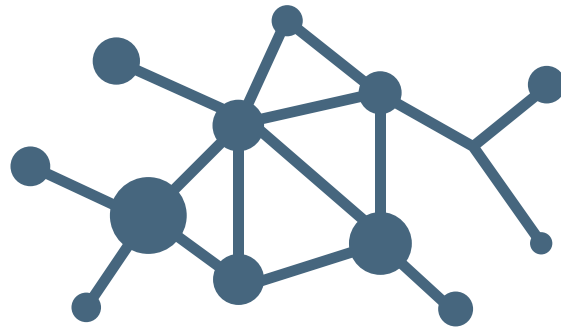




The International Association for the Engineering
Modelling, Analysis and Simulation Community



NAFEMS NORDIC CONFERENCE

22-23 May 2024 | Gothenburg, Sweden

Conference Proceedings

Gold sponsors



Silver sponsors



ISBN 978-1-83979-231-1



More NAFEMS regional conferences will take place worldwide in spring and fall 2024:

www.nafems.org/nrc24



NWC25

NAFEMS WORLD CONGRESS

19-22 MAY 2025 | SALZBURG | AUSTRIA

A WORLD OF ENGINEERING SIMULATION

Safe the date!

Abstract submission deadline likely mid November 2024

www.nafems.org/congress



Impressum

The conference is organized by NAFEMS Deutschland, Österreich, Schweiz GmbH
Griesstr. 20, 85567 Grafing, Germany, Phone: +49 176 217 984 01, Fax: +49 3 22 11 08 99 13 41
E-mail: info@nafems.de. www.nafems.org

ISBN 978-1-83979-231-1 © 2024 NAFEMS. All rights reserved. No part of this publication may be reproduced or distributed in any form or by any means, or stored in a data base or retrieval system without prior permission of the publisher.

First published: 2024, Order Reference NRC24Nordic



Dassault Systèmes, the 3DEXPERIENCE Company, is a catalyst for human progress. Operating in three sectors – Life Sciences & Healthcare, Infrastructure & Cities, and Manufacturing Industries – we provide businesses and people with collaborative 3D virtual universes to imagine sustainable innovations. A pioneer in computer-aided design founded in 1981, Dassault Systèmes has expanded into a diverse range of software categories, including 3D modeling, simulation, information intelligence, and social and collaborative processes. By creating virtual experience twins of the real world, our customers push the boundaries of innovation capable of harmonizing product, nature and life.

Dassault Systèmes' customers use our 3DEXPERIENCE platform to design and test their ideas in the virtual world so they can better respond to today's experience economy where consumers value experiences over products. 3DEXPERIENCE also extends into the organic world, where the human body can be modeled with a virtual experience twin and tested as precisely, safely and effectively as products in traditional industry. Dassault Systèmes' corporate culture promotes a questioning mindset, exploring possibilities and connecting people to bring about meaningful change. Dassault Systèmes' 20,000 employees bring value to over 300,000 customers of all sizes, in diverse industries, in 140 countries.

www.3ds.com



Established in 2003, Noesis Solutions, a trusted digital engineering innovation partner, has empowered customers adopt a transformational strategy that resolves their toughest multi-disciplinary engineering challenges of today. Our continuously evolving product portfolio, state-of-the-art technology, and unmatched customer services enable customers transform the way they build their products in a much faster and an efficient manner.

Noesis Solutions is a majority-owned subsidiary of Cybernet Systems, a leading provider of multi-domain CAE solutions covering a vast range of engineering problems. Headquartered in Leuven, Belgium, Noesis Solutions operates through a network of subsidiaries and representatives in key locations around the world.

www.noesissolutions.com



Rescale's AI-powered cloud high performance computing (HPC) platform makes accelerating innovation possible for any organization. Innovators use Rescale to provide R&D teams the world's largest library of fully managed software applications and performance-driven computing architectures, robust data security, intelligent controls, and a seamless AI-driven experience. Leveraged by a majority of Fortune 500 companies to accelerate time to market, Rescale has been recognized by Gartner as a Cool Vendor for Cloud Infrastructure, by Deloitte as a Technology Fast 500 company, and by the World Economic Forum as a Global Innovator Unicorn.

www.rescale.com

SIEMENS

Simcenter portfolio, part of Siemens Xcelerator, is a flexible, open, and scalable suite of industry-leading engineering simulation and test solutions and associated services.

Simcenter uniquely combines powerful multiphysics engineering methodologies across system simulation, computer-aided engineering (CAE) simulation and physical testing. It leverages AI capabilities for faster decisions and improved user experience and enables productivity through cross-domain workflow automation as well as process and data management.

Simcenter provides engineers with detailed insight into the real-world performance of their product or process, allowing them to increase productivity, shorten time to market, and accelerate innovation over the entire product lifecycle. Simcenter solutions are integral to delivering the comprehensive digital twin that connects the physical and virtual world.

www.siemens.com/simcenter/



Professional Simulation Engineer

It's Time
to Get Certified

nafems.org/pse



atNorth is a leading Nordic data center services company that offers sustainable, cost-effective, scalable colocation and high-performance computing services trusted by industry-leading organizations. The business acquired leading High Performance Computing (HPC) provider, Gcompute, in 2023 enabling a compelling full stack offering tailored to AI and other critical high performance workloads. With sustainability at its core, atNorth's data centers run on renewable energy resources and support circular economy principles. All atNorth sites leverage innovative design, power efficiency, and intelligent operations to provide long-term infrastructure and flexible colocation deployments. The tailor-made solutions enable businesses to calculate, simulate, train and visualize data workloads in an efficient, cost-optimized way. atNorth is headquartered in Reykjavik, Iceland and operates seven data centers in strategic locations across the Nordics, with additional sites to open in Helsinki, Finland and in Denmark in Q4 2024, as well as its tenth site ready for operation in Kouvola, Finland in 2025. For more information, visit atNorth.com or follow atNorth on LinkedIn or Facebook.

www.atnorth.com



BETA CAE Systems transformed CAE by introducing revolutionary automation software and practices into Simulation and Analysis processes more than 30 years ago.

Committed to our mission to enable engineers to deliver results of high value, we continue to offer state-of-the-art, high-performance software and best-in-class services. Our simulation solutions liberate low risk and high Return-On-Investment innovation.

The ground-breaking technology, the excellent services and our high standards of business ethics are the three pillars on which BETA was founded and grows since then.

www.beta-cae.com



The Magna Powertrain Engineering Center in St. Valentin is a globally recognized development partner for vehicle engineering, alternative propulsion systems, application software and a full range of testing services.

Its own software product FEMFAT (Finite Element Method Fatigue) is the globally leading software for finite element based fatigue life prediction. It increases the reliability and robustness of components in the automotive industry as well as in machinery & plant construction. Based on stresses from finite element analysis, FEMFAT delivers analysis results such as fatigue life or damage as well as safety factors. This enables the identification of lightweight design potentials and potential weak spots already at an early product development phase.

www.femfat.magna.com

KEYNOTE PRESENTATIONS - 1

Simulation-Based Decision Support for Transport System Development M. Eek (VTI The Swedish National Road and Transport Research Institute)	11
From CAE to SAE - From Computer- to Software Aided Engineering E. Drenth (Volvo Autonomous Solutions)	12

ARTIFICIAL INTELLIGENCE / MASCHINE LEARNING - 1

AI in FEM Simulation: Accelerated Optimization of Plastic Snap Hook Designs in the Automotive Industry F. Dirisamer (Digital Physics AI)	13
Machine Learning Optimization and Quick Verification of an Electric Vehicle Rocker Design A. Papadopoulos, D. Drougkas (BETA CAE Systems)	17
Machine Learning to Empower Engineering Organizations: Technology & Applications A. Timofeev, T. Le Clerc, T. Margaritis (Neural Concept).....	22
Hydrogen Storage 3D Architecture Automated Generation with AI J.-P. Roux (DessIA Technologies); H. Massé (OP Mobility)	25

COMPUTATIONAL FLUID DYNAMICS / MBD

Evaluation of the Munk Moment on a Wind Assisted Oil Tanker with CFD A. Ommundsen (cDynamics)	29
Electric Motor Direct Cooling: Assessment of Coolant Flowrate and Viscosity on Cooling Efficiency M. Galbiati (Particleworks Europe).....	43
ODS&ODF - A Comprehensive Approach to Evaluate the Vehicle Stiffness using MBD J. Weber, P. Ugale (Zeekr Technology Europe); M. Pena, J. Bäcklund, P. Appelgren (Beta CAE Nordic); M. Berggren (AFRY); H. Marberg (Marberg Engineering)	49
Analysing Ride Comfort in Realtime by Integrating Flexible Body in White A. Chauhan (Dassault Systemes)	51

FATIGUE / FRACTURE / DURABILITY

The Discontinuous Strain Method: Accurately Representing Fatigue and Failure L. Herrmann, A. Daneshyar (Technical University of Munich); S. Kollmannsberger (University of Weimar)	55
Enhanced Low Cycle Fatigue Analysis G. Spindelberger, K. Hofwimmer (Magna Powertrain Engineering Center Steyr).....	66
Integration of Fatigue Analysis in FEA Solver for a Faster and More Reliable Process R. Helfrich, M. Klein (Intes); L. Dastugue (Intes France).....	70
Fatigue Life Investigation as a Part of a Complete Design Optimization Process G. Korbetis, C. Tegos (BETA CAE Systems).....	82

ARTIFICIAL INTELLIGENCE / MASCHINE LEARNING - 3 / HPC

Enhancing Aircraft Safety Through Data-Driven Reduced Order Modelling for Birdstrike Analysis R. Lombardi, C. Sahin (Noesis Solutions); L. Hootsmans, W. Van de Waerdt (GKN Fokker Aerospace)	86
Automated Report Generation: Utilizing Machine Learning and Python for Automation in FEA A. Alper Akis (Enabl).....	92
Enabling Specialized Architectures for High-Performance Computing (HPC) S. Zakrzewski (Rescale).....	97

MATERIALS / MANUFACTURING**Fracture Modeling of Layered Composites in a Specialized Off-Axis Finite Element Framework**

L. Herrmann, F. Duddeck (Technical University of Munich);
 L. P. Mikkelsen, B. Nyvang Legarth, C. Niordson (DTU) 111

Upgrade Parts' Crashworthiness by Exploiting Injection Molding Manufacturing Effects

Panagiotis Fotopoulos (BETA CAE Systems); Michael Richter (MATFEM Ingenieurgesellschaft) 125

Post-Buckling Analysis of Composite Stiffened Panels using FEM

H. K. Almaz, S. Giovani Pereira Castro (TU Delft) 129

KEYNOTE PRESENTATIONS - 2**Simulation Driven Development at Volvo Car Corp.**

H. Hasselblad (Volvo Cars) 135

Highlights from Project TRUSTIT (Towards a Rational Approach to Credibility of Numerical Simulations in Industrial Applications)

F. Santandrea (RISE Research Institutes of Sweden) 136

MULTIPHYSICS**EV Battery Structural Simulation at Volvo Cars**

P. Gustavsson (Volvo Cars) 143

Design Space Exploration of Battery Pack / Body in White Integration

F. Rosenlund, T. Khalitov, K. Govindarajan, M. Lampin (Siemens Digital Industries Software) 156

Strongly Coupled Multiphysics Simulation of a Loudspeaker Driver using a Multiharmonic Approach

A. Deshmukh, A. Halbach, B. Khouya, R. Kikkeri Nagaraja, V. Lahtinen (Quanscient) 160

Electric Drive Virtual Development and Thermal Management – Project Presentation

M. Hood, F. Colas, D. Nunes, J. Brunel (Siemens Digital Industries Software) 164

VERIFICATION & VALIDATION**Building Simulation Models Credibility: What Gain can we Expect from Test-Simulation Data Fusion in Solid Mechanics?**

P. Baudoin, F. Mathieu (Eikosim); N. Swiergiel (ArianeGroup) 167

EVIDENT: Investigating Model Validation Approaches

E. Dartfeldt, T. Sjögren (RISE Research Institutes of Sweden);
 T. Bogdanoff, J. Olofsson (Jönköping University) 170

Structural Numerical and Experimental Investigation of Urea Mixer Component Thickness to Reduce Cost, Weight and Thermal Mass

H. K. Kuna (Dinex) 173

PLENARY PRESENTATIONS - 3**Modern Digital Twin Solutions - Overview and Applications**

P.-O. Jansell (Altair Engineering) 179

Recent Advances in Non-linear Industrial Non-parametric Optimization

A. Jurinic, C. B. W. Pedersen (Dassault Systemes) 180

Simulation-Based Decision Support for Transport System Development

Magnus Eek

Research Director – Vehicle and Driving Simulation

The Swedish National Road and Transport Research Institute

The presentation will give a brief overview of the Swedish National Road and Transport Research Institute (VTI) operations, with a special focus on modeling and simulation related research and development. Examples on the use of simulation in the transport systems domain will be highlighted as well as perspectives on how simulation facilitates decision support for addressing current challenges in the development of the transport system.

Dr. Magnus Eek is Research Director at VTI, heading a research unit focused on vehicle systems, simulation, and visualization. Furthermore, he is leading VTI's strategic initiative to enhance research capability in sustainable air transport systems. He has extensive experience from the defense industry, working at Saab with Model-based Systems Engineering, Research & Technology strategy, as well as research project- and program management. The time at Saab Aeronautics included an industrial PhD connected to Linköping University, focusing on methods for verification, validation, and credibility assessment of simulation models and large-scale aircraft system simulators.

From CAE to SAE

From Computer- to Software Aided Engineering

Edo Drenth

Acting Group Manager – Nominal Software & Motion Models
Volvo Autonomous Solutions

The keynote presentation will address following topics:

- Interoperability between simulation tools
- Impact of physics-based modelling on business:
- Where does it create most value? For hardware sizing or controlling software development? Only in concept phase or even at later stages of product development?
- Verification and Validation of complex system models:
- How to manage these tasks effectively within large organizations?

AI in FEM simulation: Accelerated Optimization of Plastic Snap Hook Designs in the Automotive Industry

Florian Dirisamer (Digital Physics AI GmbH)

1 Summary

At the heart of product development in the automotive industry is the continuous optimization of components, especially plastic components, in order to achieve goals such as lightweight construction, durability, cost efficiency and reliability. The introduction of artificial intelligence (AI) into this process marks a revolutionary change, particularly through the use of neural networks. These technologies make it possible to learn from a variety of data and predict the behavior of materials and components under different loads with high precision. The use of AI in finite element method (FEM) simulation leads to a drastic reduction in the time required for simulations. Instead of spending days or weeks running complex simulations, trained systems can achieve results in minutes or even seconds. This allows for much faster iteration of design variants, which can shorten development cycles and improve time-to-market. The application of AI also enables in-depth analysis and optimization of designs without the need for an exponential increase in computing resources. This results in the development of lighter, more cost-efficient, and higher-performance components with longer lifetimes, which is crucial in the automotive industry where every gram counts. To illustrate the practical application and benefits of these technological advances, the presentation will introduce a case study on the optimization of plastic snap hooks. We will demonstrate how the use of AI-supported FEM simulations can not only accelerate development processes, but also improve their quality. We will outline the technical challenges, present the solutions applied and discuss the improvements achieved. This case study highlights how AI technologies are driving innovative developments in the automotive industry and opening up new opportunities for product development.

2 Motivation

The integration of Artificial Intelligence (AI) has led to profound changes across industries, and computer-aided engineering (CAE) is also experiencing a profound impact. This article explores the potential of AI in the Finite Element Method (FEM), with a particular focus on optimizing system efficiency and addressing challenges posed by inverse problems and black-box components. Innovative approaches are highlighted to show how AI can be used to make FEM simulations more efficient and manageable when dealing with inverse problems or black-box components. Optimizing efficiency is of utmost importance in technical development, as it directly affects time and resource allocation. By employing AI techniques such as machine learning and optimization algorithms, FEM simulations can be accelerated without sacrificing accuracy.

3 Method

Presented here is a case study from the field of FEM, which is besides CFD one of the most commonly used method in engineering simulations. Usually simulations in this environment is time-consuming and often takes several hours for a single design point. Furthermore, determining meaningful boundary conditions (BC) poses a particular challenge, as a multitude of geometry, material parameters, BCs as well as production information and machine settings have a significant influence on deformation properties and failure types, such as no failure, too high bending stress, too high notch stress, etc. The schematic component for this presentation is shown in Fig. 1.

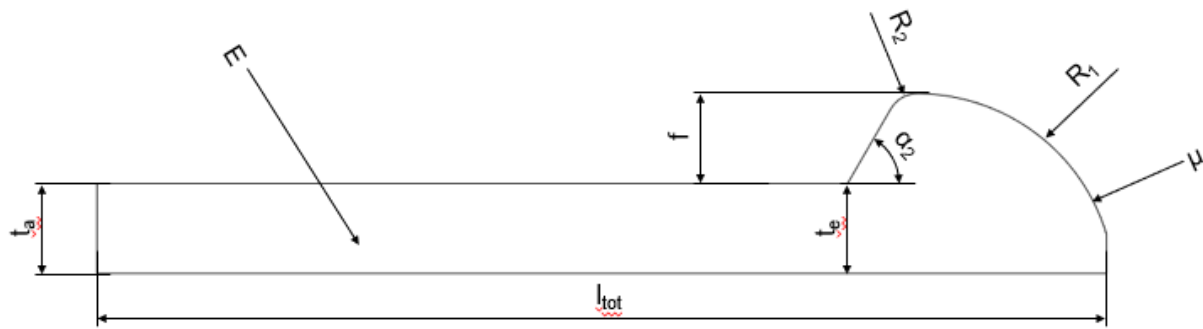


Fig. 1
Schematic component illustrating the applicability of AI predictions in FEM-Simulations

The simulation results for a combination of geometry and material parameters, as well as boundary conditions, with the simulated deformations and stresses, is simulated using FEM. Furthermore, failure types are determined by evaluating the deformation and stress behavior. One single simulation result for the plastic snap hook is shown in Fig. 2.

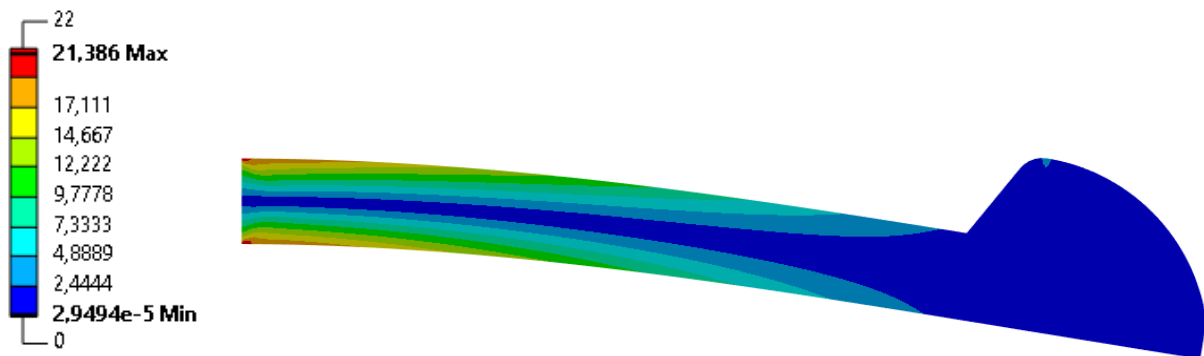


Fig. 2
Schematic result of an examined geometry, material property and BC combination

Through the utilization of Artificial Intelligence (AI), simulations are expedited, and inverse problem formulations can be efficiently resolved, as this enables the inference geometry, material properties and BCs based on desired max. stresses and failure types. Machine learning (ML) is employed to leverage simulation data and capture complex relationships between input parameters and desired output variables. Fig. 3 presents the utilized parameters along with their corresponding ranges. It also indicates which parameters are specified as boundary conditions (input parameters) in the simulation and which parameters are evaluated as outcomes (output parameters) through the simulation. Additionally, it illustrates which parameters are utilized as input parameters for the inverse prediction by the AI and which parameter the AI is tasked with determining. Input parameters for the AI training may include, as in this case, the max. stress, the failure type and some fixed geometry and material parameters, while output variables could include, for instance a missing geometry parameter. The trained AI model facilitates rapid predictions and the resolution of inverse problems to determine optimal parameters based on desired behavior.

Category	Parameter		Limits		Unit	Sim*	AI-P**
Geometry	Total length	l_{tot}	1	50	mm		
	Deflection	f	1	5	mm		
	Joining radius factor	f_{R1}	2,2	3	1		
	Rounding radius factor	f_{R2}	0,22	0,33	1		
	Joining partner radius factor	f_{RF}	0,09	0,2	1		
	Release Angle	α_2	30	90	°		
	Radius	R	0	10	mm		
	Cantilever thickness beginning	t_a	1	10	mm		
	Cantilever thickness end	t_e	1	10	mm		
	Snap arm width	b	1	20	mm		
Material model	Young's Modulus	E	500	100 000	MPa		
BC	Coefficient of friction	μ	0,1	1	1		
BC	Max. Stress	σ_{max}	1 Parameter		MPa	○	○
BC	Failure Type	F	7 Categories		-	-	○

Fig. 3

Representation of the investigated Geometry, material property and BCs with the individual limits

The presented approach combines physical simulations with AI to achieve time savings in simulations and to determine optimized boundary conditions. In doing so, prediction accuracy is maintained, and the efficiency of FEM-simulations is enhanced. Due to the inverse prediction using AI, problems can be quickly resolved that would otherwise often only be solved as optimization problems without AI, where in this case, a large number of simulations with adapted boundary conditions lead to a step-by-step approximation of the desired geometry. However, this is very time- and resource-intensive, which can be greatly shortened and reduced by AI. This is even more significant when actual machine measurement data and associated component manufacturing are used instead of simulation data because it significantly reduces the number of components to be produced with different parameter sets and can be optimized by AI, leading to significant time, resource, and cost reductions, and promoting sustainability.

4 Results

Based on the max. stress and failure type in the inverse prediction, the required length of the plastic snap hook was predicted using AI. A comparative simulation was conducted with the previously unknown parameter set, evaluating the max. stress and the failure type. These results were then compared, achieving a >95% match between the desired max. stress and the simulated max. stress (Fig. 4).

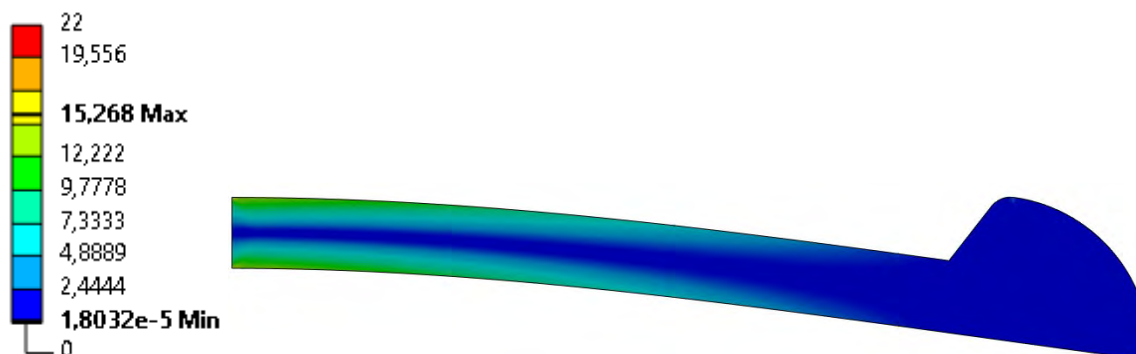


Fig. 4

Schematic result of an examined geometry, material property and BC combination

Since the length of the snap hook was obtained from the defined parameter sets of geometry, material parameters, and BCs from the previous simulations, no additional simulation was necessary for further analysis of the max stress. By utilizing the training of the AI through rearranging the structure of the existing dataset, the time and resource requirements could be significantly reduced.

5 Summary

The paper aims to provide a comprehensive understanding of the impact of AI in FEM and CFD simulations, particularly in optimizing system efficiency and effectively handling inverse problems and black-box components. By employing AI techniques, engineers can unlock new avenues for efficiency optimization and ensure the management of complex components. These advancements enable the design of safer, more innovative, and more efficient systems, contributing to progress across various industries.

It is demonstrated that determining necessary process and machine parameters for desired component quality through the inverse solution of a task by AI without solving an optimization problem is feasible. This significantly reduces development time, as well as material and resource expenditure. Furthermore, by shifting the problem statement to direct prediction, the max. stress in a component can be inferred without additional simulations and calculations. These predictions of geometry and material property, as well as BC parameters can be realized with high accuracy depending on data availability.

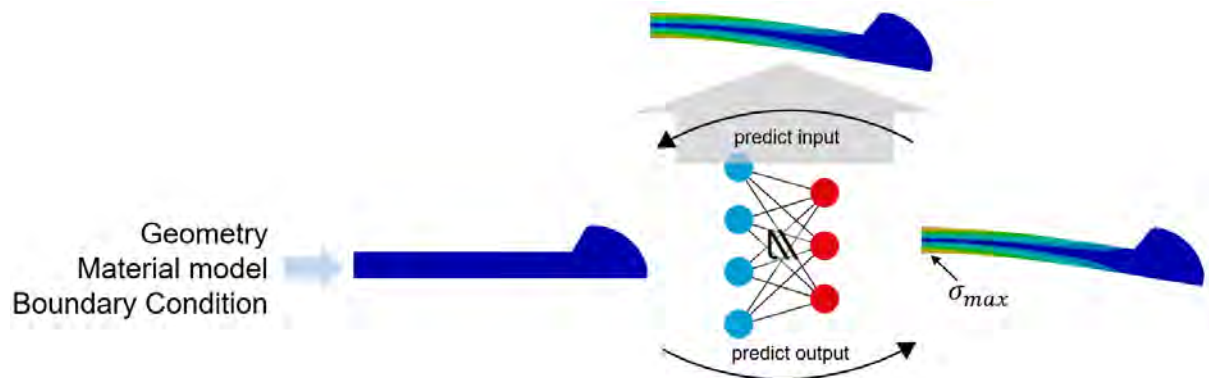


Fig. 5
Visualization of the prediction of output parameters (predict output) and the inverse prediction of input parameters (predict input) using AI, using the example of a plastic snap hook

Machine Learning Optimization and Quick Verification of an Electric Vehicle Rocker Design

MSc Dipl.-Ing. A. Papadopoulos,
MSc Dipl.-Ing D. Drougkas
(BETA CAE Systems, Greece)

Abstract

Prior to their market debut, all prototypes of vehicles undergo validation for their crashworthiness. Achieving compliance with safety standards, while simultaneously avoiding compromises in other crucial design aspects, demands a highly detailed engineering simulation approach during the product design phase. These processes become even more complicated, and time-consuming, with electric vehicles, such as Lithium-ion battery-powered cars. In many cases to accomplish the safety aims during product design, while also meeting time limitations and deadlines, sophisticated simulation tools need to be employed. Such tools are those that enable optimization studies and that take advantage of Machine Learning capabilities.

In this study, an optimization and a quick verification of an electric vehicle rocker design were performed with the aid of an Optimization tool and Machine Learning methods.

This Optimization tool employs Design Experiments and a Machine Learning predictive model (referred to as a "Predictor") to approach optimal design parameters for a given objective and constraints. This extends to quick verification of new designs, enabling rapid testing of modifications without re-solving the model. To enhance efficiency, a macroscopic battery model is used, allowing the ML Predictor to consider electromagnetic phenomena in damaged batteries without increasing solution time in side-crash simulations.

All in all, using the Machine Learning based Optimization tool, and the Transfer Learning related functionality, an already trained predictive model was able to estimate the optimal design of the vehicle with updated components and verified the updated designs without having to re-run the complete optimization and solution processes.

1. Optimization Method and Model Description

The current study focuses on the crash simulation of a Li-ion battery-powered EV module platform which is imposed to a side collision with a rigid pillar at 60 km/h. For the battery modeling of the li-ion batteries located inside the platform, the macroscopic battery model “BatMac” based on the equivalent Randles circuit was used. For the investigation of an internal battery short, LS-DYNA provides a keyword that triggers the short when the criteria defined inside the function are met. In the current case, the shorting conditions are based on the stress values applied to each cell. When the stress exceeds a particular value, an internal battery short occurs.

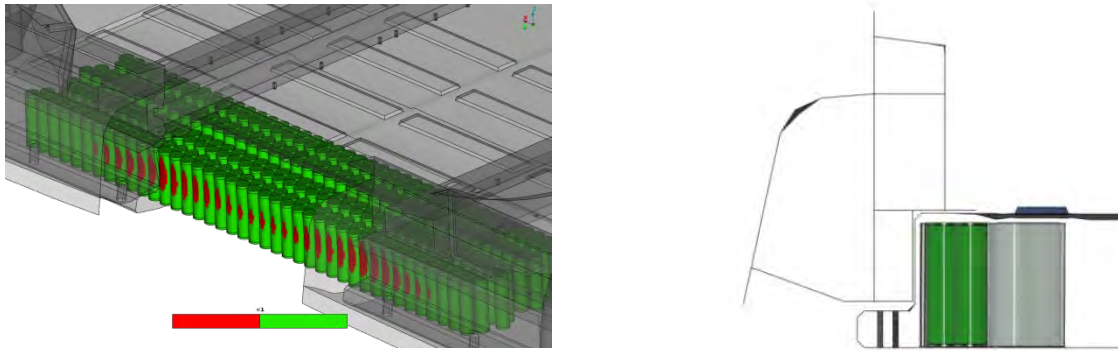


Figure 1: Side-crash simulation model of the electric vehicle

Regarding the optimization workflow, a set of pre- and post-processing functionalities were used, accelerating the optimization process of an electric car platform design, using the embedded Machine Learning Optimization tool. Specifically, the process consists of setting up an Optimization Task which embeds the Design of Experiment method to produce several DOE studies. The design parameters whose value varies from study to study, are referred to as Design Variables, and the dependent critical results as Responses. Based on these datasets, an ML Predictor is trained using the Response Surface Model. Then, the objective and constraints of the Optimization Study are defined, and finally, by utilizing the predictive model of the Predictor, the Optimizer returns the optimal solution. In the studied optimization scenario, the objective is to minimize the number of damaged batteries without increasing the rocker's mass, and hence, the corresponding values were assigned as Responses. The defined Design Variables are the rocker plates' thickness and location variation along the y-axis.

2. Predictive Model and Optimization Results

The values of the design variables are obtained by the Uniform Latin Hypercube DOE generation algorithm. For each iteration, the generated experiments with the different DV values are solved and post-processed as assigned in the Optimization Task workflow. This way, a file repository occurs, containing all the necessary data to train a predictor. In this case, 100 DOEs were solved.

To evaluate the quality of this dataset, information can be retrieved from the Correlation Matrix and the Pair Plot of the DVs versus the Responses, as well as the Power Predictive score. In the following matrix, the correlation is described through a factor that fluctuates between -1 and 1. Values close to 0 mean that there is not any relationship between the DVs and responses, and values closer to 1 and -1 mean that there is a strong correlation. In this case, it is highlighted that the mass is mainly affected by thicknesses 1 and 2 and the number of damaged cells is affected mostly by Plate Location and Thickness 2. The positive and negative signs imply that the variables are proportional and reversely proportional, respectively.

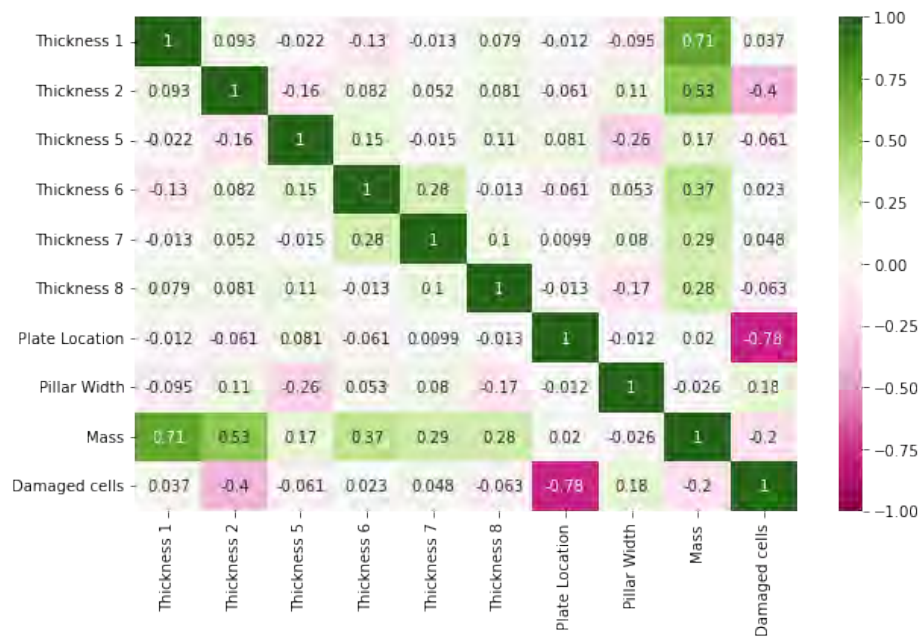


Figure 2: Correlation Matrix

In the following pair plots, each DV's values are depicted versus the corresponding response value. In the plots where patterns are noted e.g., in thickness 1 vs mass or Plate Location vs Num. of damaged cells, it is safe to assume that there is a linear correlation between the corresponding variables.

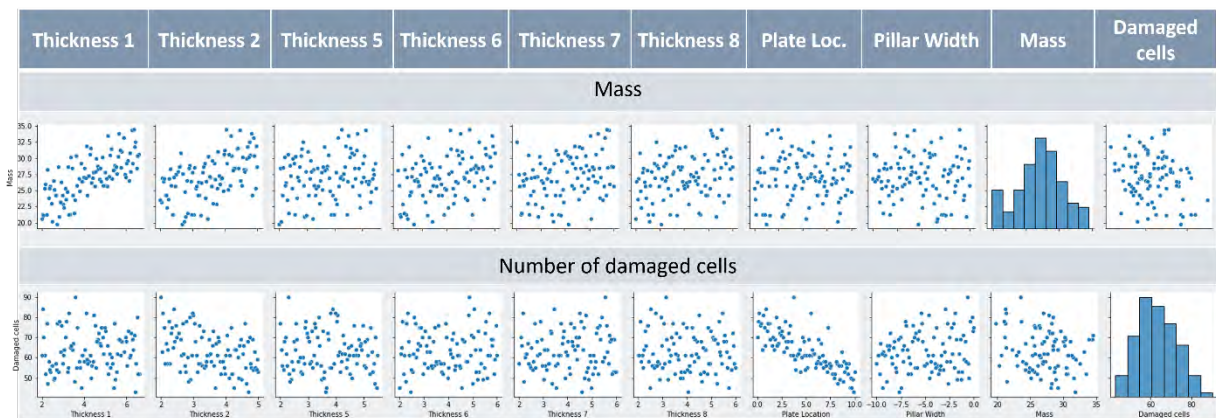


Figure 3: Pair Plots of the Responses vs. DVs

Lastly, the predictive power score (PPS) is an asymmetric, data-type-agnostic score that can detect linear or non-linear relationships between two columns. The score takes values between 0 (which means no predictive power) and 1 (which means perfect predictive power). For the Mass, the PPS is 0.98 whilst for the Number of Damaged Cells is 0.64.

The occurring calculated predictive model calculates the relationship between the Design Variables and the Responses using a Regression method. Once the predictor is trained, graphs are reported giving information about the quality of the Predictor. The shown bar chart sorts the design variables according to their importance in the optimization process. As shown, the number of damaged cells is mostly affected by the plate location, whilst the mass mostly depends on the thickness of plate 1. Then, from the variance estimation graph, the predictions with their confidence bounds are indicated. The Minimum Average Error of Variance is the minimum error of the confidence bounds for each prediction and the Accuracy is the percentage of the configuration bounds that correctly include the ground truth value.

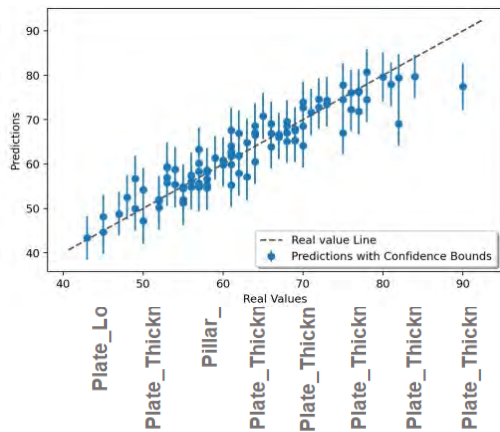


Figure 4: (a) Left: Ranking of DVs Importance regarding the number of damaged cells.
(b) Right: Variance Estimation graph.

Finally, using the Differential Evolution method, the Optimization Study is run resulting in the optimal solution. As shown below, all the studies explored by the Optimizer do not exceed the Mass constraint of 36 kg. The optimal solution is the last study which suggests that the predicted mass is at 24.5 kg whilst the predicted damaged batteries are 37.

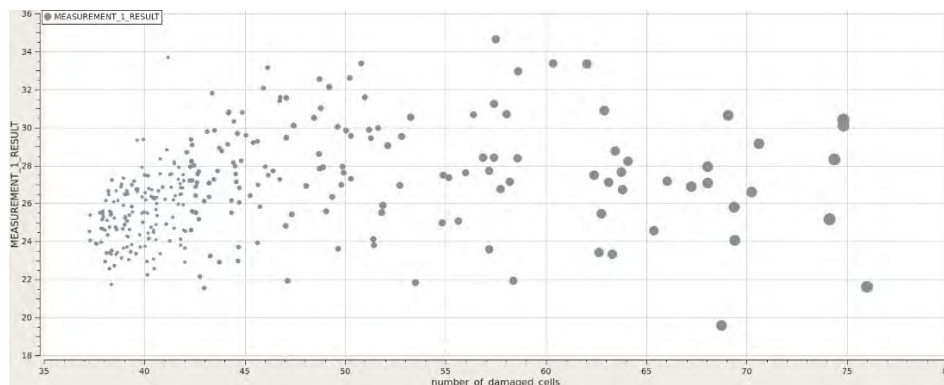


Figure 5: Optimization Studies: Mass vs Number of Damaged Cells

Moreover, the optimized model is solved conventionally to validate the optimization process, while also the optimization results are evaluated overall.

Response	Initial Model	Predicted Optimal	Validated Model
Mass [kg]	37.56	24.57	24.39
Num. of damaged cells	68	37	46

Table 1: Evaluation of Optimization Results

3. Quick Verification of the Modified EV Model

The predictive model trained previously can be used in cases where the initial model has been slightly modified on areas affected by the design variables and they have a relatively high similarity factor among the parameters of the baseline model. The response values can be quickly predicted without requiring solving the model. So, this way, the changes in the geometry can be quickly evaluated. Again, the results were validated and they highlight that the particular change in the plate's thickness will worsen the crash behavior of the vehicle. This way, the designers can save a significant amount of time during the early design stages, as they are prevented from following the wrong design direction without requiring solving numerous design scenarios.

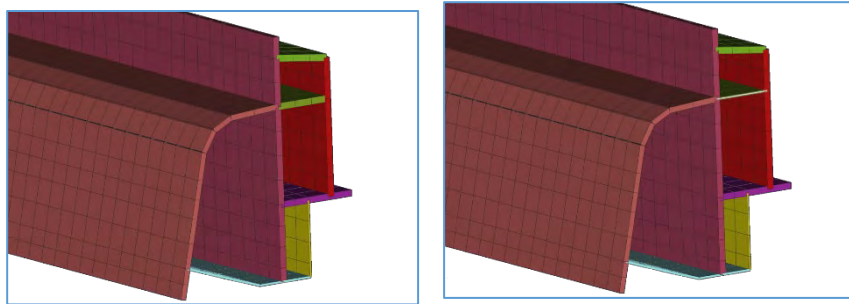


Figure 6: (a) Left: Initial rocker design, (b) Right: Modified rocker design

Response	Initial Model	Predicted	Real Modified
Mass [kg]	37.56	35.8	35.82
Num. of damaged cells	68	72	73

Table 2: Evaluation of Quick Verification Results

4. Conclusions

To conclude, the ML Optimization process discussed in this study introduces a semi-automated way: (a) to produce the required data to train an ML Predictor, (b) to estimate the optimal design of an EV using the trained Predictor and (c) to quickly evaluate potential relatively small modifications to the Baseline Model without demanding training a new predictive model. Lastly, the embedded plotting functionalities facilitate the visualization of the ML-related results, allowing the inspection of the Predictor accuracy as well as to evaluate the whole Optimization process.

Machine Learning to Empower Engineering Organizations: Technology & Applications

Aleksandr Timofeev, Théophile Le Clerc, Dr. Athanasios T. Margaritis

Neural Concept SA, EPFL Innovation Park Bâtiment A, 1015 Lausanne, Switzerland

1 Introduction and context

New societal and environmental needs demand increasingly better-performing products at an accelerated rate, posing a significant challenge for engineering organizations. To meet these demands and maintain a competitive edge, engineering teams must shorten their design processes while simultaneously enhancing product quality. Engineers need radically new capabilities, including more effective ways to harness their computational resources.

Due to their historical origin, traditional simulation tools are not well adapted to design optimization in fast-paced production and design environments. It is extremely hard for design teams to leverage insights provided by advanced simulations and by the specialized teams who develop them. Deep Learning and AI-based technologies can be used to integrate knowledge from simulation and design optimization tools in the workflow of design engineers to enable faster design iterations and better results products.

Despite the recent emergence of promising AI-enhanced techniques, businesses find it difficult to transition from pilot and R&D stages to fully harnessing these capabilities within a production setting. Many AI-augmented tools available lack the necessary openness and adaptability to create custom-tailored solutions that seamlessly integrate into intricate production ecosystems across different applications.

We're entering a new era of Engineering Intelligence, which places AI as the central paradigm of the design process, delegating to computers the tasks of creating detailed designs, starting from high-level functional requirements. This transformation from a simulation-enabled to an AI-enabled design process is driven by the most advanced Deep Learning algorithms. These algorithms allow shortcutting any simulation chain through a predictive model that outputs post-processed results and optimization suggestions, directly from the geometry design. The models are being used in engineering companies to simplify processes and to emulate the expertise of simulation engineers in the hands of product or design engineers early in the development process. Moreover, complex interactions between different teams and tools involved in the design process are transferred to the computer which assumes control of component and subcomponent design based solely on provided functional requirements.

However, the key challenge for both ISVs and engineering companies is to effectively bring this technology to production. This is achieved by building an open and flexible platform that allows the synergetic interaction of multiple key enablers of engineering intelligence. This involves new fundamental technologies, a new generation of skilled engineers with expertise in data science, Large Language Models that redefine how engineers interact with the software, cloud HPC services, and further facilitators.

In this talk, we will demonstrate how the Neural Concept (NC) platform enables engineers to develop end-to-end AI-enhanced workflows, driven by historical data from simulations, completely integrated into their current workflows and with online simulation capabilities. The combination of predictive and generative AI models empowers engineers to efficiently significantly larger number of designs than with traditional simulation tools and reach optimized results with better performance much faster.

We will focus our attention on selected use cases to demonstrate this end-to-end integration of NC within comprehensive engineering workflows for complex designs. Currently, NC is being used by multiple organizations in workflows including, but not limited to, the following applications: heat exchanger design optimization, structural analysis and durability studies, internal flows, external aerodynamics for air and road vehicles, turbomachinery, electronics testing, thermal management of

batteries and power electronics, industrial process and manufacturing, such as stamping, casting, molding.

2 Data-driven AI-based workflow examples for specific applications

In this talk, we will explore the development of NC-integrated workflows for several different applications, focusing on end-to-end workflows for selected use cases, such as vehicle external aerodynamics, heat exchanger optimization, and e-motor optimization.

In vehicle external aerodynamics, the main motivation for designers is to improve performance and reduce aerodynamic drag and the corresponding fuel consumption and emissions. Evaluating multiple design variations with traditional simulation tools is extremely expensive as design iterations increase. NC enables engineers and designers to iterate fast and explore the design space efficiently, at a massively reduced computational cost and achieving improved design performance. Central to this approach is the generative design capability of the platform to explore variations of baseline designs quickly, combined with state-of-the-art predictive algorithms.

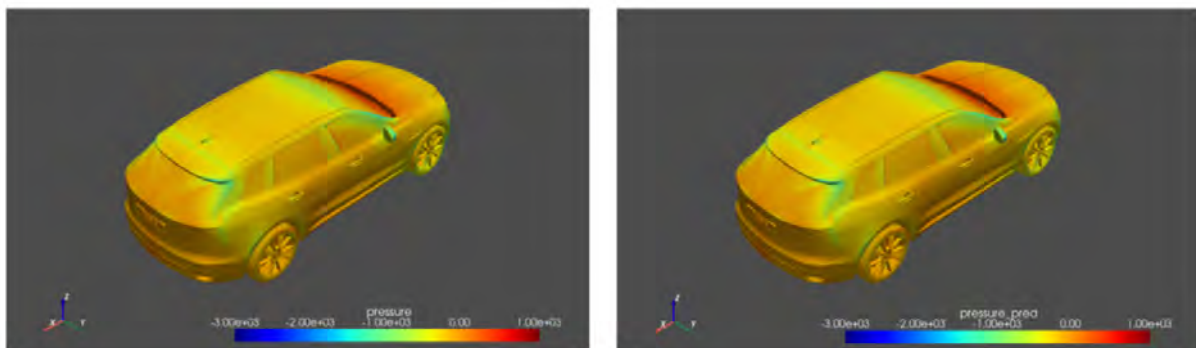


Fig. 1. Comparison of pressure field prediction on the surface of an SUV between CFD results (ground truth, left) and prediction using an NC predictive model (right).

In the application of heat exchanger design, engineers need to optimize between the competing objectives of reducing the pressure loss through the heat exchanger and ensuring the maximum heat transfer to minimize the peak temperature while maintaining uniformity to some extent. Similarly, the increasing cost of simulating multiple designs and the restricted capabilities of design generation using parametric geometry generation tools prevent engineers and designers from reaching true optimal designs within their design space. NC combines flexible, non-parametric generative models to explore new geometries with accurate predictive models to evaluate their performance, allowing designers to explore the design space efficiently and achieve improved designs while massively reducing the design cycle time.

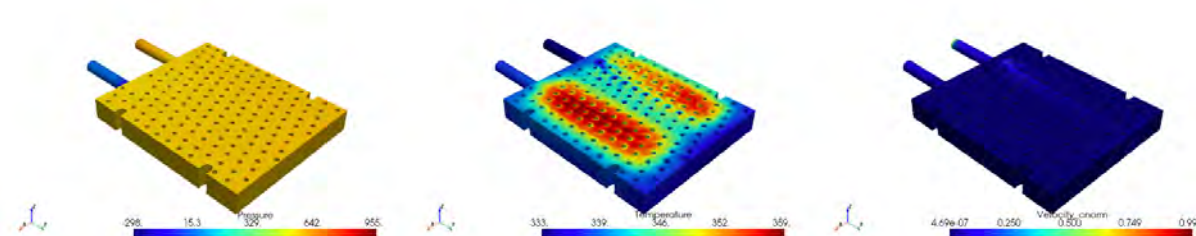


Fig. 2. Heat exchanger design. Visualization of the pressure drop (left), the temperature distribution (center), and the velocity (right) for a generated heat exchanger geometry.

Beyond aerodynamics and heat exchanger applications, we will also briefly review other related uses of NC for applications within structural mechanics, electric motor design, battery thermal management, and others.

3 Conclusions

As noted above, current engineering challenges are pushing designers and engineers to iterate and collaborate more closely than ever before, with increasing pressure to create products with improved performance with significantly shorter design cycles.

Utilizing the latest technology in state-of-the-art predictive and generative AI-based tools, Neural Concept enables engineers to create optimized products at a much faster pace than what used to be possible using traditional tools. Multiple companies and organizations around the world have been using the NC platform to integrate their traditional workflows into AI-enhanced, data-driven processes taking advantage of both historical data and designs, in-house expertise, and the latest technology in Deep Learning. In this new era of Engineering Intelligence, engineers need to adapt and use the latest technology in order to be able to develop better-performing products at a pace that was previously unattainable.

Hydrogen storage 3D architecture automated generation with AI

Jean-Pierre Roux (Dessia Technologies) - Hugues Massé (OP Mobility)

OP Mobility (ex Plastic Omnium) positions itself as a global leader in hydrogen mobility, the group directs its strategic vision in this field around a comprehensive and competitive offering covering the entire hydrogen value chain. This includes hydrogen tanks, fuel cells, and integrated hydrogen systems.

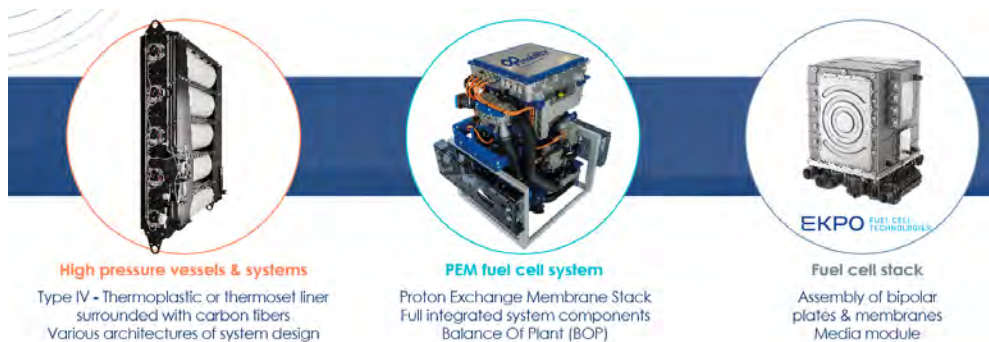


Fig1: OP Mobility H2 Product Range

Hydrogen storage in the form of compressed gas is a crucial challenge for the development of hydrogen as an energy vector in the automotive sector. Hydrogen storage is more complex and costly than that of other gases due to its very low density, thus requiring high pressures, typically 700 bars. Type IV tanks (with polymer liner) have improved these storage conditions. They separately manage the tightness and mechanical resistance to pressure, allowing the use of lighter materials while maintaining safety. However, these tanks are constrained in their shape to minimize stresses in the material due to pressure, and this shape does not allow optimal use of the available space in the vehicle.



Fig2: Type IV high pressure vessel design

Therefore, a software solution for optimizing storage architecture within the vehicle brings clear commercial interest, whether to reliably and quickly respond to RFQ or to optimize the cost-to-quantity ratio of onboard hydrogen, which is a fundamental element of storage system sizing.

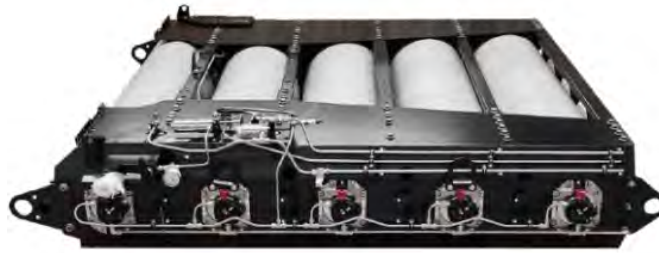


Fig3: H2 Storage system

This dedicated software solution has been developed using Dessia Technologies' process automation software platform. Leveraging the libraries of the platform, it's possible to describe a system through object-oriented modeling and associate attributes and methods such as 3D CAD generation or solution generation using AI algorithms.

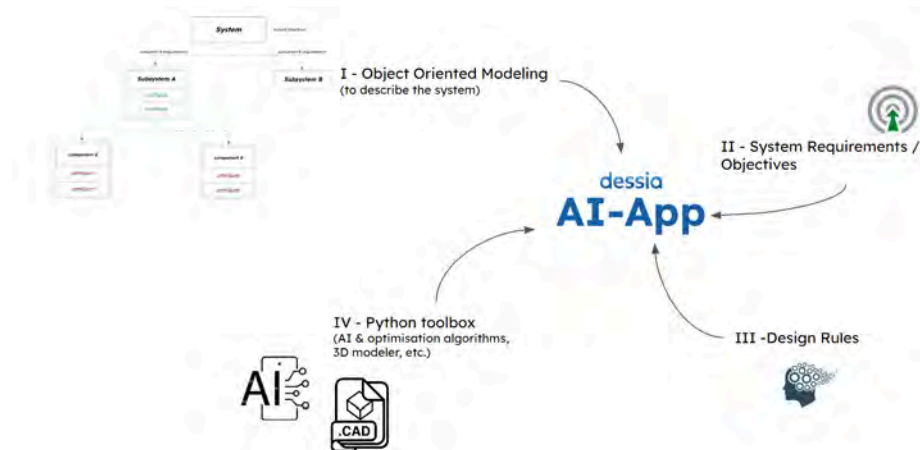


Fig4: Object Oriented System Modeling connected with AI, rules and requirements

Different types of AI algorithms are used depending on the purpose of the software application to be developed

- Generative algorithms from the symbolic or Explainable AI family are used, for instance, decision trees with pruning strategies to generate data from knowledge.
- Statistical Artificial Intelligence algorithms are used in situations where a large amount of data is available.

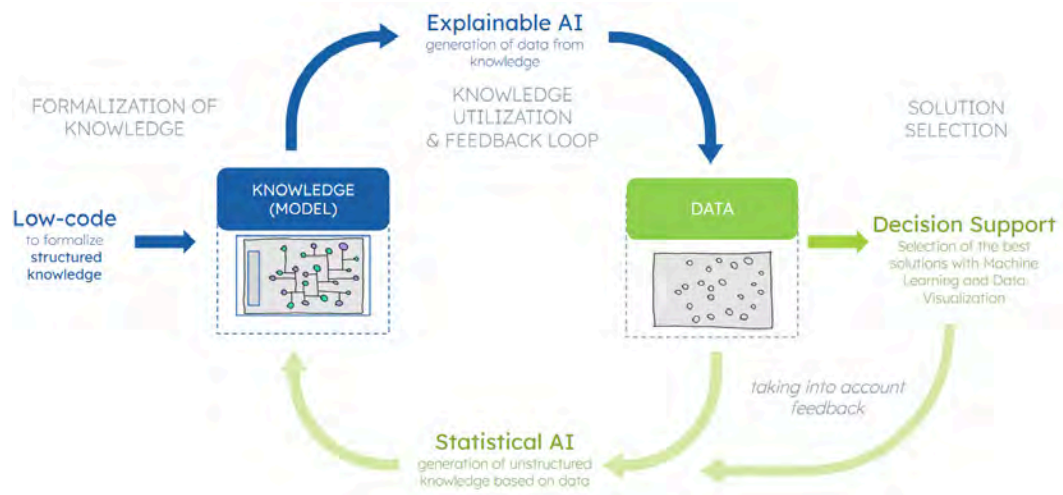


Fig5: Explainable versus Statistical AI

This software application for optimizing hydrogen storage architecture uses generative algorithms to automatically generate

- all possible solutions for integrating tanks within a given functional volume, starting from a catalog containing all possible tank models.
- the pipes routing that connect the tanks to a hydraulic collector.

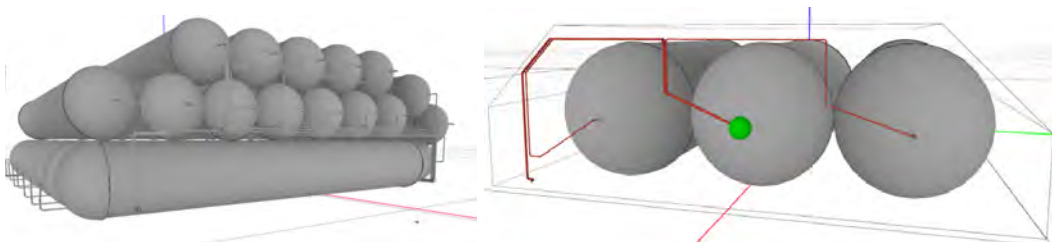


Fig6: Example of H2 Storage solution generated by the Application

- Clustering algorithms to organize the solutions into architecture families, facilitating assistance in selection and decision-making. This approach also enables the exploitation of results to quickly identify the most functionally and economically efficient solutions.

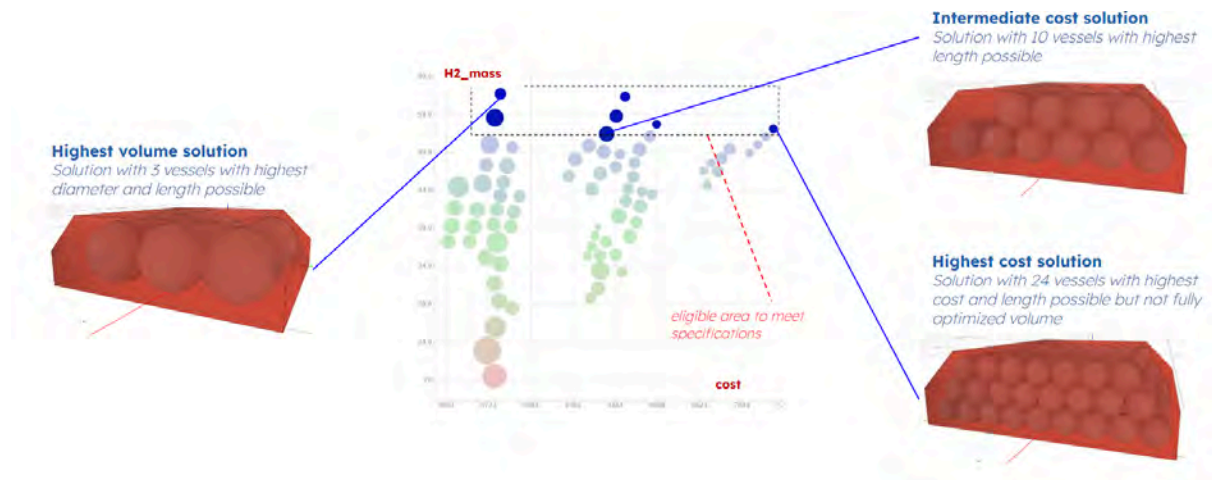


Fig7: Data driven Design Solution selection

Conclusion:

A software application combining knowledge and rules with explainable and statistical AI algorithms has been developed; it opens the capacity to explore automatically the field of all 3D architecture solutions in a few minutes where a manual process takes days to come up with a good design.

Trade-off & impact studies can be performed amongst the various solutions, and informed design decisions are taken.

Evaluation of the Munk Moment on a Wind Assisted Tanker with CFD

Andreas Ommundsen (cDynamics)

1 Summary

The ship 'Trans Tind' has been evaluated in cross flow conditions with CFD to find the centre of pressure, to aid placement of rotational sails on deck. The Munk moment arises from asymmetric locations of high-pressure stagnation points and is a major contributor to the vessels yaw moment in cross flow. It is a destabilising moment, always trying to turn the vessel perpendicular to the flow.

Three vessel velocities and three vessel headings are simulated with a heavily modified version of OpenFOAM, developed by Cloud Towing Tank [1]. The results showed that the longitudinal centre of pressure was in front of the vessel's bow, meaning that there are no points on the vessel body that when pushed will not rotate it.

2 Munk moment

2.1 Definition

The mathematical formula for the Munk moment is $\frac{1}{2} U_c^2 \sin 2\beta (A_{22} - A_{11})$, where U_c is the velocity, β is the vessel direction, and A_{11} and A_{22} are the added masses in surge and sway respectively.

This moment is always destabilising, meaning that it constantly wants to turn the hull perpendicular to the flow. The physical cause for this moment is the asymmetric location of the stagnation points. The high-pressure stagnation points in the bow and stern will exert a moment on the hull:

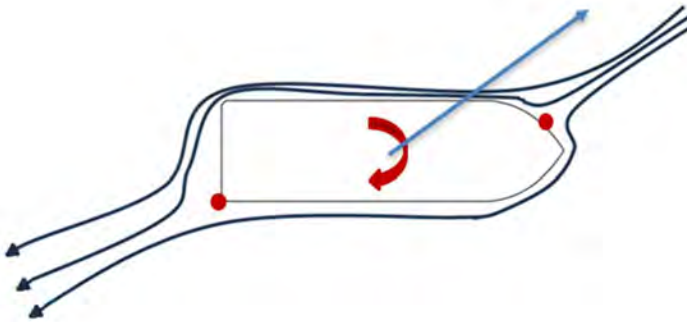


Figure 1: Hull with streamlines and location of high-pressure stagnation points. Yaw moment and vessel trajectory indicated with arrows.

2.2 Approximate value

A simplified diffraction analysis was performed to quantify the value of the Munk moment. Added mass values were calculated, and the Munk moment was found to be between 40 and 160 MNm for the chosen velocities and flow directions.

3 CFD-analyses

3.1 Software and simulations

The CFD-analyses are done in the highly modified version of OpenFOAM, developed by Cloud Towing Tank. The vessel velocities 11, 13.5 and 15 knots and directions 0°, 5° and 10° are simulated. The mesh is made with CF-MESH+ and consists of around 10 mill. cells.

3.2 Results

3.2.1 Visual results

Visual results for 10° flow angle and 15 knots velocity are shown in the figures below:

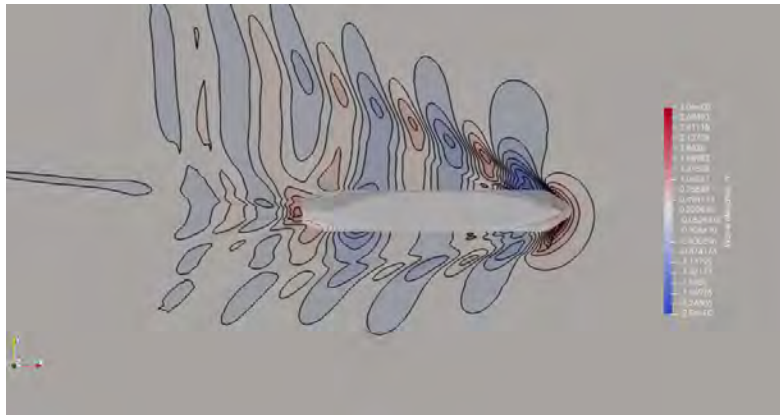


Figure 2: Wave elevation.

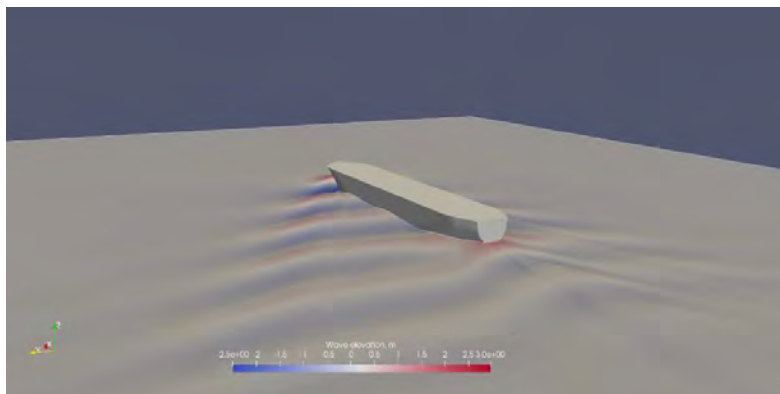


Figure 3: Wave elevation from stern.

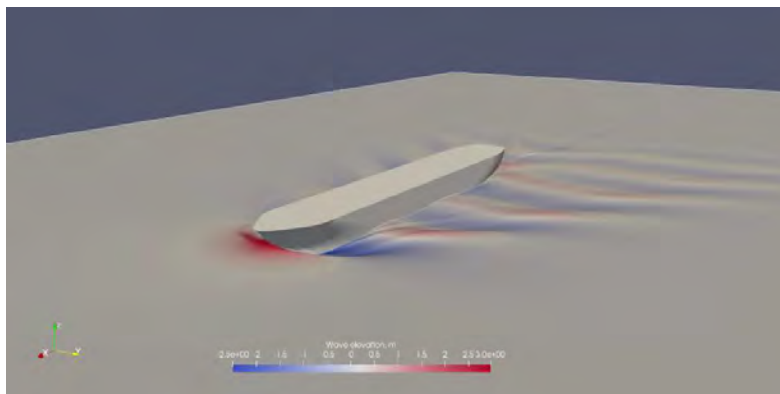


Figure 4: Wave elevation from bow.

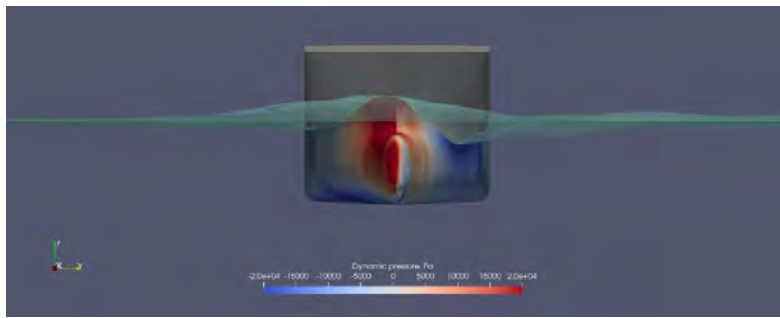


Figure 5: Hull pressure plot from bow.

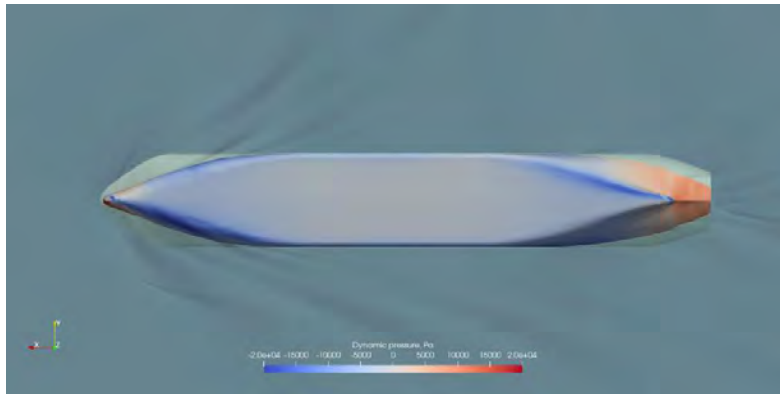


Figure 6: Hull pressure plot from below.

3.2.2 Centre of Pressure

The centre of pressure, $CoP = \frac{M_z}{F_y}$, turned out to be ahead of the bow of the vessel:

For 5° , the CoP is up to 211.4 m ahead of the stern, while the LOA is only 134 m. That is 77.4 m ahead of the bow. Subtracting the Munk moment gives a CoP up to 98.3 m ahead of the stern, i.e. within vessel boundaries. The Munk moment is therefore the biggest contributor.

This shows that M_z is large. This moment must be counteracted by the rudder and sails.

So, a centre of pressure outside of the vessel boundaries must be unphysical?

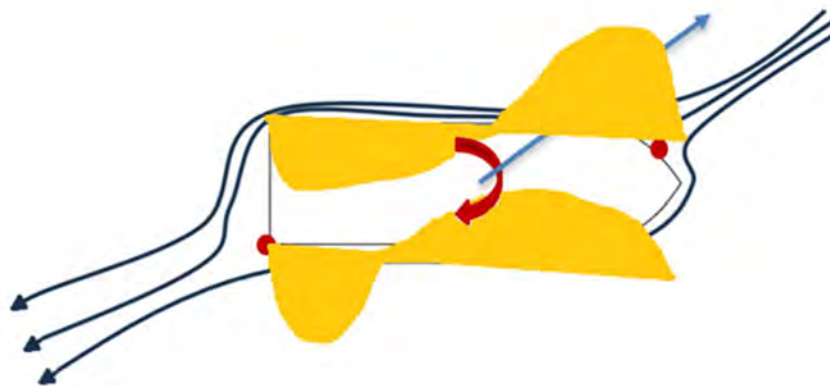


Figure 7: Orange colour is the pressure distribution of the Munk moment around the vessel.

No, the unbalanced resulting forces lead to a pressure centre outside of the vessel, i.e. you will not find a point on the vessel body anywhere that when pushed will not rotate it. It can also be interpreted as that for the transverse force resultant F_y to be able to yield a moment as big as M_z , it must have an arm equal to the distance between CoG (centre of gravity) and CoP (centre of pressure).

4 Conclusions

The CFD-analyses showed that the yaw moment in cross flow of 'Trans Tind' gave a large moment, and that the Munk moment is the largest contributor of it. The centre of pressure was calculated to be in front of the bow of the vessel, i.e. outside of the vessel boundaries.

It is wise to put the sails close to the bow in this case, as it will help counteract the moment. The rudder must compensate for the rest.

5 References

- [1] <https://cloudtowingtank.com/>

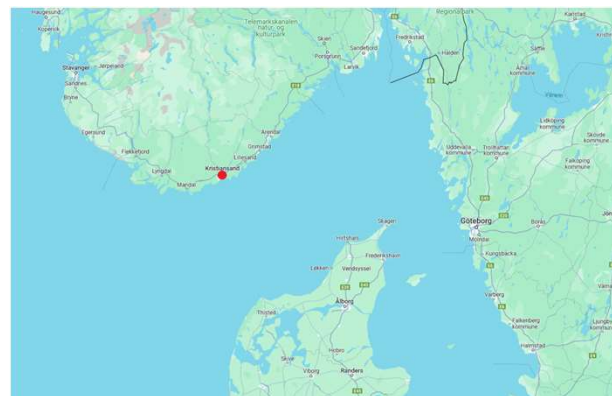
Evaluation of the Munk Moment on a Wind Assisted Tanker with CFD

Andreas Ommundsen
cDynamics

NAFEMS NORDIC Conference 2024: The Conference for Engineering Simulation and Analysis, 22 - 23 May 2024, Gothenburg, Sweden

1

- cDynamics is a consultancy company founded in 2015, located in Kristiansand.
- We are six colleagues at the moment, with main focus on composite FEA, CFD and dynamic simulations, particularly in the marine environment.



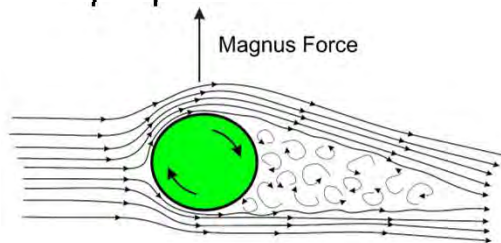
NAFEMS NORDIC Conference 2024: The Conference for Engineering Simulation and Analysis, 22 - 23 May 2024, Gothenburg, Sweden

2

- Our client is the ship owner Seatrans Group, which owns a fleet of mainly chemical tankers.
- They want to add rotational sails to the vessel 'Trans Tind' and wished therefore to do a CFD analysis on the hull beforehand.



- A rotational sail utilises the 'Magnus-effect' of a rotational body.
- Tall cylinders are put on deck and forced to rotate. The accelerated and decelerated air flow on either side due to the rotation gives rise to a thrust force perpendicular to the wind direction.
- Up to 20 % fuel reduction have been reported.



- Rotor sails work best with wind coming from the side. This will give a sideways drift of the ship.
- This combined surge and sway velocity will result in a crabbing motion of the ship, which has some unforeseen consequences.

- From Newman (1977), the moment \mathbf{M} of a body moving in an inviscid, irrotational and infinite fluid can be expressed as follows:

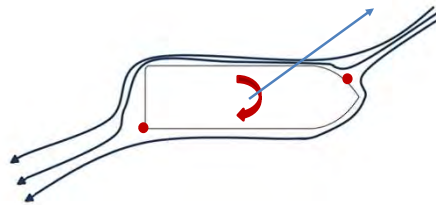
$$\mathbf{M} = -\rho \mathbf{U} \times \iint_{S_B} \varphi \mathbf{n} \, ds \quad \varphi = \sum_{i=1}^3 U_i \varphi_i \quad A_{ji} = \rho \iint_{S_B} \varphi_i n_j \, ds \quad \mathbf{M} = -\mathbf{U} \times \left[\sum_{i=1}^3 U_i \left[\sum_{j=1}^3 A_{ji} \mathbf{e}_j \right] \right]$$

$$\mathbf{M} = -\mathbf{e}_1 \left(U_2 \sum_{i=1}^3 U_i A_{3i} - U_3 \sum_{i=1}^3 U_i A_{2i} \right) - \mathbf{e}_2 \left(U_3 \sum_{i=1}^3 U_i A_{1i} - U_1 \sum_{i=1}^3 U_i A_{3i} \right) - \mathbf{e}_3 \left(U_1 \sum_{i=1}^3 U_i A_{2i} - U_2 \sum_{i=1}^3 U_i A_{1i} \right)$$

Decomposing the current velocity U_c we get $U_1 = U_c \cos \beta$ and $U_2 = U_c \sin \beta$. Inserting into the last bracket, and assuming $A_{12} = A_{21} = 0$, as well as $U_3 = 0$, we get the Munk moment:

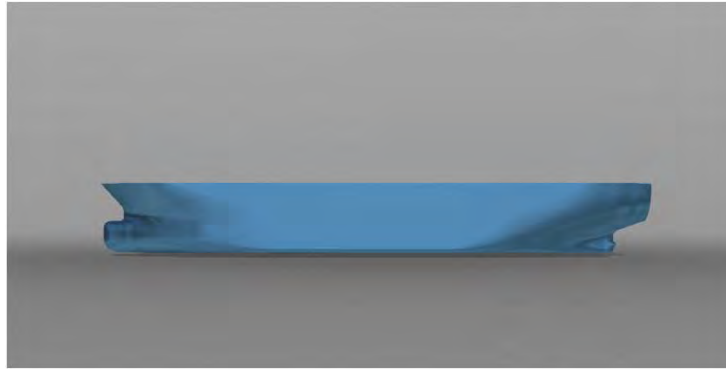
$$\frac{1}{2} U_c^2 \sin 2\beta (A_{22} - A_{11})$$

- What then is the Munk moment?
- This moment is always *destabilising*, meaning that it constantly wants to turn the hull perpendicular to the flow.
- The physical cause for this moment is the asymmetric location of the stagnation points. The high-pressure stagnation points in the bow and stern will exert a moment on the hull.

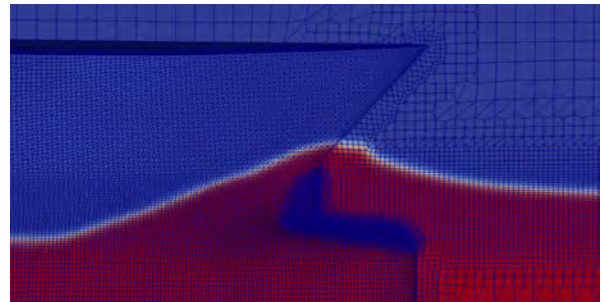
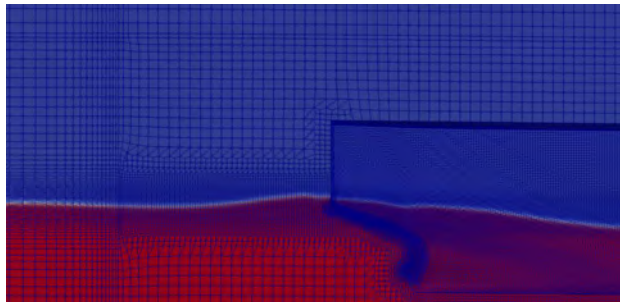


- The CFD analyses are done with a highly modified version of OpenFOAM developed by Cloud Towing Tank.
- Finite Volume discretization of the Navier Stokes equations.
- Two-phase flow, free surface capturing with level set approach.
- Ghost Fluid Method schemes for correction of the dynamic pressure and density discontinuities at the free surface interface. (Removes spurious air velocities in the air phase next to the interface.)
- $k-\omega$ turbulence model.
- Governing equations are discretized with 2nd order stencils in space and time, and time integration is done with either 1st order implicit Euler for quasi static cases or 2nd order backward for transient. Convection terms use linear upwind biased interpolation.
- Rigid body motions in heave and pitch (sinkage and trim) are calculated with a 5th order Runge-Kutta integration scheme with Cash-Karp error control.

- The CAD geometry is imported with a few modifications. This is in particular the transom, where flow separation is forced by adding a sharp edge to aid the meshing.



- Meshing is done with CF-MESH+, and the mesh used in this project had about 10 mill. cells.





- Special emphasis was put on finding the centre of pressure.
- If a force is applied to this point, no moment would act on the body.
- As the sails will apply forces to the ship, the location of this point is of interest to find the best placement of these sails.

NAFEMS NORDIC Conference 2024: The Conference for Engineering Simulation and Analysis, 22 - 23 May 2024, Gothenburg, Sweden

11

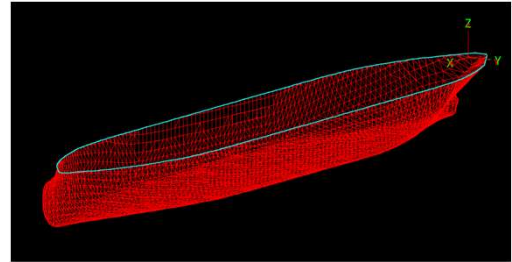


- The simulations are done without sails.
- Three vessel velocities; 11, 13.5 and 15 knots.
- Three directions; $\beta = 0^\circ$, 5° and 10° .
- All velocities in the direction of travel (following β angle).
- Calm water.
- Simulations are quasi-static, run for 1000 s.

NAFEMS NORDIC Conference 2024: The Conference for Engineering Simulation and Analysis, 22 - 23 May 2024, Gothenburg, Sweden

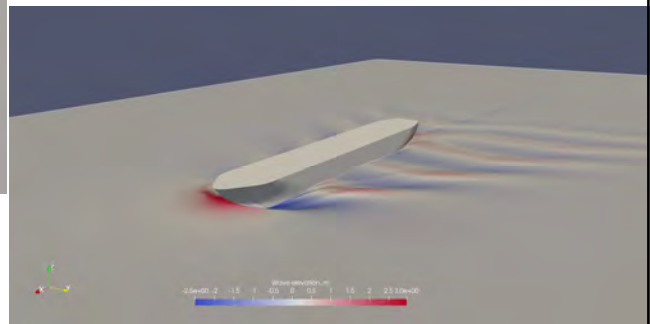
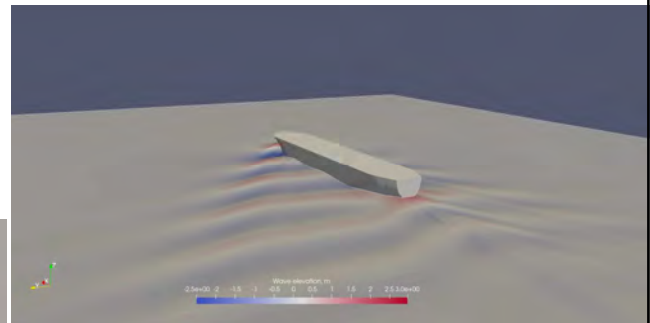
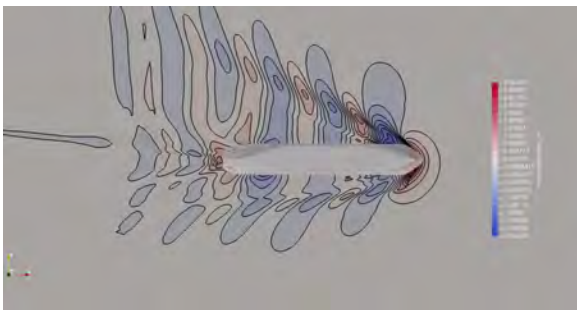
12

- What values of Munk moment to expect?
- A simplified diffraction model of the hull was made to find values for the added masses.
- $A_{11} = 920$ tonnes
 $A_{22} = 16\,640$ tonnes
- M is between 40 and 80 MNm for 5° , and between 86 and 160 MNm for 10° .

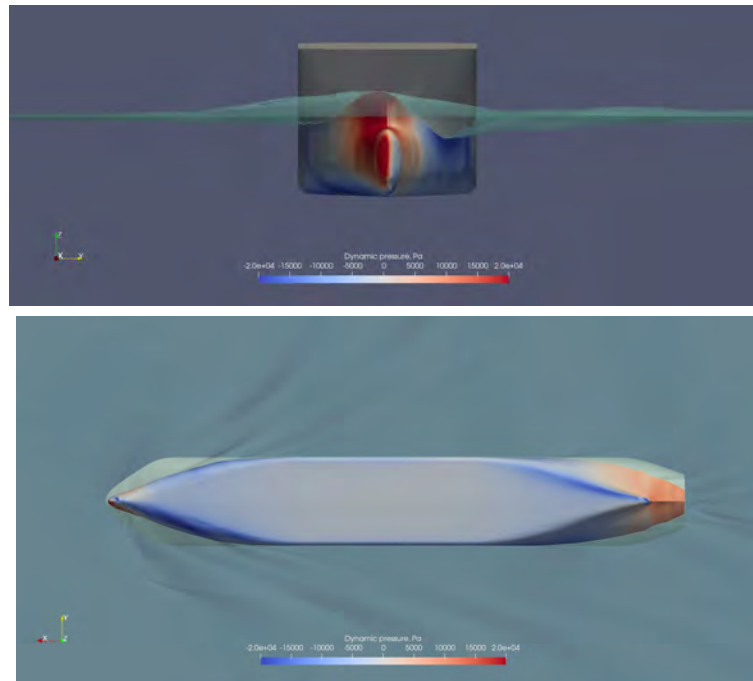


13

- 10 degrees, 15 knots:



14

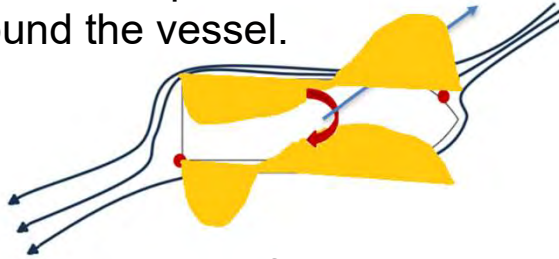


15

- The centre of pressure turned out to be ahead of the bow of the vessel:
- $CoP = \frac{M_z}{F_y}$
- For 5°, the CoP is up to 211.4 m ahead of the stern, while the LOA is only 134 m. That is 77.4 m ahead of the bow. Subtracting the Munk moment gives a CoP up to 98.3 m ahead of the stern, i.e. within vessel boundaries. The Munk moment is therefore the biggest contributor.
- Shows that M_z is large. This moment must be counteracted by the rudder and sails.

16

- Centre of pressure outside of the vessel boundaries?
- Orange colour is the pressure distribution of the Munk moment around the vessel.



- The unbalanced resulting forces lead to a pressure centre outside of the vessel, i.e. you will not find a point on the vessel body anywhere that when pushed will not rotate it.

- It is wise to put the sails close to the bow in this case, as it will help counteract the moment.
- The rudder must compensate for the rest.



Thank you for your attention

NAFEMS NORDIC Conference 2024: The Conference for Engineering Simulation and Analysis, 22 - 23 May 2024, Gothenburg, Sweden

Electric Motor Direct Cooling: Assessment of Coolant Flowrate and Viscosity on Cooling Efficiency

Massimo Galbiati 1 (Particleworks Europe)

1 Summary

Electric machines and e-axes design requires the management of a large number of parameters. Numerical simulation can give an insight into the effect of different design variables and can be useful both during the initial screening of different concepts and in the optimization the Electric-Drive-Unit geometry, coolant injection, power consumption and coolant / lubricant selection.

This paper describes a novel approach to simulate and optimize the direct cooling of electric motors using mesh-less thermo-Fluid Dynamics simulation. The Moving Particle Simulation method integrates the fluid and thermal simulations in one digital model of the complete e-machine, with the detailed geometry of the end-windings.

The thermo-fluid model allows to compare the cooling efficiency for different coolant flowrates and coolant properties.

Increasing the oil flow rate improves the cooling efficiency, but it has a cost in terms of power to circulate the coolant and in terms of drag losses, due to the interaction of the oil with the rotor and with the air-gap.

Oil viscosity has an impact on the cooling efficiency too, lower viscosity allows to reduce the machine temperature. At the same time the coolant viscosity has an effect on the lubrication of bearings and gears in integrated powertrain, where the same fluid is used both as coolant and lubricant.

The paper mainly focuses on the oil flow and temperature in the electric-machine, but oil flow simulation and drag losses in the reducer will be discussed as well.

2 Introduction

High-power density electric motors require high-efficiency cooling with a limited amount of coolant, that is directly injected into the motor on the most critical components, like end-windings. Different cooling lay-outs have been conceived, developed and tested by different manufacturers over the last years [3], [4], [5], [6], [7].

The dielectric coolant can be injected from the rotating shaft or through internal channels, running through the rotor or through the stator. In some cases, there can be both rotating and static coolant jets.

The cooling efficiency, temperature peaks, power consumption and drag losses depend on several factors. Just to mention some of these factors: the complex 3D geometry of the e-motor and the way the coolant is injected affect the interaction of the fluid with the parts to be cooled, but also with the rotating parts and can produce high drag losses [6].

Different injection concepts can affect the air-gap pollution. For this reasons, baffles or flanges can be designed to prevent the coolant from polluting the air-gap or to properly direct the coolant onto the most critical areas [3], [5].

Other relevant parameters are the oil flow rate and its distribution between the different injection points, the coolant viscosity and the interaction of the coolant itself with the air flow at different rpm conditions.

The investigation of all these design parameters and the understanding of the complex fluid and heat transfer phenomena require the use of simulation tools since the early stages of the e-motor design.

Simulation is key to optimize the coolant injection and its scavenging, to predict hot spot locations at different operating conditions and to design the internal geometry of the e-machine.

In this paper a mesh-less CFD method for gas-liquid flow and thermal analysis is introduced. The method allows to simulate windage effects, liquid coolant injection in geometrically complex systems and it can calculate the temperature of solid bodies (coils, magnets, rotor and stator) by considering the electromagnetic heat sources and the cooling effect of the air and liquid coolant.

The paper explains the effect of coolant viscosity and flow rate on heat transfer and temperature of the coils.

3 Model and simulation method

3.1 E-motor model

The geometrical model of the oil cooled e-motor with integrated gearbox is shown in Figure 1.

The digital model includes the electric motor (with housing, stator, coils, rotor, magnets and shaft) cooled by six static oil jets, three on each side of the e-motor. The oil jets are located in the upper part of the motor and they inject oil directly onto the end-windings.

The reducer gears and bearings are included, so that the same model and simulation can predict the lubrication of gears and bearings.

The oil is injected at 100°C. Heat sources are applied to stator, rotor, magnets and windings. Heat sources were previously calculated by means of 3D electromagnetic analysis of the motor for a specified operating point of the e-machine.

The aim of the model is to simulate the air and oil flow and the temperature of gears and e-machine components for an operating point at 10.000rpm.

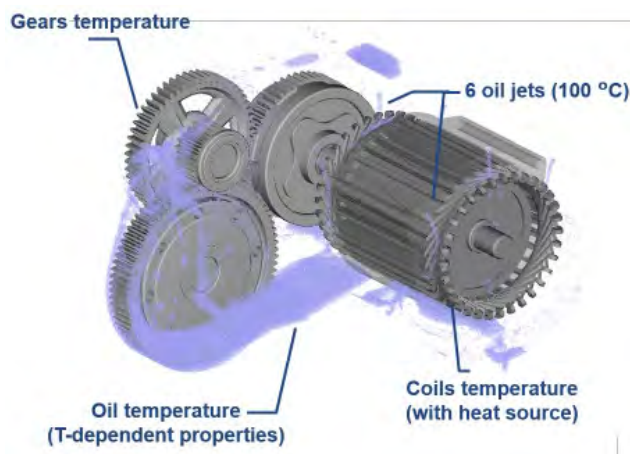


Figure 1: model of the oil-cooled electric motor with integrated gearbox.

The oil properties are reported in the table below:

Density	800 kg/m ³
Viscosity	2-20 cSt (ISO VG2, VG10, VG22)
Surface Tension Coeff	36 mN/m
Specific Heat	2000 J/kg K
Thermal conductivity	0.4 W/m K

Table 1: model of the oil-cooled electric motor with integrated gearbox.

3.2 Simulation method

The Moving Particle Simulation (MPS), formerly Moving Particle Semi-Implicit method, is a particle method to solve the incompressible Navier-Stokes equations [1], [2]. It's a mesh-free method, which solves the continuity, momentum conservation and energy equations by means of a Lagrangian method.

The main field of application of MPS is liquid flow analysis, in particular the solution of free-surface flows with high deformations of the free surface or liquid jets.

The mesh-less nature of the solver allows to easily handle complex geometries and moving parts, like end-windings and rotating gears and bearings.

The MPS solver does not even require the generation of the fluid volume, because it directly reads the CAD geometries and uses them as wall boundary conditions for the fluid flow.

The rotation of gears, bearings, shafts and rotor can be directly applied to the solid bodies in the model, so that rotating parts transfer their momentum to the fluid.

The fluid is discretized by “particles”. The size of the particles defines the accuracy of the simulation. Smaller particles allow for a finer resolution of the flow features.

Each particle is a calculation point and the size of the particles can be locally refined to better solve the flow in narrow gaps, like the air-gap or between the end-windings and in the bearings area.

Moving Particle Simulation can simulate air and liquid flow (2-phase flow) and it solves the energy equation for fluids and heat conduction in solids.

In this way the coolant velocity and temperature fields can be resolved at the same time.

3.3 Simulation process

As stated above the MPS method allows for a complete simulation of all the fluid and thermal phenomena in one model and one simulation.

There is one major drawback in this process and it is mainly related to the different time-scales of the fluid flow and thermal phenomena.

If we take an oil cooled e-machine, the air and coolant flow take a few seconds to stabilize. On the other hand, heat conduction and temperature stabilization in the solid parts of the machine is a much slower process, that can take several minutes to stabilize.

From the simulation viewpoint, this means that it is more efficient to segregate the two phenomena and simulate the fluid flow and the temperature in two separate simulations.

The fluid-flow analysis is the most expensive one in terms of computational time, but the fluid-flow phenomena are relatively fast: the fluid-flow requires a few seconds to stabilize. In this time frame instead, the temperature does not change a lot in the solid bodies.

So, it is more efficient to calculate the flow field until stabilization, without including the temperature calculation.

From the flow-field it is possible to extract the heat transfer coefficient on the e-machine surfaces. The heat transfer coefficient (HTC) is a 3D map and it represents the local cooling efficiency on the e-machine components.

The HTC map is then transferred to a steady state or transient thermal analysis of the solid parts.

The thermal simulation includes the heat sources due to the electromagnetics effects, the local cooling efficiency of the fluids (air and liquid coolant) and the heat dissipation to the external environment.

Moreover, it can also simulate local effects of insulating and potting materials and contact resistance between different bodies, like magnets and rotor.

In summary the proposed simulation process is:

1. 3D simulation of the air and liquid flow. The output of this first simulation step are the air and liquid velocity fields, the coolant impingement and filming on the e-machine surfaces, coolant accumulation and scavenging, drag losses due to the fluids on the rotating parts and heat transfer coefficient distribution
2. mapping of the cooling efficiency (HTC) both due to air and coolant on the internal surfaces of the e-machine
3. 3D steady state heat conduction analysis. The output from this simulation is the temperature distribution in the e-machine, hot spots, heat fluxes between the different parts of the machine.

This is a multi-step simulation process, but it is carried out on one single Moving Particle Simulation model, that includes both the fluid and thermal parts.

3.4 Cooling efficiency calculation

In the MPS method the cooling efficiency is expressed by the heat transfer coefficient, which is calculated by forced convection, starting from the local flow conditions.

Local Nusselt number Nux , local Reynolds number Rex and Prandtl number Pr are expressed as follows:

$$Nu = hx/\lambda \quad [1]$$

$$Re = ux/\nu \quad [2]$$

$$Pr = \rho v c_p / \lambda \quad [3]$$

Where h , x , λ , u , ν , ρ , c_p , ν represent heat transfer coefficient, distance from the beginning of the plate, thermal conductivity, average velocity, fluid density, specific heat and kinematic viscosity, respectively. The relation between the local Nusselt number and Reynolds number is defined by the following equations for both laminar and turbulent flow.

$$Nux = (a Pr^b Re^c) \quad [4]$$

In the MPS method the coefficients of equation [4] depend on the type of flow, that means that the simulation uses specific heat transfer coefficient correlations depending on the fact that the coolant is impinging on the surface, or it is sliding on the surface or, again, a different type of correlation is used locally if the coolant tends to accumulate and creates a slow-moving film on the surfaces of the e-machine.

3.5 Simulated conditions

The e-machine coolant flow and temperature distribution are calculated for different combinations of coolant flow rates and coolant viscosities, in order to assess the effect of these two design parameters on the cooling efficiency.

Two oil flow rate values are simulated: 1 [litre/min] and 2.5 [litre/min].

Three viscosity values are considered: 2 [cSt], 10 [cSt] and 20 [cSt].

4 Results

The first output from the fluid-flow simulations is the cooling efficiency, expressed in terms of Heat Transfer Coefficient.

Figure 2 shows the heat transfer coefficient on the end-windings for different combinations of coolant flowrate and viscosities.

The red regions show the areas where the coolant directly impinges on the end-windings and produces high HTC values (high cooling efficiency).

The highest HTC values occur at high coolant flow and at low viscosity: 2.5 [liter/min] and 2 [cSt].

The effect of different Heat Transfer Coefficient on the end-windings is shown in Figure 3 and Figure 4 in terms of end-windings average temperature.

The last set of results of this study is shown in Figure 5. In this case the heat conduction model of the e-machine is run in transient mode, to monitor the temperature evolution in the system for different flowrates and viscosity and to predict the time to stabilize the coils temperature. The chart shows that 5 minutes or more are required to reach a flat temperature behavior.

This confirms that while the fluid process is quite fast and tends to stabilize in a few seconds, the thermal stabilization requires a much longer time.

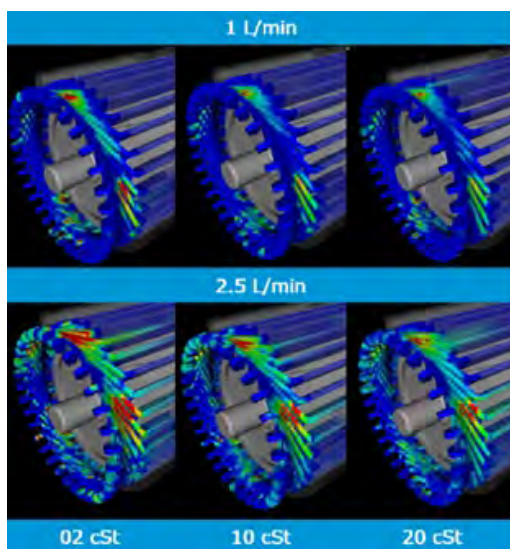


Figure 2: comparison of the heat transfer coefficient on the end-windings for different combinations of coolant flowrate and viscosities.

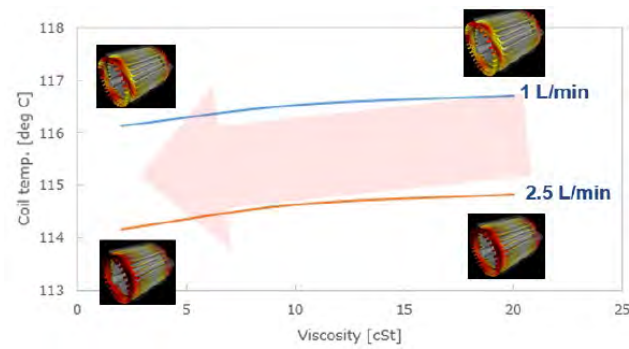


Figure 3: end-windings average temperature versus viscosity.

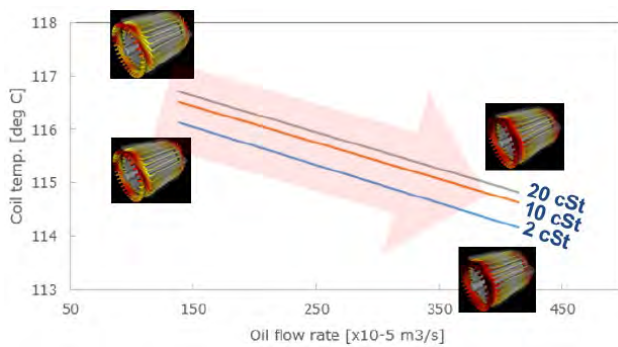


Figure 4: end-windings average temperature versus coolant flowrate.

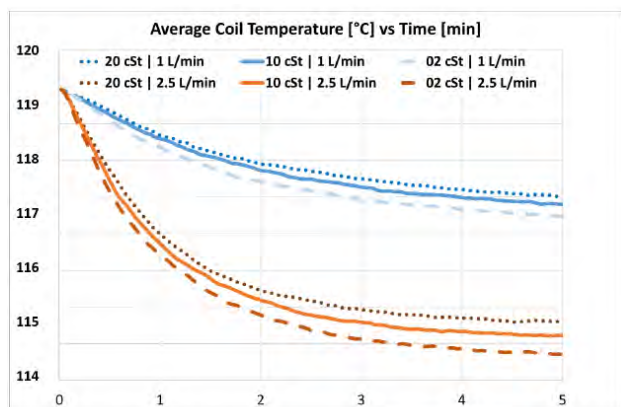


Figure 5: history of end-windings average temperature versus coolant flowrate and viscosity.

5 Conclusions

This paper assesses the effect of the coolant flowrate and coolant viscosity on the temperature of an oil-cooled electric motor.

The study is carried out by using a mesh-less thermo-fluid-dynamic model based on the Moving Particle Simulation method, that allows to simulate both the fluid flow and the heat transfer phenomena in one single model.

In order to speed up the simulation process, the fluid flow analysis is carried out separately from the heat conduction analysis. The fluid analysis allows to predict the windage effects, the liquid coolant impingement on the end-windings and its scavenging. The cooling efficiency (Heat Transfer Coefficient map) is the final output from the fluid flow simulation and it's the input for the temperature

calculation. The two-steps simulation process is the best trade-off between accuracy and calculation time and it's based on one single model.

Results show a relevant impact of the coolant flow rate on the end-windings temperature. A low viscosity coolant improves the cooling efficiency. For this reason, the fluid properties should be accurately selected, above all when the same fluid is used both as coolant and lubricant in integrated powertrain

6 References

- [1] S. Koshizuka Y. Oka, "Moving-particle semi-implicit method for fragmentation of incompressible fluid," Nuclear science and engineering, vol. 123, no. 3, pp. 421–434, 1996.
- [2] S. Koshizuka, K. Shibata, M. Kondo, and T. Matsunaga, Moving particle semi-implicit method: a meshfree particle method for fluid dynamics. Academic Press, 2018.
- [3] I. Deac et al., "Optimizing the spray cooling of e-drives," Futurities, vol. 1, no. 1, pp. 23–25, 2022.
- [4] J. Raisin, "Electric motor cooling simulation: direct vs indirect," Proceedings CAE Conference 2021, 2021.
- [5] G. Puccio, M. Raimondo, S. Nategh, D. Barater, D. Ericsson, and A. Carlsson, "An advanced thermal modeling method for directly oil cooled traction motors," in 2023 IEEE Workshop on Electrical Machines Design, Control and Diagnosis (WEMDCD), pp. 1–6, IEEE, 2023.
- [6] L. Boscaglia, Y. Liu, H. Avsar, J. Tang, and M. Galbiati, "Convective heat transfer coefficients and mechanical loss evaluation of oil splashing in direct cooled electrically excited hairpin motors," in 2022 International Conference on Electrical Machines (ICEM), pp. 496–503, IEEE, 2022.
- [7] M. Brada, "Thermal simulation of an oil-cooled e-motor," Proceedings CAE Conference 2020, 2020.
- [8] J. H. Lienhard, "Heat transfer by impingement of circular free-surface liquid jets," in 18th National and 7th ISHMT-ASME, Heat and Mass Transfer Conference, Guwahati, India, 2006.

7 Glossary

MPS: Moving Particle Simulation
CFD: Computational Fluid Dynamics
HTC: Heat transfer Coefficient
Re: Reynolds number
Pr: Prandtl number
Nu: Nusselt number

ODS&ODF – A COMPREHENSIVE APPROACH TO EVALUATE THE VEHICLE STIFFNESS USING MBD

¹Jens Weber, ¹Pravin Ugale, ²Milton Pena, ²Jesper Bäcklund, ²Peter Appelgren, ³Mats Berggren, ⁴Henrik Marberg

¹Zeekr Technology Europe AB / CAE Solidity, ²Beta CAE Nordic AB, ³AFRY, ⁴Marberg Engineering AB, Sweden

1 Increased usage of MBD

The complete vehicle simulation using Multi Body Dynamics (MBD) offers a wide range of complex load cases for both Durability and Solidity. Some of these load cases are either very hard or not possible to simulate by only using FEM. By increasing the complexity of the flexible models (mnf), e.g. the trimmed body, the response of the body can be evaluated directly based on the MBD results. The MBD simulation is also closest to the real test scenario when it comes to correlation between test and simulation.

2 Multi Stethoscope MSS

The Multi Stethoscope (MSS) is used for evaluating the body response, where the acceleration is calculated at a number of different body locations. The acceleration is then evaluated in both the existing ODF (Opening Distortion Fingerprint) tool and the new ODS (Operational Deflection Shape) tool in Meta.

In order to enable an efficient simulation and test procedure, the MSS output has to be processed before evaluating it in the ODF and ODS toolbar. For this purpose, an ODF&ODS preparation toolbar has been implemented.

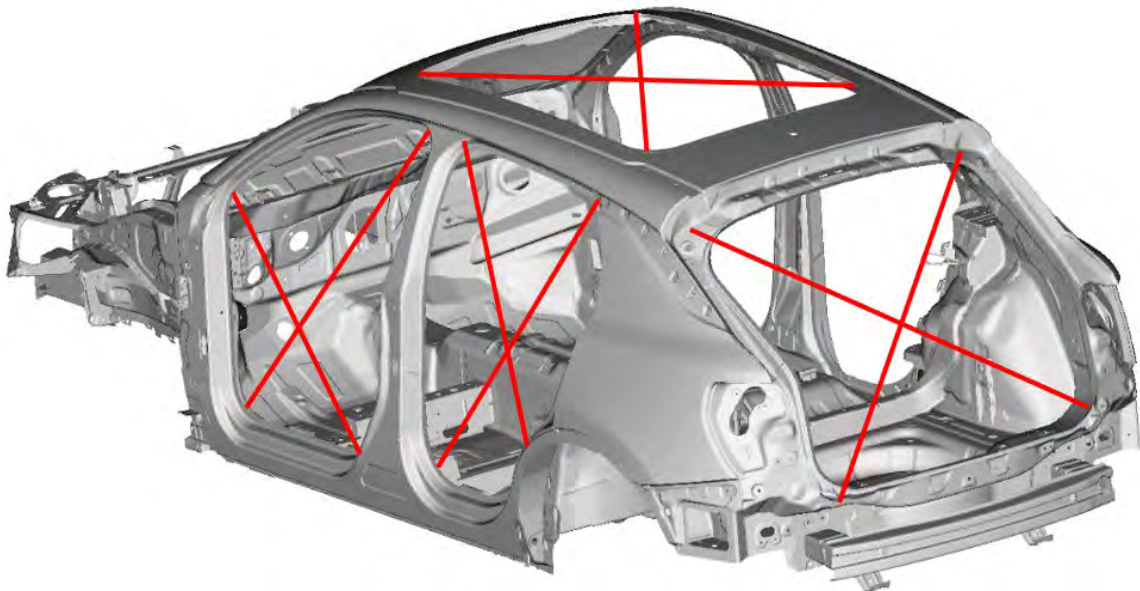


Fig. 1
Multi Stethoscope MSS

3 Summary

The first part of this presentation shows a deeper insight into the capabilities of the full vehicle MBD simulation regarding both the vehicle representation itself and the available load cases. The second

part shows how the static and dynamic vehicle body response can be assessed by using the ODF and ODS toolbar in Meta. A special focus will be on the new ODS toolbar.

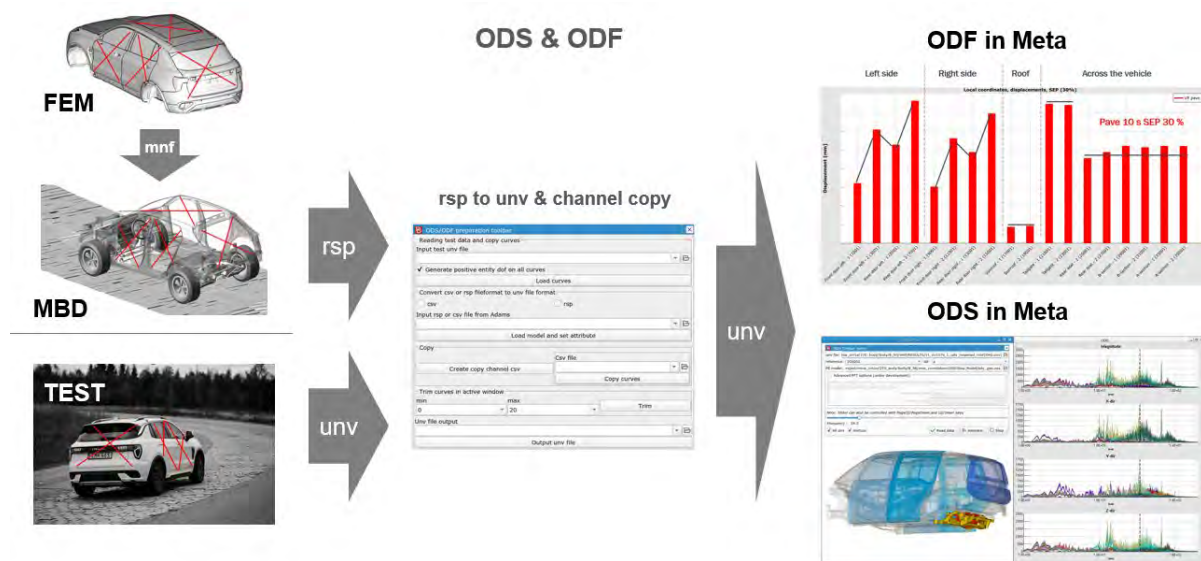


Fig. 2
ODF & ODS evaluation process based on both simulation and test

4 References

- [1] Weber J., Ugale P., Olsson S. et al., "Vehicle Stiffness Evaluation in MBD Simulation Using the ODF Method (Opening Distortion Fingerprint)," VDI-Berichte Nr. 2407, 2022.
- [2] Weber, J., Jönsson, V., Hansson, L., Varela, R. et al., "Opening Distortion Fingerprint (ODF) - A New Body Evaluation Method for Perceived Quality and Vehicle Dynamics," SAE Technical Paper 2022-01-0950, 2022
- [3] Weber, J., Faria, L., Bäcklund, J., Vignati, M. et al., "A New Equivalent Static Load (ESL) Creation Procedure for Complete Vehicle," SAE Technical Paper 2024-01-2944, 2024

Analysing Ride comfort in Realtime by integrating Flexible Body in White

Avijit Chauhan (Dassault Systemes UK)

1 Summary

With the ever more competitive automotive industry, the requirement to focus on simulations has become extremely critical. One of the main focuses is to reduce the number of physical prototypes required for testing vehicle characteristics. This can significantly reduce vehicle development costs. Hence driving simulators have become evermore popular and a powerful tool to achieve the goal of zero prototypes. As much as the technical development of these simulators is important, developing a high-fidelity multibody dynamics physics model is equally important to experience accurate feedbacks from the realtime rigs. Full vehicle attributes can be broadly classified in two categories based on frequency range: Handling (upto 5-7 Hz) and Ride (upto 30-35 Hz). This paper intends to investigate integrating an optimized flexible body in white into a full vehicle MBD model and run it in realtime on a rough road to analyse ride dynamics of a passenger car.

A full component based multibody dynamics was developed in Simpack using all rigid bodies. An FE model was created in Abaqus where all the required attachment points were defined which included damper top mounts, subframe mounts etc. This FE model was modally reduced using Craig Bampton reduction method and then integrated into the Simpack model. The hence developed vehicle model was run on a rough road surface using a semi-physical tyre model and accelerations at the seat rails were extracted. Results were compared between:

- Full rigid BiW
- Full Flex BiW (All Eigen Modes enabled) using a variable step size solver
- Optimized Flex BiW (Eigen modes affecting Ride) using a variable step size solver
- Optimized Flex BiW (Eigen modes affecting Ride) using a fixed step size solver – to understand possible realtime capability

Full vehicle model with optimized Flex BiW run on a realtime platform (redhawk Linux)

2 Introduction

Comparison between Multibody Simulation and Physical tests:

	Multibody Simulation	Physical Test
Detecting problems already in earliest design phases	Possible	Impossible
Detailed variant studies	Possible	Very expensive
Measuring motion and forces	Any place in the system	Only at limited places
Design changes	Easy	Difficult, expensive
Analyzing misuse and abuse cases	Possible	Difficult or impossible

It is understood that even though Simulations are much more cost effective and earlier to perform, it's almost always necessary to carry out physical tests to have the subjective feel of a car. Driving simulators aim toward zero prototypes, but the feedback is only as good as the physics models/solvers used. Lateral Dynamics (handling) are low frequency analysis and low fidelity models could provide good enough feedbacks, but to accurately extract upto the secondary ride frequencies, the flexibility of the Body in White (BiW) is extremely important.

3 Vehicle model

A full vehicle component based model was created with required fidelity such Ride frequencies could be captured. The model contained:

- Rigid Suspension Front McPherson Strut and Rear Multi-link
 - Flexible Body in White using Craig Bampton Reduction method
 - Simple Driveline driving rear wheels
 - Overall full vehicle degrees of freedom observed in case of the optimised Flex BiW were 264.
- This model was run in Realtime later after various offline simulation validations

3.1.1 Simulations Ran:

- Offline Simulation with Vehicle running on Belgian Pave rough road represented by crg format. The Vehicle was run on a straight line with controlled velocity
- Offline Simulation as above but the Flex BiW was optimized to include only the modes upto 45 Hz. Simpack's^[1] Auto Eigen Mode feathure was used to automatically find the required modes
- Realtime Simulation using the Optimised Flex BiW with Driver and Hardware (Steering wheel and pedals) in the loop

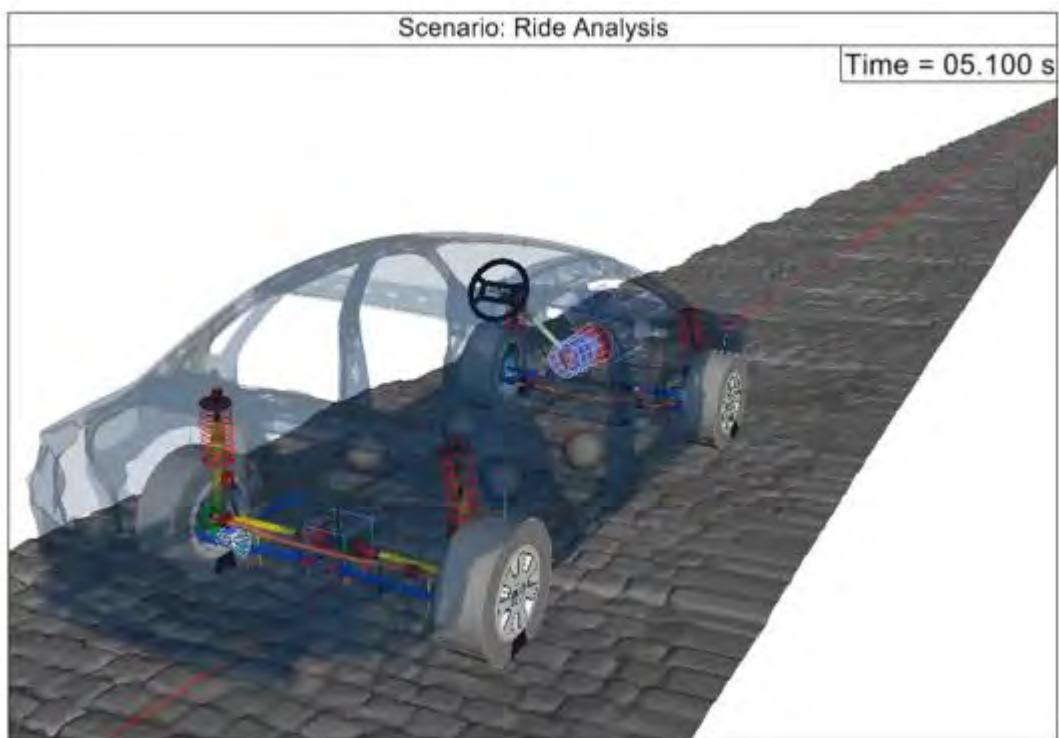


Fig. 1 Full Vehicle model run on Belgian Pave Rough Road Scenario

3.1.2 Results

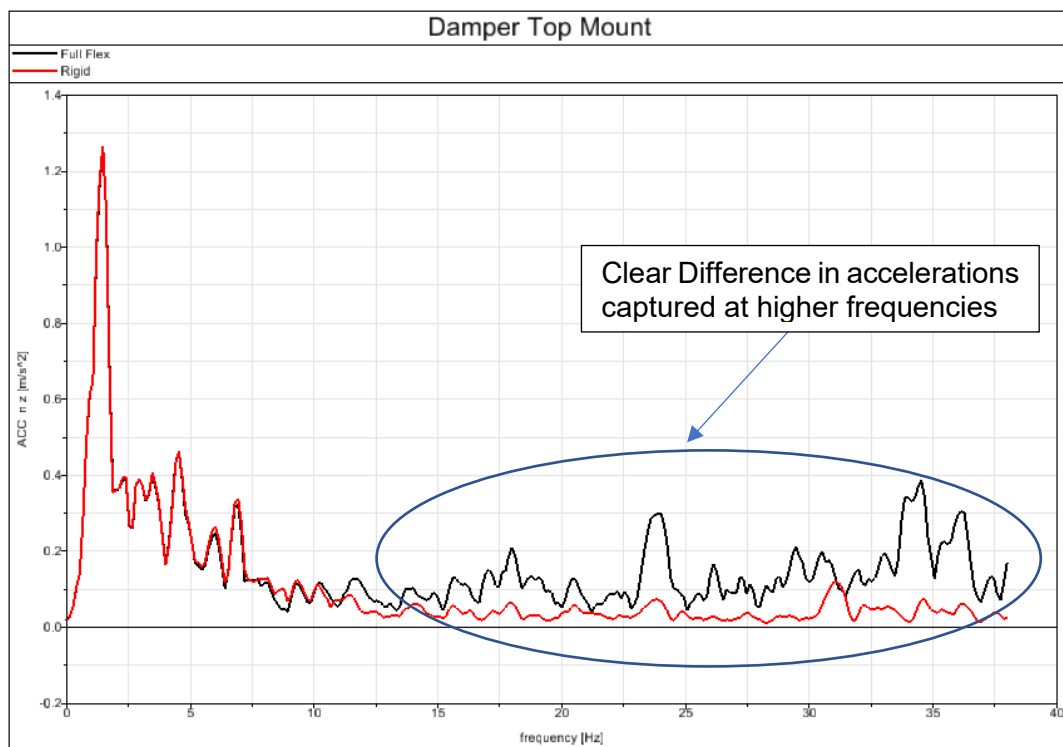


Fig. 2 Full Flex vs Rigid BiW Accelerations at Damper Top Mount

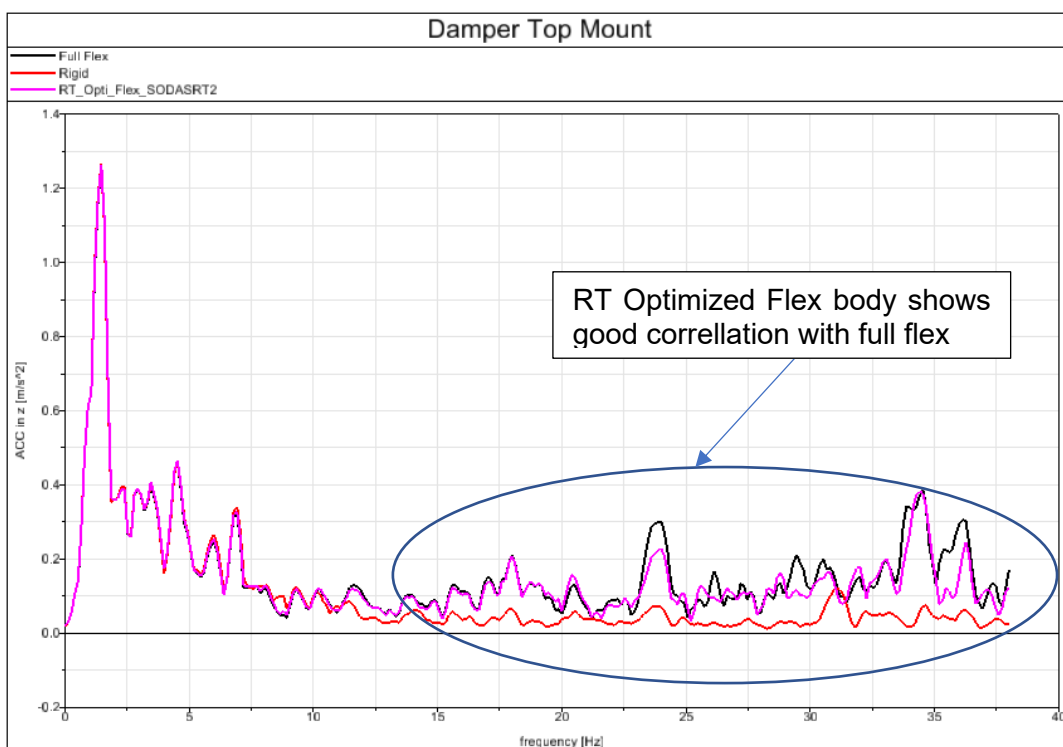


Fig. 3 Full Flex vs Rigid vs RT Optimized Flex BiW At Damper Top Mount

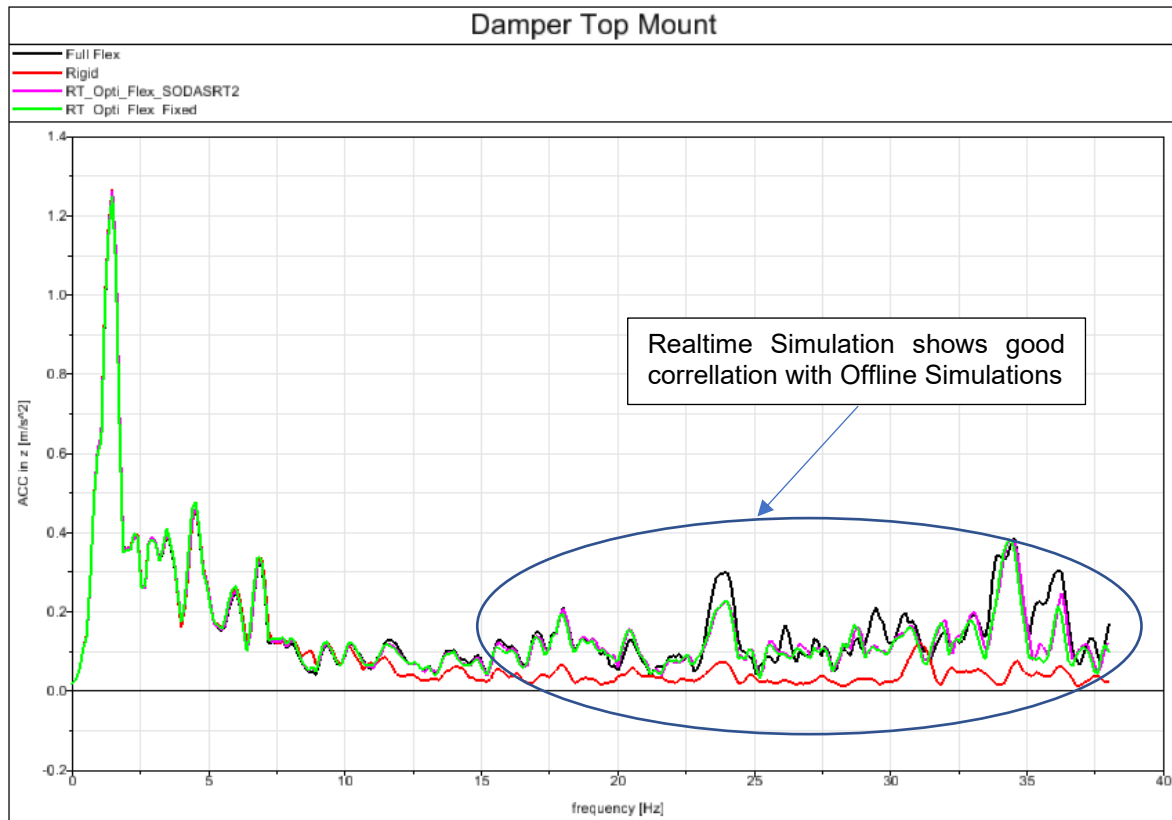


Fig. 4 Full Flex (run Offline) vs Rigid vs RT Optimized Flex BiW (run on Realtime Simulator)
Accelerations at Damper Top Mount

4 Conclusions

- Optimised Flex BiW was able to run in Realtime upto Secondary Ride Comfort using a static simulator
- Good Correlation between Full Flex BiW Offline simulation and Optimised Flex BiW Realtime Simulation
- Realtime Factor well below 1 means including more fidelity in model is possible
- Users able to make changes in the model and run in Realtime immediately
- Allows for much more agile approach in vehicle development than traditional methods

4.1 Future Work

- Run Simulations with Higher Fidelity tyres
- Parameter Variations to improve Ride Comfort
- Include Active Systems (eg. Active Dampers)
- Include Air Springs
- Scale parallelization to more cores to include more overall model fidelity
- Model to be run on full Motion Simulators

5 References (Überschrift 1)

- [1] Simpack 2024x Documentation

The Discontinuous Strain Method: accurately representing fatigue and failure

Leon Herrmann (TUM), Alireza Daneshyar (TUM), Stefan Kollmannsberger (Bauhaus-Universität Weimar)

Abstract

Accurate modeling of unloading and reloading is crucial for fatigue simulation. Yet, traditional ductile damage models consider deformations after complete failure as irrecoverable, causing unphysical behavior during unloading. This unphysical behavior arises due to the continued accumulation of irrecoverable plastic strains after failure, where the post-failure strains are not recovered during unloading. Thus, erroneous stresses would arise at the point of crack closure. As a remedy, we introduce a discontinuity strain in the additive elasto-plastic strain decomposition, which absorbs the excess strain after failure and thereby leads to a more realistic unloading and reloading behavior. The proposed extension requires only minor modifications of conventional plastic-damage routines and only leads to a minor increase in computational effort. Furthermore, a characteristic length scale --- based on the discretization's resolution --- is employed to provide mesh-independent results. This new methodology is referred to as the discontinuous strain method.

The theoretical aspects and algorithmic adjustments are first discussed for the one- and subsequently for the two-/three-dimensional case. For the sake of simplicity, the proposed method is presented with a basic ductile constitutive model and validated against established benchmarks from literature. However, the discontinuous strain method is independent of the constitutive model. Thus, elastic, plastic, and damage models may be chosen arbitrarily, thereby making the methodology applicable to low-cycle fatigue modeling. Additionally, the method can potentially be applied in other scenarios requiring a discontinuity representation within a plastic-damage framework.

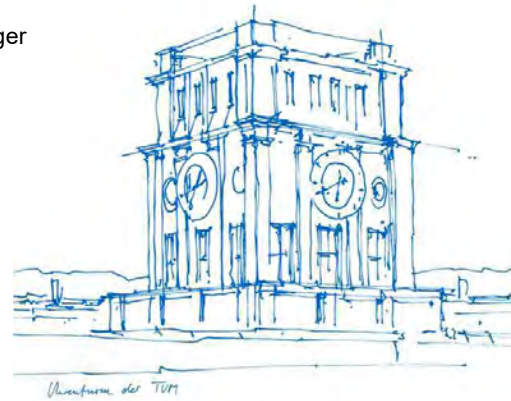
The Discontinuous Strain Method: accurately representing fatigue and failure

Leon Herrmann, Alireza Daneshyar, Stefan Kollmannsberger

Technical University of Munich

Chair of Computational Modeling and Simulation

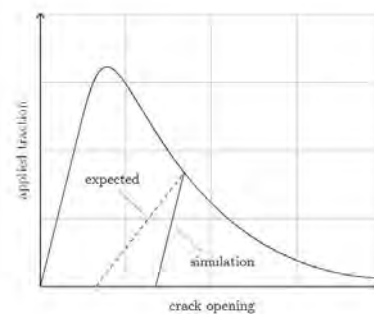
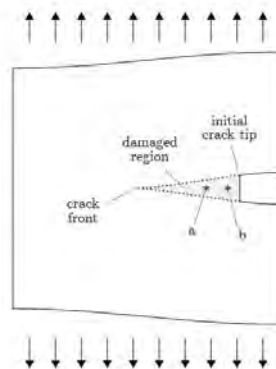
Gothenburg, 24.05.2024



1

Motivation

- Problem with ductile damage models
 - Irreversible strain accumulation after failure
 - Unphysical unloading (and reloading) paths after failure

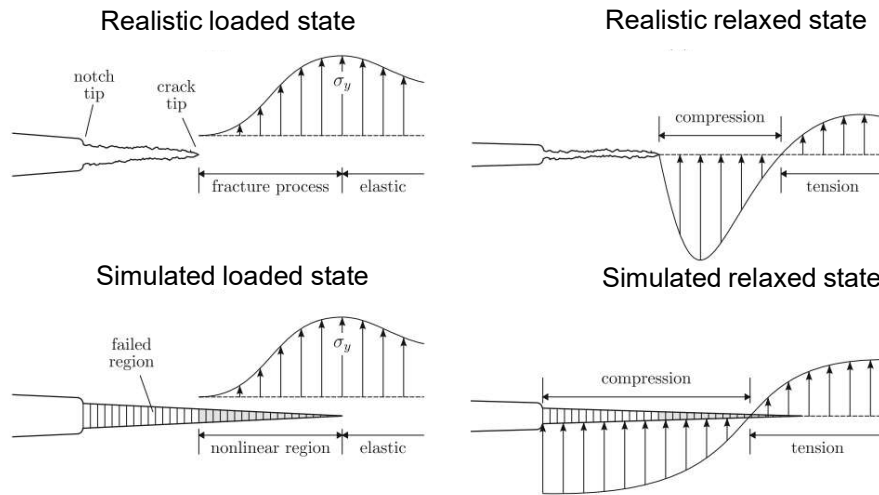


Leon Herrmann | Nafems Nordic Conference 2024 | Gothenburg

2

2

Motivation

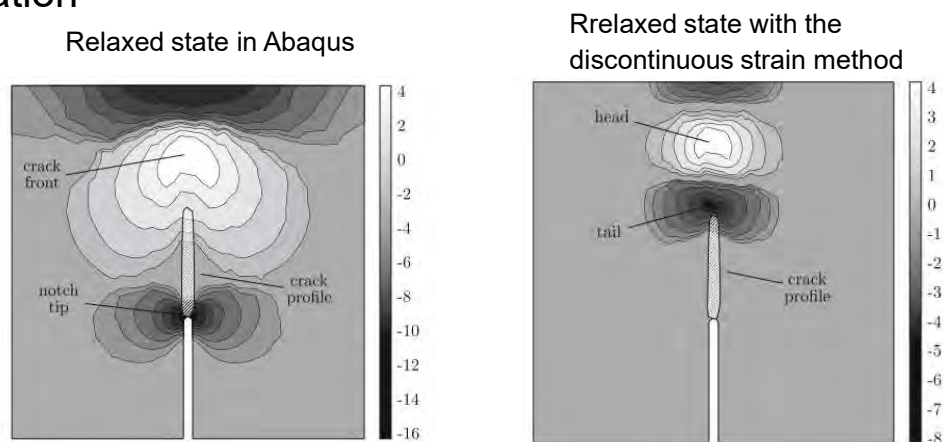


Leon Herrmann | Nafems Nordic Conference 2024 | Gothenburg

3

3

Motivation



Leon Herrmann | Nafems Nordic Conference 2024 | Gothenburg

4

4

Plasticity & Damage Model

- Strain decomposition

$$\boldsymbol{\varepsilon} = \boldsymbol{\varepsilon}^e + \boldsymbol{\varepsilon}^p$$

- Linear elastic constitutive law

$$\tilde{\boldsymbol{\sigma}} = \tilde{\mathbf{D}} : (\boldsymbol{\varepsilon} - \boldsymbol{\varepsilon}^p)$$

- Rankine maximum stress criterion

$$f(\tilde{\boldsymbol{\sigma}}) = \hat{\sigma}_{\max} - \sigma_y$$

- Flow rule based on Drucker-Prager potential function

$$\dot{\boldsymbol{\varepsilon}}^p = \dot{\gamma} \left(\beta \mathbf{I} + \frac{3}{2} \frac{\tilde{\boldsymbol{\sigma}}}{\tilde{q}} \right)$$

- Damage Evolution via accumulated plastic strain $\dot{\varepsilon}_{\max}^p$

$$d = 1 - \exp(-\alpha k)$$

$$\dot{k} = w(\tilde{\boldsymbol{\sigma}}) \dot{\varepsilon}_{\max}^p$$

Weight function

$$w(\tilde{\boldsymbol{\sigma}}) = \frac{\sum_{i=1}^3 \langle \hat{\sigma}_i \rangle}{\sum_{i=1}^3 |\hat{\sigma}_i|}$$

Leon Herrmann | Nafems Nordic Conference 2024 | Gothenburg

5

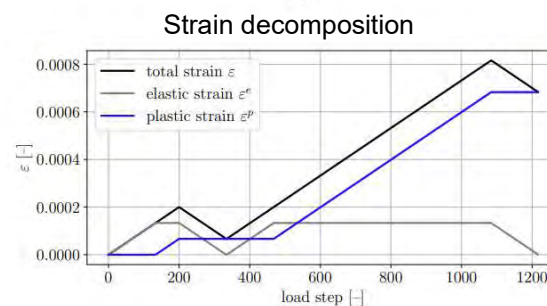
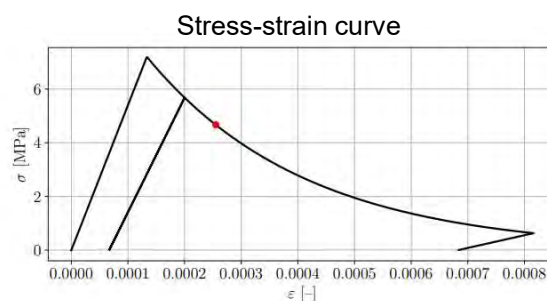
5

1D Example

- Plastic damage model
 $d = 1 - \exp(-\alpha k)$

- Strain decomposition
 $\boldsymbol{\varepsilon} = \boldsymbol{\varepsilon}^e + \boldsymbol{\varepsilon}^p$

- Plastic strain accumulation after failure is unphysical



Leon Herrmann | Nafems Nordic Conference 2024 | Gothenburg

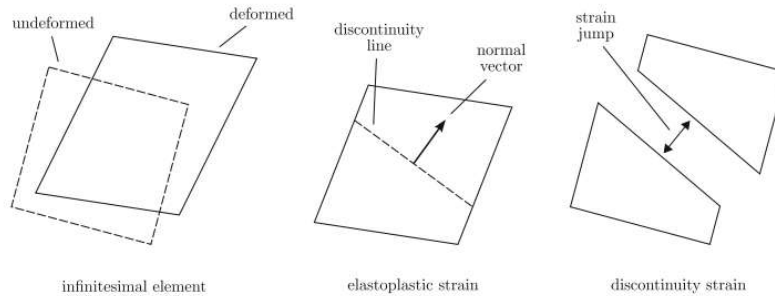
6

6

Discontinuity Strain

- Introduction of discontinuity strain to absorb the excess strain after failure
- Extension of strain decomposition with **discontinuity strain**

$$\boldsymbol{\varepsilon} = \boldsymbol{\varepsilon}^e + \boldsymbol{\varepsilon}^p + \boldsymbol{\varepsilon}^d$$



Leon Herrmann | Nafems Nordic Conference 2024 | Gothenburg

7

7

Modification of Damage Model

- Accumulated plastic and maximum discontinuity monitored with internal damage variable k

$$d = 1 - \exp(-\alpha k)$$

– Before failure

$$\dot{k} = w(\bar{\sigma}) \dot{\varepsilon}_{\max}^p$$

– After failure

$$k = k_c + \max_{\tau \leq t} (\varepsilon_n^d)$$

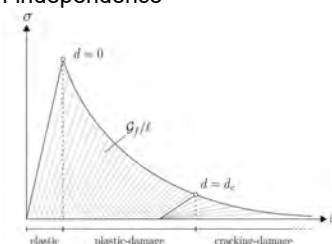
- Energy equivalence to ensure mesh-independence

– Fracture toughness \mathcal{G}_f

– Length scale ℓ

– Encoded as $\alpha = \frac{2E\ell\sigma_y}{2E\mathcal{G}_f - \ell\sigma_y^2}$

– Minimum length scale $\ell < \frac{2E\mathcal{G}_f}{\sigma_y^2}$



Critical k_c

$$k_c = -\frac{1}{\alpha} \ln(1 - d_c)$$

Crack opening strain

$$\varepsilon_n^d = \mathbf{n}^T \boldsymbol{\varepsilon}^d \mathbf{n}$$

Normal vector to the cracking plane \mathbf{n}

Leon Herrmann | Nafems Nordic Conference 2024 | Gothenburg

8

8

Implementation

- Modified plastic-damage routine

Require: strain increment $\Delta\varepsilon$, history variables from last load increment $\tilde{\sigma}, \varepsilon^p, \varepsilon^d, k, d$, material properties $E, \nu, \sigma_y, \beta, d_c, \alpha$ (cf. Equation (59)), k_c (cf. Equation (44)), length scale ℓ

```

1: if  $\varepsilon^d \neq 0$  then
2:    $\Delta\varepsilon, \varepsilon^d, k \leftarrow \text{checkCrackClosure}(\Delta\varepsilon, \varepsilon^d, k)$ 
3: end if
4: if  $\varepsilon^d = 0$  then
5:    $\tilde{\sigma} \leftarrow \text{stressIncrement}(\tilde{\sigma}, \Delta\varepsilon)$ 
6:   if  $f(\tilde{\sigma}) > 0$  then
7:      $\tilde{\sigma}, \Delta\varepsilon^p \leftarrow \text{returnMapping}(\tilde{\sigma})$ 
8:      $\varepsilon^p, \varepsilon^d, \tilde{\sigma}, k \leftarrow \text{checkCrackOpening}(\Delta\varepsilon, \Delta\varepsilon^p, \varepsilon^p, \tilde{\sigma}, k)$ 
9:   end if
10: end if
11:  $d \leftarrow \text{updateDamage}(k)$ 
12:  $\text{updateHistoryVariables}(\tilde{\sigma}, \varepsilon^p, \varepsilon^d, k, d)$ 
13: return total stress  $\sigma$ 

```

Leon Herrmann | Nafems Nordic Conference 2024 | Gothenburg

9

9

Checking for Crack Closure

- The strain increment fully contributes to the discontinuity strain as long as it is non-zero

Require: $\Delta\varepsilon, \varepsilon^d, k$

```

1:  $\varepsilon^d = \varepsilon^d + \Delta\varepsilon$ 
2: if  $\varepsilon^d < 0$  then                                ▷ check crack closure
3:
4:    $\varepsilon^d = 0$                                     ▷ deactivate  $\varepsilon^d$  at crack closure
5: else
6:    $k = k + \langle \Delta\varepsilon \rangle$ 
7: end if
8: return  $\Delta\varepsilon, \varepsilon^d, k$ 

```

Leon Herrmann | Nafems Nordic Conference 2024 | Gothenburg

10

10

Checking for Crack Opening

- The crack opens at a critical damage threshold k_c

Require: $\Delta\varepsilon, \Delta\varepsilon^p, \varepsilon^p, \tilde{\sigma}, k$

```

1: if  $(k + \langle \Delta\varepsilon^p \rangle) > k_c$  and  $\Delta\varepsilon > 0$  then
2:    $\varepsilon^d = \Delta\varepsilon$ 
3:    $\tilde{\sigma} = \tilde{\sigma} - E(\Delta\varepsilon - \Delta\varepsilon^p)$  ▷ reset stress
4:    $k = k + \langle \Delta\varepsilon \rangle$ 
5: else
6:    $\varepsilon^p = \varepsilon^p + \Delta\varepsilon^p$ 
7:    $k = k + \langle \Delta\varepsilon^p \rangle$ 
8: end if
9: return  $\varepsilon^p, \varepsilon^d, \tilde{\sigma}, k$ 

```

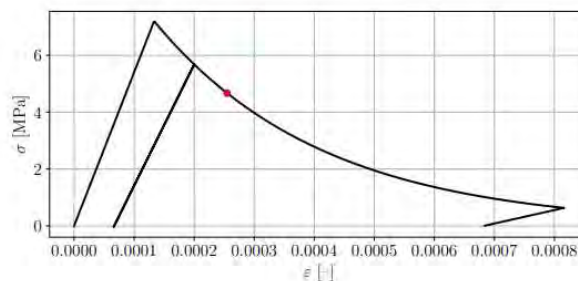
Leon Herrmann | Nafems Nordic Conference 2024 | Gothenburg

11

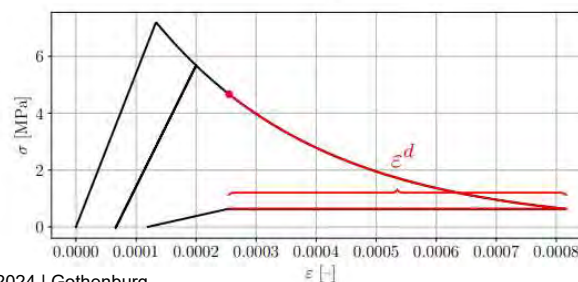
11

1D Example

- Stress-strain curve
 - Without discontinuity strain



- With discontinuity strain



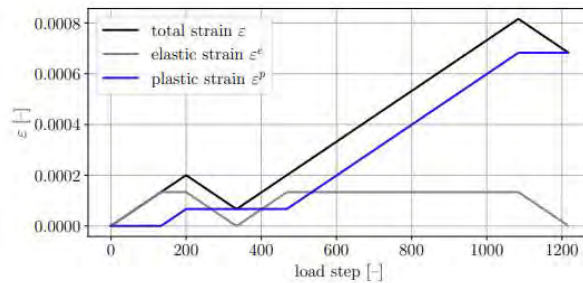
Leon Herrmann | Nafems Nordic Conference 2024 | Gothenburg

12

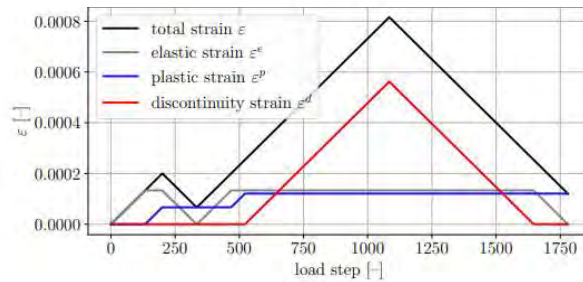
12

1D Example

- Strain decomposition
 - Without discontinuity strain



- With discontinuity strain



Leon Herrmann | Nafems Nordic Conference 2024 | Gothenburg

13

13

2D and 3D

- Crack opening can be checked with normal to crack surface \mathbf{n}

$$\varepsilon_n^d = \mathbf{n}^T \boldsymbol{\varepsilon}^d \mathbf{n}$$
- Normal is identified by the maximum principal stress during the initial crack opening

```

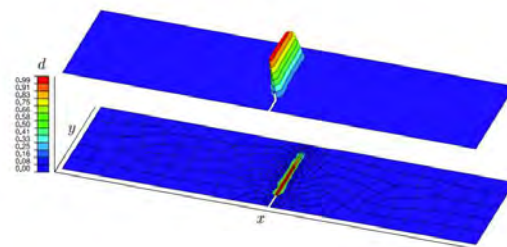
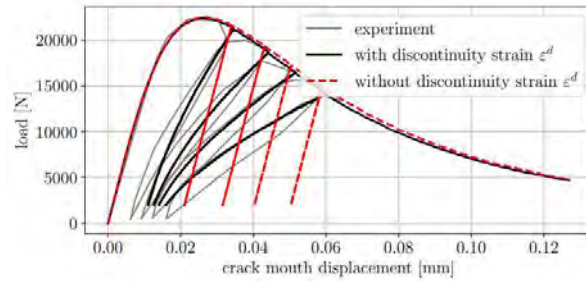
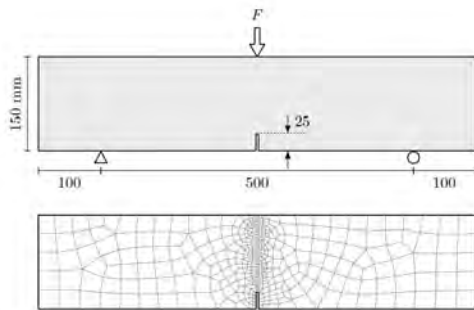
Require:  $\Delta \varepsilon, \Delta \varepsilon^p, \varepsilon^p, \tilde{\sigma}, k$ 
1: if  $(k + w(\tilde{\sigma}) \Delta \varepsilon_{\max}^p) > k_c$  and  $\mathbf{n}^T \Delta \varepsilon \mathbf{n} > 0$  then
2:    $\varepsilon^d = \Delta \varepsilon$ 
3:    $\tilde{\sigma} = \tilde{\sigma} - \tilde{D}(\Delta \varepsilon - \Delta \varepsilon^p)$   $\triangleright$  reset stress
4:    $k = k + w(\tilde{\sigma}) \Delta \varepsilon_{\max}^p$ 
5:   if crackInitiated=False then
6:     crackInitiated=True
7:      $\mathbf{n} \leftarrow \text{getCrackNormal}(\tilde{\sigma})$   $\triangleright$  using  $\hat{\sigma}_{\max}$ 
8:   end if
9: else
10:   $\varepsilon^p = \varepsilon^p + \Delta \varepsilon^p$ 
11:   $k = k + w(\tilde{\sigma}) \Delta \varepsilon_{\max}^p$ 
12: end if
13: return  $\varepsilon^p, \varepsilon^d, \tilde{\sigma}, k, \mathbf{n}, \text{crackInitiated}$ 
  
```

Leon Herrmann | Nafems Nordic Conference 2024 | Gothenburg

14

14

Center-Notched Beam



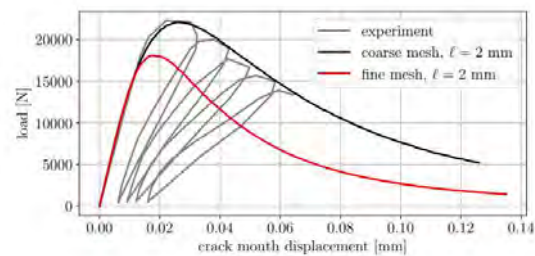
Leon Herrmann | Nafems Nordic Conference 2024 | Gothenburg

15

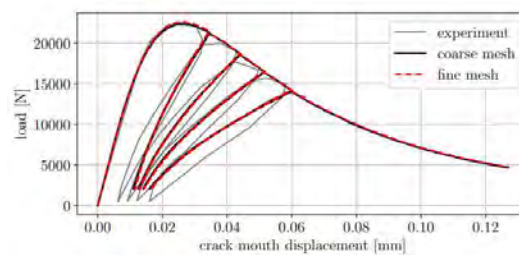
15

Center-Notched Beam

- Without length scale ℓ



- With length scale ℓ

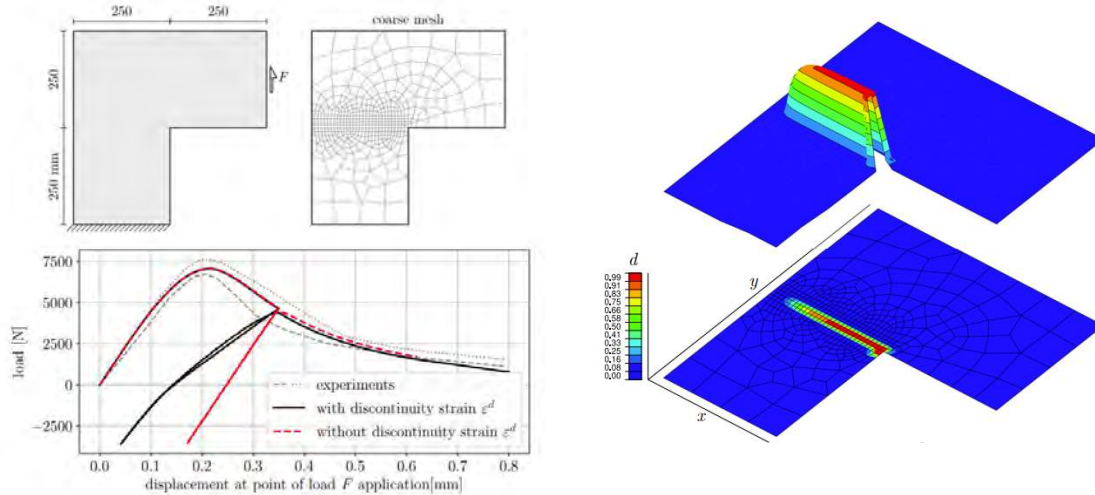


Leon Herrmann | Nafems Nordic Conference 2024 | Gothenburg

16

16

L-shaped panel



Leon Herrmann | Nafems Nordic Conference 2024 | Gothenburg

17

17

Conclusion

- Accurate representation of unloading and reloading
 - Necessary for low-cycle fatigue
 - Accurate identification of crack closure and opening
- Global Newton-Raphson iterations do not increase
- Additional history variable: discontinuity strain
 - Memory increase of about 1.6

Leon Herrmann | Nafems Nordic Conference 2024 | Gothenburg

18

18

References

A. Daneshyar, L. Herrmann, and S. Kollmannsberger, „From ductile damage to unilateral contact via a point-wise implicit discontinuity“, *Computational Mechanics*, Sept. 2023

L. Herrmann, A. Daneshyar, and S. Kollmannsberger, „The discontinuous strain method: accurately representing fatigue and failure“, *arXiv*, Nov. 2023

The Discontinuous Strain Method: accurately representing fatigue and failure

Leon Herrmann, Alireza Daneshyar, Stefan Kollmannsberger

Gothenburg, 24.05.2024



Enhanced Low Cycle Fatigue Analysis with FEMFAT

Gerhard Spindelberger, Klaus Hofwimmer (MAGNA Powertrain, Engineering Center Steyr)

1 Summary

This paper explores the application of enhanced low cycle fatigue analysis with FEMFAT to address the challenge of predicting plastic deformation in materials subjected to stresses that exceed their yield strength. Mathematical models, such as the von Mises yield criterion and strain hardening models, have been traditionally used to estimate the plastic deformation of metals. However, considering material non-linearity in finite element analysis (FEA) significantly increases analysis time, making it impractical for many engineering applications.

To overcome this problem, this paper proposes the use of PLAST methods in FEMFAT for estimating elasto-plastic stresses. The PLAST methods involve two main components: fitting a kinematic hardening model to the initial branch of the stress-strain curve and employing stress rearrangement methods based on the Neuber method or the equivalent strain energy density (ESED) method. Additionally, the influence of load peak sequence on damage results will be discussed.

A case study focusing on the plates of a rotor in an electric motor is presented to demonstrate the effectiveness of the FEMFAT PLAST approach. The results of the case study show that the new PLAST approach can achieve comparable results to elastoplastic FE analysis while significantly reducing analysis time. Furthermore, the paper discusses how the sequence of load peaks influences the resulting damage predictions, providing valuable insights for engineers in designing fatigue-resistant components.

2 Introduction

In many engineering applications, the stresses experienced by materials can exceed their yield strength, resulting in plastic deformation. The accurate prediction of this plastic deformation is crucial for assessing the structural integrity and fatigue life of components. Mathematical models, such as the von Mises yield criterion and strain hardening models, have been widely used to estimate the plastic deformation of metals. Hardening models describe the behavior of materials under load over the yield point. The hardening process in materials can occur through the expansion or translation of the yield surface. This concept is fundamental in understanding the behavior of materials under plastic deformation. The two primary types of hardening mechanisms based on the nature of yield surface changes are isotropic hardening and kinematic hardening.

2.1 Isotropic and kinematic hardening

Isotropic hardening refers to the expansion of the yield surface in all directions uniformly. In this case, the size of the yield surface increases as plastic deformation progresses. Isotropic hardening is commonly observed in materials that undergo uniform plastic deformation, such as mild steels. As the material experiences more plastic deformation, the yield surface expands – the yield stress increases, indicating a higher resistance to further deformation.

On the other hand, kinematic hardening involves the translation of the yield surface while maintaining its size. This type of hardening is associated with materials that exhibit non-uniform plastic deformation, such as certain types of metals and alloys. As the material undergoes plastic deformation, the yield surface shifts, indicating a change in the material's ability to accommodate further deformation. Kinematic hardening is often characterized by a Bauschinger effect, where the material's yield strength decreases after reverse loading.

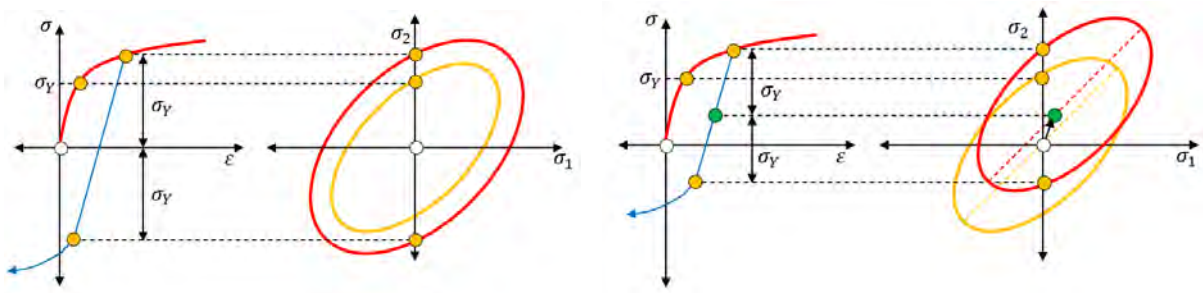


Fig. 1: Yield surface for isotropic hardening (left) and kinematic hardening (right)

However, incorporating material non-linearity in finite element analysis (FEA) can significantly increase computational time and complexity. This poses a challenge for engineers who need to perform efficient and reliable low cycle fatigue analysis.

3 New PLAST method

To address the problem of increased analysis time due to material non-linearity, the use of PLAST methods in FEMFAT for estimating elasto-plastic stresses was proposed. The PLAST methods offer an alternative approach that reduces computational time while maintaining accuracy. The two major components of the FEMFAT PLAST approach are as follows:

1. Fitting a kinematic hardening model to the initial branch of the stress-strain curve: The kinematic hardening model captures the material's behavior during cyclic loading and provides a more accurate representation of the stress-strain response, especially in the plastic range. By fitting this model to the initial branch of the stress-strain curve, the PLAST method accounts for the material's hardening behavior.
2. Stress rearrangement according to Neuber or ESED method: Stress rearrangement methods are employed to account for the redistribution of stresses due to cyclic loading. The Neuber method and the ESED method are commonly used approaches for stress rearrangement. These methods ensure that the elasto-plastic stresses are appropriately distributed, leading to more accurate fatigue life predictions.

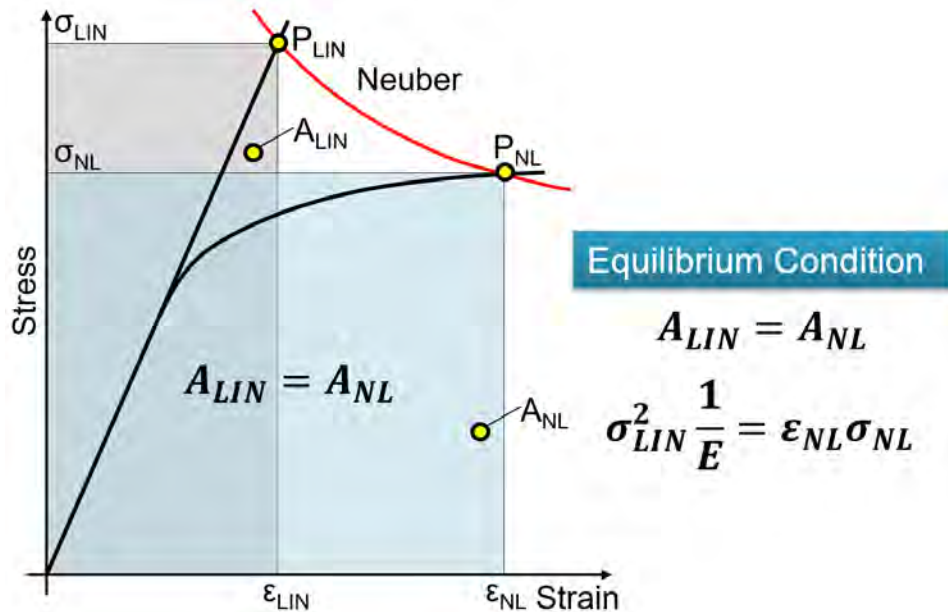


Fig. 2: Stress rearrangement according to Neuber

Procedure of the new PLAST method:

1. Computation of Material Parameters: For each material pair (C_i, γ_i) , an optimization process is conducted to determine the values that minimize the error to the cyclic stabilized stress-strain curve. These parameters are specific to the material being analyzed and are crucial for accurately predicting its behavior under cyclic loading. The Ramberg-Osgood parameters K' and n' , which define the cyclic stabilized data, serve as reference values for the optimization process.

2. Kinematic Hardening Model: In the cutting plane, the equivalent stress history is rearranged using the kinematic hardening model. This model utilizes the optimized parameters obtained in step 1 for each sample of the load time history. The kinematic hardening model considers the material's response to cyclic loading, accounting for the accumulation and redistribution of plastic deformation.
3. Rainflow Counting: The rearranged stress history obtained from the kinematic hardening model undergoes rainflow counting.

4 Benefits and Case Study:

The advantage of the FEMFAT PLAST approach is to avoid the need for computationally expensive elastoplastic FE analysis. Engineers can significantly reduce analysis time without compromising the reliability of their predictions.

To demonstrate the effectiveness of the FEMFAT PLAST approach, a case study focusing on the plates of a rotor in an electric motor is presented. The case study compares the results obtained using the new PLAST approach with those obtained from an elastoplastic FE analysis. The findings show that the PLAST approach yields similar results to the elastoplastic FE analysis while significantly reducing analysis time.

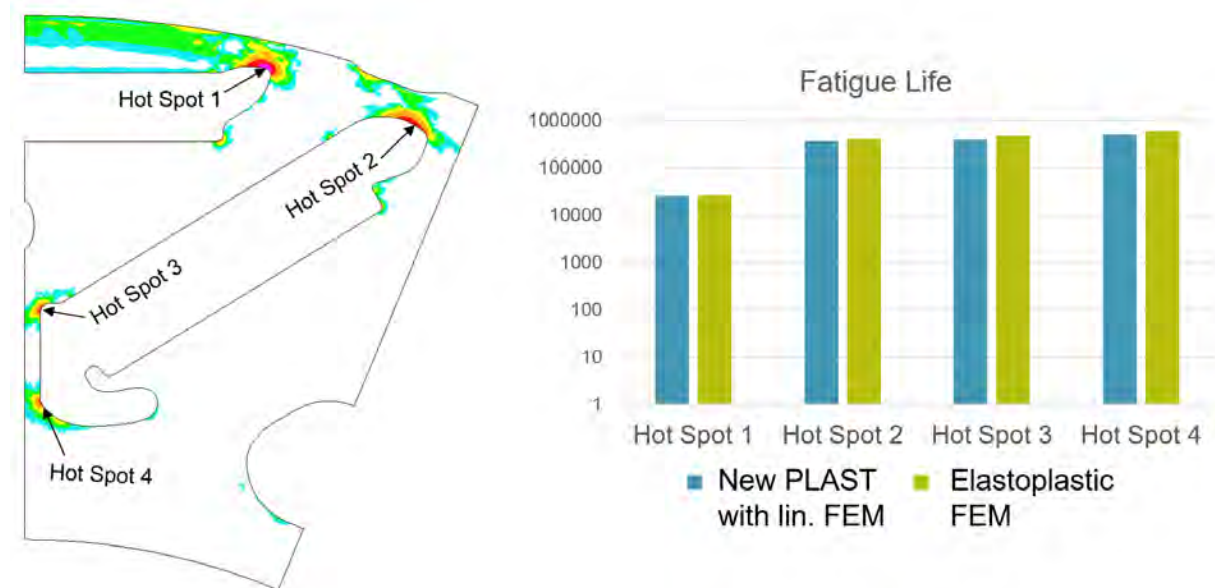


Fig. 3: Comparable fatigue life results for new PLAST with linear FEM and elastoplastic FEM

In Fig. 3 it can be seen that the fatigue results between the new PLAST approach with linear FEM and elastoplastic FEM are very similar. But the total analysis time (FEM + fatigue analysis) of the new method is about 25 times faster!

Additionally, it was discussed how the sequence of load peaks influences the resulting damage predictions. To illustrate the sequence influence, two signals with same rainflow matrix are investigated. The second signal was generated by just flipping the first signal.

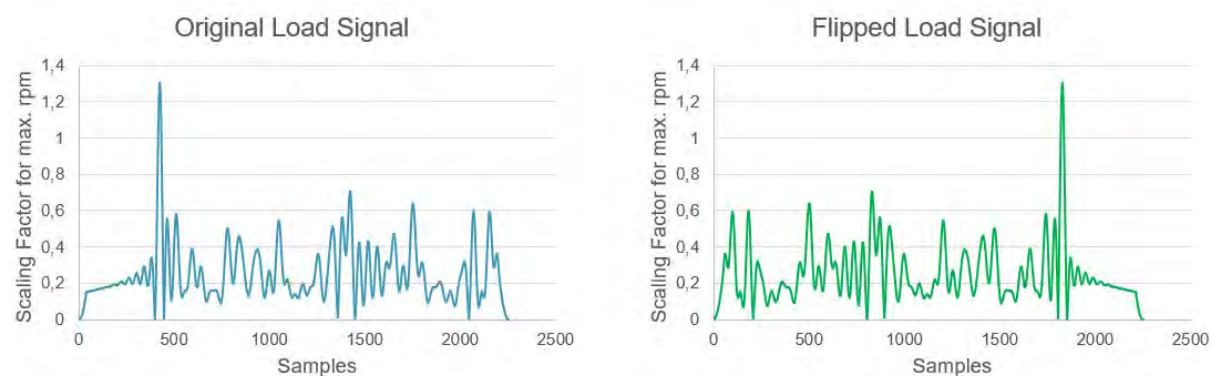


Fig. 4: original signal (right) and flipped signal (left) to study the sequence influence

Both signals were analysed with the old and new FEMFAT plast method. Both signals provides the same rainflow matrix, thus the old method provides the same damage, independent if the high load peak is at the beginning or at the end of the signal. In contrast, the new methods demonstrate, that the stress peak at the beginning leads to plastic hardening, thus reducing the damage of the subsequent cycles.

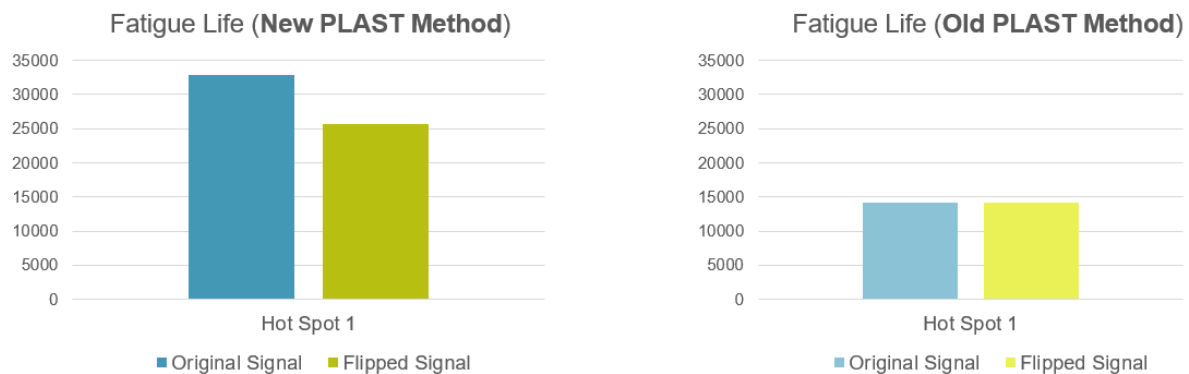


Fig. 5: original signal (right) and flipped signal (left) to study the sequence influence

5 Conclusions

In conclusion, the enhanced low cycle fatigue analysis with the new FEMFAT PLAST method offers a practical and efficient solution for engineers to accurately predict the fatigue life of components subjected to high-stress applications.

By incorporating kinematic hardening in multiaxial fatigue analysis, the influence of the sequence of high load peaks can be predicted with high accuracy even for long time histories.

Integration of Fatigue Analysis in FEA Solver for a Faster and More Reliable Process

R. Helfrich (INTES), L. Dastugue (INTES France), M. Klein (INTES),

1 Summary

Fatigue analysis is established in industrial applications. The findings are used for the design of components. The classic fatigue analysis leads to additional requirements for the simulation process. The exchange of large amounts of data between software/compute servers with different interface formats is necessary. The implementation and error-free use of this process is the responsibility of the user. In addition to data handling, the different release periods of the software involved must also be considered.

The full integration of the fatigue analysis into a general FEA solver solves the process issue. Both parts of the analysis, the classic stress analysis, and the fatigue analysis, are based on a common data model and use the same resources. This ensures data efficiency (large data stays internal, double data handling is avoided) and the import/export of intermediate results is no longer necessary.

Stress gradients, which were previously additionally calculated by the fatigue software based on its own model data, are now available in better quality directly within the FEA software based on the original FEA model. This can be used to increase the quality of the results. Due to the elimination of data exchange and the HPC orientation of the FEA software, the integrated fatigue analysis benefits significantly in terms of performance.

New analysis classes are made possible by reduced amounts of data. Thanks to the integration, the complete stress results for all calculation steps no longer must be saved, but are used directly ("on-the-fly") by the fatigue analysis in each calculation step and then immediately deleted again. This significant process improvement means that new classes of model variables and significantly more result steps can be considered. The results are then much more accurate.

The focus of the paper is on process simplification and reducing computing time for industrial applications.

2 References

- [1] Alexander Berndt, Jens Michy, Daimler Truck AG, Markus Ast, Eric Heinemeyer, Michael Klein, INTES, Reduktion der Prozesskomplexität durch Integration der Lebensdauerberechnung in die FEM-Simulation, VDI SIMVEC, November 22nd – 23rd, 2022
- [2] Alexander Berndt, Jens Michy, Daimler Truck AG, Michael Klein, INTES, Integrated Fatigue Lifetime Prediction of a Differential Case, PERMAS Web Conference, June 29th – July 7th, 2022
- [3] Jakob Häckh, Steinbeis Transferzentrum, Andreas Schünemann, INTES, Integrated Fatigue Analysis in PERMAS – Development Preview –, PERMAS Tech Meeting, April 22nd, 2021
- [4] Prof. Dr.-Ing. G. Willmerding, M.Sc Dipl.-Ing.(FH) Jakob Häckh, Steinbeis Transferzentrum, Fatigue Life estimation using winLIFE and PERMAS, PERMAS Tech Meeting, 11. April 2019

Integration of Fatigue Analysis in FEA Solver for a Faster and More Reliable Process

R. Helfrich, M. Klein, L. Dastugue
INTES



INTES
INTES Ingenieurgesellschaft
für technische Software mbH

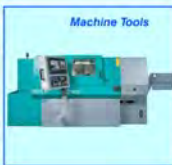


*Privately held and independent Finite Element Technology company since 1984
located in Stuttgart, Paris, Tokyo and Ann Arbor.*

*Developing and marketing of the FE analysis software **PERMAS** with graphical
user interface **VisPER**.*

Unified software for thermo-mechanics, vibro-acoustics, and optimization.

*High-level specialists with many years of experience form a powerful team. High
performance solvers and functional innovations account for the team's success.*



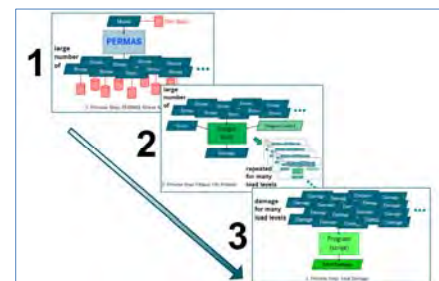
1. Motivation
2. State-of-the-art industrial process
3. Step by step description of the process
4. Innovation: New simulation process by integration of fatigue in FEA solver
5. Description of new process
6. Summary and outlook

Fatigue analysis is part of the virtual development process of single parts up to complete assemblies. Characteristics of the development demands: many variants, mathematical optimization.

Fatigue Life Prediction is very important, but it is an additional step with additional software, additional interfaces and high demands on disk space for the stress tensors!

The issues are:

- Interfaces between different software programs,
- Cache the results on disk,
- Long computing times,
- Different responsible hotlines,
- Process by proprietary scripts or manual copy and execution,
- User is responsible for the process and its maintenance, and
- Fatigue analysis has no access to FEA's internal model and results.

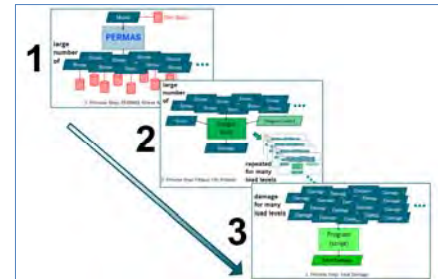


Several steps, several softwares, several scripts
A process with extensive file handling

Motivation

It's obvious that there is room for major improvements:

- Simplifying the process chain, reducing complexity
 - Reducing number of file formats
 - Reducing sources of (handling) errors
 - Reducing number of responsible software vendors
 - Aligning maintenance cycles of different process parts
- Accelerating virtual product development
 - Faster design decisions by reduced run times
- Implementing technological lead
 - New innovative opportunities
 - Increasing accuracy

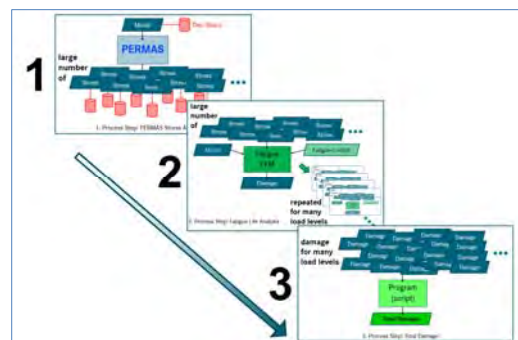
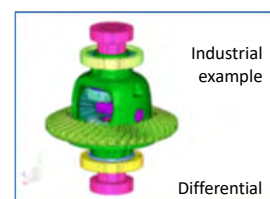


Several steps, several softwares, several scripts
A process with extensive file handling

**Focus of this presentation: Fatigue process improvements for industrial applications!
by integration of fatigue analysis in an existing FEA software**

State-of-the-Art Industrial Process

- Industrial process example: Total damage requested of a solid structure differential assembly.
- Many load cases of a nonlinear static analysis including contact describe the recurring stress.
- Stresses for different load levels are considered.
- Stresses from assembly are correctly considered (no load levels).
- The total damage results from the different number of damage repetitions at different load levels.
- This requires several main steps (3 steps in this industrial case) with different software and data transfer via files and interfaces.
- Description and analysis of the 3 steps follows.



Classic process with 3 steps

Step 1: Stress Analysis

State-of-the-Art Industrial Process:

- Simplified cutout

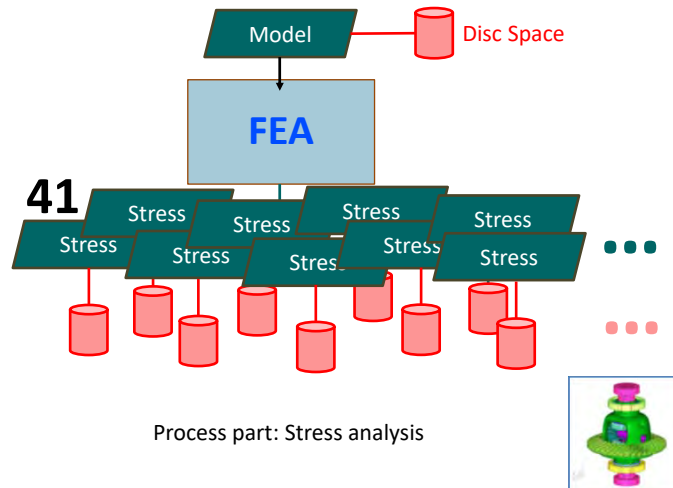
Analysis case:

- Prepare 41 stress result files (one for each analysis step) for further processing:

- Ideally reduced to surface nodes.
- Gradients still possible?
- More results necessary for gradients.
- Efficiency and quality dependent on interfaces and disk I/O speed.

(Remarks:

- Main gear has 41 teeth.
- Number is often a prime number.)



Step 2: Many Fatigue Analyses

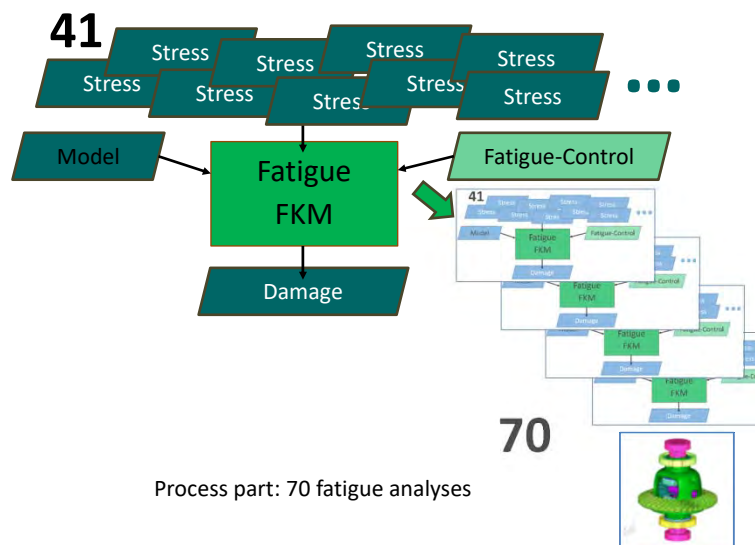
State-of-the-Art Industrial Process:

- Simplified cutout

Analysis case:

- Create 70 single damage files for 70 load levels by 70 fatigue analyses each out of the 41 stress data files.

- 70 fatigue analyses!
- Repeated model and stress result reading.
- Many read and write actions.
- Extended data handling!



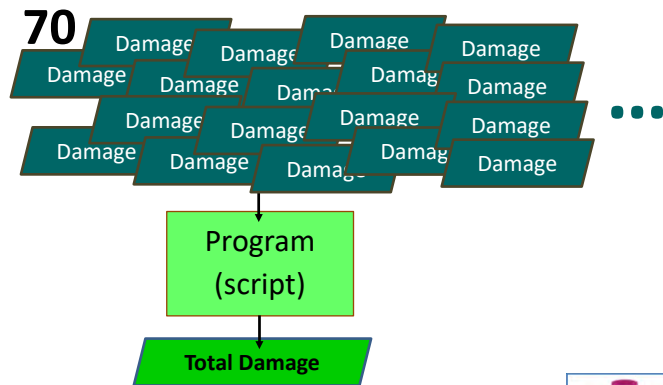
Step 3: Total Damage

State-of-the-Art Industrial Process:

- Simplified cutout

Total damage task:

- Consider individual (location-dependent) usage profiles via repetitions of the load levels.
- Read 70 single damage files.
- Combine them by proprietary program script.
- Use individual number of cycles (repetitions) for the 70 load levels (collectives).
- Calculate total damage.
- Write total damage file.



Process part: Total damage



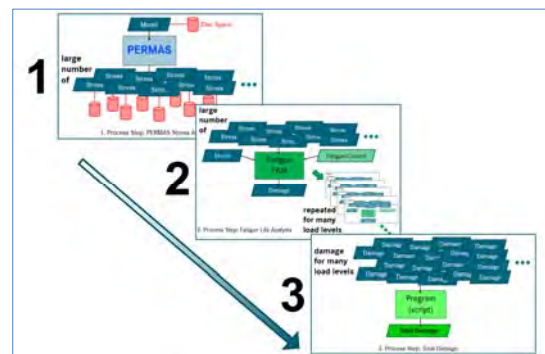
3 Steps Process

Complete task:

1. FEM stress analysis (>40 load steps)
2. 70 fatigue analyses
3. Combine fatigue results for total damage

Characteristic of the process:

- For the complete process, a large amount of data is frequently written out and read in.
- The amount of data limits the model size.
- The data organization is manual and therefore not process-safe.
- Individual interfaces are additional sources of errors.



Classic process with 3 steps



Solution Approach

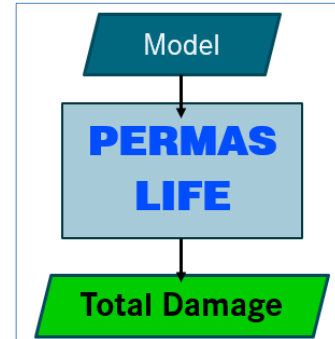
Solution: New integrated process!

Integration of fatigue analysis in FEA software.

(Integration = completely new development of fatigue analysis in the FEA software for common model description, common data management, and common post-processing).

Three major improvements by integration:

1. Process simplification (standardized process definition)
2. Accuracy
3. Data efficiency
4. Shorter time to make design decisions



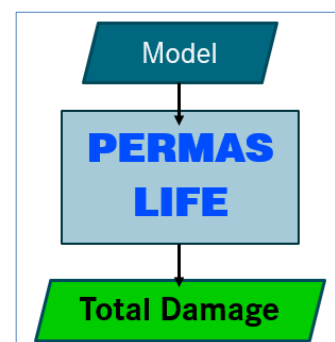
New integrated process

1. Process Simplification

Three major improvements by integration:

1. Process simplification

- Nodal stresses are already available in FEA
 - Direct processing step for fatigue
- All analysis steps are part of a maintained software
- The management of the complete process is part of one software
- High-performance solver infrastructure
 - Experienced in dealing with large amounts of data
 - Parallelization is present throughout
 - Specialists for HPC
- Fatigue analysis benefits from this software base
- Data caching on disk deleted (no longer necessary)



New integrated process

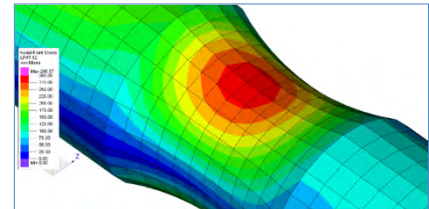
2. Accuracy

Three major improvements by integration:

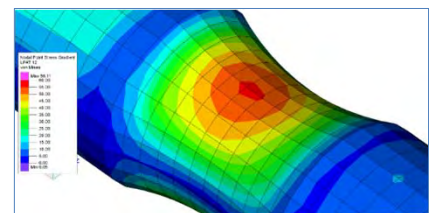
1. Process simplification

2. Accuracy

- Stresses in internal accuracy (more digits)
- Stresses inside structure available (not only on surface) anyway (no additional data write/save/read)
- Nodal point stresses (at nodes) and element stresses (at Gaussian points)
- High quality stress gradients
 - Accurate normal direction (complete element information)
 - Stress gradients consider element shape functions
- FEA-Solver based stress gradients are more accurate
 - → more accurate fatigue analysis



Stress results



Nodal stress gradients normal to the surface

3. Additional Data Efficiency – “On-the-fly”

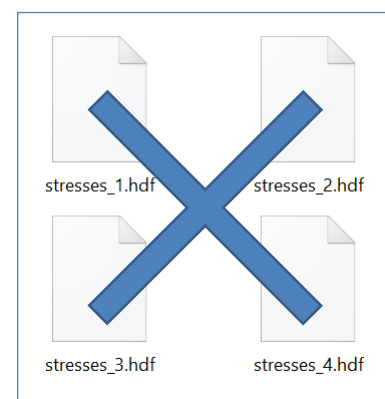
Three major improvements by integration:

1. Process simplification

2. Accuracy

3. Data efficiency

- Stress data and fatigue results in the same database.
- **“On-the-fly”**: Faster calculation of results when needed, no storage .
- **Instead of saving all intermediate results** like stress data, including gradients, stack wise until they are used later to calculate damage results, the integrated approach allows to **calculate the final result stepwise** and to **release the intermediate results right away from storage**.
- Much faster, no storage space, no manual administration.
- This allows formerly impossible model sizes.

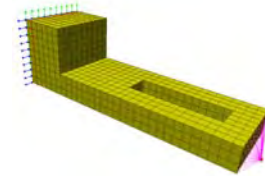


Stress data not on files

Illustration of “On-the-Fly”

Why is „On-the-fly“ a game changer?

Transient Analysis	Stress Tensors	Timesteps	Binary Storage [GB on HDF file]
Small example	1,500	10,000	0.403
	*400	*100	*100,000
Realistic model	600,000	1,000,000	16,120 = 16 TB



Small example structure with 1500 nodes

Required disk space exceeds available capacities in most cases.

But computing is here faster than storing and retrieving data.

That is the solution “On-the-fly”

- Stresses are calculated stepwise, and as intermediate results they are released right away from storage
- Stresses are never written to disk => disk limit solved! + run time drastically reduced.



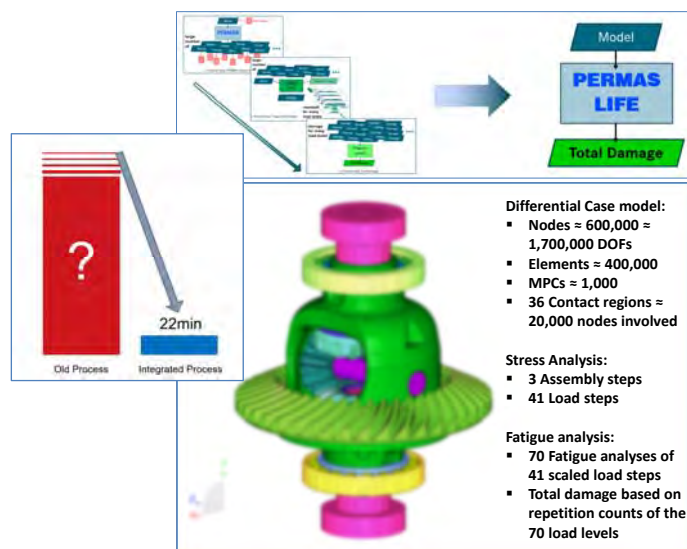
Truck on torture test track

Customer response: “On-the fly makes it possible to do fatigue life analysis with my new models of larger size!”

“on-the-fly” of integrated fatigue analysis is a breakthrough in saving disk capacity!

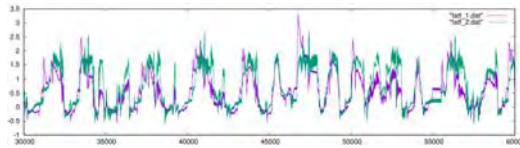
Industrial Example

- Complex industrial process in one single run
- Process organization completely in FEA solver
 - Creation of time step history load spectra
 - Individual damage results for different load levels
 - Accurate stress gradients
 - Collect damage results
 - Combination of each damage level with individual number of cycles
 - Export total damage result
- **Short run time: 22 min on 18 cores** (usage of high-performance infrastructure of solver)
 - Stress analysis with 41 load steps
 - 70 fatigue analyses
 - Total damage based on repetition numbers
- Process directly usable to new model variants



Run Time Example

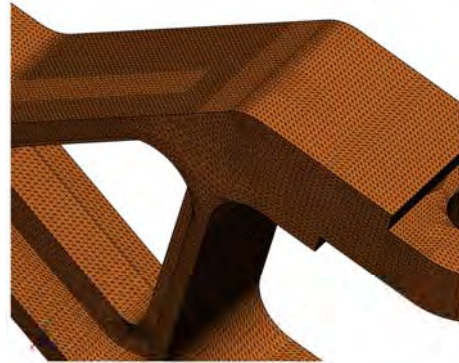
Yoke with fine mesh



2 time functions (164 548 steps each) for 2 load pattern



Damage result



1 259 616	Nodes
889 088	Elements
146 810	Fatigue nodes

Run Time Example

Yoke (fine mesh)

- Characteristics: 146,810 fatigue nodes, two time functions with 164,548 steps each, 40 cutting planes & 200 rainflow stress classes per node
- Run time:

Elapsed Run Times	24 Cores	48 Cores
static+fatigue	21min 56sec	12min 49sec
fatigue	19min 43sec	10min 45sec

System: 2 * Intel Xeon 8260L, 24/48 cores, 288/576 GiB memory

- Excellent run time, parallelization performance of HPC infrastructure

Current Features of Implementation

- Fully integrated fatigue analysis directly in FEA Solver PERMAS
- Stress based high-cycle fatigue (long term loading, typ. >1000 cycles)
- Multi-axial stress state on structural surfaces (FKM 7.0 and more)
- For all volume elements
- Classical nodal point stresses and gradients or highly accurate SPR stresses and gradients (Smooth Patch Recovery by Zienkiewicz)
- Multiple S-N curves for each material, surface hardness and roughness, support factor, mean stress correction, Neuber correction
- Loads
 - Collectives: of loads or modes (like differential example)
 - Timeline: time amplitude functions for load pattern or modes
 - Timehistory: samples out of primary analysis' load/time history

Summary and Outlook (1)

- The new integrated fatigue life analysis improves the process by orders of magnitude.
- Stress calculation and fatigue life analysis are integrated in one software and do not require any interfaces.
- Accuracy is increased through improved accuracy for the stress gradients.
- Run time has been drastically reduced.
- Basic technology and infrastructure for fatigue analysis in the FEA solver PERMAS is developed.
- This is the perfect starting point for functional expansion, like extension by further fatigue approaches, optimization with damage as objective function or as design constraint.
- Integration, process reliability and short run times allow in future the industrial usage of fatigue optimization and fatigue sampling.



From classic manual 3 step process to an efficient integrated process

Summary and Outlook (2)

- The new integrated fatigue life analysis improves the linked process in key manner.
- Stress calculation and fatigue life analysis are integrated in one software and do not require any interfaces.
- Accuracy is increased through high accuracy stress and stress gradients.
- Run time has been drastically reduced and larger model sizes are enabled.
- Basic technology and infrastructure for fatigue analysis is available in PERMAS since 2022.
- The functional capabilities will be extended and combined analyses with other integrated functions like sampling or optimization will soon be established.



From classic manual 3 step process to an efficient integrated process

Thank you for your kind attention!

More information?

www.intes.de

or

Reinhard.Helfrich@intes.de

Fatigue life investigation as a part of a complete design optimization process

George Korbetis, Christos Tegos (BETA CAE Systems)

1 Summary

Product design in the automotive industry is becoming increasingly demanding as new products should reach high performance standards in very short development cycles. Engineering simulation, using FEA, comes to assist in most product development stages to substitute costly experiments for new designs while speeding up the overall processes. In this direction, optimization procedures are increasingly employed during the design.

Apart from FEA, fatigue analysis is a mandatory process which assures product integrity by accurately predicting products' life. Using fatigue analysis, the engineer is able to construct stronger yet lighter structures while avoiding overdesign.

Fatigue analysis is often incorporated into the product design workflow through an optimization process that fine-tunes structures' efficiency.

In this case study, a structural part of a car is subjected to a cyclic load. Several design variables are defined directly to the part's FE model to control its shape. The fatigue analysis as a part of an optimization loop analyzes the model and locates critical areas for improvement.

2 Problem set-up

The target of this case study is to perform design optimization on a certain part of a car model. The optimization goal is to reduce fatigue damage while keeping mass and stress within specific range. The input load of the case is calculated by running the car kinematic model on a Belgian block road. All actions that are used to complete this task are set-up in an automatic way so they are able to run in a optimization loop. These actions are described in the following sections.

2.1 Design changes

The selected part for this investigation is subjected to several shape changes. These changes are applied directly on the FE model using the ANSA morphing tool so there is no need for remeshing or FE model update. Six design variables are defined which control the model geometrical changes. The shape changes are selected to handle areas with high stress but also to reduce mass in non-critical areas. The design variables are shown in Figure 1 and in Table 1.

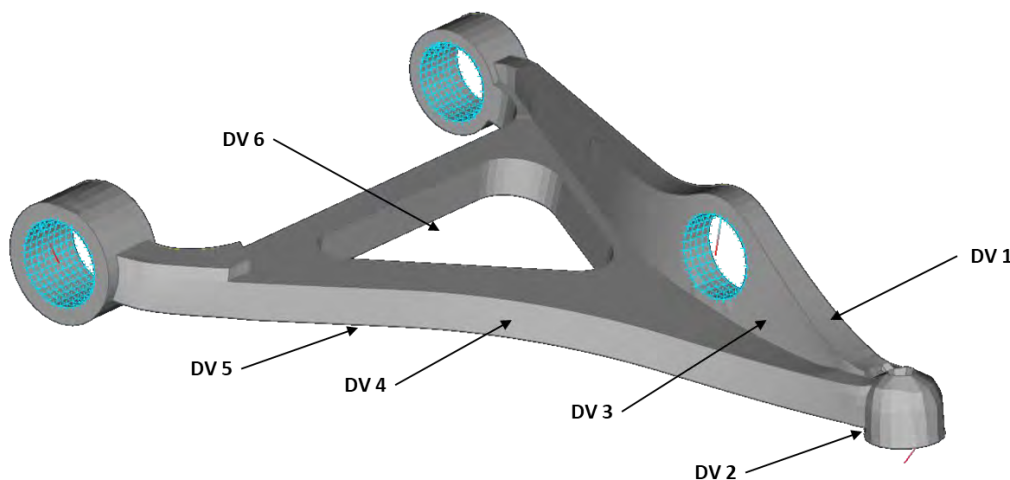


Fig. 1
Shape changes on the FE model

DV name	Initial	Min.value	Initial value	Max value
DV1	curvature	0	0	1
DV2	thickness_1	-4	4	4
DV3	fillet_1	0	0	3
DV4	Internal_hole	-5	4	8
DV5	external_curvature	0	0	1
DV6	bottom_offset	-5	0	5

Table 1
The design variables

3 The Kinetics model

The kinetics model is defined from the car's FE model. All bodies are considered rigid except for the wishbone part which is set as a flexible body. An eigenvalue analysis has been applied for the flexible body to calculate the stiffness matrix and the eigenmodes. Then the car runs on a Belgian block road for three seconds and the ANSA Multi Body Dynamics solver calculates the dynamics of the whole assembly and the stresses that appear on the wishbone part.

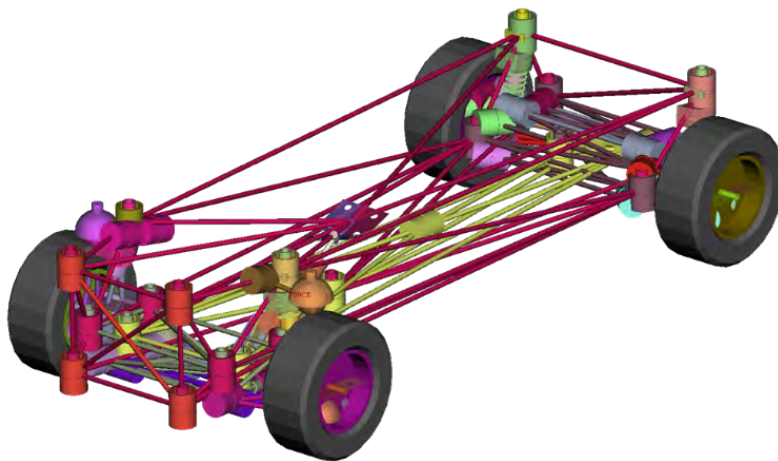


Fig. 2
The kinematics model

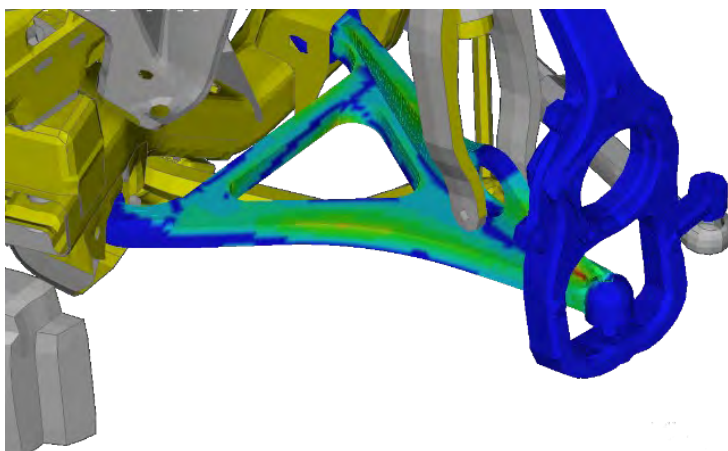


Fig. 3
Flexible body calculation

3.1 Fatigue calculation

The fatigue analysis is performed in the FATIQ software. The input data for this analysis are nodal stresses from the wishbone model, computed from the kinematic model. Damage calculation is carried out by applying Miner's rule to cycles extracted through the Rainflow counting algorithm. The method employed for fatigue analysis has been structured in a way that allows it to be stored for subsequent reuse in batch mode and coupled to the optimization workflow.

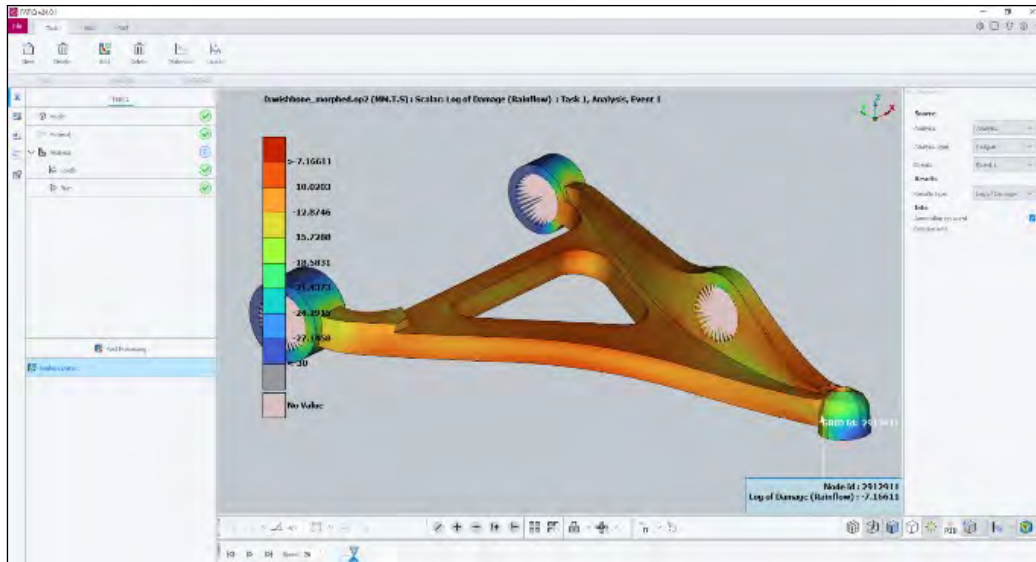


Fig. 4
Fatigue analysis

4 Optimization

Optimization is done in two steps. At first, a DoE analysis runs to identify design variables with significant influence on the model behavior. As a next step the optimization problem runs. The ANSA Optimization controls all tools and processes which are seamlessly run at the optimization iterations (Fig. 5). The Simulated annealing algorithm is used.

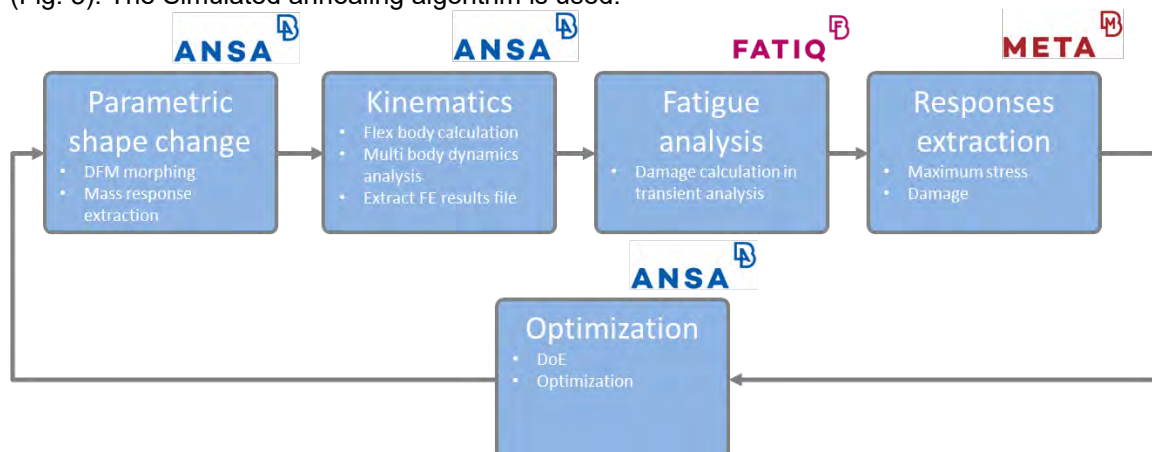


Fig. 5
The optimization workflow

5 Results

The optimization converges after 38 iterations. A significant reduction in fatigue damage has been achieved while the maximum stress and mass has been kept within acceptable range. The shape changes and objective and responses values are shown in figure 6 and table 2.

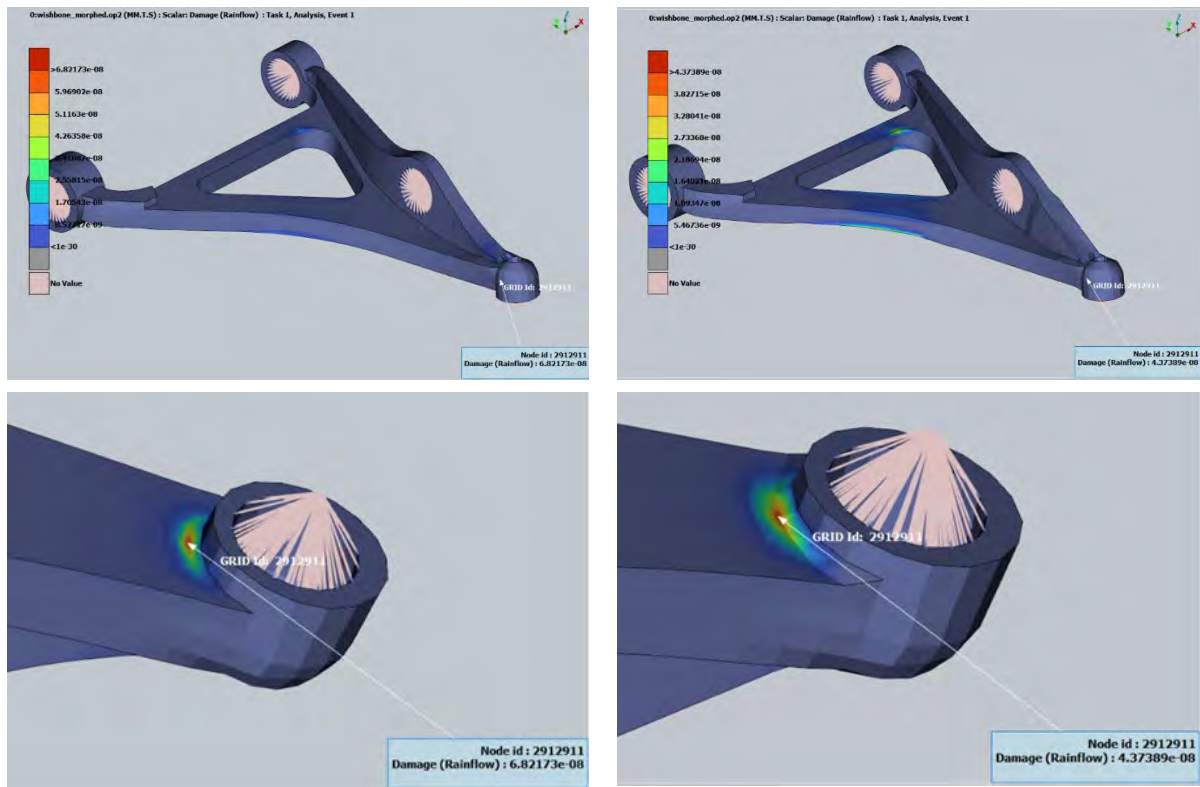


Fig. 6
The initial and final designs

	Initial	Optimum	Improvement [%]
Max Damage	6.82173e-8	4.37389e-8	35.8
Max Stress	106.643	121.192	-13.6
Stress at max Damage	98.594	86.997	11.7
Mass	0.00267	0.00273	-2.2

Table 2
Objective and responses

6 Conclusions

A long process with different types of analyses has been seamlessly combined into a single workflow, capable for model behavior exploration and optimization. The converge was fast with relatively small number of iterations and thus, the same process can be applied into all critical parts of the car model. The same process can be extended in other kinds of optimization such gauge optimization. In this case model thickness, kinematic parameters and fatigue analysis properties can be defined as design variables.

Enhancing Aircraft Safety Through Data-Driven Reduced Order Modelling for Birdstrike Analysis

Dr. R. Lombardi, Dr. C. Sahin (*Noesis Solutions NV, Belgium*)
L. Hootsmans, W. Van de Waerdt (*GKN Fokker Aerospace, The Netherlands*)

Summary

Bird strikes are a significant threat to aircraft safety, as such events could lead to severe damage to exposed structures such as wing and tail leading edges, engines and engines' nacelles, and cockpit windows. To mitigate this risk, manufacturers must prove that their structures can fulfill strict airworthiness specifications prescribed by transportation agencies. This represents a design constraint whose satisfaction must be verified by means of physical and numerical impact simulations. The latter is being investigated and developed for the significant improvements in terms of flexibility, time, and cost-effectiveness that it would bring, with respect to practical experiments.

However, crash analyses are complex, resource-intensive, and require expert personnel to be prepared and analyzed. The substantial number of CPU hours needed to perform a single simulation is going to be a burden if the simulation itself is part of a complex, multi-disciplinary analysis framework tasked for component optimization (e.g. minimizing mass). An accepted approach to streamline the process under similar circumstances involves surrogate models, which are mathematical representations of the original problem behavior; however, many modelling approaches are not well suited to deal with time-dependent and/or dimensionally large problems commonly found in crash simulations.

Reduced Order Modelling (ROM), and more specifically, data-driven ROM, is one of the methodologies that could help with this kind of analyses, and generate a model that, once trained, can replace the real simulation during the initial stages of the design study, allowing for a significant reduction in evaluation time, at the cost of some accuracy.

In this paper, data-driven ROMs were used to reproduce the behavior of aluminum leading edges, of different thicknesses and radii, upon impact by simulated birds of variable speed. The objective was to determine:

- If the model could deliver realistic deformation simulations.
- the amount of time and resources compared to the original computation.
- the impact of the model's parameters on the quality of the results.

The paper is organized as follows: a brief introduction on data-driven reduced order models; a description of the leading-edge bird-strike test case; model training implementation and achieved results for single geometry, with a focus on the model's performances, and for multiple geometries, followed by planned future activities.

Data-Driven Reduced Order Models

Data-driven ROMs can be described as a class of methodologies that, starting from an existing database of the time history of the full-order solutions of the outputs of interest, can generate a reduced model that provides a reliable evaluation at a lower computational cost. The price to be paid to achieve easier/faster computation takes the form of a controlled loss of accuracy [1].

Several approaches have been developed in the last decades, ranging from general-purpose solutions to tailored, problem-specific ones. Most methodologies, although different in terms of implementation and specific algorithms, share the offline-online framework, and can be split into 3 main operations: dataset generation, model training, and model evaluation. The first two operations, by far the most time-consuming and expensive to perform, belong to the offline stage. The database generation is

independent from the ROM itself, thus allowing for pre-existing datasets (e.g., from previous designs of experiments) to be efficiently repurposed.

In this work, the projection of the full-order snapshots into reduced basis is achieved by means of the proper orthogonal decomposition (POD). POD is a dedicated application of Single Value Decomposition (SVD) to analyze and extract the modes that dominate the variation of the data over time, and it is performed independently on both design variables (when function of time, e.g. external structural or thermal loads) and responses. The reduced parameters are used to train a fully connected Deep Neural Network (DNN); PODs drastically reduce the size of the input and output layers, with direct effects on the DNN structure, both in batch size and number of layers. The DNN models the relationship between reduced state design variables and reduced state responses.

The DNNs constitute a layer of the complete model, that requires access to the projection/un-projection matrixes determined by the PODs. The model is generated during the offline training when all its constituents are determined and then stored; the operation leads to an object that can be queried to determine the full-order solution generated by new values of the design variables [2].

With this type of approach, the absolute reliability of the model is influenced both by the accuracy of the POD (specifically, how faithfully the reduced space represents the full-order one) and by the accuracy of the NN (quantifiable through the training losses). The latter can be influenced by the former.

The reliability and quality of the model are determined by the complexity of the responses being modeled and the number of available training experiments. For a fixed-size training dataset, the overall accuracy of the model and its training time can be leveraged by acting both on SVD truncation (therefore the error committed projecting the modes by removing the least relevant components), and DNN hyper-parameters such as number of epochs, learning rate, and/or the NN layout.

The time-dependent component of the responses is compressed through the POD approach. The geometry-dependent aspect of the model (namely, the number of nodes in a Finite Element Model) is addressed by partitioning the full mesh into smaller sub-subproblems, each assessed by a dedicated, interconnected sub-model. The partitioning allows for a significant reduction in the system's requirements to generate and use the model; compared with the full problem, multiple, smaller SVDs and DNN trainings can be performed (potentially in parallel) without the need for purpose-built high-performance computers.

The online evaluation stage inherits the saved projection matrices and normalization boundaries, which are then used to cast the design variables associated with the new experiment into their reduced state. DNNs are then queried using projected design variables to determine the estimated reduced-order states of the responses. Finally, these are projected back to their full-order state (by means of the associated design variables projection/un-projection matrixes). The operations are repeated across all the partitions (if required) and the final, full-order, response is made available.

Leading Edge Test Case

In a previous work [3] the ROM methodology was used on a simplified bird strike simulation, using an Aluminum octagonal, flat plate as the target. The plate itself had fixed dimensions but its thickness, along with the bird's impact speed and mass, were used to investigate their influence on the deformation over time. The simulation already had several aspects of interest, including modelling of the soft-body behavior of the bird, bird-plate contact, plate damage initiation, and later accumulation, high deformation, elements' failure, and removal.

As the ROM approach was being developed, a more realistic scenario was generated. The objective was to assess the performances using a geometry that better represented the engineering challenges associated with designing structures able to survive a strike.

The plate was replaced with a model of the wing leading edge (LE), represented as a uniform-thickness, aluminum sheet; its geometry is defined by flat, parallel, upper, and lower sides, joined by a constant radius, semi-cylindrical nose, Figure 1. The bay length (rib-to-rib span) was set to 600 mm. The simulation software was Abaqus 2022. The resulting mesh had 14558 total elements of type PC3D and S4R, with upper and lower straight sides constrained. In order to properly investigate the behavior of the material, two failure modes were considered, material failure and maximum deformation.

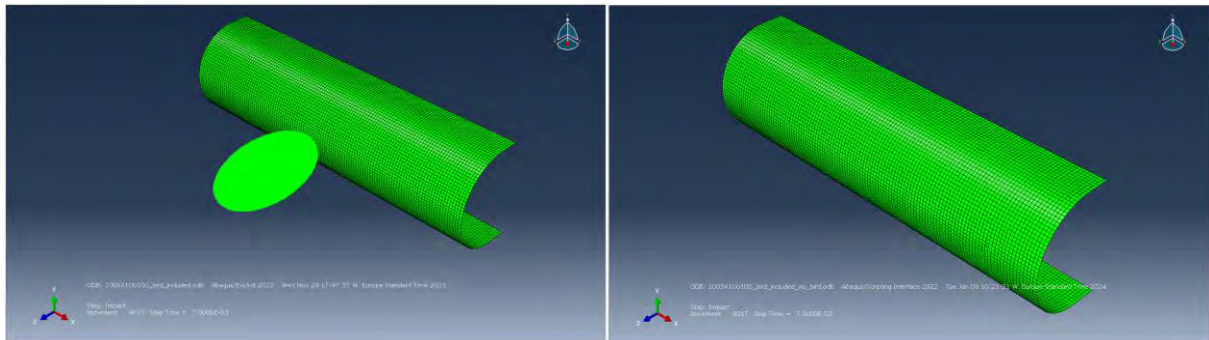


Figure 1: Leading edge (width 600 mm, height 170 mm, depth 120 mm, radius 85 mm), bird strike analysis setup, with and without simulated (2.2 lbs., 10k elements) bird.

The two selected design variables were used to perform a Design of Experiments (DOE) and generate the dataset that later drove the creation and validation of the reduced models, Figure 2.

For every impact speed, the range of thicknesses between 0.5 and 5 mm with a step of 0.5 mm was explored. The selected speed of the simulated bird was between 50 and 200 m/s, compatible with bird strike requirements that regulate weight and speed according to the class of aircraft, flight envelope (take-off, cruise, landing), and the type of component (wing, engine, tail). The images at the corners represent the final simulation step for the scenarios at the boundaries of the design space, which could lead to negligible deformation (high thickness, low speed), deformation without damage to the surrounding structure (high thickness, high speed), significant deformation and likely damages to the spar behind the leading edge (low thickness, low velocity) and destruction of the LE (minimum thickness, maximum strike velocity).

The green line separates the regions of the design space with (below) or without (above) cracks in the structure. The area delimited in red marks the experiments with detached and removed elements, as (but not necessarily that catastrophic) the bottom right scenario.

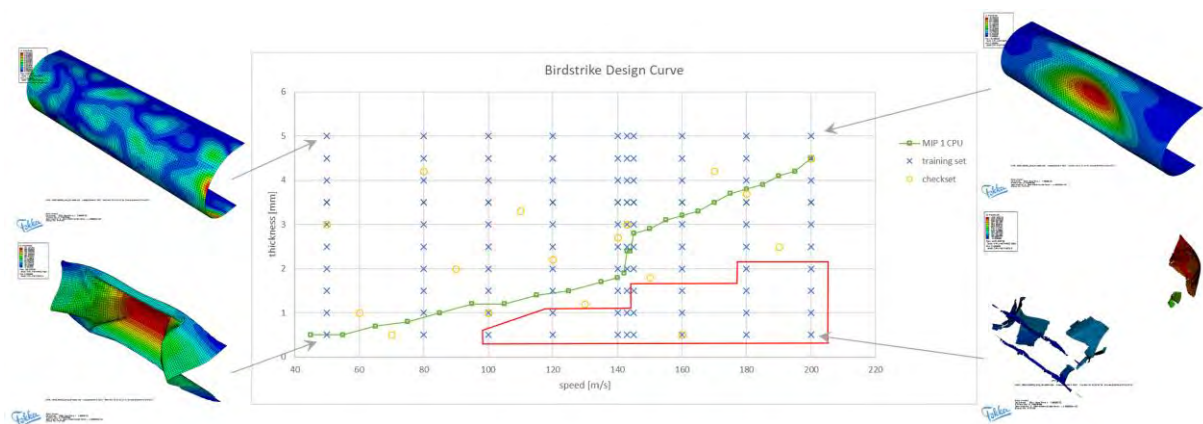


Figure 2: LE DOE investigation. Performed Abaqus simulations, targeted to be used as training set, are represented by the blue crosses.

Single LE Geometry

The DOE-generated dataset explored designs of limited interest, such as maximum thickness plate / minimum impact speed or events with very extensive failures due to unrealistic couplings of minimum thickness/maximum speed. Subsets of the dataset, tailored to describe the region where the transition between no failed elements / failed elements occurs and boundaries, and or according to front spar penetration/not penetration criteria, were used to train different ROMs and investigate their modelling quality (accuracy in reproducing the responses for a design that was included in the training set), predictive capability (accuracy of the responses predicted for a new design point), the influence of the

model settings and finally compare the evaluate the model evaluation time with the equivalent native simulation.

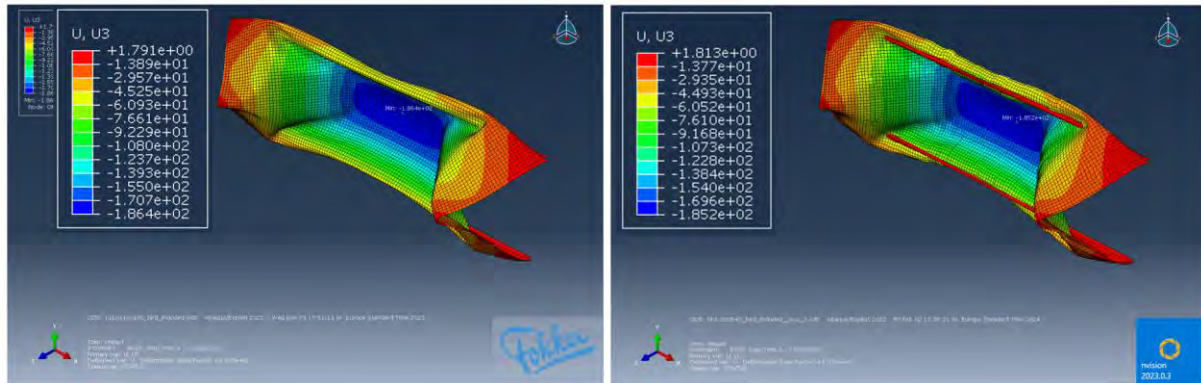


Figure 3: Comparison native (left) and surrogate model (right) results, for bird speed 100 m/s and LE thickness 2.0 mm. The maximum difference in displacement is 0.3%.

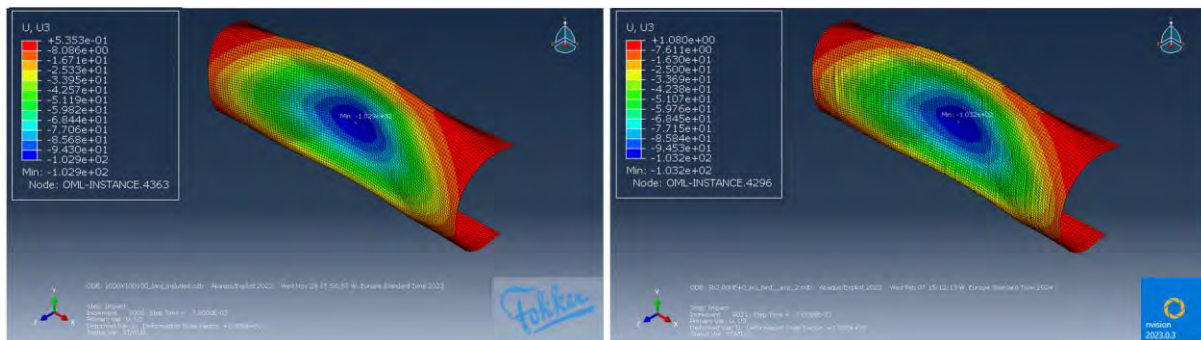


Figure 4: Comparison native (left) and surrogate (right) results, for bird speed 100 m/s and LE thickness 1.0 mm. The maximum difference in displacement is 0.3%. No material failure detected.

Table 1 highlights a comparison between the results achieved by the reduced model and the equivalent simulations for 8 cases that were part of the training dataset and cases at an impact speed that was unseen by the model. The maximum displacement in the model was used as the metric for the model accuracy. Except for 2 experiments, the difference is below 5%, which is often considered the upper threshold for acceptable surrogate model accuracy; in both cases where the difference exceeds this value, the model overestimated the displacement. Figure 3 and Figure 4 illustrate reference results achieved through simulation and the corresponding ROM predictions for high and low deformation cases.

Table 1: Comparison of Abaqus-simulated and ROM-predicted maximum displacements. Experiments with speed 90 m/s were not part of the training dataset.

Speed	Thickness	Simulation displacement	Predicted displacement	Percentage difference
50	0.5	-181.5	-180.9	0.3%
50	1.5	-55.52	-59.26	6.7%
80	1.0	-166.7	-171.9	3.1%
80	2.0	-72.55	-70.06	3.4%
100	1.0	-186.4	-186.3	0.1%
100	2.0	-102.9	-107.5	4.5%

120	1.5	-166.3	-165.0	0.8%
120	2.5	-98.54	-106.6	8.1%
90	1.0	-176.3	-178.9	1.5%
90	1.5	-138.8	-136.1	1.9%
90	2.0	-87.44	-86.31	1.3%

With the achieved results as a testament to the accuracy of the approach, the models were integrated into an optimization workflow to determine the minimum skin thickness able to withstand an impact without contact between the elements of the LE and those of the front spar. To this end, the full extent of the training dataset was restricted to exclude experiments that were less relevant for this kind of analysis, which led to the training dataset illustrated in Figure 5 as the orange-bounded area.

The model training time for this scenario (43 experiments, 14558 elements) was about 1800 seconds. The total time required to set up the workflow (integrate the simulations in the optimization framework) and evaluate the results was less than 2 hours.

For each impact speed between 50 and 200 m/s, with incremental steps of 10 m/s (step selected to include speeds not directly investigated by the training dataset), two optimizations were performed, using native simulations and model-based analyses. The minimum thickness increment was set to 0.1 mm.

In the plot optimized thicknesses were reported using green boxes for the Abaqus and yellow circles for the ROM. The global trend of thickness vs speed for the 2 sets is similar, with model-based optimization results being slightly less conservative and somewhat thinner.

Optimization time was unique for every speed, between 600 and 1400 seconds for the ROM-based investigations and 900 and 2200 seconds for the native ones.

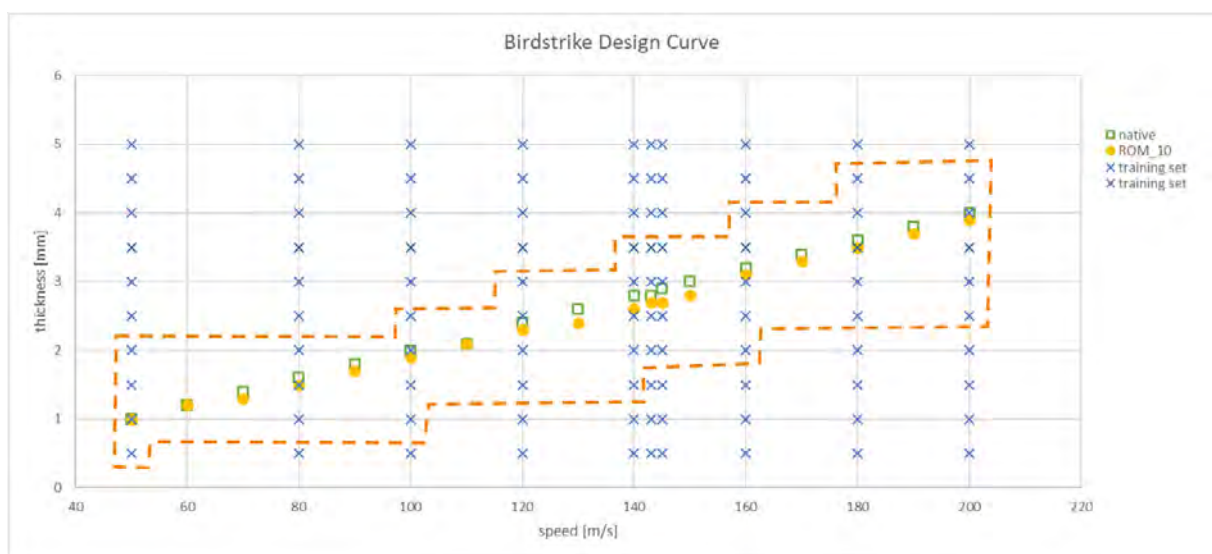


Figure 5: Comparison of the optimized minimum skin thicknesses, function of impact speed, required to ensure no front spar contact, native simulation (green) and ROM results (yellow).

Multiple LE Geometries

Leading edge geometry has a relevant impact on the evolution of the deformation after the strike. The implemented ROM approach requires the snapshots to be dimensionally consistent. A pre-processing step was introduced with the objective of mapping different but similar geometries (the design variable being the LE radius) to a standardized one, whose snapshots were later used for the model training and evaluation, Figure 6.

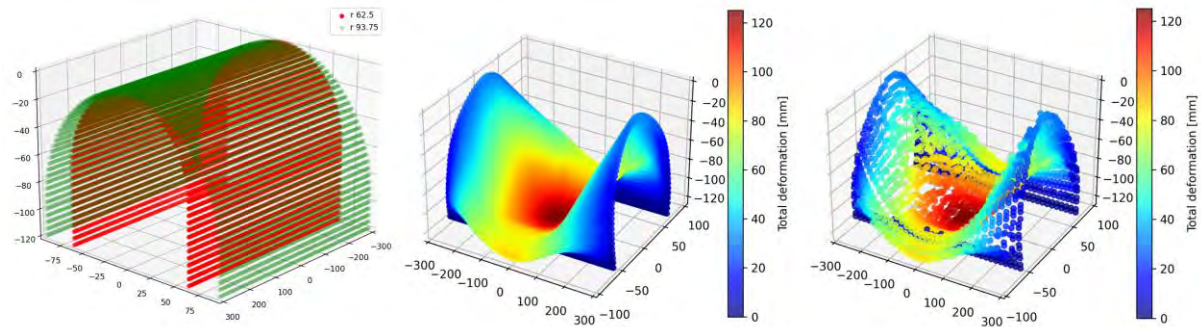


Figure 6: Point clouds representing the nodes of different LE geometries (left), deformation reported for all the vertices in the original mesh (center) and deformation on the standardized point-cloud (right).

The mapping process, performed through conversion to voxels and matching of similar features, introduces approximation both in the generation in the trainable snapshots (as the responses for the coarser standardized point-cloud are inferred from the parent vertexes in the source meshes) and in the reverse operation after evaluation. In addition to DNN models and projection /un-projection matrixes, ROM based on multiple geometries also requires the standardized point cloud and the generated association maps to be saved.

Conclusions and further developments

The paper presents and discusses a data-driven ROM methodology applied to a simplified crash simulation from the aerospace industry. Predictions achieved by means of the Reduced Order Models are consistent with the reference results from the original simulations, both in single design validations and when integrated as part of more advanced design processes (as optimization). Simulation time was in favor of the models but less than expected. Later investigations identified the performance bottleneck not in the model itself but rather overhead from the integration interface, which was corrected. Future developments will be aimed at improving the approach flexibility in dealing with multiple geometries, expanding the underlying modelling methodology.

References

- [1] Benner, Peter & Gugercin, Serkan & Willcox, Karen. (2015). A Survey of Projection-Based Model Reduction Methods for Parametric Dynamical Systems. SIAM Review. 57. 483-531. 10.1137/130932715.
- [2] Qian Wang, Jan S. Hesthaven, Deep Ray, Non-intrusive reduced order modeling of unsteady flows using artificial neural networks with application to a combustion problem, Journal of Computational Physics, Volume 384, 2019, Pages 289-307, ISSN 0021-9991.
- [3] Lombardi, Panzeri, Sahin, Hootsmans, Van de Waerdt. (2023). Reduced Order modelling for bird strike simulations – Extended abstract – Nafems World Congress 2023.

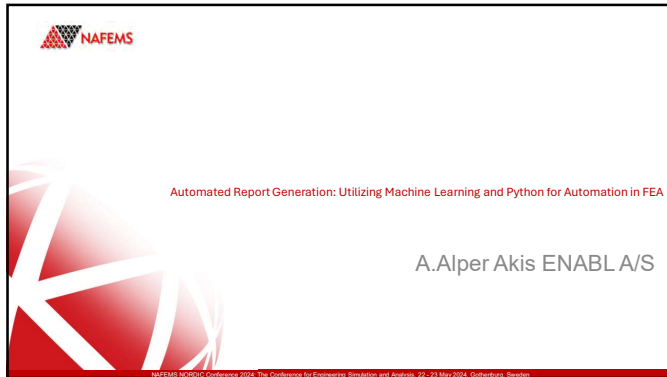
Automated Report Generation: Utilizing Machine Learning and Python for Automation in FEA

Ahmet Alper Akis (Enabl)

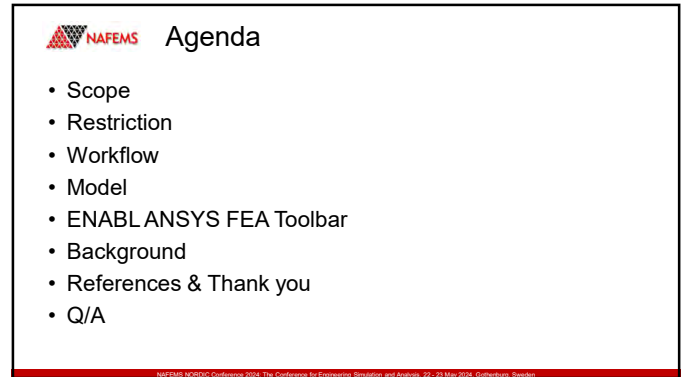
This study introduces an innovative approach to automating report generation from ANSYS Mechanical simulations using the Report Builder, incorporating machine learning techniques and Python scripts for FEA. Traditionally, creating comprehensive reports for engineering simulations requires tedious manual effort, often leading to errors and inconsistencies. Our solution simplifies this process by directly integrating with ANSYS Mechanical to extract relevant simulation data and automatically populate predefined report templates. The key component of our approach is the enhancement of the Finite Element Analysis (FEA) model through machine learning techniques, with decisions made prior to simulation.

The culmination of these advancements is the automatic generation of comprehensive reports, documenting the verification and validation options, as well as detailing the improvements made to the FEA model. This automated process not only streamlines workflow efficiency but also ensures accuracy and reliability in engineering simulations, marking a significant advancement in the field. In conclusion, our work presents a robust solution for automating report generation from ANSYS Mechanical simulations using the Builder framework.

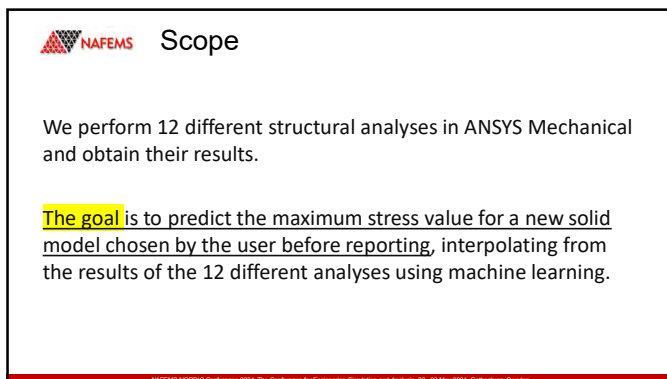
By incorporating machine learning techniques and Python scripts for FEA, we enhance the efficiency and reliability of engineering simulation workflows, enabling engineers to focus more on analysis insights and decision-making processes. Additionally, our approach provides inspiration for companies utilizing FEA to enhance their own work.



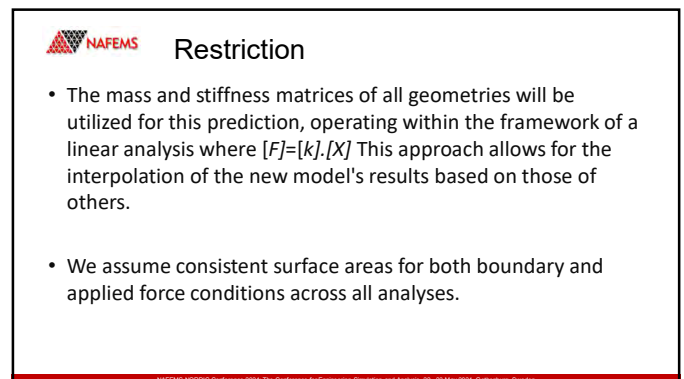
1



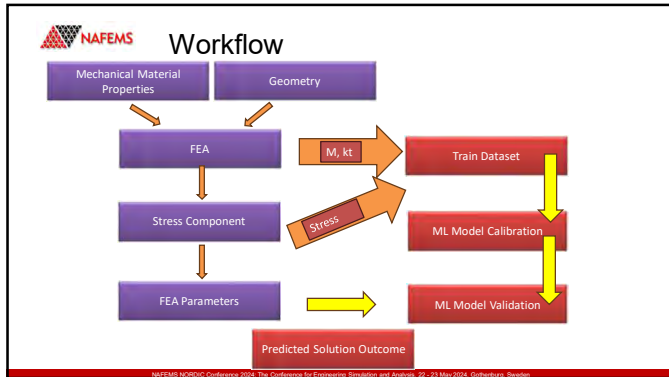
2



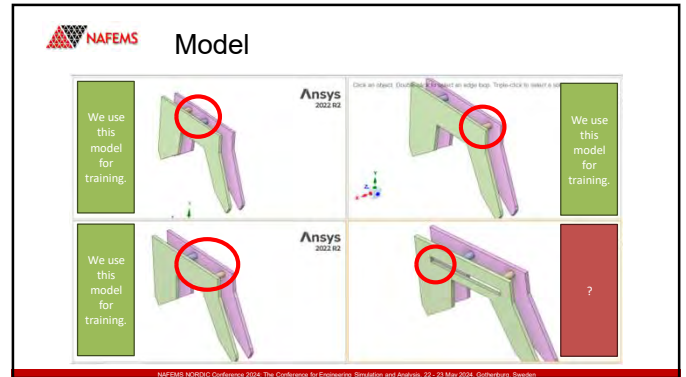
3



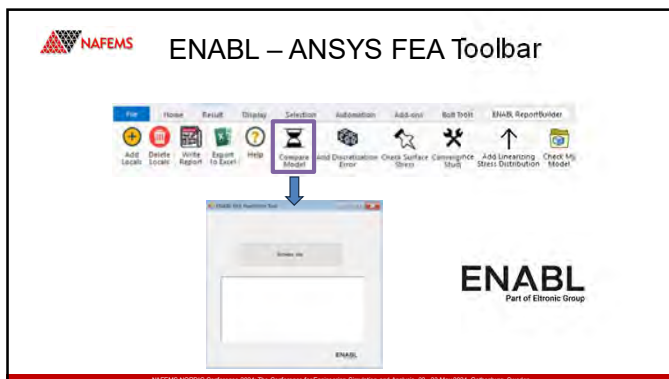
4



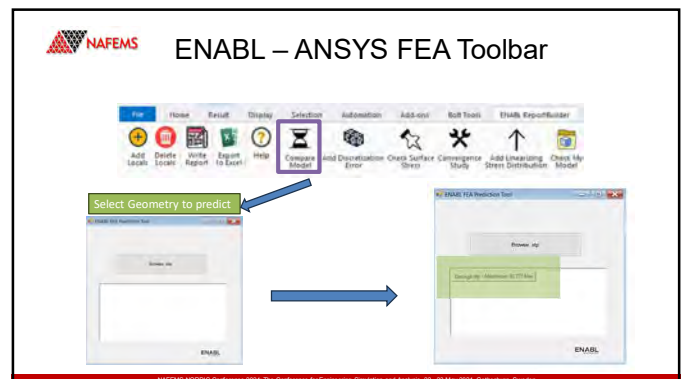
5



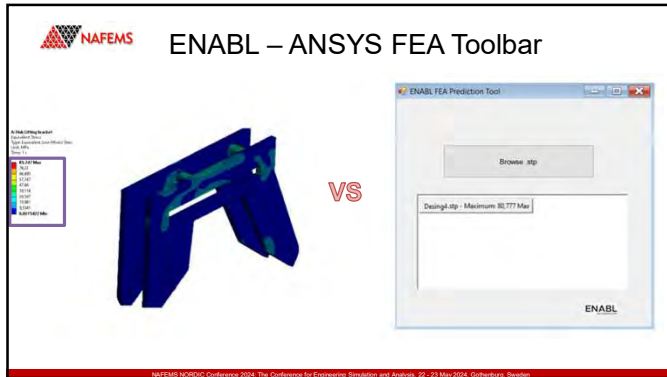
6



7



8



9

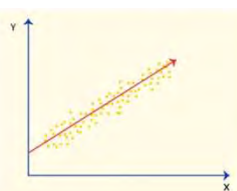
Background

- **Data Collection**
PyANSYS - Exporting .dat, stiffness and mass matrix
- **Data Preprocessing**
PyANSYS
- **Model Selection and Training**
Linear regression

10

Machine Learning - Linear Regression

- The Linear regression is used when you try to find the relationship between variables.



$$F = K \cdot X$$

The scatter plot shows a positive linear correlation between variables X and Y, with a red regression line and yellow data points.

11

General Approach

The diagram illustrates the workflow for machine learning-based FEA. It starts with a code editor showing Python scripts for data collection and preprocessing. An arrow points from the code to a 3D FEA model of a mechanical part, which is color-coded to show stress distribution. A second arrow points from the model back to the code editor, indicating an iterative or feedback process.

12



References

1. <https://docs.pyansys.com/>
2. https://www.w3schools.com/python/python_ml_getting_started.asp

NAFEMS NORDIC Conference 2024: The Conference for Engineering Simulation and Analysis 22 - 23 May 2024 Gothenburg, Sweden

13



Thank you

- ENABLA/S
- Michell Mirsbach Olsen & Anne-Mette Nils Ebbesen
- NAFEMS

NAFEMS NORDIC Conference 2024: The Conference for Engineering Simulation and Analysis 22 - 23 May 2024 Gothenburg, Sweden

14

Enabling Specialized Architectures for High-Performance Computing in Engineering Simulation on Rescale

Sam Zakrzewski (RESCALE)

1 Summary (Überschrift 1)

This presentation explores the potential of Rescale, a leading cloud high-performance computing (HPC) platform, in harnessing specialised architectures for Computational Fluid Dynamics (CFD) and Finite Element Analysis (FEA) workloads. With an increasing demand for faster and more efficient simulations, Rescale aims to optimise its infrastructure by incorporating specialised processing units, particularly Arm architecture and Nvidia GPUs.

Arm chip sets offer energy-efficient and scalable solutions, making them an attractive choice for HPC applications. Rescale's integration of Arm-based processors enables users to achieve high computational throughput while minimising energy consumption, resulting in improved cost-effectiveness for CFD and FEA simulations. Furthermore, the platform's support for Nvidia GPUs provides engineers and scientists access to powerful parallel processing capabilities, accelerating complex calculations, reducing simulation time and the opportunity to expand into AI/ML workflows.

The collaboration between Rescale and specialist HPC infrastructure developers showcases a commitment to pushing the boundaries of performance in engineering simulations. By harnessing the strengths of these specialised architectures, Rescale not only enhances the scalability and efficiency of CFD and FEA simulations but also provides users with a diverse range of hardware options to tailor their computing resources to specific application requirements. This presentation sheds light on the strategic integration of Arm and Nvidia GPUs into Rescale's HPC platform, demonstrating the diverse possibilities for advancing the capabilities of simulation-driven engineering in the cloud.

2 References (Überschrift 1)

Rescale. "Cloud Computing Infrastructure for HPC." <https://rescale.com/platform/hpc-ai-architectures/>
Rescale. "GPU Center of Excellence." <https://rescale.com/solutions/by-use-case/gpu-coe/>
Arm. "Arm HPC Ecosystem." <https://www.arm.com/solutions/high-performance-computing>
Nvidia. "NVIDIA GPU Solutions for HPC." <https://www.nvidia.com/en-us/data-center/gpu-accelerated-applications/high-performance-computing/>



Enabling Specialized Architectures for High-Performance Computing in Engineering Simulation on Rescale



2024 NAFEMS Nordic Conference
Wednesday, May 22:18:25
Session 4 A – AI/ML 3 - HPC

[Sam Zakrzewski PhD.](#), Senior Solution Architect EMEA

1



Talking Points

- ❖ Industry Trends
- ❖ Rescale Introduction
- ❖ Hardware Vendor Partnerships
- ❖ Simulation Workflows
 - Nvidia
 - Arm
- ❖ Tailoring Your Accelerator on Rescale
- ❖ AI Driven Engineering
- ❖ Conclusions

2

2

Trends Impacting Engineering Simulation Across Industries



Accelerated Computing

Performance of domain-specific architectures such as GPU and RISC (Arm), is **growing 2x faster** than traditional architectures such as x86 CPUs.



Data Sharing and Collaboration

Collaborative R&D and data sharing is reported at **70% of organizations** globally, often between academia, suppliers, & engineering services organizations.



AI-driven R&D

AI/ML enhanced R&D can **reduce product development time by 50%** while accelerating time to market and increasing efficiency.

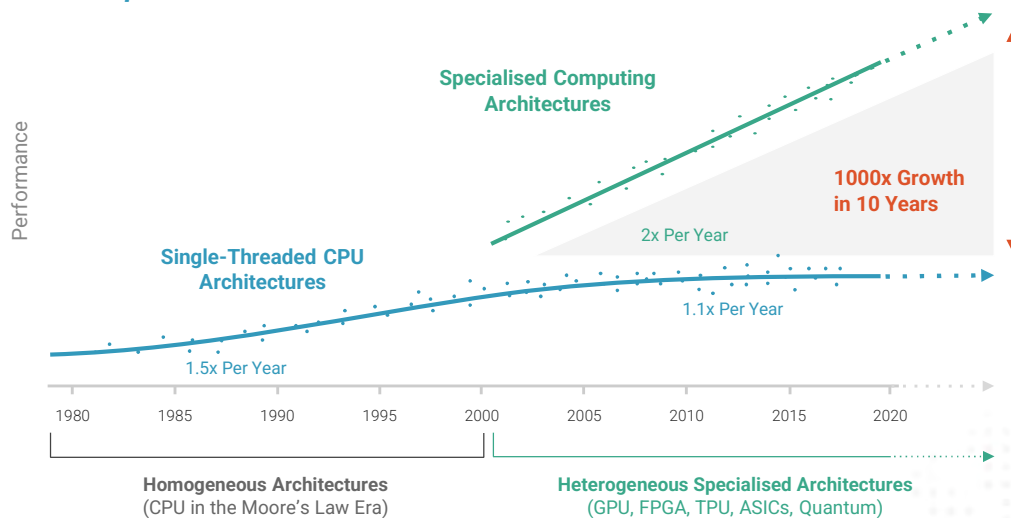


Sustainable Computing

Energy & performance improvements from new architectures in the cloud can be up to **4 times more sustainable** than on-prem.

3

New Specialised Architectures Drive Performance Gains *Domain-Specific Hardware Accelerators*

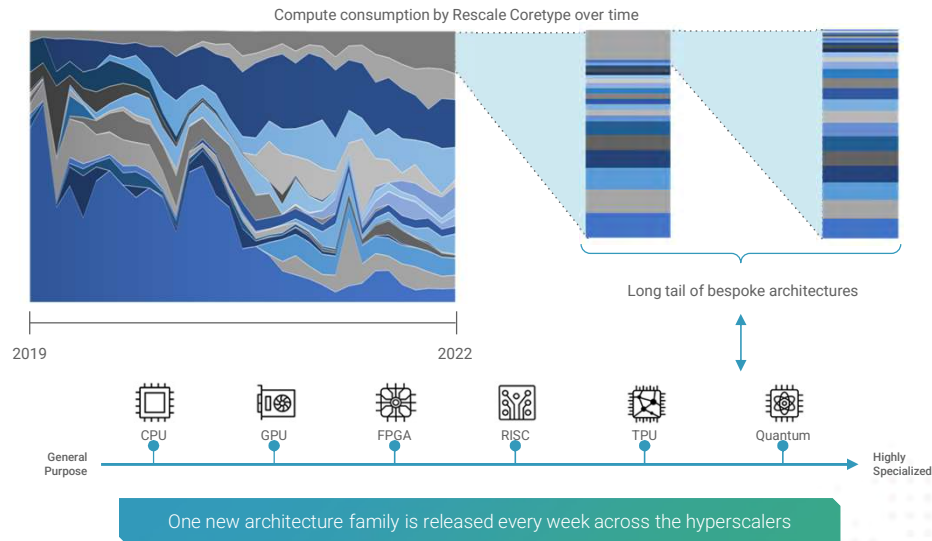


4

Source: NVIDIA

4

Rescale Customers Take Advantage of Architectural Proliferation



5

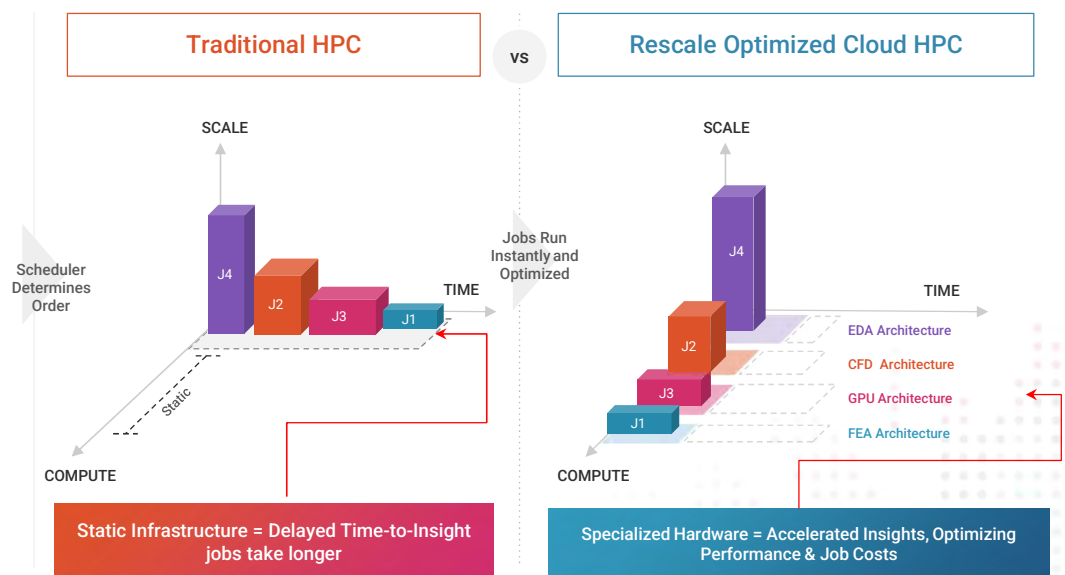
Source: Rescale Platform Intelligence

5

Specialized Architecture for each Optimized Job

Specialize Jobs with Unique Needs:

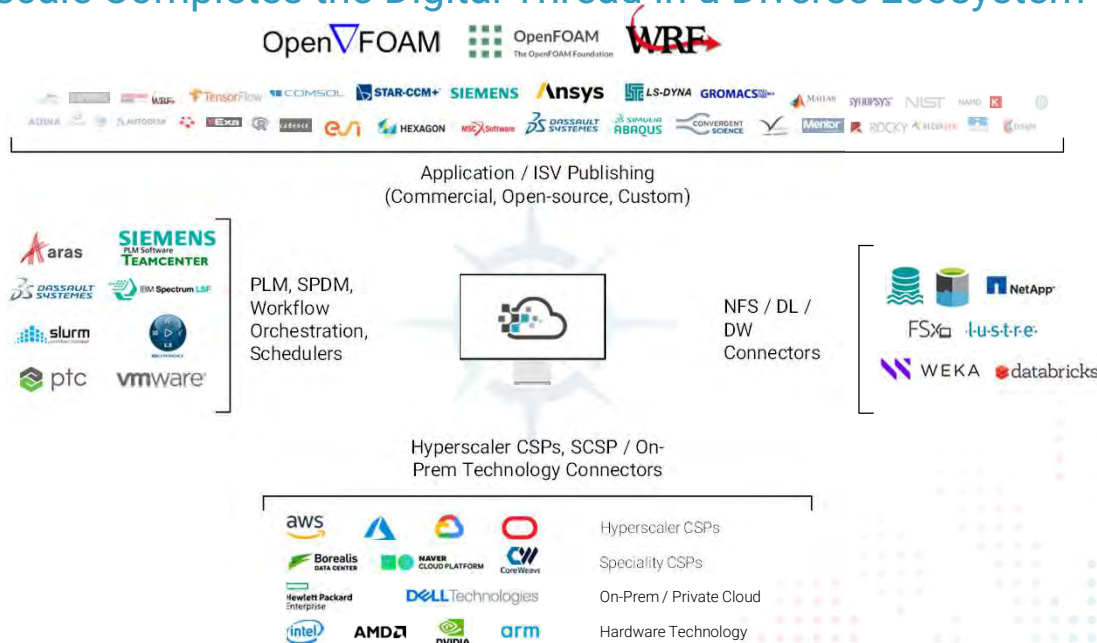
- Ansys Mechanical
High clock speed requirement
- Ansys CFX
High memory bandwidth
- Ansys Fluent
GPU requirement
- Ansys HFSS
Highly Parallelized
Large # of cores



6

6

Rescale Completes the Digital Thread in a Diverse Ecosystem



7

7

NVIDIA and Rescale: Partners in HPC and Applied AI



NVIDIA

"Rescale's cloud-based platform enables customers to run simulations on-demand and scale up or down as needed. With Rescale's performance intelligence feature, it will be easy for customers to see which applications are accelerated, and provide the best cost and efficiency benefits. **Together, we've generated tremendous cost and time savings for customers.**"

– Jensen Huang



Rescale Raises \$105M
Extended Series C

NVIDIA is a corporate investor in Rescale.



Rescale is a strategic NVIDIA go-to-market partner.



Rescale has integrated with NVIDIA NGC Catalog, NVIDIA AI Enterprise, NVIDIA DGX Cloud, and the latest NVIDIA-GPU accelerated hardware from hyperscalers.

8

8

arm



Rescale Customer Spotlight

Company: Arm
Industry: Engineering Consulting
Use Cases: Chip Design, Design Verification, High Throughput Computing

"Rescale is helping Arm usher in a new era for chip design. Arm-powered cloud computing combined with the intelligent automation of the Rescale platform brings many benefits to our design and verification processes by not only helping Arm engineers create the world's most advanced IP, but also enabling our ecosystem to take full advantage of multi-cloud resources for accelerating R&D. With Rescale, our engineering teams can access the best computing resources they need – including the price/performance and sustainability benefits of running on Arm architecture – whenever they need them."

— Mark Galbraith, VP of Productivity Engineering

9



9

Hardware Accelerators Available on Rescale



arm

- CUDA Compute / Double Precision
 - H100 - 96GB VRAM
 - Heliodor, Morganite
 - A100 - 40/80GB VRAM
 - Mallorn, Celestine, Ankerite
 - V100 - 16/32GB VRAM
 - Dolomite
 - Olive
- Visualisation, RayTracing / Single Precision
 - RTX A6000 - 48GB VRAM
 - RTX A5000 - 24GB VRAM
 - L4 - 24GB VRAM
 - A10 - 24GB VRAM
 - T4 - 16GB VRAM
 - M60 - 8GB VRAM
- Graviton 3
 - Neoverse V1 - 64 cores
 - 2662 GFlops
 - Peak Memory B/W - 307 GB/s
 - 200Gbps RDMA
 - Pectolite, Zeolite
- Graviton 2
 - Neoverse N1 - 64 cores
 - 1280 GFlops
 - Peak Memory B/W - 204 GB/s
 - Palladium, Gallium
- Ampere Altra
 - Neoverse N1
 - Azure, Google
- Grace Hopper
 - aarch64/CUDA

10

10

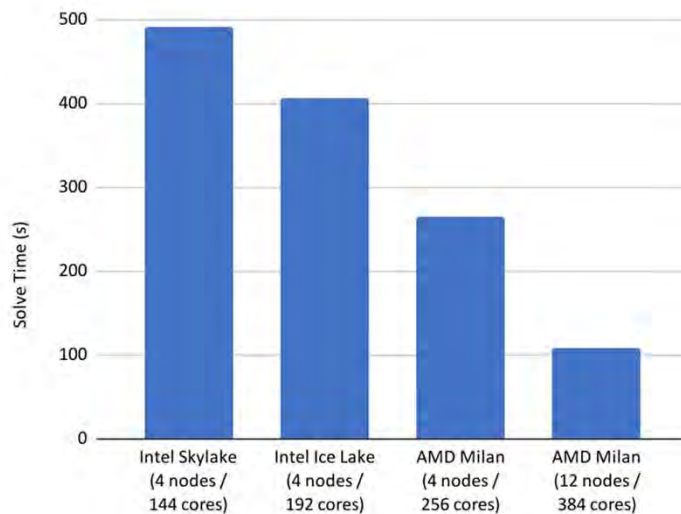
Accelerated Simulation Tools Available on Rescale



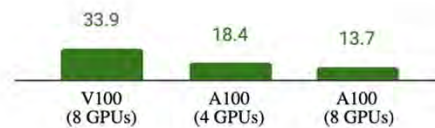
11

11

Ansys Fluent Benchmarks



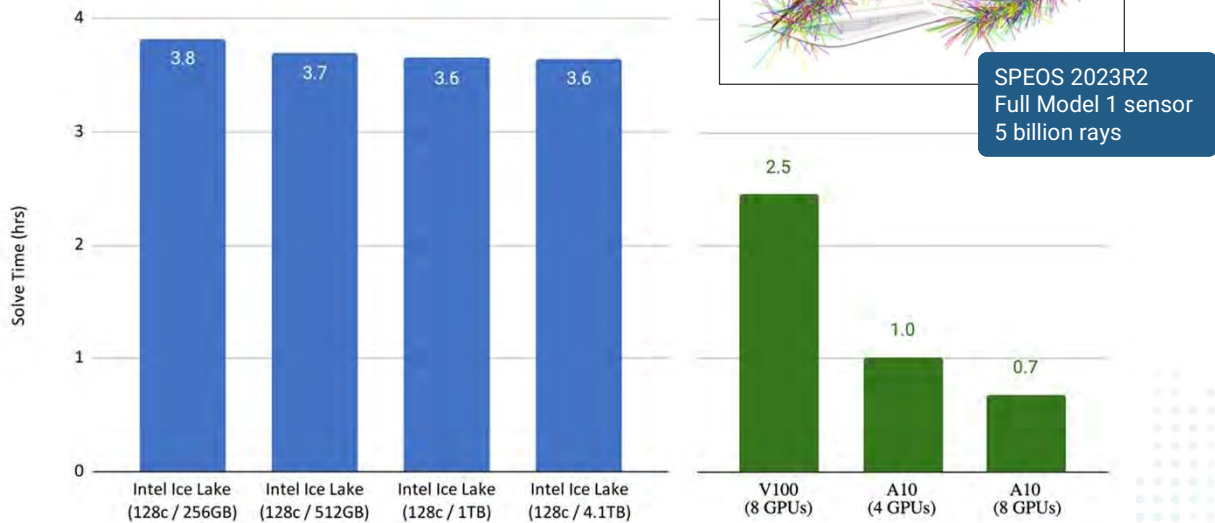
Fluent 2023R1
External Flow over Formula-1 Race Car
140 million cells
25 iterations



12

12

Ansyes SPEOS Benchmarks



13

13

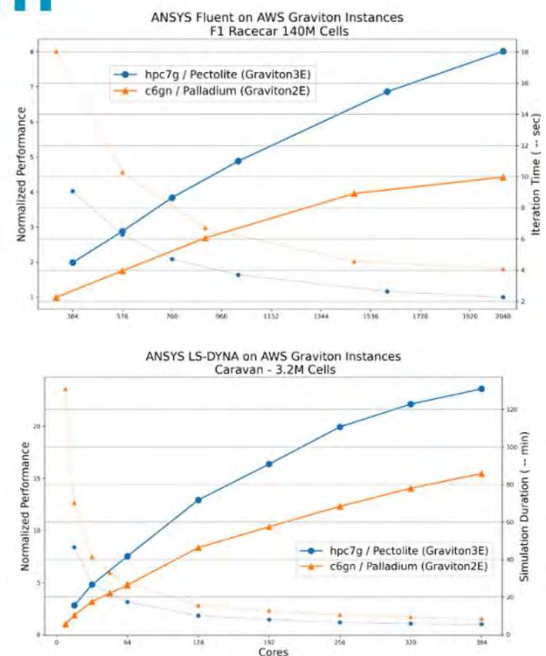
Leveraging aarch64 on Rescale



- Various ways of deploying aarch64 software:
- Most major simulations software already onboarded
- Deploy your own containerised software
 - Docker, Apptainer, Singularity
- Compile your full stack on a aarch64 instance :
 - gcc compilers available
 - acf1 and Arm Performance Libraries
- Publish your aarch64 software on the platform using [Rescale Software Publisher](https://rescale.com/blog/rescale-automates-the-deployment-of-ansys-ls-dyna-and-ansys-fluent-workloads-on-amazon-ec2-hpc7g-instances/)

<https://rescale.com/blog/rescale-automates-the-deployment-of-ansys-ls-dyna-and-ansys-fluent-workloads-on-amazon-ec2-hpc7g-instances/>

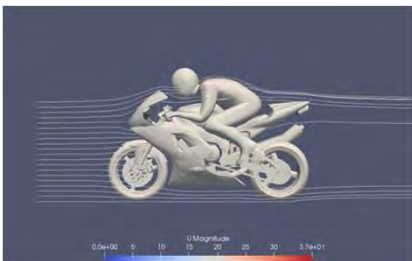
14



14

OpenFoam Single Node Benchmarks

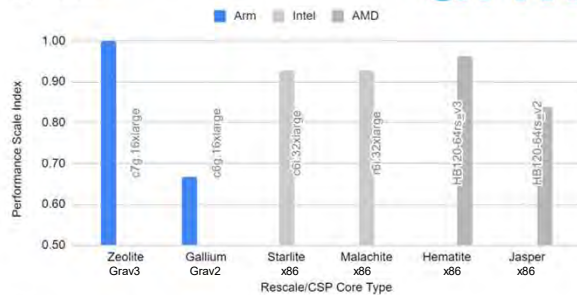
- MotorBike Tutorial simpleFoam
- OpenFOAM+ v2212
- 0.35 million cells
- 64 cores per node
- aarch64 and x86_64 compiled with gcc



15

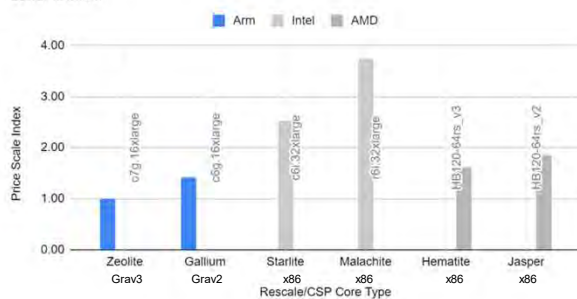
Performance Scale Index

Higher is better



Price Scale Index (CSP List Price)

Lower is better



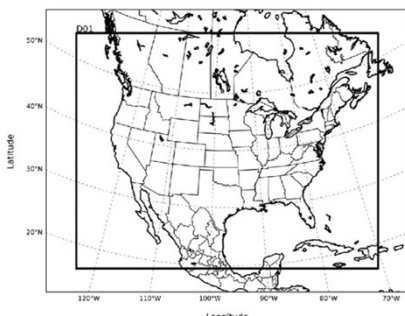
arm

rescale

15

WRF Multi Node Benchmarks

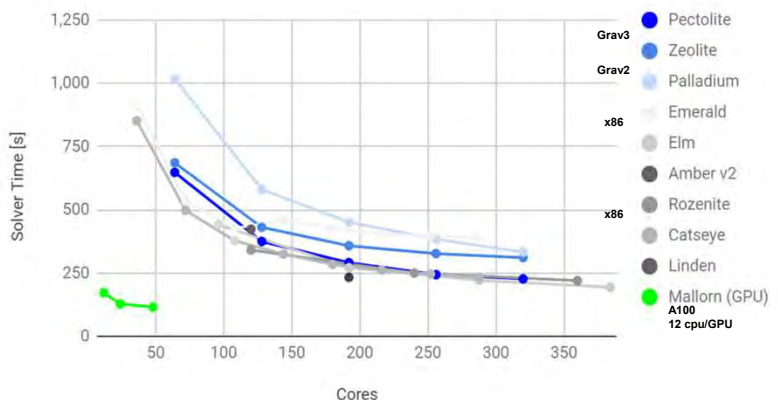
- CONUS 12km/WRF 4.x
- OpenMPI
- 425 x 300 grid points
- aarch64 compiled with aocl and x86_64 compiled with gcc
- AceCast CUDA GPU



16

Multi-node WRF 4.3

Solver Time vs Cores



- WRF has a different CPU utilisation profile than OpenFoam
- WRF is more compute bound than memory bound so floating point performance is indicative of the expected performance
- Graviton 3 comparative to Milan, Genoa and IceLake on performance and cost
- CUDA has a performance advantage
 - Not all WRF solvers have been ported

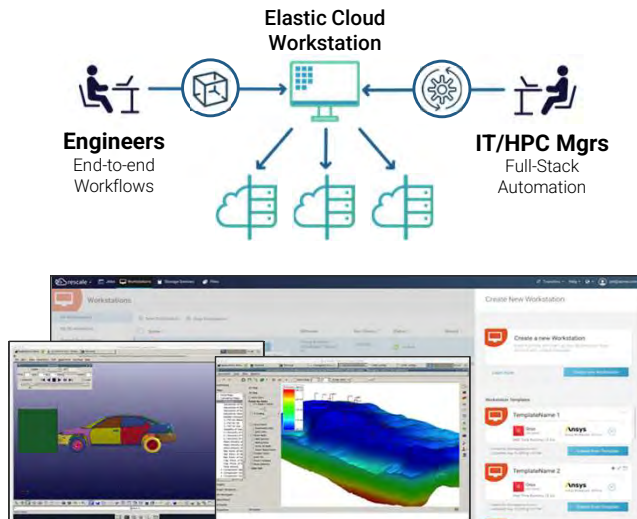
NVIDIA

arm

rescale

16

Elastic Cloud Workstations (ECW)

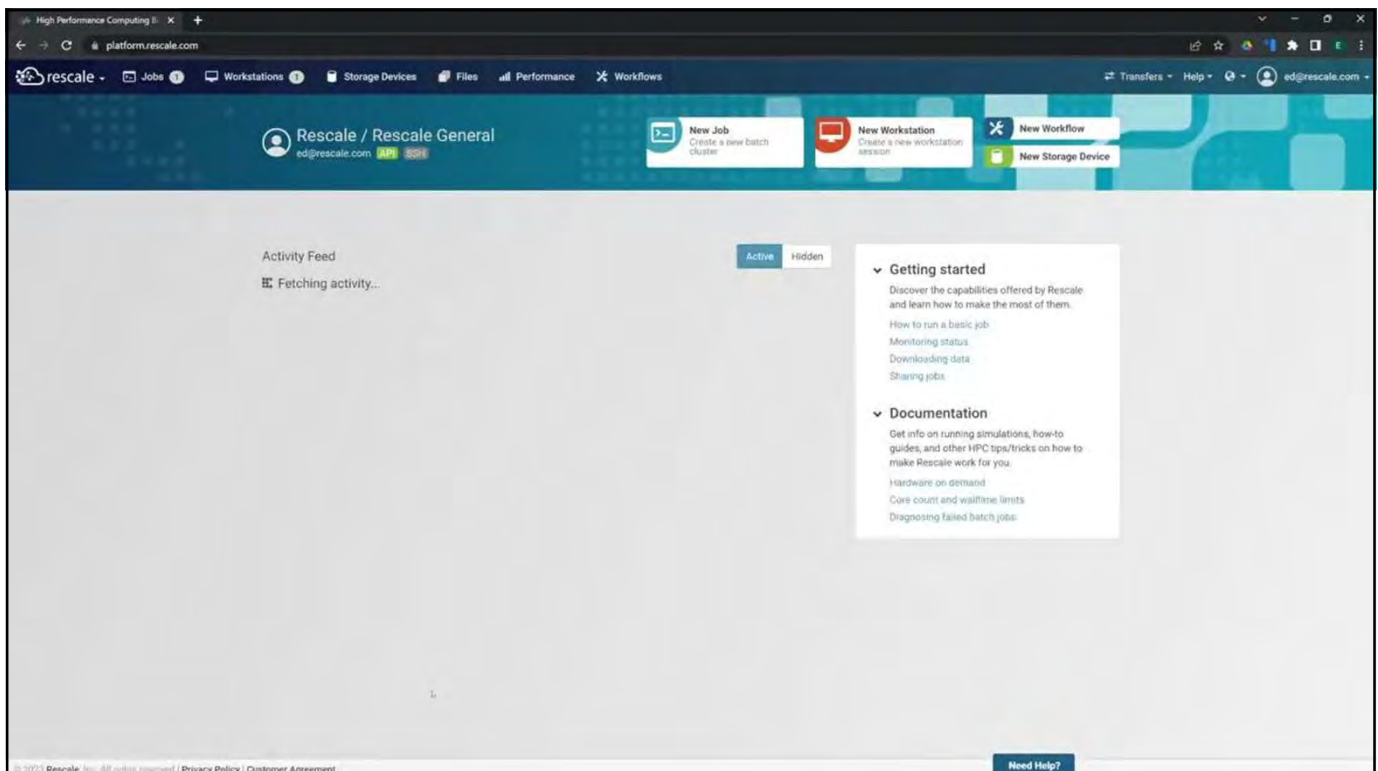


Powerful Desktop Experience at Cloud Scale

- Pre-process, solve, and post-process simulations from a rich, web-based GUI
- Launch in minutes from anywhere, and share results and collaborate with colleagues
- Access full Rescale application and infrastructure catalogs on-demand
- Accelerate your desktop simulations with the latest specialized CPU and GPU architectures
- Deploy secure desktop virtualization with Rescale's full-stack security and compliance

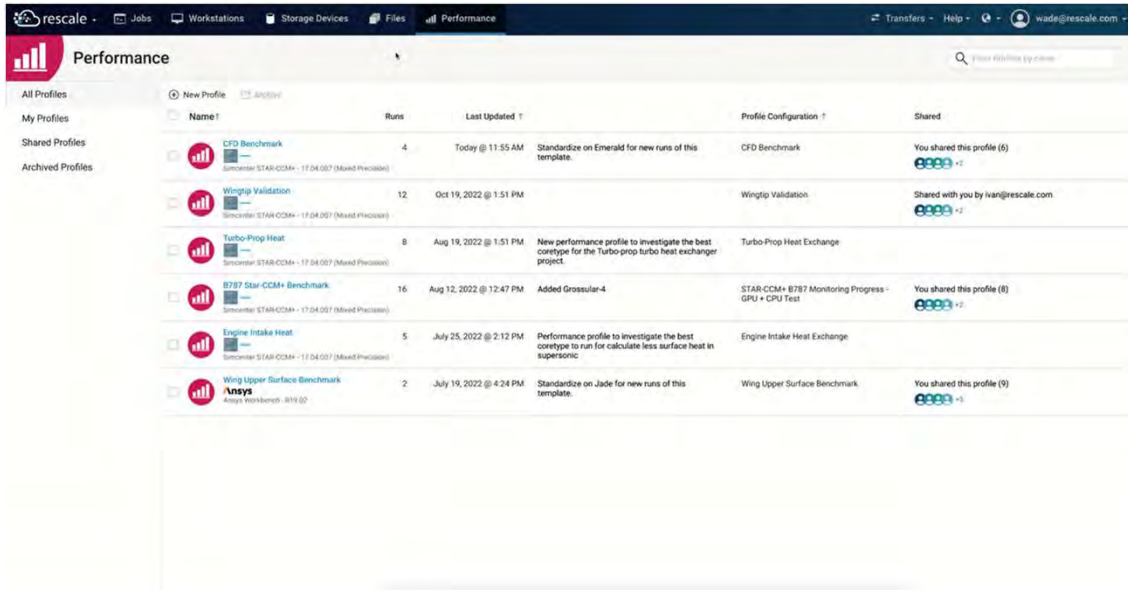
17

17



18

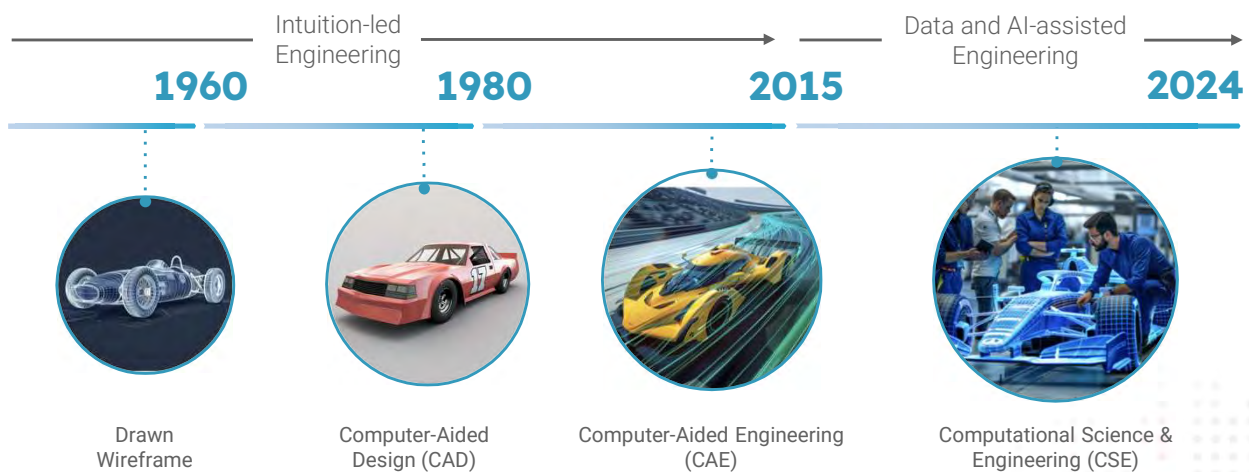
Hardware Benchmarking with Performance Profiles



Name	Runs	Last Updated	Profile Configuration	Shared
CFD Benchmark Simcenter STAR-CCM+ - 17.04.007 (Mixed Precision)	4	Today @ 11:55 AM	Standardize on Emerald for new runs of this template	CFD Benchmark You shared this profile (6)
Wingtip Validation Simcenter STAR-CCM+ - 17.04.007 (Mixed Precision)	12	Oct 19, 2022 @ 1:51 PM		Wingtip Validation Shared with you by Ivan@rescale.com
Turbo-Prop Heat Simcenter STAR-CCM+ - 17.04.007 (Mixed Precision)	8	Aug 19, 2022 @ 1:51 PM	New performance profile to investigate the best coretype for the turbo-prop turbo-heat exchanger project	Turbo-Prop Heat Exchange
B787 Star-CCM+ Benchmark Simcenter STAR-CCM+ - 17.04.007 (Mixed Precision)	16	Aug 12, 2022 @ 12:47 PM	Added Grossular-4	STAR-CCM+ B787 Monitoring Progress - GPU + CPU Test You shared this profile (8)
Engine Intake Heat Simcenter STAR-CCM+ - 17.04.007 (Mixed Precision)	5	July 25, 2022 @ 2:12 PM	Performance profile to investigate the best coretype to run for calculate less surface heat in supersonic	Engine Intake Heat Exchange
Wing Upper Surface Benchmark Ansys Workbench - 3019.02	2	July 19, 2022 @ 4:24 PM	Standardize on Jade for new runs of this template	Wing Upper Surface Benchmark You shared this profile (9)

19

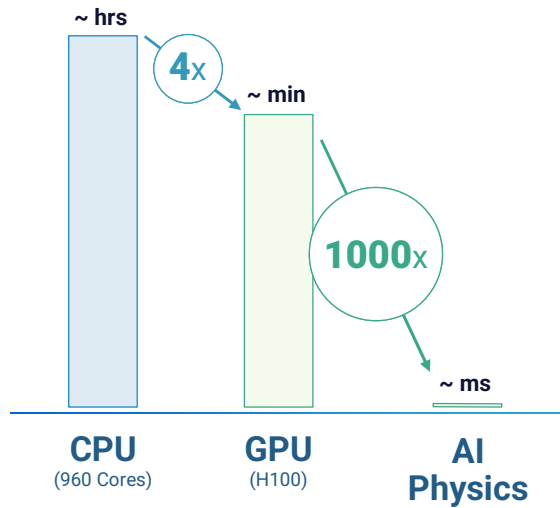
AI is Driving Transformation in Engineering



20

20

AI and Accelerated Computing Enable AI Physics Breakthroughs



- Computational reducibility unlocks accurate predictive physics
- Breakthroughs in AI frameworks, and neural network development
- Accelerated computing further fuels accelerated algorithms
- Pre-trained physics models can provide compounding advantages

21

21

Custom AI Models for Continuous Product Improvement

Design Exploration & Optimization Cycle with Simulation + AI

1 Simulation Data Generation



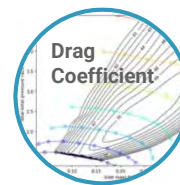
Generate physics-based CFD data, label data & prepare training datasets

2 Model Training & Deployment



Automate workflows for training & deploying custom AI models

3 Inference & Prediction



Run inference to rapidly evaluate one or many designs with AI-driven predictions

Validation & Tuning
Validate prediction accuracy and improve AI models with additional simulation

22

22

Conclusions

- ❖ The Rescale platform allows engineers to **seamlessly leverage** the latest Domain-Specific Hardware Accelerator technologies to drive their digital product development cycle
- ❖ Domain-specific accelerators are a major step forward in terms of HPC **applicability and performance** compared to traditional x86 based HPC.
- ❖ Rescale works together with the **foremost hardware manufacturers** to ensure **efficient and performant** compute resources are available at **all times** in most **regions of the world**.
- ❖ Benchmarks show that the latest **Arm** and **Nvidia** architecture chips are **industry leading** in both Performance and Cost
- ❖ Engineers are able to tailor their **bespoke pipeline** on Rescale and deploy them on the most appropriate architecture with a consistent methodology in **matter of days**
- ❖ AI/ML Physics workflows can be accelerated to gain **extensive insight** into the design space and significantly **reduce computational cost and time**
- ❖ Migrating to these accelerated workflows is a **trivial exercise** for **all compatible HPC workflows** on Rescale

23

23

Start your free trial today!

Rescale Test Drive

Instant access to high performance computing for engineering and scientific applications

Digitally transform your R&D process

Join thousands of global leaders developing new innovations across industries including aerospace, automotive, energy, government, higher education, life sciences, industrial manufacturing, semiconductor, and electronics.

Visit: <https://eu.rescale.com/signup/>

Scan Me



24

24



High Performance Computing Built for the Cloud



Digital
Engineering



Workload
Optimization



Intelligent
Automation



Security &
Compliance

Become a Rescale Certified User Expert. Learn more at rescale.com/training

Fracture Modeling of Layered Composites in a Specialized Off-Axis Finite Element Framework

Leon Herrmann (TUM), Lars Pilgaard Mikkelsen (DTU), Brian Nyvang Legarth (DTU), Fabian Duddeck (TUM), Christian Niordson (DTU)

Abstract

Fiber-reinforced composites under tension typically fail in three distinct stages: (I) tunneling crack initiation and propagation in off-axis layers, (II) delamination, and (III) fiber fracture in load-carrying layers. These processes are typically modeled by considering homogenized plies and three-dimensional simulations of the laminates. These three-dimensional simulations on small length scales are computationally expensive. To this end, we have introduced a specialized finite element, exploiting the strain field's invariance in the off-axis fiber direction. This enables a reduction to an efficient two-dimensional model with a speed-up between three and four orders of magnitude.

The specialized off-axis finite element is applied to laminates with periodic defects, enabling a further reduction in model size, namely a single period. This enables efficient stiffness degradation models with tunneling and delamination cracks for different layups, validated against experimental data from the literature. With the compliance method, stiffness degradation curves can be differentiated in order to obtain energy release rates without additional simulations, thus predicting damage propagation. Lastly, microstructures have also been incorporated into the individual layers in order to determine the accuracy of the corresponding homogenized models, where we found that homogenized models capture the fracture behavior sufficiently well.

In summary, an off-axis finite element framework is presented, which is able to simulate arbitrary layups with tunneling and delamination cracks with and without microstructures. From these, both stiffness and energy release rates are extracted.

Fracture modeling of layered composites in a specialized off-axis finite element framework

Leon Herrmann

Chair of Computational Modeling and Simulation, Technical University of Munich

leon.herrmann@tum.de

<https://www.cee.ed.tum.de/cms/team/leon-herrmann/>

Lars Pilgaard Mikkelsen

Brian Nyvang Legarth

Fabian Duddeck

Christian Frithiof Niordson

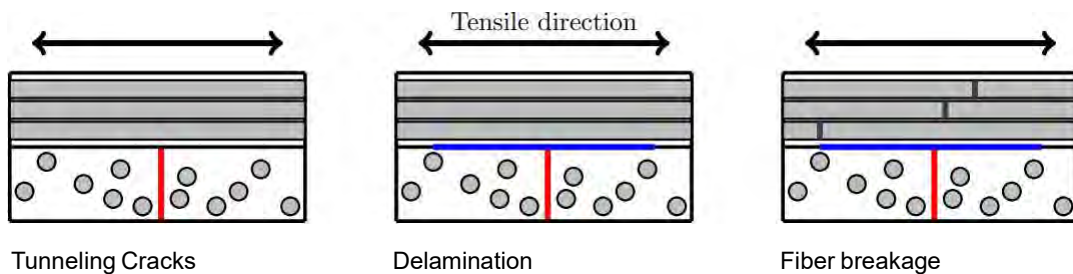
Leon Herrmann

22.05.2024

1

1

Damage mechanisms in fiber-reinforced composites under tension



Leon Herrmann

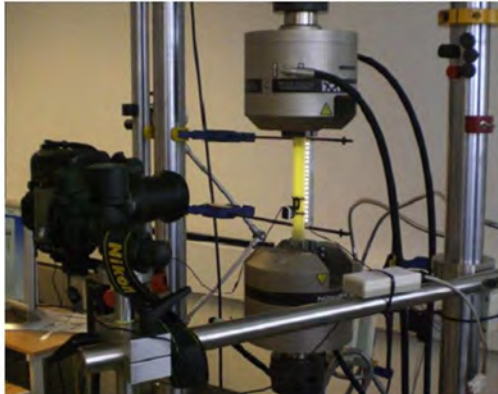
22.05.2024

2

2

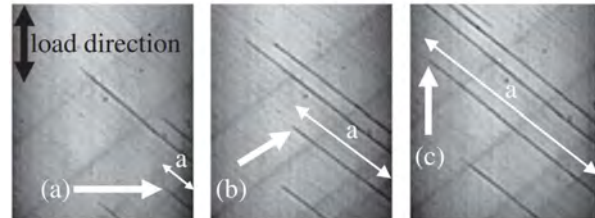
Tunnel cracking during fatigue loading $[0/\theta/0/-\theta]_s$

Fatigue test set-up and acquisition system



(Quaresimin et al. 2014)

Off-axis crack growth during fatigue loading

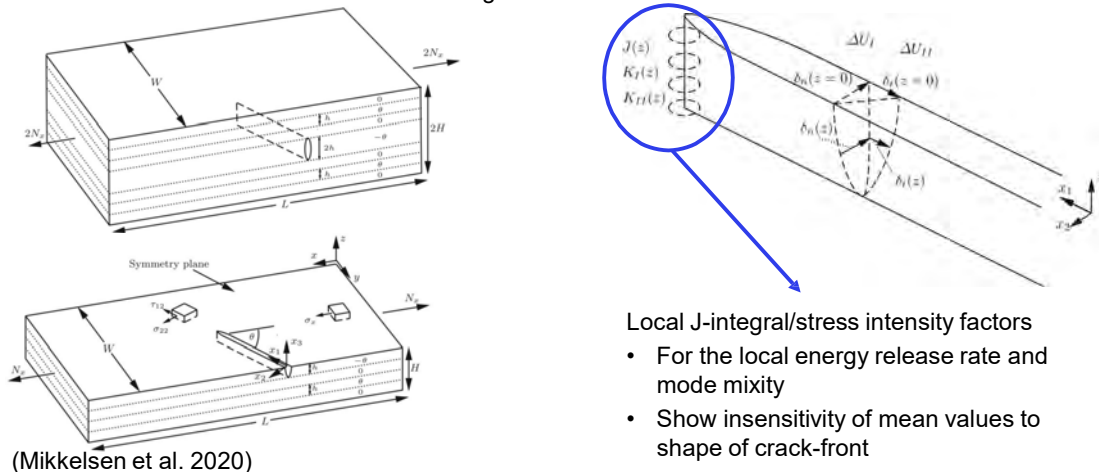


Steady-state crack growth

- Energy release rate estimation $G_{ss} = ?$
- Mode mixity estimation $\psi = ?$

Crack-tip condition along straight crack-front

Estimation of fracture behaviour through 3D finite element simulations



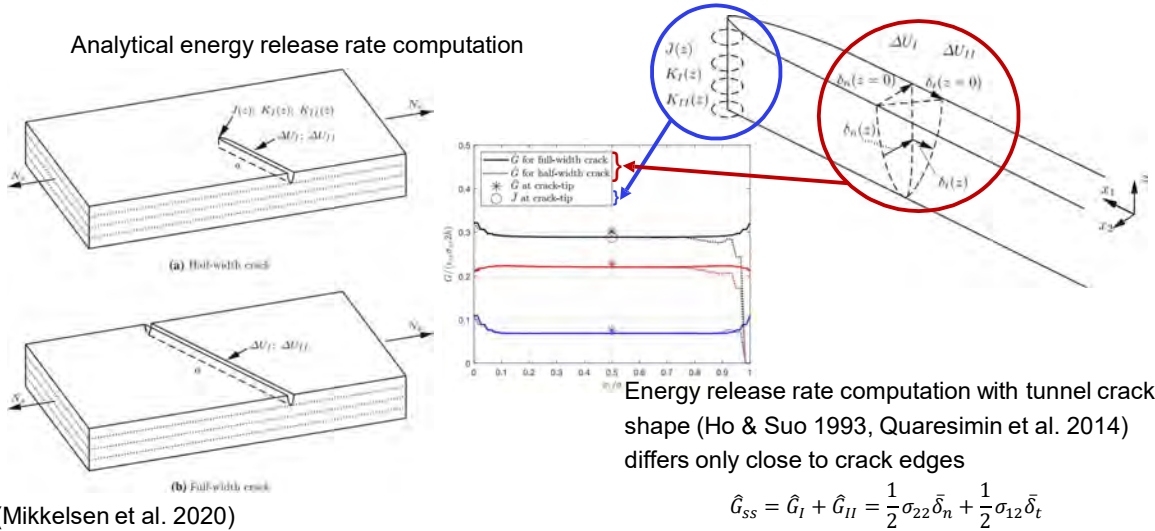
(Mikkelsen et al. 2020)

Local J-integral/stress intensity factors

- For the local energy release rate and mode mixity
- Show insensitivity of mean values to shape of crack-front

From crack-tip to tunnel crack shape

Analytical energy release rate computation



Leon Herrmann

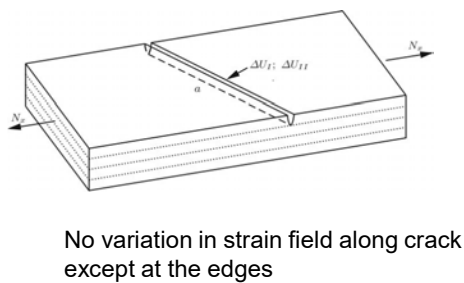
22.05.2024

5

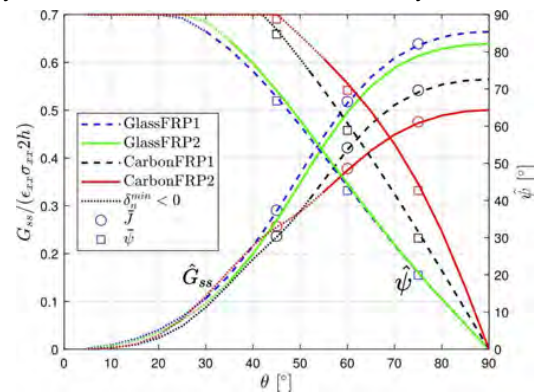
5

Tunneling crack: Crack-tip and energy method

Without consideration of the crack-tip, the energy release rates are estimated accurately



(Mikkelsen et al. 2020)



Leon Herrmann

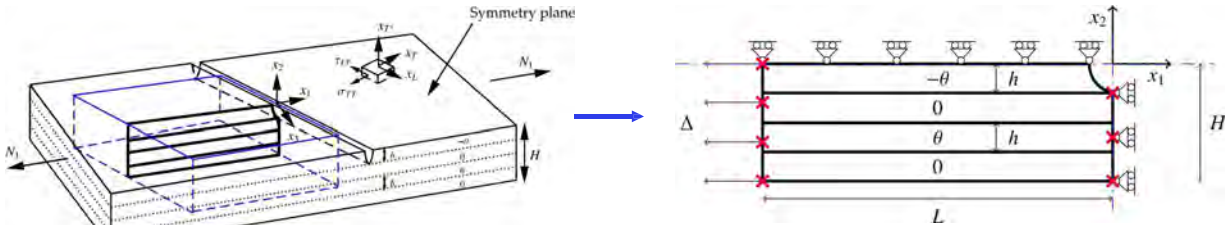
22.05.2024

6

6

3D full-width crack → 2D off-axis model

Due to lack of variation, i.e. a steady state along the crack, a 2D representation is possible

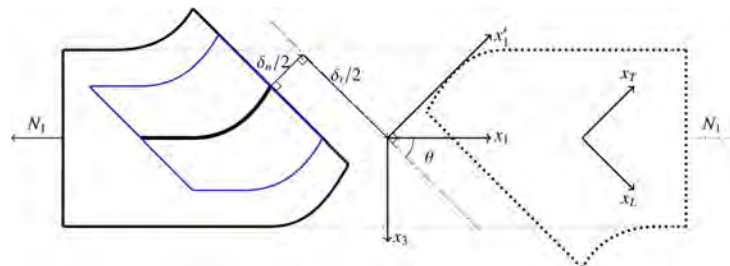


The deformation field on the 2D plane is still 3D. How can this be modelled?

(Mikkelsen et al. 2022)

2D off-axis finite element framework

Top view to illustrate the kinematics of the problem



Out-of-plane strain components can be defined in terms of in-plane derivatives

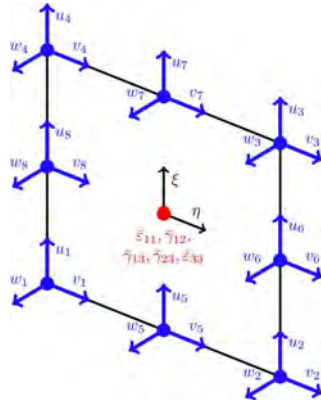
$$\begin{aligned}\gamma_{13} &= \bar{\gamma}_{13} + \cot(\theta)\bar{\epsilon}_{11} - \cot(\theta)u_{1,1} + \tilde{u}_{3,1} \\ \gamma_{23} &= \bar{\gamma}_{23} + \frac{1}{2}\cot(\theta)\bar{\gamma}_{12} - \cot(\theta)u_{2,1} + \tilde{u}_{3,2} \\ \epsilon_{33} &= \bar{\epsilon}_{33} - \cot(\theta)\tilde{u}_{3,1}\end{aligned}$$

$\bar{\epsilon}_{11}, \bar{\gamma}_{12}, \bar{\gamma}_{13}, \bar{\gamma}_{23}, \bar{\epsilon}_{33}$ are the far-field components

(Mikkelsen et al. 2022)

2D off-axis finite element framework

Discretization via finite elements. Here using a quadratic quadrilateral serendipity element



$$B = \begin{bmatrix} N_{1,1} & 0 & 0 & \dots & N_{M,1} & 0 & 0 & 0 & 0 & 0 & 0 & 0 \\ 0 & N_{1,2} & 0 & \dots & 0 & N_{M,2} & 0 & 0 & 0 & 0 & 0 & 0 \\ N_{1,2} & N_{1,1} & 0 & \dots & N_{M,2} & N_{M,1} & 0 & 0 & 0 & 0 & 0 & 0 \\ -c'N_{1,1} & 0 & N_{1,1} & \dots & -c'N_{M,1} & 0 & N_{M,1} & c' & 0 & 1 & 0 & 0 \\ 0 & -c'N_{1,1} & N_{1,2} & \dots & 0 & -c'N_{M,1} & N_{M,2} & 0 & \frac{1}{2}c' & 0 & 1 & 0 \\ 0 & 0 & -c'N_{1,1} & \dots & 0 & 0 & -c'N_{M,1} & 0 & 0 & 0 & 0 & 1 \end{bmatrix}$$

$$\epsilon = BD$$

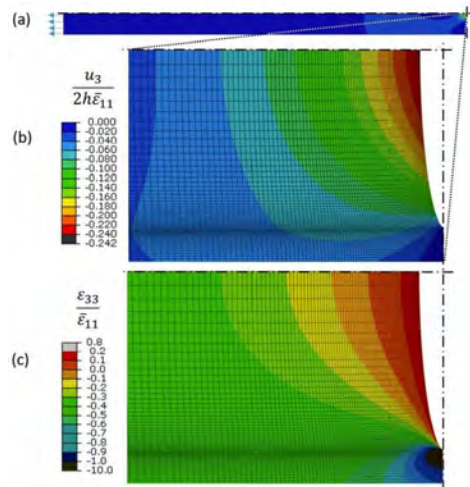
$$\epsilon^T = \{\epsilon_{11}, \epsilon_{22}, \gamma_{12}, \gamma_{13}, \gamma_{23}, \epsilon_{33}\}^T$$

$$D^T = \{u_1^{(1)}, u_2^{(1)}, \bar{u}_3^{(1)}, \dots, u_1^{(M)}, u_2^{(M)}, \bar{u}_3^{(M)}, \bar{\epsilon}_{11}, \bar{\gamma}_{12}, \bar{\gamma}_{13}, \bar{\epsilon}_{33}\}^T$$

The far field strains are global degrees of freedom shared by all elements

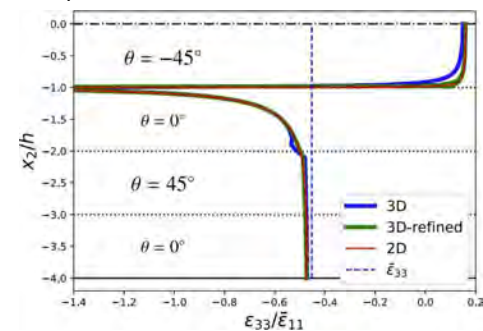
(Mikkelsen et al. 2022), Illustration from (Herrmann et al. 2022a)

Predictions by the 2D off-axis model



(Mikkelsen et al. 2022)

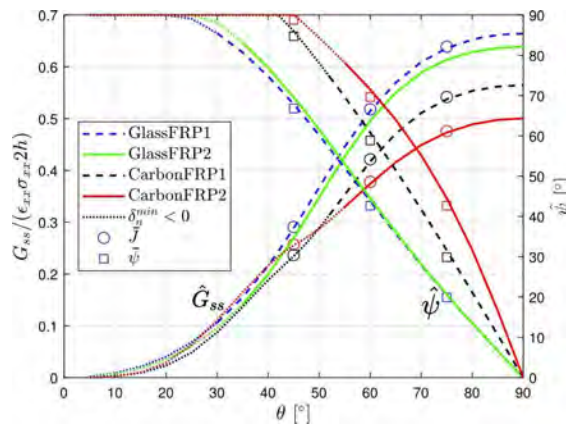
Comparison of deformations



Comparison of computation times

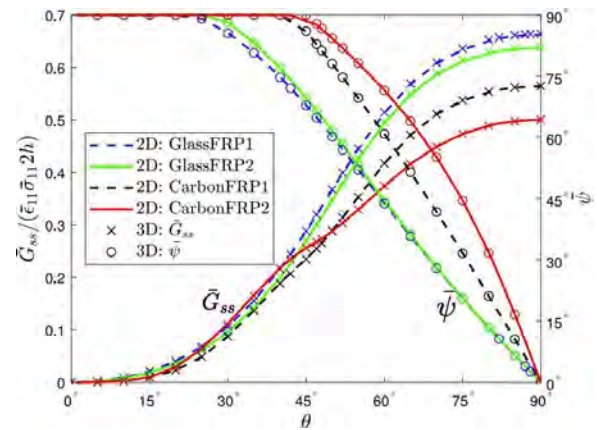
- 3D on 200 CPUs: 2-5 hours
- 2D on 1 CPU: 5 seconds

Crack-tip → 3D full-width



(Mikkelsen et al. 2020)

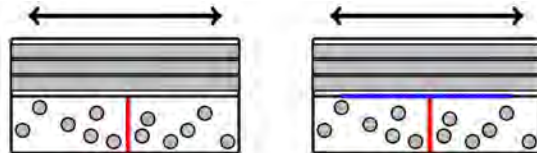
3D full-width → 2D off-axis



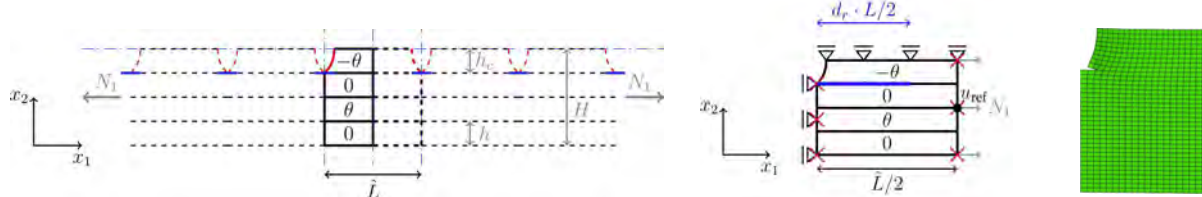
(Mikkelsen et al. 2022)

Stiffness degradation predictions

Application of the off-axis framework to stiffness degradation caused by Tunnel cracks Delamination cracks



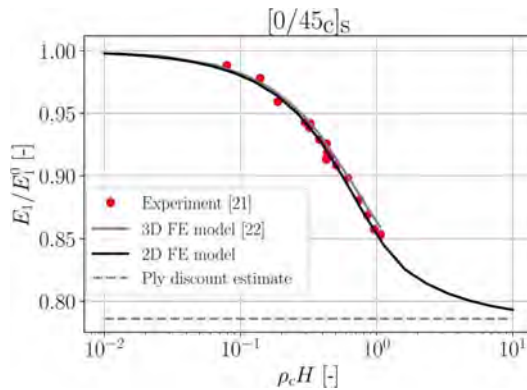
Modeling by assuming periodicity and exploiting symmetry



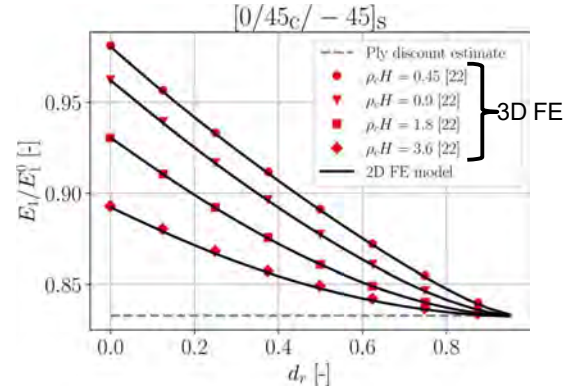
(Herrmann et al. 2022a)

Validation of predictions of stiffness degradations

Tunnel crack density $\rho_c H$



Tunnel crack density and delamination ratio



(Herrmann et al. 2022a)

Leon Herrmann

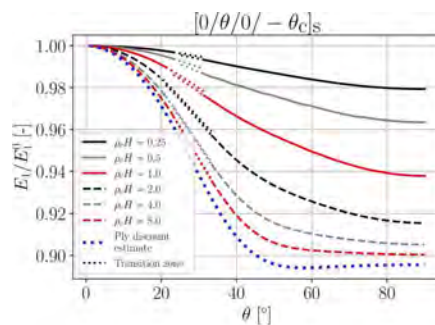
22.05.2024

13

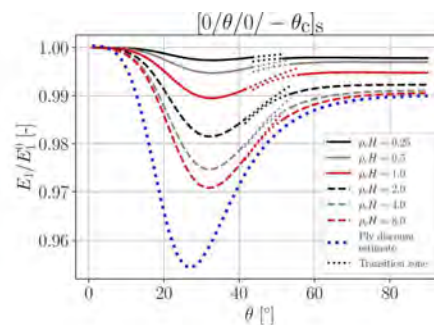
13

Cheap parametric studies of stiffness degradations

Influence of the orientation θ on the stiffness degradation for various tunnel crack densities



(a) GlassFRP.



(b) CarbonFRP.

(Herrmann et al. 2022a)

Leon Herrmann

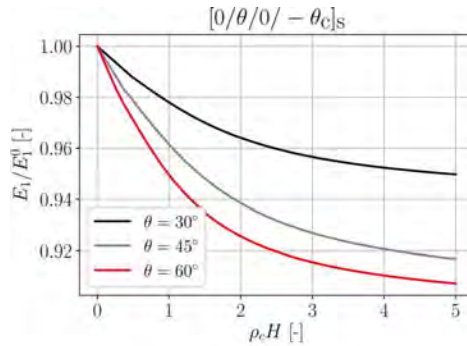
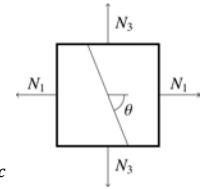
22.05.2024

14

14

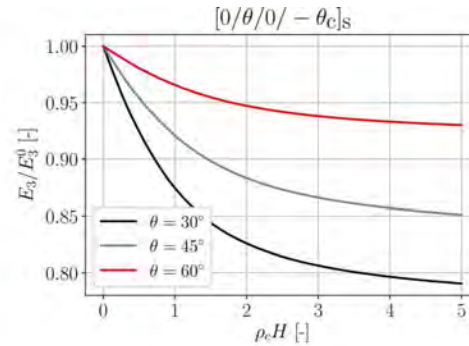
Stiffness degradation in two directions

Axial and transverse stiffness degradation for different tunneling crack densities ρ_c



(a) Axial stiffness degradation E_1 .

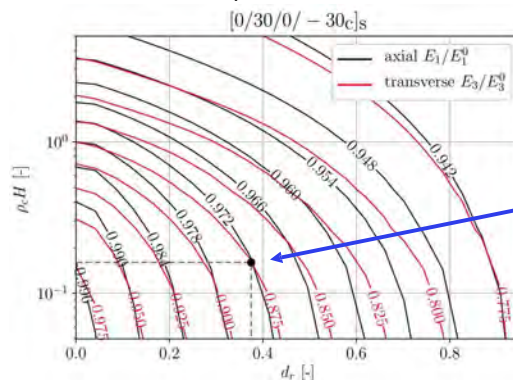
(Herrmann et al. 2022a)



(b) Transverse stiffness degradation E_3 .

Predicting $\rho_c H$ and d_r from stiffness degradation

Solving the inverse problem of identifying state of cracks from stiffness observations by generating entire contoursurface of the problem



Example identification at intersection of contourlines for the measurements

- Axial 0.875
- Transverse 0.972

(Herrmann et al. 2022a)

From stiffness degradations to energy release rates

The energy release rate in terms of change in internal energy ΔU and external work ΔW

$$\mathcal{G} = -\frac{\Delta \Pi}{\Delta A} = -\frac{\Delta U + \Delta W}{\Delta A} = -\frac{\Delta W}{2\Delta A}$$

The external work is the work during crack propagation, i.e. going from Δ_1^0 to Δ_1^1

$$\Delta W = (\Delta_1^0 - \Delta_1^1)N_1$$

The energy release rate can thus be related to the compliance $C_1 = \Delta_1/N_1$

$$\mathcal{G} = \frac{\Delta C_1 N_1^2}{2\Delta A}$$

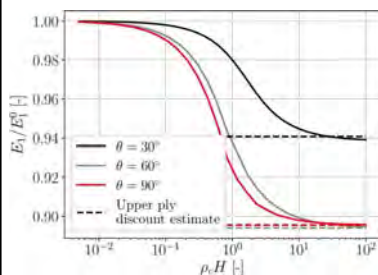
Possibility of going from stiffness degradations to energy release rates without simulation

(Herrmann et al. 2024)

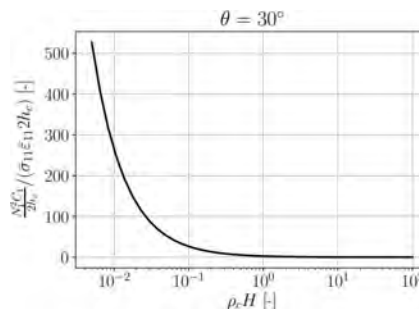
From stiffness degradations to energy release rates

The energy release rate can thus be related to the compliance

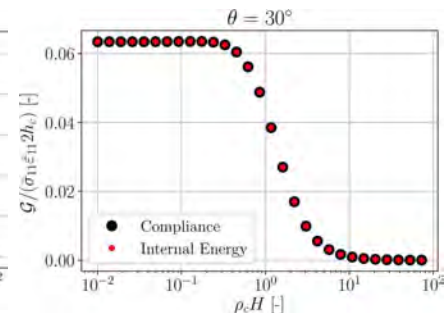
$$\mathcal{G} = \frac{\Delta C_1 N_1^2}{2\Delta A}$$



Stiffness



Compliance

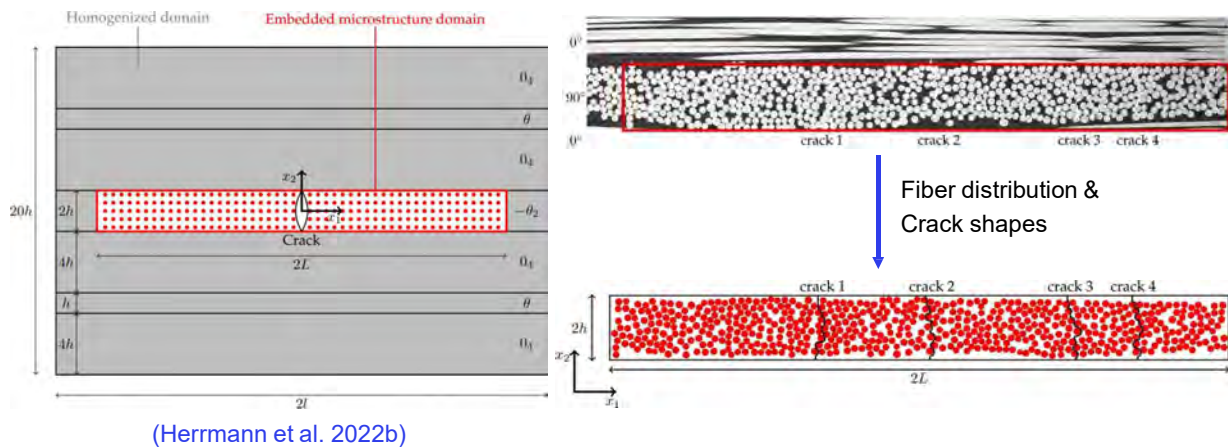


Energy release rate

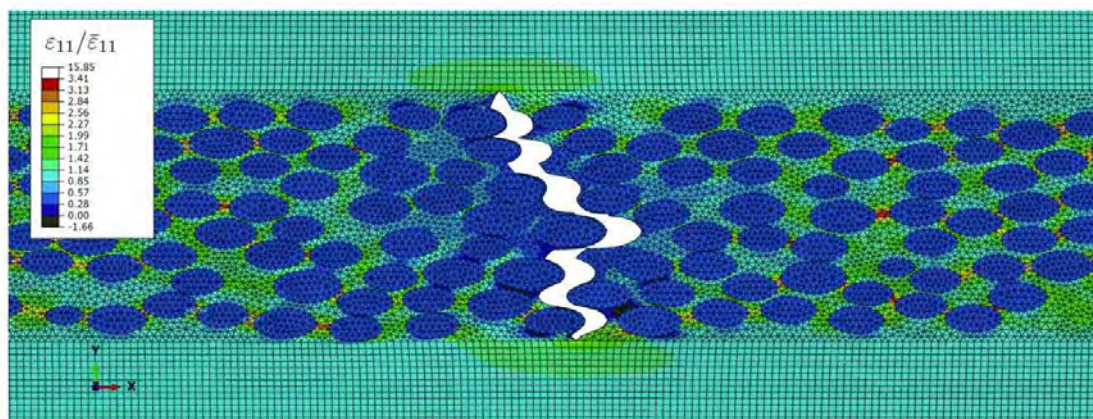
(Herrmann et al. 2024)

Effect of micro-structure in center tunneling crack in $[0_4/\theta/0_4/-\theta]_s$

Realistic microstructure from (Mortensen et al. 2022) is modeled in the cracked layer



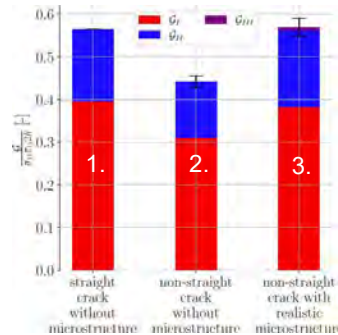
Modelling off-axis cracks in realistic microstructures



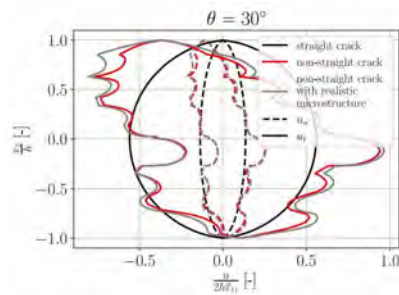
Effect modeling the micro-structure on the energy release rate

Three cases

1. Straight crack without microstructure
2. Non-straight crack without microstructure
3. Non-straight crack with microstructure



(Herrmann et al. 2022b)



The energy release rate is captured well by the homogenized model with a straight crack

Adding only a non-straight crack is a bad idea

Conclusion

The specialized off-axis finite element framework was used to create a model, that is able to tackle a variety of problems related to the damage mechanisms in fiber-reinforced composites

- Energy release rate predictions of tunneling cracks
- Energy release rate predictions of delamination cracks
- Axial stiffness degradation predictions
- Fatigue predictions using Paris-like power laws
- Possible inclusion of
 - Fiber-matrix microstructure
 - Non-straight cracks

Future work could include material non-linearities, fiber breakage, more in-depth fatigue studies and much more!

Publications

(Mikkelsen et al. 2022)

A special finite element method applied to tunnel cracking in laminates

Mikkelsen, L. P., Legarth, B. N., Herrmann, L., Christensen, M. M., Niordson, C. F., *Engineering Fracture Mechanics*, 2022

(Herrmann et al. 2022a)

An efficient stiffness degradation model for layered composites with arbitrarily oriented tunneling and delamination cracks, Herrmann, L., Mikkelsen, L. P., Legarth, B. N., Duddeck, F., Niordson, C. F., *Composites Science and Technology*, 2022

(Herrmann et al. 2022b)

The influence of the fiber-matrix microstructure on off-axis tunnel cracking in laminates, Herrmann, L., Mikkelsen, L. P., Legarth, B. N., Niordson, C. F., *Composites Part B: Engineering*, 2022

(Herrmann et al. 2024)

The compliance method for tunnel and delamination cracks, Herrmann, L., Mikkelsen, L. P., Legarth, B. N., Niordson, C. F., *in review at International Journal of Solids and Structures*, 2024

References

(Ho & Suo 1993)

Tunneling Cracks in Constrained Layers, Ho, S., Suo, Z., *Journal of Applied Mechanics*, 1993

(Quaresimin et al. 2014)

Damage evolution under cyclic multiaxial stress state: A comparative analysis between glass/epoxy laminates and tubes, Quaresimin, M., Carraro, P. A., Mikkelsen, L. P., Lucato, N., Vivian, L., Brøndsted, P., Sørensen, B. F., Varna, J., Talreja, R., *Composites Part B: Engineering*, 2014

(Mikkelsen et al. 2020)

Tunneling cracks in arbitrary oriented off-axis lamina, Mikkelsen, L. P., Klitgaard, S. J., Niordson, C. F., Sørensen, B. F., *International Journal of Fracture*, 2020

(Mortensen et al. 2022)

Observations of fatigue damage in uni-directional non-crimp fabric composites subjected to cyclic bending loads, Mortensen, U. A., Mikkelsen, L. P., Andersen, T. L., *Journal of Composite Material*, 2022

Fracture modeling of layered composites in a specialized off-axis finite element framework

Leon Herrmann
Chair of Computational Modeling and Simulation, Technical University of Munich
leon.herrmann@tum.de
<https://www.cce.ed.tum.de/cms/team/leon-herrmann/>

Lars Pilgaard Mikkelsen
Brian Nyvang Legarth
Fabian Duddeck
Christian Frithiof Niordson

Upgrade parts' crashworthiness by exploiting injection molding manufacturing effects

Panagiotis Fotopoulos (BETA CAE Systems S.A.),

Michael Richter (MATFEM Ingenieurgesellschaft mbH)

1 Introduction

The recent trends towards more lightweight and autonomous vehicles have elevated plastics' importance increasingly, by replacing metallic parts.

In this direction, essential exterior components of a vehicle formed by plastics are required to sustain important mechanisms and apparatus which assist the autonomous driving of the car. These parts must be able to sustain and to cope with harsh environments and impacts at low speeds.

Design freedom of the mold injection process allows to produce complex geometries of big parts. To mold these complex parts in low cycle times multiple inlets are needed. This entails the creation of weld lines with local varying material properties and moreover a local fiber orientation.

To meet such requirements, the injection molding manufacturing process characteristics play an important role in the overall behavior of components and for their mechanical properties. Specifically, the local fiber orientation and the weld lines formation are amongst the most important concerns during the manufacturing process.

Weld lines are locations where two or more melt fronts meet. These influence the local fibers direction which is described by the material orientation and consequently the local orthotropy. As a result, weld lines and material orientation have significant impact not only on the visual appearance of a component but also on its mechanical strength.

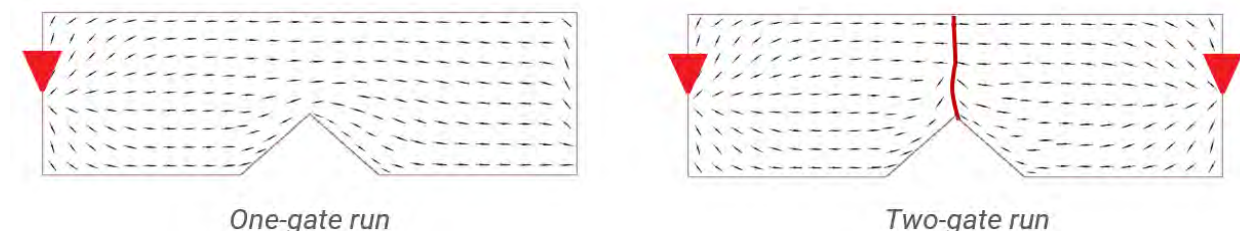


Fig. 1
The influence of the gates on the mechanical properties

Thus, a great challenge for such an approach is to connect the two worlds of injection molding and the FEA analysis successfully and accurately. However, to accomplish simulation results of high quality and accuracy within time constraints, the right pre- and post- processing tools and methodologies are important to facilitate the mapping as well as the handling of the necessary data.

The extracted results by this simulation are coupled with a comprehensive material and failure model MF GenYld+CrachFEM (further referenced as CrachFEM).

BETA CAE Systems provides a complete tool package to transfer and pre-process the injection molding manufacturing process results to the currently working model. After that, it generates the necessary solver files used by CrachFEM material model to initialize locally varying material properties. The results of the structural simulation can then be post-processed by META.

A great solution is provided by the ANSA one-step molding solver which can provide results calculated directly for the working model. Its easy set-up and the considerably short running time, makes it an extraordinary solution to conduct quickly multiple optimization loops on early design stage product development, with minimum resources.

2 Process overview

The goal that is achieved by the proposed solution is that the final calculations by the FEA solver have counted the behavior of the fibers and weld lines which affect the local orthotropy.

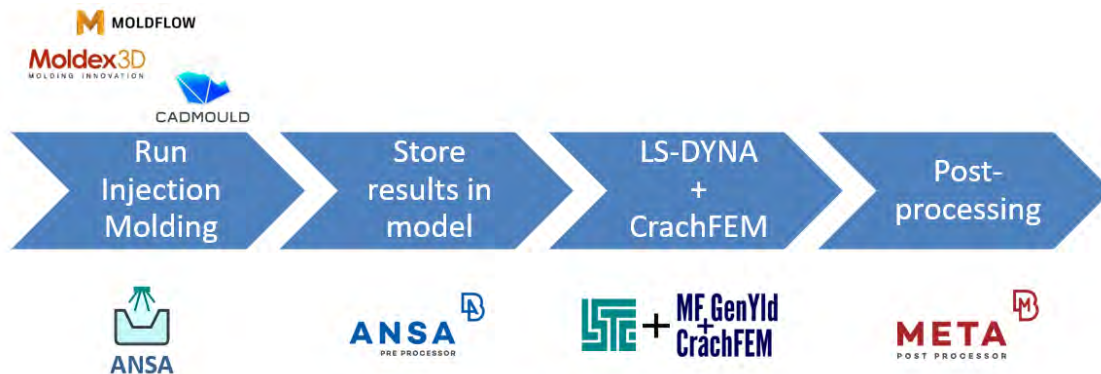


Fig. 2
The proposed CAE process loop

The above figure illustrates the process loop of an integrative simulation approach with a seamless integration of the CrachFEM material model in BETA CAE Systems suite. The ANSA one-step-molding solver can be coupled directly in this loop (skipping mapping step) but even third party software results such as from Moldflow, Moldex3D or Cadmould can also be used. In the latter case (third party solver), since the modelling as well as the mesh types are usually different between the Moldex3D/Moldflow/Cadmould and the FEA solver, the advanced Results Mapper tool of ANSA can bridge this gap properly.

Diving into more details, the weld lines and orientation tensor results from the injection molding analysis are:

- Handled directly on the FEA model when the ANSA one-step-molding solver is used because the solver runs directly on the working model.
- Transferred and mapped into the FEA model using ANSA advanced tools under Plugins>Molding group of functions. The tools are architected in a way to simplify the process and complexity of choices per case by providing the relevant-to-case options only.

The storage of the above results takes place per element by a specific way via *INITIAL_STRESS_SHELL or *INITIAL_STRESS_SOLID of LS-DYNA which enables the data to initialize at the beginning of simulation. Then, the model is ready to be output in the standard LS-DYNA format for the calculation of the material model by CrachFEM.

Furthermore, the calculated results by CrachFEM coupled with LS-DYNA solution can directly be read by META thus, under dedicated labeling of the results, evolving a wide range of capabilities and tools for advanced post-processing solutions such as reporting. Note that automation can cover the entire post-processing actions and tools and even run in batch mode.

ANSA GUI can further be used to inspect visually the donor and target mesh in an overlay plot to analyze if both meshes are consistent. Even if small geometrical changes occur and the meshes are not 100% congruent, isotropic properties are assumed as the default material properties in the CrachFEM-material card.

3 The material model

The user-defined material model can be coupled with the explicit solvers as a shared object and exchanges data. It obtains strains and returns the corresponding stresses in accordance with the material model/parameters. The material card itself summarizes the material parameters.

The material model MF GenYld+CrachFEM is applicable both to shell and solid elements alike and suitable for meeting industrial requirements of a Crashworthiness simulation.

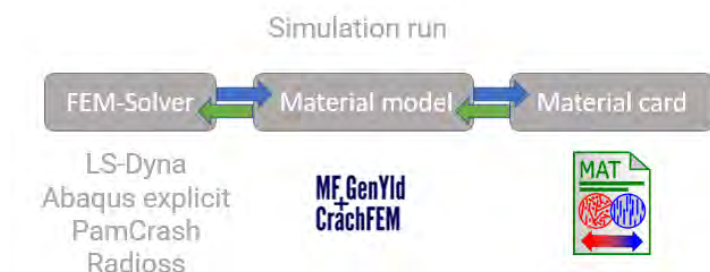


Fig. 3
The material model process

To prove the concept of the suggested solution process with the accuracy of the CrachFEM material model, an experiment was conducted in a laboratory on a coupon level. The outcome is then compared to both the simulated isotropic and orthotropic CrachFEM modeling materials, verifying that the orthotropic material modeling provides high accuracy on the simulation.

Moreover, the simulation of a hat profile model with two different variations of injection molding gating proves the high quality of the material as well as the importance of the suggested solution for injection molded parts.

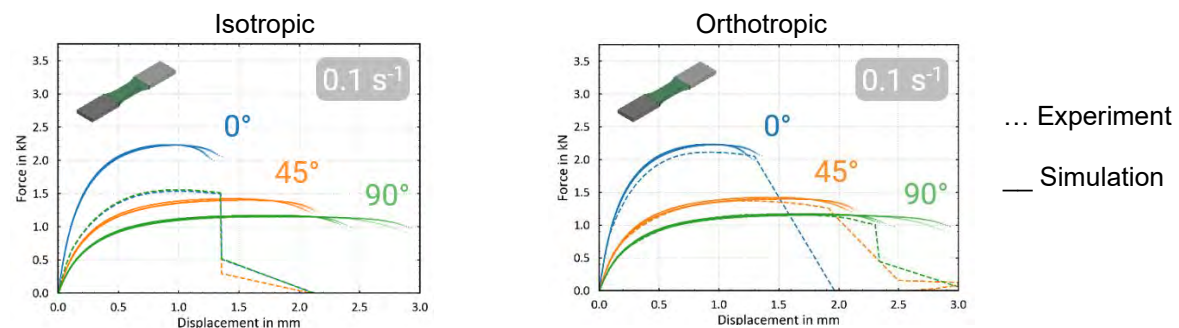


Fig. 4
Experiment vs simulated material model

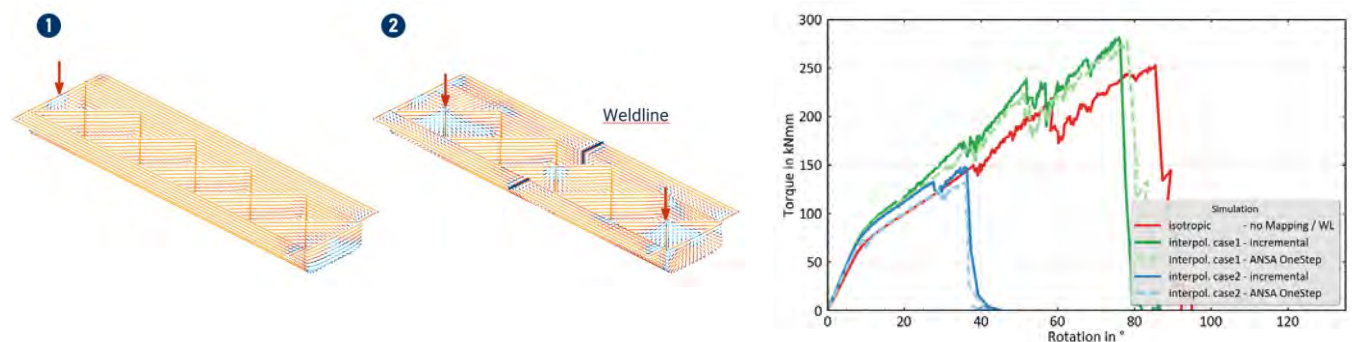


Fig. 5
Axial torsion simulation on a hat profile part with two gate scenarios

4 Conclusions

In this work, the improved accuracy of the simulated material properties is proved to be met, by the proposed solution which utilizes the injection molding manufacturing process and effects. The solution is a full cycle of steps, tools and software products which establish high quality result, by using advanced methods for pre-processing the injection molding results and provide detailed information to the CrachFEM material model.

Thus, the harmonic connection between ANSA-CrachFEM-META can serve highly accurate results for plastics to undergone a crash analysis.

The entire process is verified by the experiment results as well as, simulation tests on a hat profile part with different gating scenarios, to justify the efficiency and elevated quality of the proposed solution.

Furthermore, the dedicated tools as well as the one step molding solver ensure the minimum effort for the pre- and post- process of the model as well as the detailed examination of the results when necessary.

Post-buckling analysis of composite stiffened panels using a FEM approach

H.K. Almaz (TU Delft), S. Giovani Pereira Castro (TU Delft)

1 Abstract

Pushing the envelope of aerospace structures requires the complete exploitation of their potential in terms of load-carrying capacity per unit weight for both economic and ecological reasons: the two most important being the reduction of fuel consumption and greenhouse gas emissions. A key approach involves allowing structures like stiffened panels to function within the post-buckling range domain while in service. To do so, the finite element approach allows a broad design space for researching the post-buckling behaviour of such structures.

Accurately representing post-buckling behaviour in finite element models requires accounting for geometric and loading imperfections. The present study explores their effects on the post-buckling behaviour of a composite L-stiffened panel. A finite element model is created and validated based on an experimental case. This is then further modified to incorporate imperfections. Geometric imperfections are modelled using linear eigenvalue modes, while loading imperfections are introduced via a rigid loading plate making contact at an angle.

The research showed that first eigenmode combinations for geometric imperfections influence post-buckling behaviour. Their shape and amplitude impact the transition into post-buckling and their ultimate loads. Similar behaviour was also observed for loading imperfections. Additionally, their configuration also showed an offset in axial displacement results. These insights emphasise the need for precise imperfection modelling to promote safer and more efficient post-buckling design of aerospace structures.

2 Research Objective

Based on a literature review, it was understood that imperfections influence the post-buckling behaviour of composite-stiffened panels. Geometric imperfections are usually modelled using either measured imperfections, or, eigenmodes. In the case of the latter, the first few modes are often imposed from an eigenvalue analysis as an initial state for a non-linear analysis. This second method is used in the present study.

To the authors' knowledge, loading imperfections for straight stiffened composite panels are only included in the study from Park et al. [6]. However, they do not mention the influence of such imperfections on post-buckling behaviour. This presents a notable research gap, necessitating further investigations for more conclusive results. They are to be verified with the trends observed in the research from Park et al.

The presented study focussed on a low-torsional panel with L-shaped stiffeners, due to their common use in aerospace applications. The study also includes the systematic analysis of the inclusion of geometric imperfections in an Finite Element (FE) paradigm. Literature has demonstrated the importance of including these imperfections to obtain more accurate models that allow for a better understanding of the observed post-buckling behaviour. Additionally, loading imperfections are modelled in this research to study how they affect post-buckling.

To study the influence of imperfections on post-buckling behaviour, a baseline FE model was desired. For this, a stiffened panel design from Lanzi et al. [1,2,3,4] was modelled in ABAQUS, whose buckling behaviour was validated using their experimental data.

3 Finite Element Implementation

The FE models are created in the commercial software ABAQUS 2023. Two modelling approaches are followed to create a model with the closest characteristics to the design by Lanzi et al., from now on referred to as Lanzi case. The first model employs conventional S4R¹ [5] elements, and the second SC8R² continuum shell elements. The former requires less computational effort than the SC8R element-containing models. Both element types account for transverse shear deformation. However, their through-the-thickness behaviour differs: the S4R elements capture the properties in the mid-plane of the element and are formulated assuming plane stress, whereas the SC8R continuum shell model allows for stacking of the elements and features a constitutive relation for out-of-plane stresses. In the present study, SC8R elements are implemented by stacking four elements along the thickness direction, one for each ply.

A mesh convergence study is performed to ensure that the final load-displacement curves are mesh-independent. The axial compression load as well as the corresponding displacement (axial shortening) are important outputs for the studies performed on imperfections. The study resulted in a mesh size of 5 mm x 5 mm for both the S4R and SC8R models, with their respective element types assigned, after refining the mesh until the loads converged. However, further mesh refinement was required around the stiffener fillet to cover the high-stress gradients in this region adequately. The fillet region is depicted in an enlarged view within Figure 2. Along the curvature of the stiffener fillet, 10 elements are used. No further mesh study was needed through the thickness of the SC8R model as the four-element mesh already gave converged results.

¹Quadrilateral conventional 4-node general purpose shell with reduced integration

²Quadrilateral continuum shell element with 4-nodes facing the bottom-, and 4-nodes facing the top surface [5]

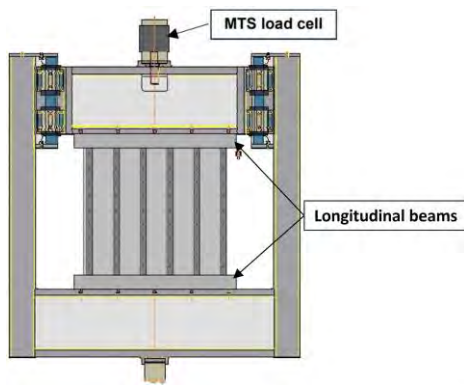


Figure 1: Schematic overview of the testing setup, copied from [1].

Table 1: Mechanical properties of the L-stiffened panel, copied from [1].

Property	Value	Unit
Elastic modulus $E_{11}=E_{22}$	55700	[N/mm ²]
Shear modulus $G_{12}=G_{13}=G_{23}$	3060	[N/mm ²]
Poisson coefficient $\nu_{11}=\nu_{22}$	0.048	[-]
Tensile strength $\sigma_{11}=\sigma_{22}$	431	[N/mm ²]
Compression strength $\sigma_{11}=\sigma_{22}$	467	[N/mm ²]
Shear in-plane strength τ	99	[N/mm ²]
Ply thickness	0.33	[mm]

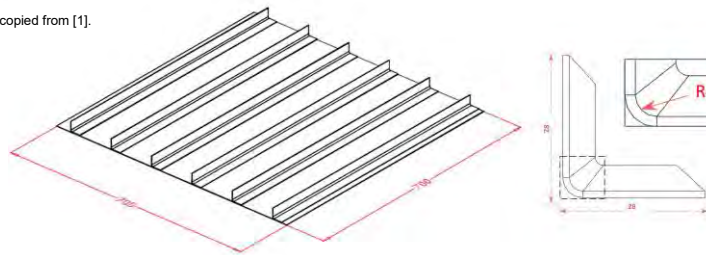


Figure 2: The stiffened panel with six L-shaped stiffeners.

3.1 Boundary Conditions

The boundary conditions are selected to replicate the experimental setup as accurately as possible. Referring to the setup illustrated in Figure 1 the panel is clamped on both the top and bottom sides, except for the loading direction (U2) at the top. In ABAQUS, this is modelled by tying the top and bottom edges of the skin and stiffeners to their respective reference points with the corresponding restricted degrees of freedom. This is depicted on the left in Figure 3 for the S4R model. The longitudinal edges are left free. While conventional shell models have displacement and rotational degrees of freedom, continuum shell models are restricted solely using the displacement degrees of freedom.

The Lanzi case specifies that the skin and stiffeners undergo separate curing processes before bonding and riveting. In the FE model, the lack of available data on the adhesive used prevented modelling this region. As for the rivets, it is assumed that these joints are sufficiently rigid to act collectively as a single rigid body. This has been represented using a tie "surface-to-surface" constraint, allowing the stiffener flange to deform alongside the skin. In the model illustrated on the right side in Figure 3, this feature is depicted by yellow symbols, indicating the tied regions. Not previously mentioned, but to prevent mesh distortion caused by the tie constraint, the meshes for the skin-stiffener interface have been aligned resulting in coinciding nodes.

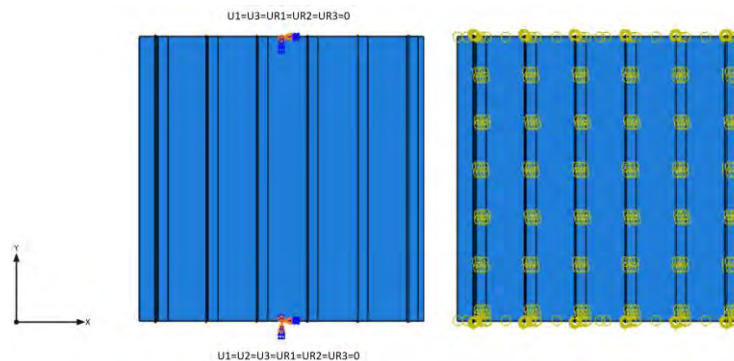


Figure 3: Applied boundary conditions and visualisation of the tie-constraint.

3.2 Analysis Methods

An eigenvalue and a dynamic implicit (DI) analyses were performed for the FE models. The eigenvalue analysis is based on a linear pre-buckling state, and is used to determine the linear buckling load. In addition to this, the linear buckling eigenmodes are used to model geometric imperfections. The DI analysis has the benefit of considering inertia effects and improved convergence behaviour compared to general static analysis, especially during dynamic events such as the stiffness reduction at buckling and the later buckling mode changes.

A challenge imposed by DI analysis is the selection of the correct displacement velocity rate, as it can affect both the computational time and the convergence of the solution. At high velocities coupled with sudden changes in the stiffness of the structure, the solution may diverge. ABAQUS's built-in automatic time incrementation algorithm

attempts to mitigate this by reducing the time increment. However, even with a decreased time increment, the solver may still encounter overshooting issues followed by sudden load drops rather than normal convergence. Low velocities on the other hand, lead to increased computational costs. The shortening velocity by Lanzi et al. [1] is for this reason not adapted. Based on a convergence study that concentrated on the load-axial shortening relation, the analysis initially commenced with a velocity of 1.3 mm/s and subsequently decreased to a rate of 0.13 mm/s. Ultimately, this study led to the selection of a velocity of 0.13 mm/s for both the S4R and SC8R models.

4 Imperfection Modelling

4.1 Geometric Imperfection

Various methods for modelling geometric imperfections exist. One approach involves incorporating measured data directly from experimental observations. Alternatively, eigenmodes derived from a linear eigenvalue analysis can be employed. The first approach is not feasible due to the insufficient data available from the Lanzi case regarding the measurements of geometric imperfections. The second option, which assumes a shape based on linear buckling modes and modifies the respective nodes accordingly in FE method, is preferred. In this method, eigenmodes derived from a linear buckling analysis are used as the initial geometric state for DI analysis. These can be implemented as either a single mode or as a linear combination of multiple modes. This approach for the geometric imperfection (w_0) is mathematically represented by the following equation:

$$w_0(x, y, z) = \sum_{i=1}^p c_i w_i(x, y, z) \quad (\text{Eq. 1})$$

where c_i are arbitrary scalar weighting factors applied to each linear buckling mode $w_i(x, y, z)$.

The modelling strategies proposed by Schafer and Pekoz [7] and Gardner [8] are adapted as a modelling approach: combining at least two early linear buckling modes with different shapes. Choosing different mode shapes are crucial to prevent mode cancellation, which can occur when two modes with inverse deformations are superimposed. The weighting factor (c_i), as shown in Eq. 1, will be referred to as the amplitude from this point onward. These amplitudes are expressed as percentages of the skin thickness, which is 1.32 mm. The study by Lynch et al. [9] specifies 10% of skin thickness as a typical value for riveted structures. The present research involves testing a range of amplitudes from 1% to 10% to observe their influence on the stiffened panel. A curve-fitting approach reveals that imperfection amplitudes up to 5%, yield results closely aligning with the initial baseline model. While real-life structures typically exhibit deformations equivalent to higher amplitudes, as also noted by Lynch et al. [9], it is important to clarify that these geometric imperfections do not manifest in mode-shaped deformations. This study imposes the buckling modes on the initial geometry to represent the geometric imperfections observed in experimental data. The modes are rather a tool to represent them within the FE paradigm.

In Figure 4, the first five eigenmodes for the baseline model are presented. Since modes 1 and 2 closely resemble each other, as the half-waves appear at the same location, only the first one is considered in the analysis.

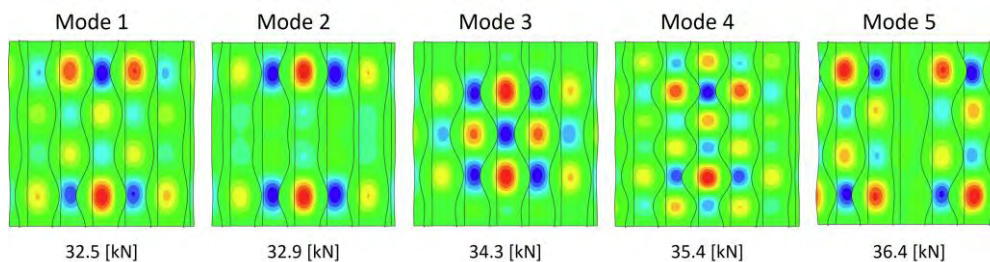


Figure 4: The first five eigenmodes of the baseline model.

Different combinations are made and implemented in the models in ABAQUS. The initial state of the model with the mode combinations were not able to be visualised due to the limitation of the solver used.

4.2 Loading Imperfection

Adjustments are made to the baseline model to account for the impact of the loading imperfection. A loading plate is introduced as a discrete rigid body to transfer the loads to the stiffened panel. Previously, the loads were uniformly applied through reference points, tied to the edge of the panel. The addition of the loading plate was omitted due to the inclusion of a contact formulation, which imposes some stiffness between the stiffened panel and the loading plate. This adjustment is only made for the SC8R model. In the case of the S4R model, contact was not possible because of the element type that could not establish contact on the edge with the loading plate. Since the stiffnesses seem almost equal between the baseline model and model including a loading plate. A small offset was present in the axial shortening, leading to a clear difference at the final axial shortening. This could be caused by the contact formulation that includes a default value for an artificial contact stiffness, which introduces additional compliance to the model. This decreases, in this case, the overall stiffness.

Park et al. [6] placed in their work the loading plate at a tilted angle of 0.005 and 0.01 degrees with respect to their stiffened panel. This was done to resemble a less ideal loading scenario at the start of the experiment. A similar approach is taken in the present study and the loading imperfections are modelled using SC8R models in order to compare their (post-)buckling behaviour with the baseline model.

As an initial step, four different configurations are tested in two setups, illustrated in Figure 5. The first configuration displays the front view, labelled as *Left* and *Right*, denoting the loading plate's orientation: in this instance, the panel is inclined towards the right side. The second figure portrays the side view, similarly marked to indicate the orientation.

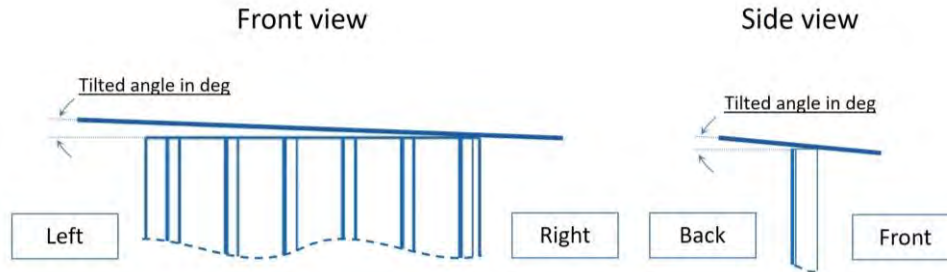


Figure 5: Configurations of the implementation of different loading imperfections.

5 Results and Discussion

5.1 Results

Before discussing the results obtained from the models with imperfections, it is important to highlight differences between the two panels tested by Lanzi et al. [1] and point the main sources of uncertainty. In Figure 6 a clear difference between the tested panels, especially in their ultimate loads, is visible. In their study, Lanzi et al. attributed the discrepancy in their test results to the differences in the collapse mechanisms of their panels: Panel 1 failed at the stiffener web's half-height, while Panel 2 failed at the stiffener web's top and bottom sections. They emphasised that these variations highlight the sensitivity of post-buckling behaviour to different failure modes. Although the authors do not explicitly mention it, this study also assumes that these differences could, for example, be caused by manufacturing defects.

Regarding the comparison between the FE model and the experimental cases, it is noteworthy to recall the differences between the tested panels. The FE model exhibits a lower percentage deviation compared to the panels, especially with respect to Panel 1. Considering the deviation between Panel 1 and 2, which share the same material and design but still result in a notable difference, the presented FE model is already within an acceptable prediction range.

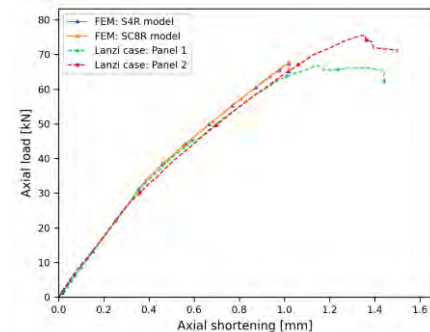


Figure 6: FE model results compared with the experimental results from Lanzi et al. [1].

As for the geometric imperfections, as visible in the first two plots in Figure 7, all the curves show similar trends up until the first buckling load at an axial shortening value of around 0.4 mm, which is expected behaviour. As for the transition into post-buckling is made visible for an amplitude of 1% in the most right figure in Figure 7, with their average loads displayed at the top row. While the perfect baseline model transitions into five half-waves, the models with imperfections exhibit four half-waves in the vertical direction.

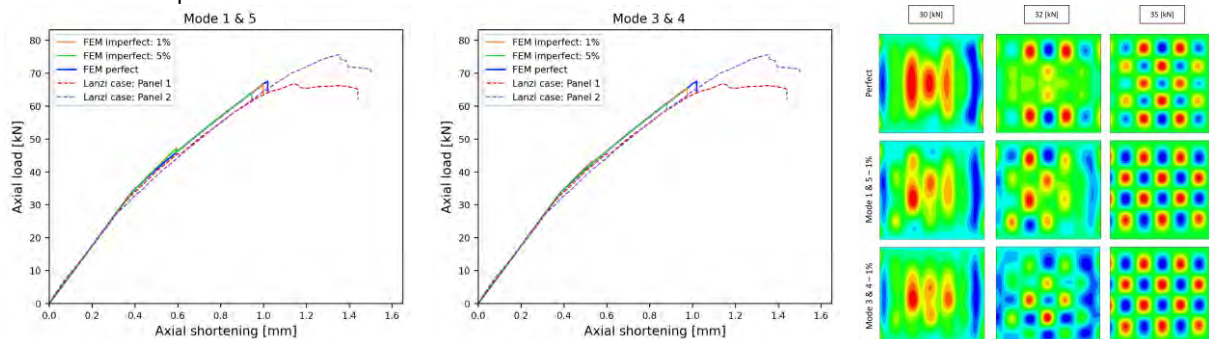


Figure 7: The first two figures compare two different mode combinations with the experimental results. The last one presents the transition from a pre-buckled to a post-buckled state.

As for the loading imperfections, the results for the different configurations are presented in Figure 8.

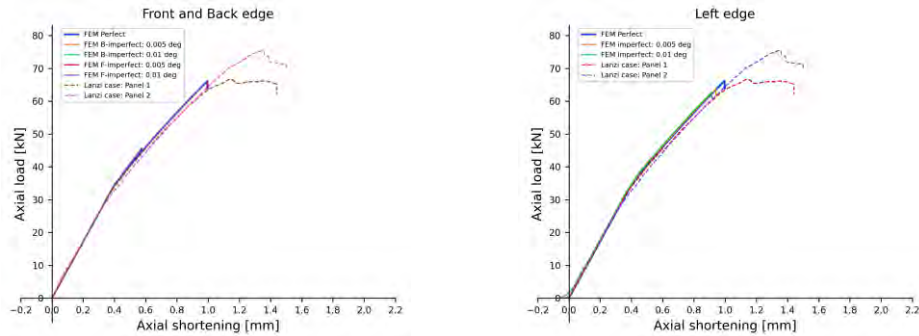


Figure 8: The results from the models including loading imperfections, compared with the results from Lanzi et al. [1].

As becomes evident from the figures, applying the loading plate in the SC8R models toward the back and front edges of the plate did not significantly alter the results. On the other hand, the tilted configurations on the Left- and Right edges of the stiffened panel did affect the results.

Recalling from earlier, the loading plate was positioned with an offset from the stiffened panel. This is evident in the negative axes since the displacement is measured in the midsection of the loading plate. In the tilted configuration, one part of the stiffened panel initiates contact first with the loading plate. Both plots demonstrate a good alignment up to 0.4 mm, marking the onset of the initial buckling.

Reduced ultimate loads are observed with increased tilted angle. Similar to models with geometric imperfections, the loading imperfections can trigger mode jumps, leading to lower ultimate load, with decreased axial shortening.

After the transition from pre-buckling into post-buckling, the panels switch modes right after the first buckling mode, which is made visible in Figure 9. This is possibly due to the modes being close to each other and the five half-waves dominating the physical realm.

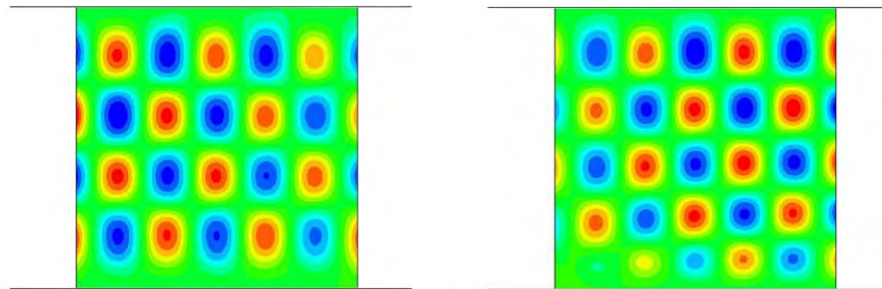


Figure 9: Mode switch from 4 (left figure) to 5 half-waves (right figure).

Overall, the main differences were observed at first initial contact, the offset from the baseline model (resulting from the initial contact) and the change in ultimate loads.

5.2 Discussion

The common detail between all models with imperfections is their influence on buckling shapes upon transitioning from the first buckling mode to post-buckling modes and the decrease in their ultimate loads. This highlights the close correlation with the observations made in the literature in the case of geometric imperfections. Also, the included from the eigenvalue analysis for the geometric imperfections were mainly present in the panel's skin. This is logical, as the stiffeners are designed to counteract this out-of-plane behaviour. The eigenmodes depicted in this study emphasise solely the out-of-plane displacement in the skin, as their magnitude substantially surpasses that observed in the stiffeners.

One type of geometric defect that could have resulted in stiffness reduction is introducing geometric imperfect stiffeners. The study by Prato et al. [10] included uneven stiffener length compared to the skin, resulting in stiffness differences in the post-buckled region. It is believed that adding such imperfections to the present model would decrease the ultimate load even further and could also result in stiffness loss since the stiffeners are the main load carriers in the post-buckling region.

Models with loading imperfections exhibit similar behaviour to what was observed for the ones with geometric imperfections: with increasing tilted angles, their ultimate loads decrease. In addition to this, the structure loses possibly a certain amount of stiffness, given that a part of the structure is loaded earlier and encounters higher stresses. This results in an offset in the load-shortening results. Also, the design of the structure is highly relevant: here, the right segment of the panel, where stiffeners are closer to the edge, showed a better resistance for non-uniform loading since the stiffeners carry more loads. One aspect not addressed in the previous sections is the use of carriage guides by Lanzi et al. to prevent non-uniform loading. An often overlooked consideration is that such a system does not directly establish uniform contact with the panel. The current research substantiates this

by demonstrating that initial load application at an angled position unveils variations when compared to the baseline model.

The perfect baseline model showed a transition to five half-waves (vertical direction) upon entering post-buckling. The models with imperfections first showed four half-waves in the vertical direction, followed by five. However, this buckling pattern cannot be exactly validated as the experimental data for these loads (between 30-35 kN) are unavailable.

Failing to include actual potting may impact the variance between the shape changes observed in the FE model and the experiment. For instance, models with loading imperfections demonstrate a smooth transition from four to five half-waves, whereas those based on geometric imperfections undergo a more abrupt change. This could be due to the gradual transfer of load in the case of loading imperfections. The sudden shift observed in geometric models can be attributed to the absence of potting.

6 Conclusions

The present study on the influence of geometric and loading imperfections on post-buckling behaviour has yielded several insightful conclusions. Regarding geometric imperfections, the analysis revealed that different eigenmode shapes and amplitudes significantly impact behaviour beyond the first buckling load. Some configurations exhibited small mode jumps due to mode interaction, whilst others did not display such behaviour. A key observation was the variance in ultimate load: at higher amplitudes some modes intuitively resulted in lower ultimate loads, while some showed counter-intuitive results with increased loads. This emphasises the crucial need for the careful selection of the appropriate eigenmode shape and amplitude to accurately represent geometric imperfections in post-buckling behaviour.

Similarly, loading imperfections demonstrated behaviours akin to those of geometric imperfections, notably affecting the ultimate loads. Beyond this, they also introduced an offset in the load-axial shortening behaviour from the perfect baseline model, dependent on the specific configuration and tilt angle. Based on these observations, it can be concluded that their influence should be accounted for.

In summary, this study highlights the importance of a detailed and meticulous approach in the selection and incorporation of both geometric and loading imperfections in structural modelling. In the case of geometric imperfections, the first eigenmodes can represent the geometric imperfections. As for loading imperfections, the configurations where the loading plate tilted towards the left- and right edge resulted in a significant difference with respect to the baseline model. Acknowledging and including these imperfections is crucial for a more realistic representation of post-buckling behaviour and for accurately predicting ultimate load capacities.

7 References

- [1] Lanzi, L., & Bisagni, C. (2003). Post-Buckling experimental tests and numerical analyses on composite stiffened panels. In 44th AIAA/ASME/ASCE/AHS/ASC Structures, Structural Dynamics, and Materials Conference (p. 1795).
- [2] Lanzi, L. (2004). Composite stiffened panels in postbuckling: experiments and dynamic explicit analyses with LS-DYNA.
- [3] Lanzi, L. (2004). An experimental investigation on the post-buckling behavior of composite stiffened panels. In 45th AIAA/ASME/ASCE/AHS/ASC Structures, Structural Dynamics & Materials Conference (p. 1566).
- [4] Lanzi, L. (2004). A numerical and experimental investigation on composite stiffened panels into post-buckling. *Thin-walled structures*, 42(12), 1645-1664.
- [5] Simulia. (2023). ABAQUS/Standard User's Manual 2023. Retrieved from <https://help.3ds.com/>
- [6] Park, O., Haftka, R. T., Sankar, B. V., Starnes Jr, J. H., & Nagendra, S. (2001). Analytical-experimental correlation for a stiffened composite panel loaded in axial compression. *Journal of Aircraft*, 38(2), 379-387.
- [7] Schafer, B. W., & Peköz, T. (1998). Computational modeling of cold-formed steel: characterizing geometric imperfections and residual stresses. *Journal of Construction Steel Research*, 47(3), 193-210. Elsevier.
- [8] Gardner, L. (2002). A new approach to structural stainless steel design. Imperial College London (University of London).
- [9] Lynch, C., Murphy, A., Price, M., & Gibson, A. (2004). The computational post buckling analysis of fuselage stiffened panels loaded in compression. *Thin-Walled Structures*, 42(10), 1445-1464. Elsevier.
- [10] Prato, A., Al-Saymaree, M. S. M., Featherston, C. A., & Kennedy, D. (2022). Buckling and post-buckling of thin-walled stiffened panels: modelling imperfections and joints. *Thin-Walled Structures*, 172, 108938. Elsevier.

Simulation Driven Development at Volvo Car Corp.

Harald Hasselblad

Technical Expert – Weight Management and Optimization

Volvo Cars

Light weight and well balanced design is becoming more and more important. To support this challenge, the use of CAE and optimization needs to be efficiently introduced during the development process. This presentation will give you an overview of how Volvo Cars strategically work with simulation driven development to support light weighting. Benefits and challenges with simulation driven development will be presented along with a number of inspirational cases with focus on topology optimization.

Harald Hasselblad works as a Technical Expert within weight management at Volvo Cars. He is responsible for corporate weight strategies and driving an Optimization Competence Arena, supporting Simulation Driven Development within the company. The arena supports the development and implementation of methods and tools for efficient engineering and optimization in early and late project phases. Harald also coordinates a national network between OEMs, institutes and universities in Sweden. Harald started his carrier as a PhD student at Volvo Cars 1999. His research area was focusing on topology optimization and methods for the early concept phases. Harald's expertise lies within conceptual analysis and optimization and working with development of methods and tools for structural optimization. He received his PhD in Mechanical Engineering from the Linköping University, Sweden. He has now worked at Volvo Cars for 25 years.

Highlights from Project TRUSTIT

(Towards a Rational Approach to Credibility of Numerical Simulations in Industrial Applications)

Fabio Santandrea (RISE)

1 Summary

Numerical simulations play a pivotal role in the development of manufactured products, as they enable systematic quality improvement whilst reducing costs and time-to-market. The possibility to explore design variants in a virtual environment, with limited use of physical prototyping and testing, contributes to make production processes more sustainable, as suggested by several industrial cases. The envisaged positive implications of the more extensive use of numerical simulations to support decisions are conditional upon their credibility. In this paper, we report on the ongoing project TRUSTIT, a joint research initiative of RISE and Volvo Cars. The main purpose of the project is to facilitate the transfer of knowledge about uncertainty quantification (UQ), sensitivity analysis, and related concepts from research to industrial environment, in order to improve the credibility of the results generated by numerical simulations and enable more robust and transparent decision-making processes based on computational models.

2 Introduction

Numerical simulations play a pivotal role in the development of manufactured products, as they enable systematic quality improvement whilst reducing costs and time-to-market. The possibility to explore design variants in a virtual environment, with limited use of physical prototyping and testing, contributes to make production processes more sustainable, as suggested by several industrial cases [1][2].

The envisaged positive implications of the more extensive use of numerical simulations to support decisions are conditional upon their credibility. The responsibility of model developers grows with the criticality of the potential consequences of decisions made upon erroneous predictions. The mitigation of the risk entailed by overconfidence in numerical simulations requires adequate Simulation Governance, i.e., a system or collection of process-es to ensure the accountability and reliability of the information generated by numerical simulations [3]. Simulation Governance is in the list of the 20 major challenges identified by NAFEMS for the future of engineering simulations [4].

The use of numerical modelling techniques (collectively denoted as Computer Aided Engineering – CAE) in automotive industry has reached a considerable level of maturity. Nevertheless, CAE teams working on various attributes are often quite isolated. Best practices and quality standards are often developed within CAE teams built around specific product functions or attributes (e.g., Fuel Economy, Propulsion, or Crashworthiness) and rarely shared with other teams, thus creating a variegated landscape of practices to assess the credibility of numerical simulations developed within the company.

System simulations for complete vehicle virtual verification as done with VSIM are a significant example of multidisciplinary analysis where different parts of a large organization interact and exchange data, both internally and with external suppliers. VSIM is developed as a toolbox within the general-purpose mathematical package Matlab/Simulink and it simulates the longitudinal dynamics of vehicles driven along a one-dimensional trajectory with an assigned speed profile to follow (often based on synthetic driving cycles that simulate standardized laboratory tests to evaluate pollutant gas emissions). Driver behaviour, environmental factors (e.g., road roughness) as well as software and physical components of the vehicle are included in VSIM simulations through a large array of sub-models of various nature, ranging from static look-up tables (e.g., efficiency maps for internal combustion engines) to numerical implementations of equations derived from fundamental physical principles.

The industrial survey conducted in the research project SPRUCE [5] evidenced that personal responsibility of model developers, combined with (mainly, informal) assessment reviews by peers are largely commonplace in quality assurance of engineering simulations in Swedish industry, see Figure 1. The need for more structured, possibly standardized approaches to model verification and validation was identified in the survey and practical proposals on how to address it have appeared also in the recent literature [5]

The overall purpose of the project TRUSTIT is to share knowledge and to promote best practices to practically address the risks and limitations in the current practice for quality assessment and management of numerical simulations in product development. The information exchange between the participating organizations will consider the challenges faced by complete vehicle virtual verification as well as the existing concepts, methods, and tools to address them.

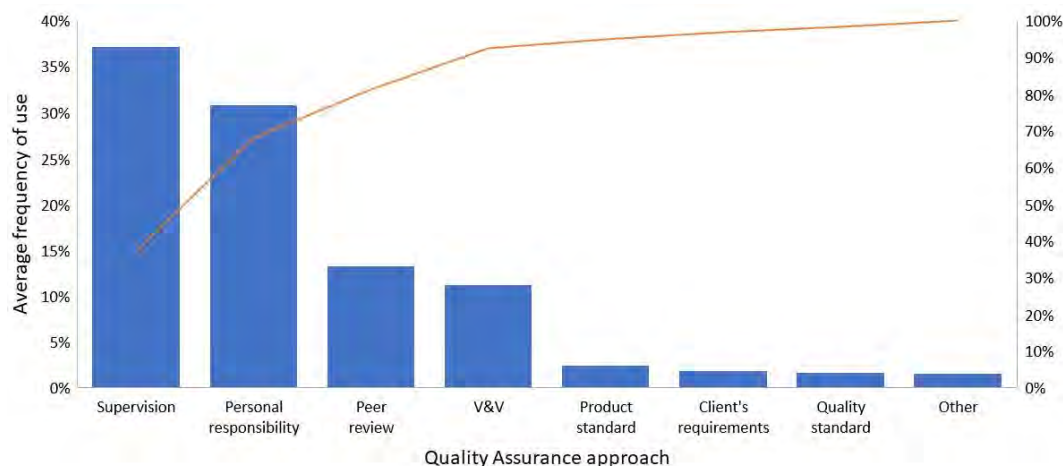


Fig. 1 Distribution of approaches for quality assurance of numerical simulation in Swedish industry, based on a survey conducted in 2020-2021 within the research project SPRUCE.

3 Uncertainty Quantification in CAE

The general workflow of Uncertainty Quantification (UQ) considered in the TRUSTIT project for complete vehicle simulations in VSIM is shown in Figure 2.

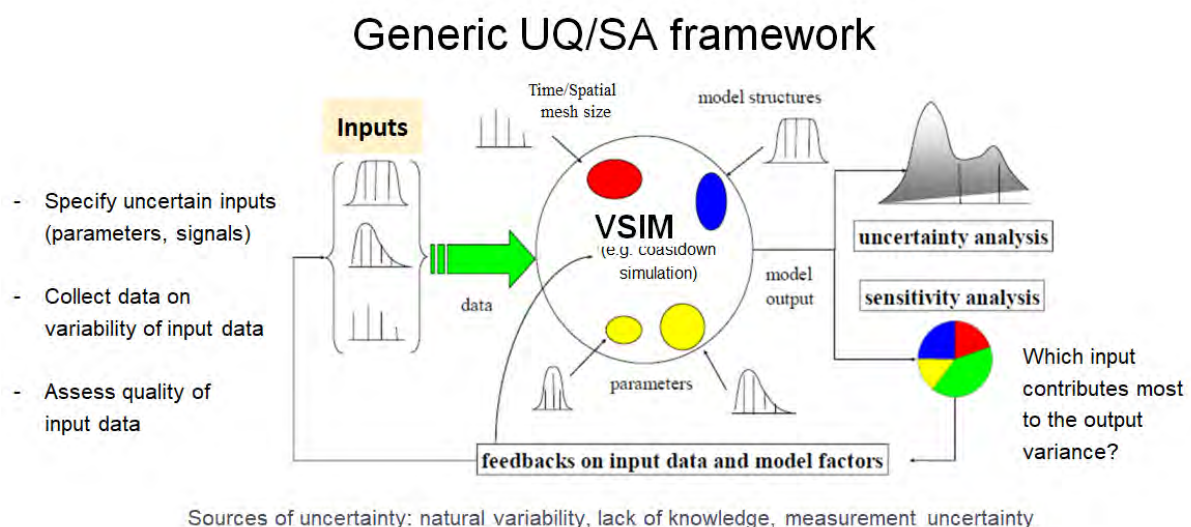


Fig. 2 The general workflow of uncertainty quantification and sensitivity analysis considered in the TRUSTIT project.

What is UQ good for? The integration of UQ in industrial CAE workflows provides invaluable support to those actors who are responsible to make decisions based on the results of numerical simulations. The possibility to make sound decisions upon simulation results is largely dependent on the credibility of the underlying computational models for their intended purpose. This point can be illustrated with an example taken from the paper of Danquah et al, where a statistical framework for the verification and validation of computational models in automotive design is put forward [5].

The example is based on the data reported in Table 1. The energy consumption of an electric Smart was measured in laboratory environment (i.e., roller dynamometer) under several standardized driving cycles (e.g., WLTC, NEDC). The same quantity of interest was also evaluated from the numerical simulation of the selected driving cycles using a longitudinal dynamics vehicle model. A conventional, deterministic validation criterion for the model might be defined by requiring that the simulated results should not deviate more than 5% from the corresponding experimental values. On the basis of this criterion and the data reported in Table 1, the vehicle dynamics model considered in [5] would be validated and that would be possibly expressed by a statement such as „the accuracy of simulation results is at least 5%“.

However, nothing prevents that additional measurements or simulation results will not invalidate such a statement. There is no estimation of the discrepancy between measured and simulated results that might be potentially generated in addition to the existing ones, besides blind belief in the accuracy of the model. This is the major intrinsic limitation of a purely deterministic approach to model validation. In contrast, probabilistic methods such as the P-boxes suggested in [5] (see the rightmost column of Table 1) enable to estimate the intervals where the discrepancy between simulated and measured data is expected to fall with predefined frequency. It is up to the user of the simulations to decide whether the size of this interval (that is, the uncertainty of simulation results) is acceptable in the application context where the numerical model is developed and used.

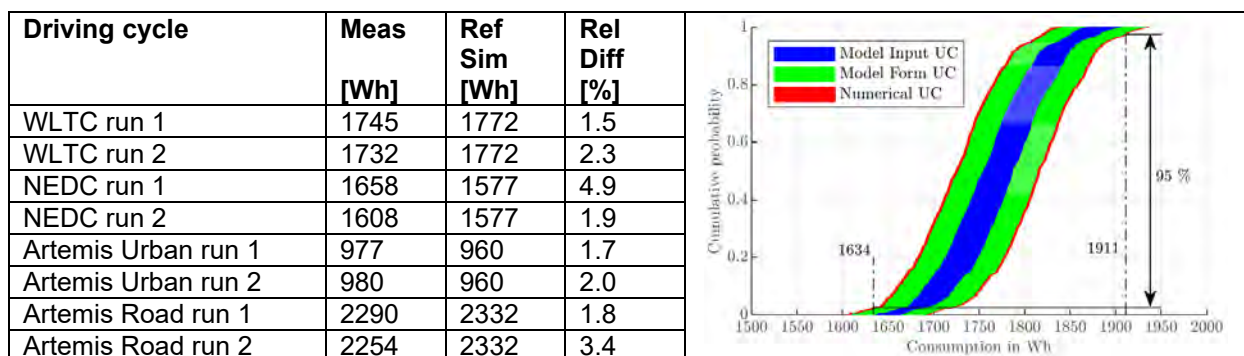


Table 1. (Left) Comparison between measured and computed energy consumption of an electric Smart for various driving cycles, adapted from [5]. The reference simulations are conducted with estimated mean values of all the input. (Right) Example of derivation of 95% confidence interval for the average energy consumption of the same vehicle in the WLTC driving cycle, based on the statistical model Verification & Validation framework proposed in [5].

In general, the challenges faced by the implementation of UQ in industrial environment can be categorized as follows:

- 1) Cultural/Strategic: understanding of the additional value that UQ can create when integrated to CAE workflows in product development. Such an understanding should spread across all levels of the organization, including simulation specialists and decision makers, namely designers and project managers. Different minimum levels of competence in UQ might be expected from different roles and possible knowledge gaps might have to be filled with tailored training initiatives for the staff.
- 2) Computational: availability of hardware and software infrastructure to streamline the execution of large amount of simulations and ensure basic data management functions such as storage, security, traceability, interoperability with internal and external partners, etc.
- 3) Accessibility: User-friendly tools for the application of UQ methods to existing simulation workflows, including appropriate resources for in-house development of tailored solutions.

4 Case study – coastdown simulation

Coastdown test is a common test in automotive industry that is used to estimate the mechanical and aerodynamic forces that act under driving against the propulsive force of the powertrain. These dissipative forces have a significant impact on the fuel economy or, more generally, the energy consumption of vehicles and, as such, they play an important role also in the certification of vehicles according to international regulations on the greenhouse gas emissions in the transportation sector.

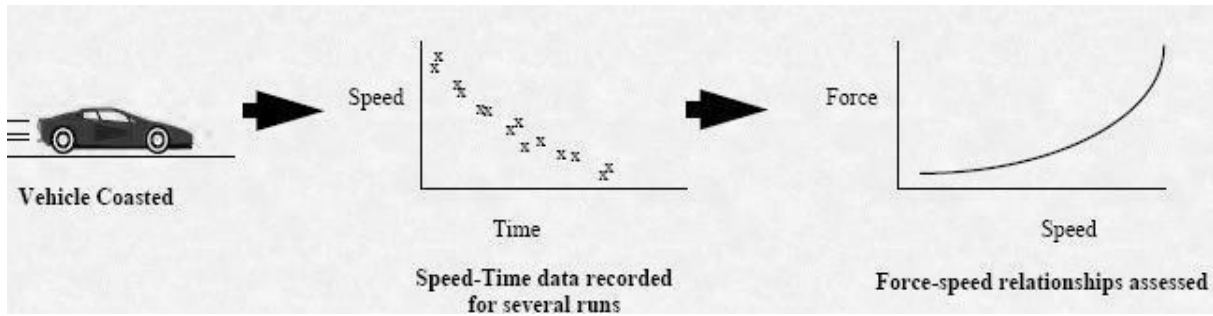


Fig. 3 Schematic representation of the coast-down test procedure [6]

The road load of a vehicle is defined as the force required to push the vehicle forward in neutral gear at constant speed on a flat road [6]. The experimental on-road procedure to determine the road load is shown in Figure 2. The vehicle is accelerated to a target speed, set on neutral and let it decelerate down to another target speed, while the time elapsed during the transition is measured. The procedure is repeated between several target speed values under nominally identical conditions. The road load is computed from deceleration data via Newton's second law and an empirical relationship between force and speed is derived (see rightmost part of Figure 2), which is typically fit with a second order polynomial function. The quadratic term dominates at higher speed and it is interpreted in terms of aerodynamic resistance, while rolling resistance and internal losses prevail at lower speed. The total rolling resistance F_{rr} can be broken down into the contributions of different components of the powertrain, that is:

$$F_{rr} = F_{EM} + F_{Trns} + F_{Drvl} + F_{Tyr} + F_{WhB} + F_{WhO}$$

The components of the powertrain included at the right-hand side of the equation above are: electrical machine, transmission, drivelines, tyres, and wheels. Various models are implemented in VSIM to represent the different components of the powertrain and they are typically developed and parameterized by different teams within Volvo Cars. Therefore, a varying level of quality might be expected from these models, which concur to determine the predictive capability of the complete vehicle model. The question then arise about how to assess the impact of the quality of component models on the credibility of the simulated coast-down results. In order to address this question, an uncertainty quantification exercise was conducted on a VSIM model to simulate on-road coastdown tests, followed by a sensitivity analysis.

The procedure followed the general workflow shown in Figure 2. The uncertainty in the input parameters was quantified using an approach proposed in the field of Life Cycle Assessment [7] and based on the concept of Pedigree Matrix, which can be seen as part of the general framework for uncertainty characterization and communication in science for policy known as NUSAP (Numeral, Unit, Spread, Assessment, Pedigree) [8].

In TRUSTIT, the focus is on the quantification of uncertainty in the parameters of VSIM simulations, which might represent properties of the vehicle (for example, mass, aerodynamic coefficient, or tyre pressure), the environment, or the driver. Normally, in ordinary VSIM simulations, these parameters are given single values that are determined by qualified operators within Volvo Cars or by external suppliers. However, these values are affected by uncertainty, which is characterized by shifting from single values to (min, max) intervals or probability distributions. The uncertainty may originate from different sources, such as scarcity of experimental data, natural variability, poor representativeness, lack of knowledge. In the approach implemented in TRUSTIT, the user is not asked to specify directly the most likely probability values or distributional forms for the uncertain parameters, but rather to

assess the quality of the available data according to a rating system that takes into account several attributes that influence the credibility of the stated values, such as the amount of available measurements, the accuracy of calculated or estimated values, and their representativeness for the system to be simulated. This approach was selected to make the framework accessible also for users who are not familiar with the concepts of probability theory, and also to mitigate the risk of making the choice of input distributions overly arbitrary or plainly wrong, which is considerable even for experts. The scores given to the quality indicators for each uncertain parameter are usually defined on an ordinal scale, for example from 0 to 4. They are aggregated into a single overall score according to some averaging procedure such as that shown in Figure 4.

The range of possible values for the aggregated quality indicator is divided up into 5 subranges, each corresponding to a different level of uncertainty (from high to low) and modelled with a 4-parameter Beta distribution with shape and range parameters shown in Figure 4. Due to its flexibility, this probabilistic model is able to represent different scenarios of uncertainty with the same mathematical object (only the parameters vary). The distributions of the uncertain inputs are centred at the nominal values that are normally used in deterministic VSIM simulations.

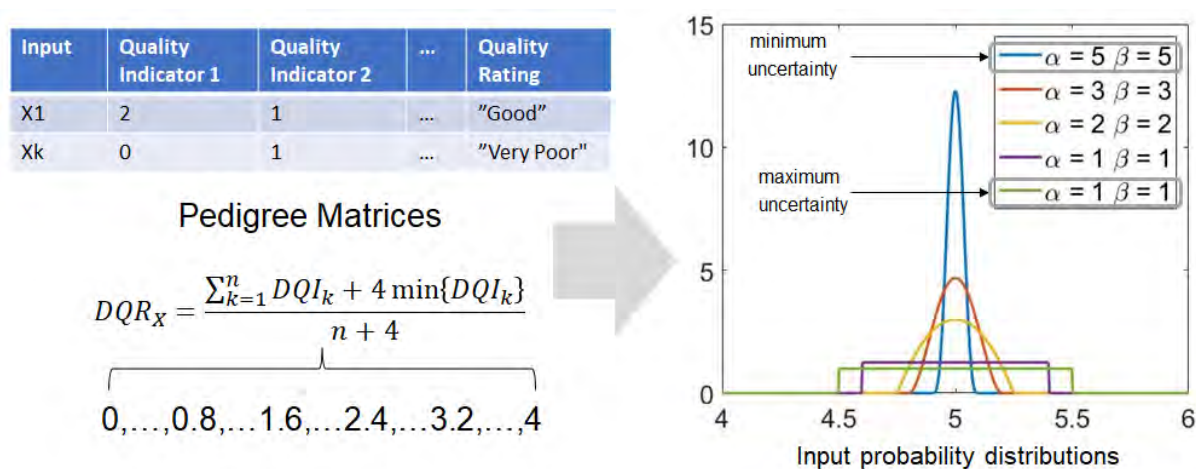


Fig. 4 Schematic illustration of procedure to quantify uncertainty in input parameters starting from a quality assessment of available data based on Pedigree Matrices.

Different choices of Pedigree Matrices are possible, depending on the application. For the preliminary analysis of uncertainty in simulated coastdown tests based on the model described by the equation above, the Credibility Assessment Scale (CAS) from the NASA 7009 standard [9] was chosen and applied to the models of the powertrain components. The model quality attributes included in the CAS are: Input Pedigree, Results Uncertainty, Results Robustness, Verification, Validation, Use History, Modelling&Simulation Management, People Qualifications.

The uncertainty in input parameters is propagated through the complete vehicle model for a given driving scenario by Monte Carlo simulation, that is by repeatedly sampling the input distribution to generate the distribution of model output, which in the case of coastdown simulations, is the total rolling resistance F_{rr} . An example of output distribution evaluated in this way using 1000 samples is shown in Figure 5, together with the results of variance-based sensitivity analysis.

In general, the term "sensitivity analysis" denotes a large family of methods to quantitatively characterize the importance of input factors in computational models, that is to what extent their variability can shift the output of the model. Variance-based methods characterize the spread in model output through its variance and decompose it into the sum of separate contributions that can be interpreted as the effect of individual inputs, either alone or in interactions with other inputs. Statistical indicators such as first order Sobol indices are evaluated by Monte Carlo simulation to measure the contributions of input parameters to the output variance (we refer to [10] for a thorough introduction to the subject).

An example of first order Sobol coefficients for the resistance forces of each powertrain component in simulated coastdown tests is shown in Figure 5. The calculation of the Sobol coefficients in this case

was performed with the SAFE toolbox [11]. The major role of the tyre model suggested by the deterministic simulations is confirmed by the uncertainty analysis, which also indicates that the other components contribute significantly to the variance of model output (at least, 10%).

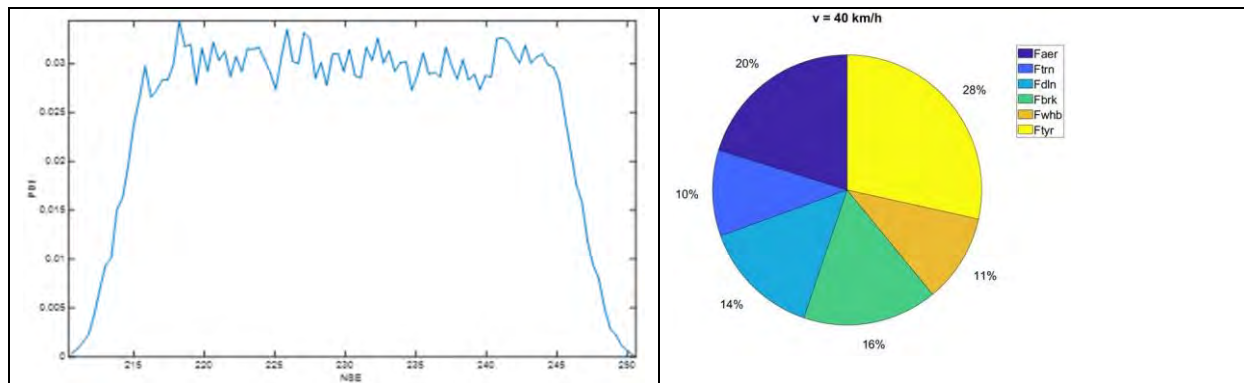


Fig. 5 (Left) Example of Monte Carlo-generated distribution of VSIM model output for simulated coastdown tests. (Right) Sobol coefficients of contributions to total road load evaluated from simulated coastdown tests in VSIM.

5 Conclusions

There is a need for more UQ in industrial CAE. The TRUSTIT project is a good opportunity to explore the challenges of implementation and demonstrate realistic case studies. Current work on development of a general-purpose framework to conduct uncertainty quantification and sensitivity analysis on input parameters in complete vehicle simulations based on Python, particularly on the UQpy toolbox [12]. The project is planned to end in September 2024.

From the industrial standpoint, the project has a significant potential to generate useful knowledge and processes to overcome the challenges identified in the development of electrified and autonomous vehicles, two business areas which have significant implications for the future of sustainable and safe transportation. Due to the uncertain market when it comes to electrification and autonomous drive, the substantial increase of software components, and mechatronic complexity in the cars, there is a need to improve our virtual product development process. Furthermore, when it comes to emission regulations and testing of active safety functions in a very large number of traffic scenarios, it will not be possible to rely only on physical test, but we need to increase the use of virtual verification. One big challenge when it comes to increasing the use of virtual methods in the complete product development process is that there currently is a lack of standardization when it comes to model verification and model fidelity.

From the standpoint of applied research, the project represents a major opportunity for the re-searcher involved in the exchange to translate concepts and ideas about quality assurance of numerical simulations into processes that can be tested and optimized in an industrial environment, thus enabling research work to have a tangible impact. The proximity and continuity ensured by the placement in industry facilitate the acquisition of hands-on experience that is quite limited in research projects, where the focus is typically not aligned with daily industrial practice.

Furthermore, the many lessons that are expected to be learned during the project might create the conditions to replicate similar initiatives with other industrial stakeholders. Project TRUSTIT might be seen as a pilot case that could motivate the creation of an open forum where industrial stakeholders and research organizations could share ideas about quality assurance of numerical simulations and how to integrate them in product development.

Financial support from the Swedish Innovation Agency (VINNOVA) is gratefully acknowledged (Diarienummer 2022-0313).

6 References

- [1] <https://www.visualcomponents.com/resources/blog/the-role-of-simulation-in-sustainability-exploring-the-five-core-areas/>.
- [2] <https://digitallabs.edrmedeso.com/blog/sustainability-in-technology-design-and-engineering-how-engineers-and-simulation-can-help>.
- [3] B. Szabó, R. Actis, Simulation governance: Technical requirements for mechanical design, Computer Methods in Applied Mechanics and Engineering, 249–252, 2012, 158-168, <https://doi.org/10.1016/j.cma.2012.02.008>.
- [4] <https://www.nafems.org/community/the-analysis-agenda/upcoming-topics/>.
- [5] B. Danquah, S. Riedmaier, J. Rühm, S. Kalt, M. Lienkamp, Statistical Model Verification and Validation Concept in Automotive Vehicle Design, Procedia CIRP, 91, 2020, 261-270, <https://doi.org/10.1016/j.procir.2020.02.175>.
- [6] P. Norrby, Prediction of coast-down test results - A statistical study of environmental influences, Master Thesis, 2012, Department of Product and Production Development, Chalmers University of Technology, Gothenburg, Sweden, <https://hdl.handle.net/20.500.12380/160184>.
- [7] Chen, X., Lee, J. (2021). The Identification and Selection of Good Quality Data Using Pedigree Matrix. In: Scholz, S.G., Howlett, R.J., Setchi, R. (eds) Sustainable Design and Manufacturing 2020. Smart Innovation, Systems and Technologies, vol 200. Springer, Singapore. https://doi.org/10.1007/978-981-15-8131-1_2
- [8] Funtowicz, S. O., Ravetz, J. R., Uncertainty and Quality in Science for Policy, Springer Dordrecht, 1990, <https://doi.org/10.1007/978-94-009-0621-1>.
- [9] NASA-STD-7009A W/CHANGE 1, Standard for Models and Simulations. <https://standards.nasa.gov/standard/nasa/nasa-std-7009>.
- [10] Saltelli, A., Ratto, M., Andres, T., Campolongo, F., Cariboni, J., Gatelli, D., Saisana, M., Tarantola, S., Wiley, 2007, <https://doi.org/10.1002/9780470725184>.
- [11] <https://safetoolbox.github.io/>.
- [12] <https://uqpyproject.readthedocs.io/en/latest/>.

EV battery structural simulation at Volvo Cars

Peter Gustavsson (Volvo Cars)

1 Summary

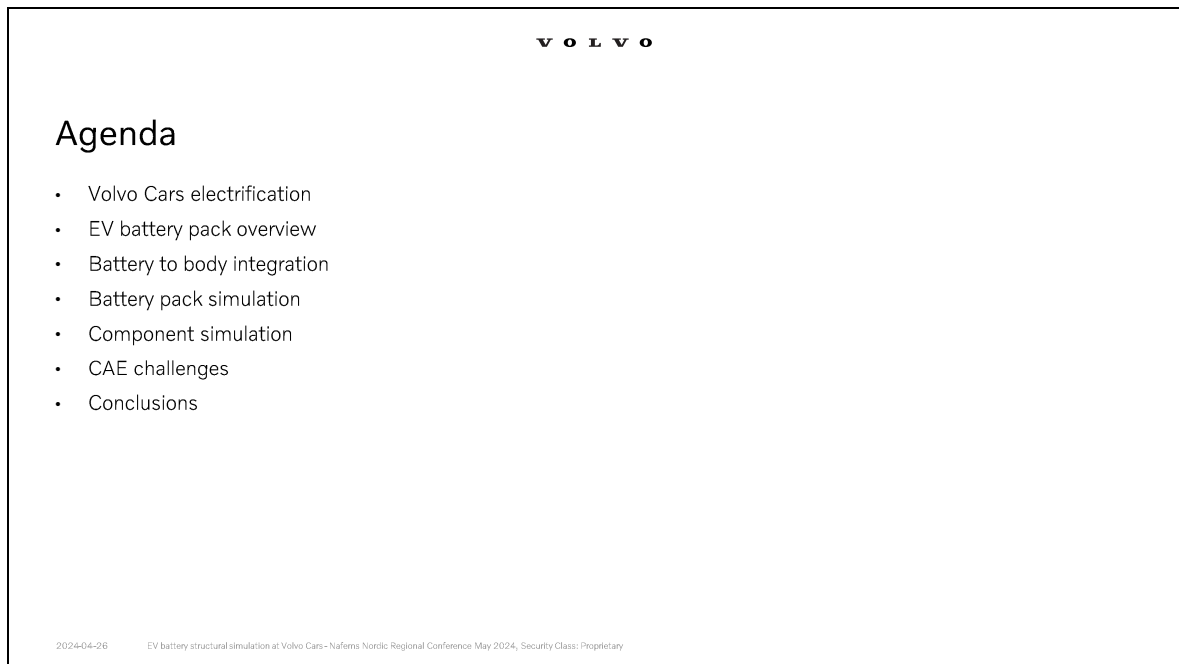
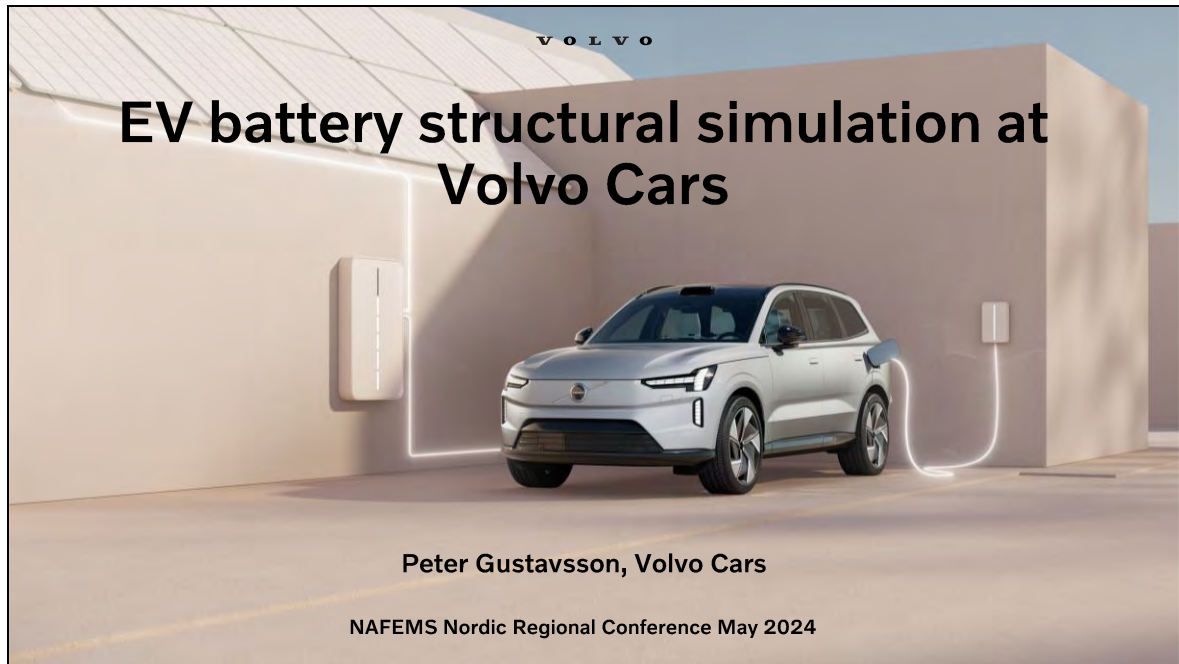
Volvo Cars plan to become a fully electric car company by 2030. The automotive industry is a highly competitive landscape where a lot of new OEMs are aiming to increase their market share. Using CAE simulations during the development of new car models is the established way of working at Volvo Cars, it reduces lead time, improves component design, and makes sure that in verification testing no major issues are found.

Evolving into a fully electric car company brings new challenges to the organization. New certification load cases on battery packs need to be passed before vehicles can be sold. Furthermore, integrating the battery pack into the complete vehicle mean that the attributes Safety, Durability and NVH must include the battery structure in their simulations and learn how it influences the vehicle performance. This presentation will give an overview of some of the battery structural simulations that are performed at Volvo Cars to help the company become a leading electric car OEM.

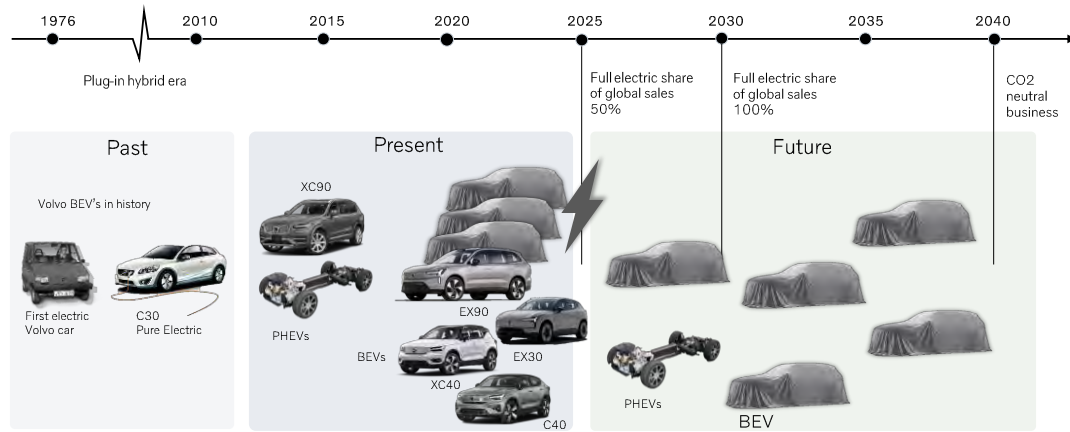
2 Battery structural simulations

Battery structural CAE team at Volvo Cars performs various simulation on the battery pack to make sure that the design fulfills the set requirements. The team also work in close collaboration with complete vehicle attributes Safety, Durability and NVH. All battery packs are modeled according to Dura/NVH and Safety best practices and delivered to the complete vehicle CAE departments for further analysis.

Some of the load cases that are analyzed at Volvo Cars during EV development are presented in the following pages.



Volvo Cars electrification journey



2024-04-26 EV battery structural simulation at Volvo Cars - Nafems Nordic Regional Conference May 2024, Security Class: Proprietary

Geared for premium growth with a balanced portfolio

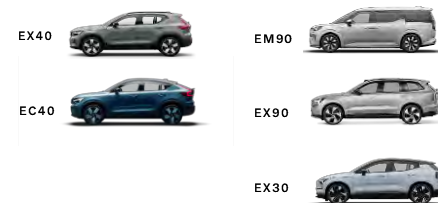
All models available are available as plug-in hybrids or fully electric. Since 2020 all new models have been fully electric. During 2023, we revealed two new cars, the EX30 in June and EM90 in November.



PLUG-IN AND MILD-HYBRIDS



FULLY ELECTRIC



2024-04-26 EV battery structural simulation at Volvo Cars - Nafems Nordic Regional Conference May 2024, Security Class: Proprietary

<https://investors.volvocars.com/en/results-and-reports/results-centre>
Annual & Sustainability report

Overview of an EV battery pack



Lid

Thermal
barrier

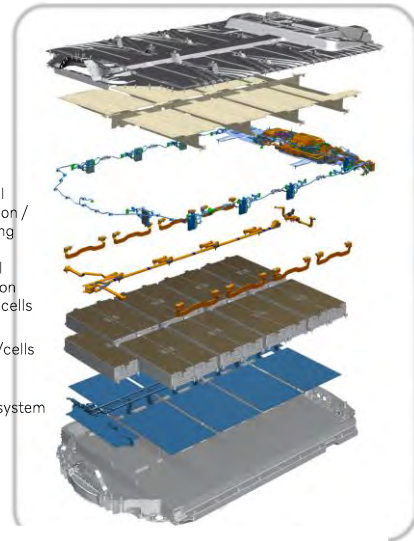
Electrical
distribution /
monitoring

Electrical
distribution
between cells

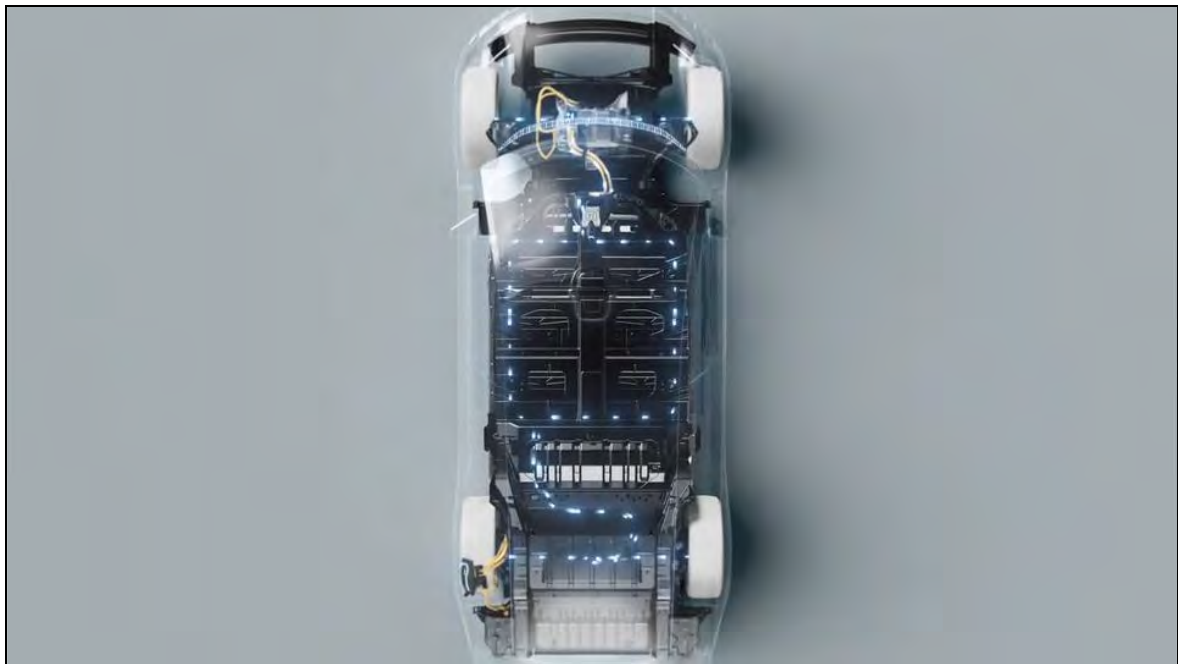
Modules/cells

Cooling system

Tray



2024-04-26 EV battery structural simulation at Volvo Cars - Nafems Nordic Regional Conference May 2024, Security Class: Proprietary

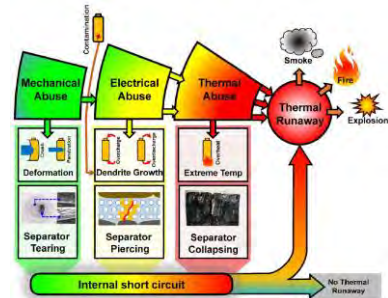


Battery integration – Safety

Volvo Cars is synonymous with safety.

Cells are sensitive to mechanical, electrical and thermal abuse.

They need to be protected by surrounding structure!



"Thermal Runaway Mechanism of Lithium Ion Battery for Electric Vehicles: A Review"
X. Feng, et al Tsinghua University – Beijing
2024-04-26 EV battery structural simulation at Volvo Cars - Nafems Nordic Regional Conference May 2024, Security Class: Proprietary

SAFE - FOR LIFE

In 1927 one of our founders, Gustaf Larsson, stated: "Cars are driven by people. The guiding principle behind everything we make at Volvo, therefore, is and must remain, safety." This principle made our brand synonymous with safety and is today as relevant as ever before. We will continue to aim to pioneer the safest, most intelligent technology solutions in mobility and everyday life to protect what is important to people. Their lives, and the lives they are living.

<https://investors.volvocars.com/en/results-and-reports/results-centre>
Annual & Sustainability report

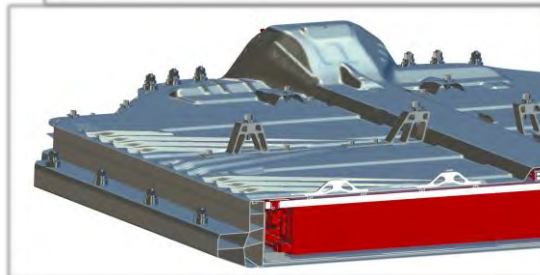
Battery integration – Safety

Complete vehicle side pole impact

- Body and battery working together to protect cells

Also looking into these safety loadcases:

- Front
- Rear
- De-road (stone impact)
- Etc.



2024-04-26 EV battery structural simulation at Volvo Cars - Nafems Nordic Regional Conference May 2024, Security Class: Proprietary

Battery integration – Durability & NVH

New system with large mass and stiffness influences complete vehicle attributes.

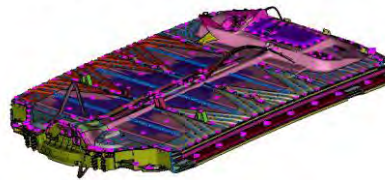
Vehicle stiffness

- Torsional / bending

Complete vehicle durability

- Fatigue test track virtual loads
- Fatigue on base material and joining
- Bolt forces

NVH (Noise, Vibration and Harshness)



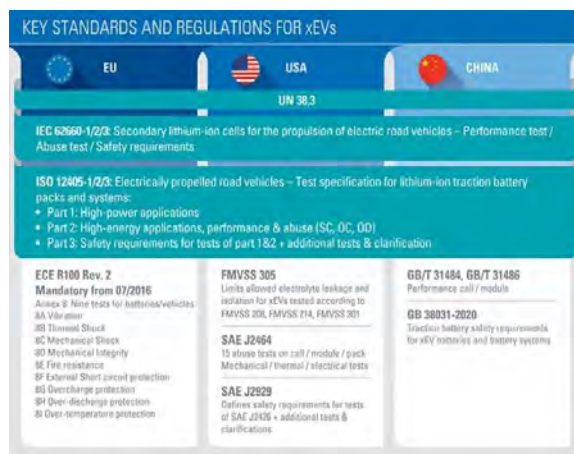
2024-04-26 EV battery structural simulation at Volvo Cars - Nafems Nordic Regional Conference May 2024, Security Class: Proprietary

Battery pack certification

There are different legal requirements/standards that should be passed to allow certification of the battery pack for different markets. For example:

- GB38031-2020 in China
- ECE R100 in Europe

To pass the certification process the Battery pack is subjected to different physical tests and the results are reported (and/or the testing is supervised) to the authorities that issues the approval to sell the car/battery pack on the specific market.



2024-04-26 EV battery structural simulation at Volvo Cars - Nafems Nordic Regional Conference May 2024, Security Class: Proprietary

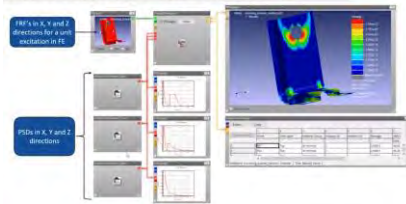
<https://www.tuvsud.com/en/industries/mobility-and-automotive/automotive-and-oem/automotive-testing-solutions/battery-testing/traction-battery-approval-according-to-international-standards>

Battery pack simulation – Vibration

Legal requirement on battery pack

- X, Y, Z direction
- PSD random and fixed frequency or logarithmic sweep depending on market
- Fatigue on base material and joining

Random Vibration Fatigue Process – Virtual Shaker Table



https://www.hbkworld.com/en/knowledge/resource-center/recorded-webinars/random-vibration-fatigue-capabilities-in-ncode-designlife#ref_ncode.com

2024-04-26 EV battery structural simulation at Volvo Cars - Nafems Nordic Regional Conference May 2024, Security Class: Proprietary

Battery pack simulation – Mechanical integrity / Crush

Legal requirement on battery pack

- X, Y direction
- Different impactors in regulations
- Reach 100 kN force

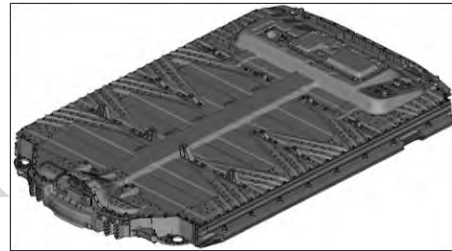
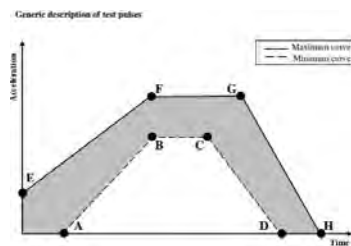


2024-04-26 EV battery structural simulation at Volvo Cars - Nafems Nordic Regional Conference May 2024, Security Class: Proprietary

Battery pack simulation – Mechanical shock

Legal requirement on battery pack

- Acceleration pulses in X, Y, Z direction
- Evaluate stresses and displacements of parts inside battery pack.



2024-04-26

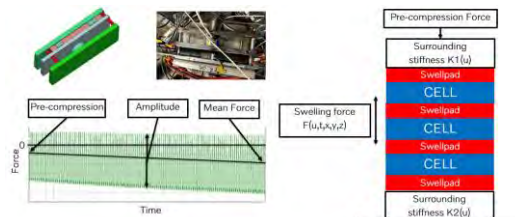
EV battery structural simulation at Volvo Cars - Nafems Nordic Regional Conference May 2024, Security Class: Proprietary

Battery pack simulation – Swelling

Cell swelling forces are one of the more complex type of loading that battery modules and packs are subjected to.

Pulsating load from charging and discharging of the cell and steadily increasing mean force due to ageing of the cell.

- Evaluate surrounding structure load capability
- Cell compression force evolution
- Consequences seen after years of service



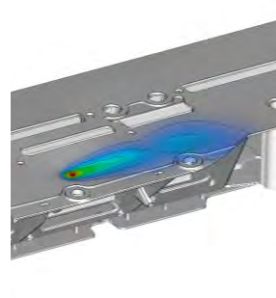
2024-04-26

EV battery structural simulation at Volvo Cars - Nafems Nordic Regional Conference May 2024, Security Class: Proprietary

Battery pack simulation – Weld process

Different manufacturing load cases are simulated, for example welding process.

- Temperature distribution and deformation during welding.



2024-04-26

EV battery structural simulation at Volvo Cars - Nafems Nordic Regional Conference May 2024, Security Class: Proprietary

Component simulation – CFD / FEM coupling

Cooling system

Pressure cycling & burst pressure

- Fatigue on base material and joining
- Strength on base material and joining

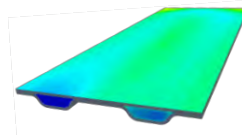
Channel pattern influenced a lot by CFD requirements on pressure drop and temperature on module / cells.

Busbars (electrical distribution)

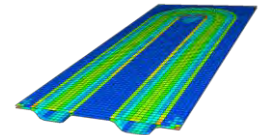
Temperatures mapped from CFD solver to busbars for different driving and fast charge scenarios.

- Fatigue on base material and joining.
- Reaction forces on electrical connector components.

CFD solver
Pressure



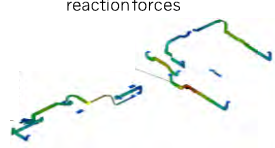
FEM solver
Stresses / displacement



CFD solver
Temperature



FEM solver
Stresses / displacement /
reaction forces



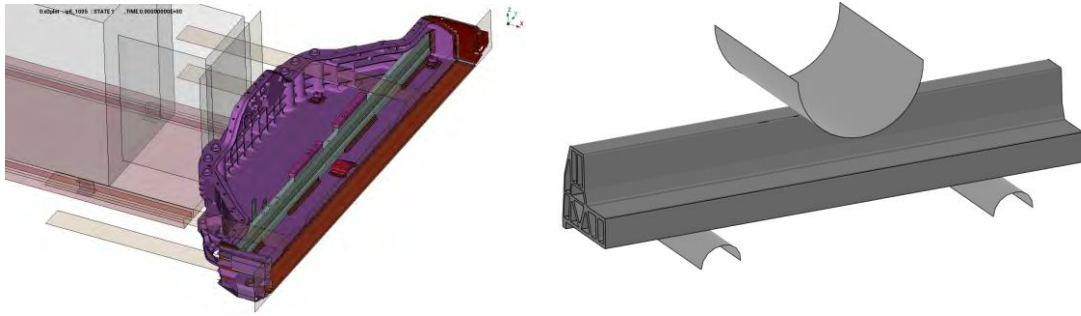
2024-04-26

EV battery structural simulation at Volvo Cars - Nafems Nordic Regional Conference May 2024, Security Class: Proprietary

Component simulation – Casting & extrusions

Correlation to testing to get correct behavior of CAE model in impact load cases

- Modeling and material parameters

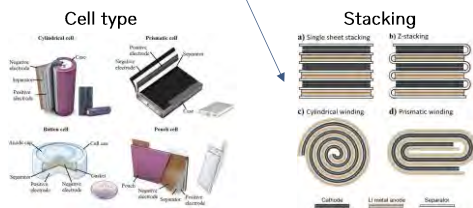


2024-04-26 EV battery structural simulation at Volvo Cars - Nafems Nordic Regional Conference May 2024, Security Class: Proprietary

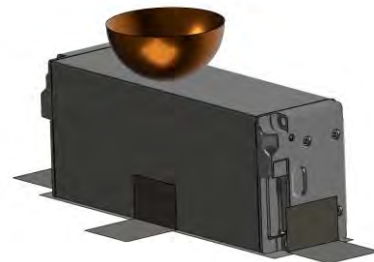
Component simulation – Cells & modules

Correlation to testing to get correct force-displacement behavior of CAE model

- Quasi-static
- Dynamic
- Optimization of "Jellyroll" material parameters



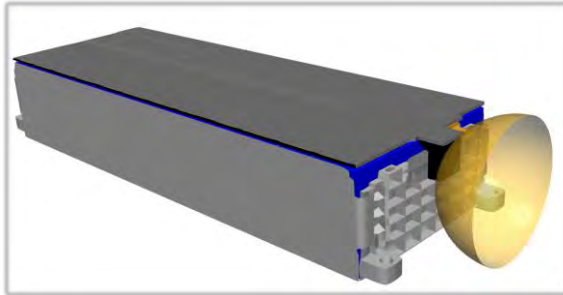
Left: Murashko, PhD Thesis Lappeenranta University of Technology, 2016
Right: Wu et al., Journal of The Electrochemical Society, 2019



2024-04-26 EV battery structural simulation at Volvo Cars - Nafems Nordic Regional Conference May 2024, Security Class: Proprietary

Component simulation – Cells & modules

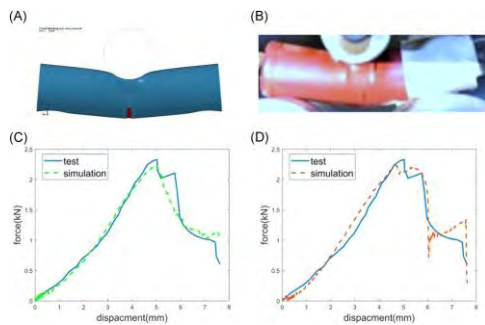
Correlation to testing



2024-04-26 EV battery structural simulation at Volvo Cars - Nafems Nordic Regional Conference May 2024, Security Class: Proprietary

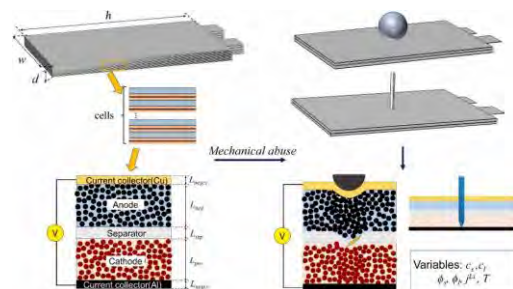
Thesis work at Volvo Cars: spring 2024

Material characterization & mechanical modelling



From: Song et al., *Energy Science & Engineering*, 2022

Short-circuit modelling



From: Li et al. *Energy*, 2023

2024-04-26 EV battery structural simulation at Volvo Cars - Nafems Nordic Regional Conference May 2024, Security Class: Proprietary

CAE challenges

Material

- Cast aluminium
- Extruded aluminium

Joining

- Aluminium welding
- Adhesive

Cell model

- Cell internal parts supplier IP (does not want to share)
- "Jellyroll" modeling & properties
 - Layered to homogenized

2024-04-26

EV battery structural simulation at Volvo Cars - Nafems Nordic Regional Conference May 2024, Security Class: Proprietary

Conclusions

- Safety - cornerstone in Volvo Cars design philosophy
- Volvo moving to 100 % electric
- Whole company need to learn about a new large subsystem
- Battery to body integration important
- Cells / modules sensitive to mechanical deformation
- New loadcases and components for Volvo Cars
- Correlation to testing to improve modeling and trust in CAE results



2024-04-26

EV battery structural simulation at Volvo Cars - Nafems Nordic Regional Conference May 2024, Security Class: Proprietary

VOLVO

More about Volvo Cars

volvocars.com



investors.volvocars.com



2024-04-26 EV battery structural simulation at Volvo Cars - Nafems Nordic Regional Conference May 2024, Security Class: Proprietary

VOLVO

Thank you!

Design Space Exploration of Battery Pack and Body in White Integration

Fredrik Rosenlund, Timur Khalitov, Karthik Govindarajan, Mark Lamping

Siemens Digital Industries Software

Abstract

Integrating the battery pack into the electric vehicle body (chassis) is often a challenging task for engineers. For example, integrating a battery pack might cause too much vibration during operation, affecting NVH performance and as a result passenger comfort and potentially the safety of the passenger.

To achieve the desired NVH performance while also not sacrificing range or comfort, engineers test various virtual model configurations which are built in standard Finite Element Analysis (FEA) software packages. This aids them in simulating the NVH characteristics to study what and how different characteristics of the battery pack in a Body-in-White (BIW) model affect performance. Manually simulating the required number of scenarios is almost an impossible task as it takes a burdensome number of man-hours.

This presentation highlights how modern simulation process automation and multi-disciplinary design space exploration (optimization) can be used to consistently deliver high-performance, low-cost designs within tight timelines. Specifically, this presentation reviews an example of a FEA model of a BIW electric vehicle and the NVH performance of the BIW when a battery pack is integrated. A key performance attribute of automotive bodies is their first torsion mode frequency. When the system operates at a higher torsional frequency, it indicates greater passenger comfort. Typically, NVH analysts will study attributes of a system to increase stiffness and reduce mass. But the mass and frequency of an electric vehicle system are competing characteristics, so, a fine balance needs to be achieved to satisfy all requirements necessary for product development.

For this type of simulation, verification is traditionally done manually by correlating the mode shapes (dynamic deflection patterns of a system) with the required reference mode shapes, in order to ensure necessary vibration characteristics. This again is challenging as it requires a lot of time and expertise to do the correlation. This presentation also demonstrates an automated mode shape correlation technique between two analysis models, incorporated within the design space exploration.

A well-qualified analysis model acts as the reference to the current model under development. Then a design space exploration (optimization) is setup that exercises a set of parameters that influence overall system stiffness and mass. These include connections (bolts, glues etc.), choice of materials of the battery pack, panel thickness assignments, as well as the inclusion/exclusion of certain components. A manufacturing cost function is applied to the exploration as well to avoid an optimal analysis solution, but an infeasible solution for manufacturing.

The objective of the design space exploration (optimization) will be to minimize the mass of the system while maintaining thresholds on cost and the first torsion modal frequency of the system. This presentation will also walk through how intelligent design space exploration and data mining of the results will help you understand your design space and your product better. This will help you in making well-informed design decisions faster and aid in rapid product development.

1 Finite element model build process

Creation of the finite element models (FEM) for the complete BIW and battery pack can take significant amount of time due to complexity of the workflow which implies preprocessing of different type of input data like CAD Bill-of-Material (BOM) data of hundreds of components, material data, joining, meta-data, etc.

This presentation highlights how CAE departments can speed-up and automate FE model build process by leveraging design data and meta-data. In particular, this includes execution of the automated batch meshing process for CAD BOM components including material physical properties assignment, automated assembling of FE models based on predefined assembly template for particular analysis discipline (structural, NVH, crash, etc) and finally connections (spot welds, seam welds, screws and bolts, adhesive, etc) are created by leveraging joining data defined in the CAD model [1].

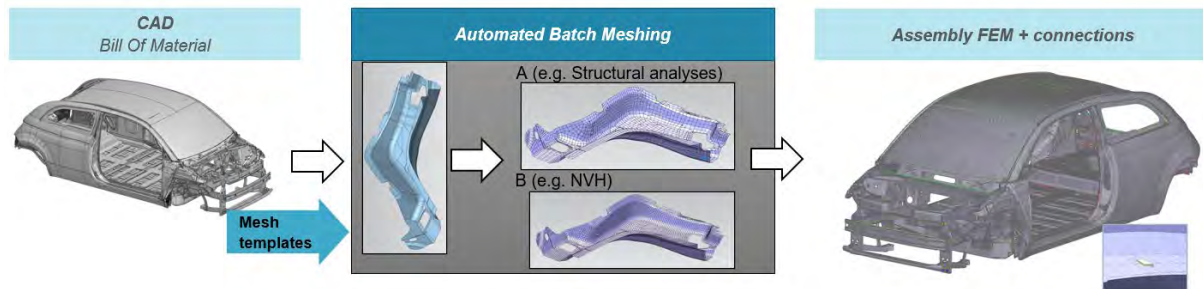


Fig. 1
Finite element model build process

2 Analytical technique to gauge NVH performance of a BIW model with an integrated battery pack

NVH performance of a BIW electric vehicle when a battery pack is integrated is gauged by analysing normal modes. The first torsion mode is observed and shape correlation for its first torsion mode to a reference model modal shape is carried out. A well-qualified reference model is used for the correlation.

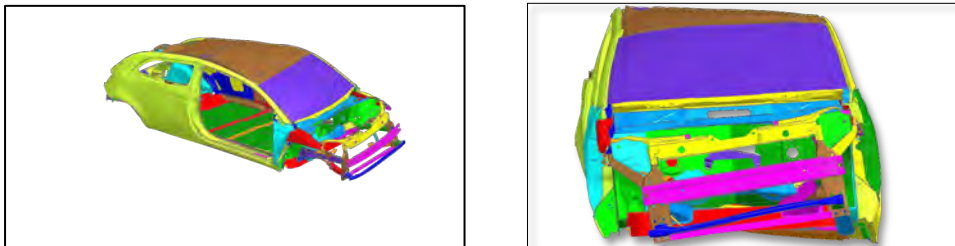


Fig. 2
First torsion mode shapes

The mode shape correlation was quantified using the Modal Assurance Criterion (MAC) [2]. MAC is a parameter indicating the degree of consistency between a mode shape from the reference data and a mode shape from the work data. These mode shapes can be real or complex. A MAC parameter is a scalar value between zero and one. The value near one indicates a high degree of correlation or consistency between two mode shapes.

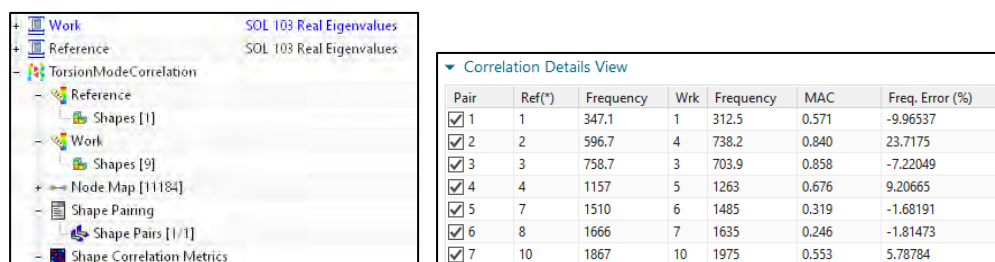


Fig. 3
Shape correlation setup

A mode pair is created based on a mode from the simulated data that yields the highest MAC value for a given mode from the test data.

3 Automation and Design Space Exploration using HEEDS

The fully validated finite element model is used to conduct a design space exploration (optimization) study of the NVH performance. Driving design changes to the model is automated using the HEEDS design space exploration software. The goal of the study is to minimize mass of the vehicle subject to constraint on the first torsion mode frequency and cost. Following are the design variables of the study:

Table 1: Design variables considered for the optimization study		
No	Variable	Range
1	Floor stiffeners	2,5
2	Number of bolts on the floor stiffeners	0,2,4
3	Number of bolts on the side	4,6
4	Rear roof stiffener	On/Off
5	Adhesive between floor and battery pack	On/Off
6	Materials for the battery pack (4 parts)	Steel, Aluminium, Composite
8	Cost function	Calculated based on material chosen

4 Design exploration results

Design space exploration study found 119 feasible design alternatives satisfying study constraints.

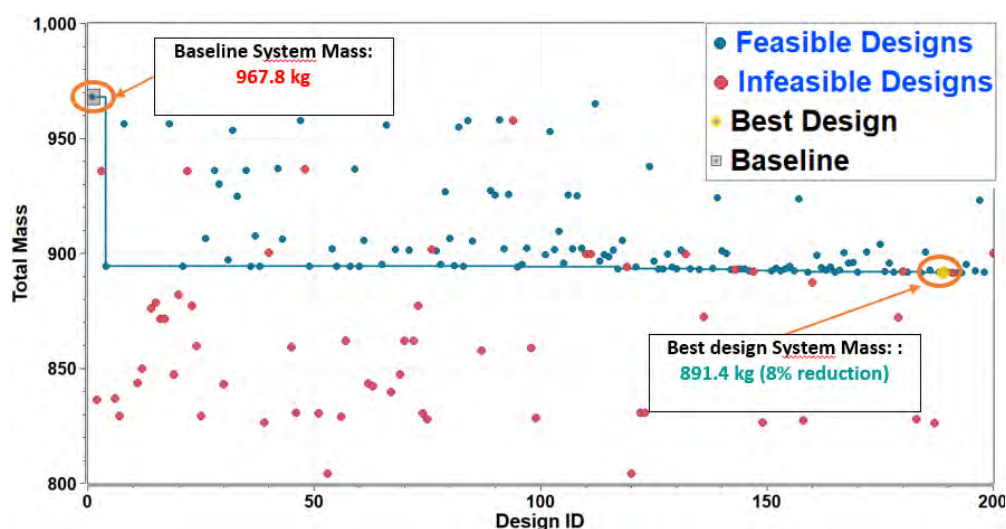


Fig. 4
Designs classified as Feasible (satisfying constraints) and infeasible (violating constraints)

Postprocessing and analysis were conducted to identify how design variables impact the overall performance of the design and to compare the best design with its close alternatives (outliers).

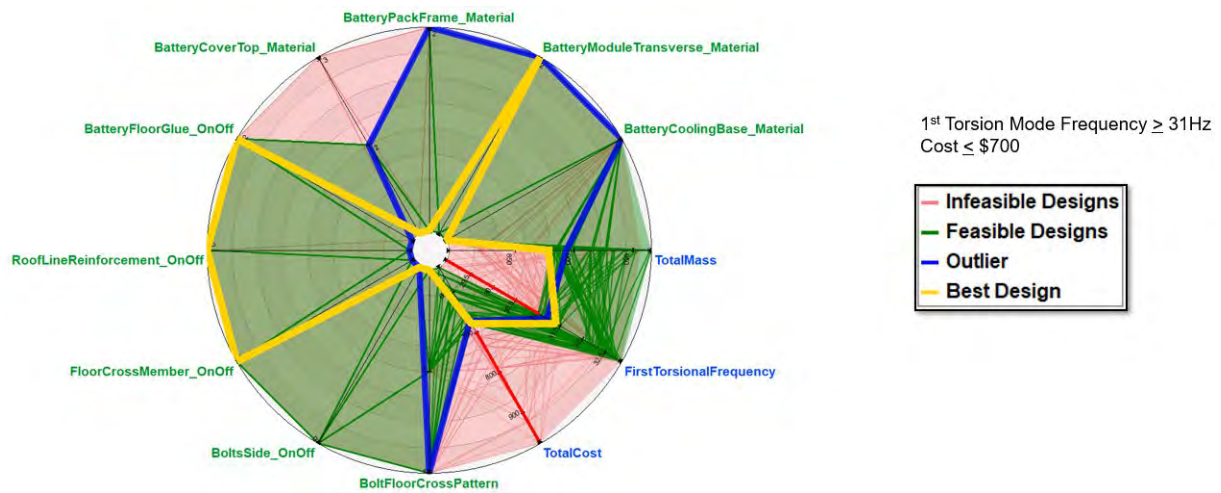


Fig. 5
Radial plot of design variables, constraints and objective

5 Conclusion

This paper demonstrates how new-age simulation and multi-disciplinary design space exploration software can be used to balance conflicting attributes while driving numerous design variables to guide engineers toward optimal design solutions.

6 References

- [1] Lamping M.: "Automated model build process through an SPDM system", 2019 NAFEMS World Congress in Quebec Canada
- [2] Allemang, R.J., "The Modal Assurance Criterion - Twenty Years of Use and Abuse", Sound and Vibration, August 2003.

Strongly coupled multiphysics simulation of a loudspeaker driver using a multiharmonic approach

A. Deshmukh, A. Halbach, B. Khouya, R. K. Nagaraja, V. Lahtinen

(Quanscient Oy, Åkerlundinkatu 8, 33100 Tampere, Finland)

1 Introduction

Designing sound systems for different applications poses different challenges. These include interactions between several loudspeaker drivers in an audio rack system for concerts. The packaging of the drivers into ever-thinning televisions or personal computers without compromising the sound quality requires ingenious designs. For such design iterations, accurate and fast numerical simulations can be very helpful. A loudspeaker driver involves several physical phenomena that eventually create the sound in the human hearing range (20 Hz - 20 kHz). An electric current through the voice coil induces the magnetic field that interacts with a permanent magnetic field, generating a vibrating motion of the cone, which in turn, emits acoustics waves creating the desired sound. In this work, we present a strongly coupled multiphysics simulation of a loudspeaker driver using Quanscient Allsolve [1]. A multiharmonic approach [2] is used to capture the nonlinear effects of the coupling among the current flow, magnetism, solid mechanics, and acoustics. The multiharmonic method allows the steady-state simulation of periodic signals without a transient analysis. In addition, in our method, as many harmonics as required can be selected, and they need not be consecutive.

2 Methods and models

2.1 Multiharmonic method

A typical transient analysis to get a steady-state periodic solution can take a very long time as shown in Figure 1 and involve manual steps, such as restart strategies if the simulation runs for multiple days. In addition, to obtain the frequency distribution in the signal, fast Fourier transform (FFT) needs to be performed on the transient signal. The frequencies extracted by using the FFT of the transient signal may contain noise if the resolution of the signal is not enough.

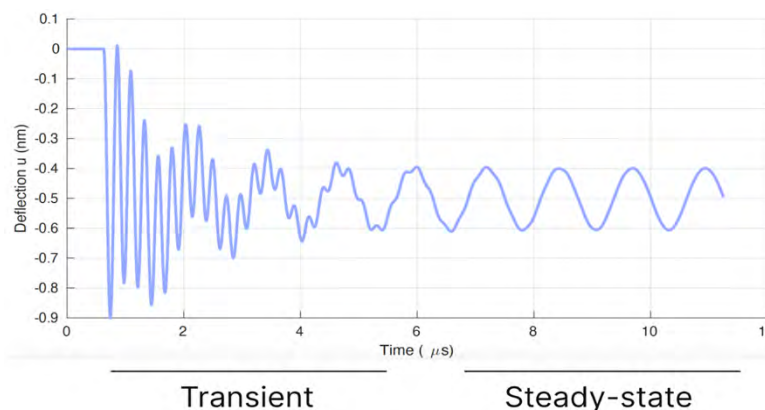


Fig. 1
Displacement over time showing transient behavior before reaching a steady periodic state [3].

Frequency domain analysis, also known as harmonic analysis is often used to avoid such transient simulations but such an analysis is limited to linear problems with one frequency. The multiharmonic (also called harmonic balance) method approximates steady-state solutions to nonlinear periodic problems in the frequency domain. Thus, this method enables to access the steady-state region without a need to simulate the initial transient simulation for complex but periodic signals. The nonlinearities in the governing equations result in harmonics other than the fundamental frequency to appear in the solution and these are naturally represented by the multiharmonic method. The fields are decomposed

with a truncated Fourier series including as many as possible of the dominant harmonics, as shown in Eq. 1. The harmonics considered are not anymore only those of the excitation field since new harmonics can appear due to the nonlinearity of the problem.

$$\phi(x, t) = \sum_{k=0}^N \phi_{sk}(x) \sin(\omega_k t) + \phi_{ck}(x) \cos(\omega_k t) \quad (1)$$

A limitation of the multiharmonic method is that the number of unknowns grows rapidly with increasing number of harmonics in the simulation, which in the finite element framework implies increasing memory requirements and increasing computational costs. Furthermore, the implementation becomes increasingly complex with the increasing number of harmonics. These limitations have been overcome by Quanscient Allsolve using a generalized scalable implementation and a cloud-based platform, which makes available the required hardware on demand.

2.2 Multiphysics model

In this work, a two dimensional (2D) axisymmetric model of a loudspeaker driver (shown in Figure 2) is simulated in Quanscient Allsolve. A typical loudspeaker driver consists of a permanent magnet, a pole piece and a plate, a voice coil attached to a former, a diaphragm that forms the cone and emits sound waves, a dust cap, a surround, and a spider that restricts the motion of the coil former in the axial direction. Figure 3 shows the domain used in the simulation, which includes the loudspeaker components as well as the outer acoustics domain with a radius of 1.25 m.



Fig. 2
Geometry of loudspeaker driver.

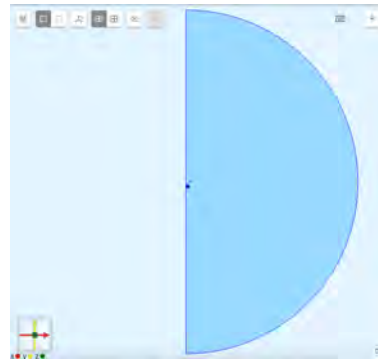


Fig. 3
Domain of simulation including the acoustics region.

The permanent magnet and the voice coil is modeled by the H-phi formulation for electromagnetics. The coil is driven by a sinusoidal current signal. The diaphragm including the former, the surround, and the spider are modeled by linear elasticity and coupled with the H-phi formulation by a magnetostatic force. The acoustics in the outer region is modeled by Helmholtz equation and coupled with the linear elasticity. All the governing equations are implemented in a single finite element formulation making them a strongly coupled system of equations. The system of equations is then solved by multiharmonic method in frequency domain as described in section 2.1. The nonlinearities in the system appear due to interaction between permanent magnetic field and the induced magnetic field in the voice coil, with a force acting on the voice coil which scales as the square of the amplitude of the current. Thus, the constant harmonic with zero frequency appears in the system. Also, higher harmonics with double the fundamental frequency appear, which are readily modeled by considering higher harmonics. An absorbing boundary condition was used on the outer spherical boundary to let the acoustic waves leave the domain without reflections.

For this work, the first three harmonics were chosen for the representation of all fields. The mesh for the domain was created with 212710 nodes and 107107 elements. This mesh with the Multiphysics formulation resulted in 2.15 million degrees of freedom (DoFs). A frequency sweep was performed in the audible sound range of 20 to 20000 Hz. The sound pressure level was computed at a distance of 1 m on the axis of the loudspeaker driver in the direction of acoustic emission. In addition, a three-dimensional (3D) simulation with the loudspeaker driver in a cabinet with a resonator (12 million DoFs) was performed as an application to demonstrate the method and solver capabilities.

3 Results and discussion

Figure 4 shows the pressure field in the outer region along with the magnetic field represented by flux lines and direction shown by the arrows at a fundamental frequency of 6000 Hz. For representation purposes, the axisymmetric field was reflected about the symmetry axis. The acoustic waves are emitted in all directions in a spherical manner. However, it can be observed that the waves have stronger amplitudes in the axial direction away from the diaphragm (positive Y-axis). This is due to the conical diaphragm that creates constructive and destructive interference, resulting in the directivity pattern of the loudspeaker.

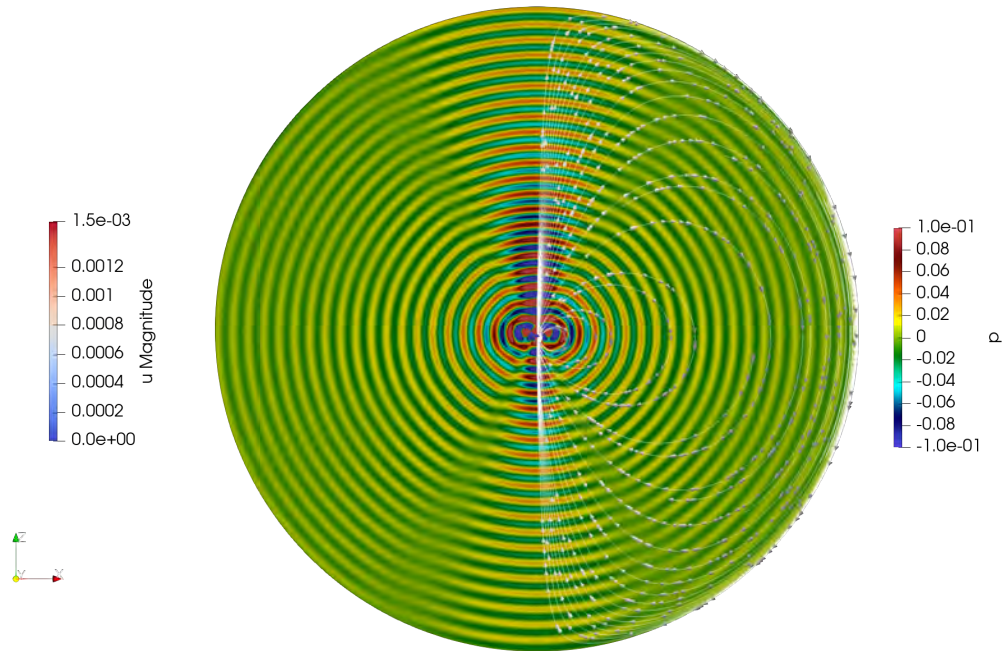


Fig. 4
Pressure contours at frequency of 6000 Hz with contour lines with arrows denoting magnetic field of permanent magnet.

Figure 5 shows the sound pressure levels (SPLs) computed in decibels as described in section 2.2 at several frequencies in the human-audible range. For this geometric configuration, the spectrum of SPLs is irregular between 800 to 1000 Hz. This warrants an optimization of the geometry and materials to obtain the desired SPL spectrum for the application in loudspeaker systems.

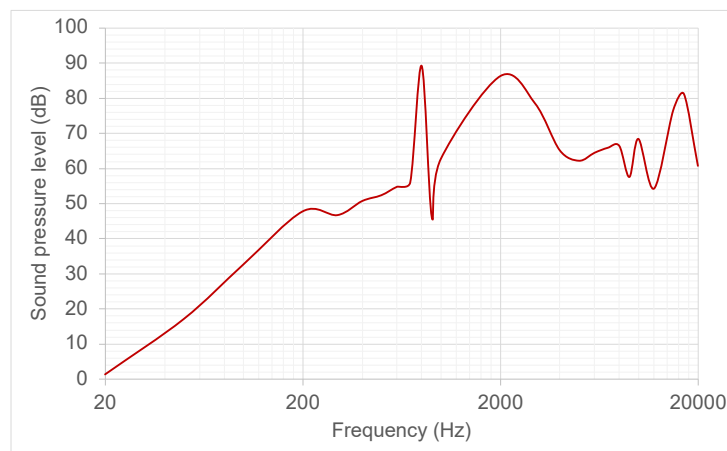


Fig. 5
Frequency sweep of sound pressure level in the human-audible range.

In addition to 2D axisymmetric simulations, the 3D simulation of the loudspeaker in the cabinet with the resonator was also carried out as an application to demonstrate the method and solver capabilities. Figure 6 shows the pressure field emitted by the loudspeaker system with a mannequin representing a human. The corresponding loudspeaker driver is shown colored by displacement field and magnetic field lines. Once the pressure field is calculated, it can be interpolated on any external object to analyze the SPLs at desired locations and their potential effects on the objects, in this case, the mannequin.

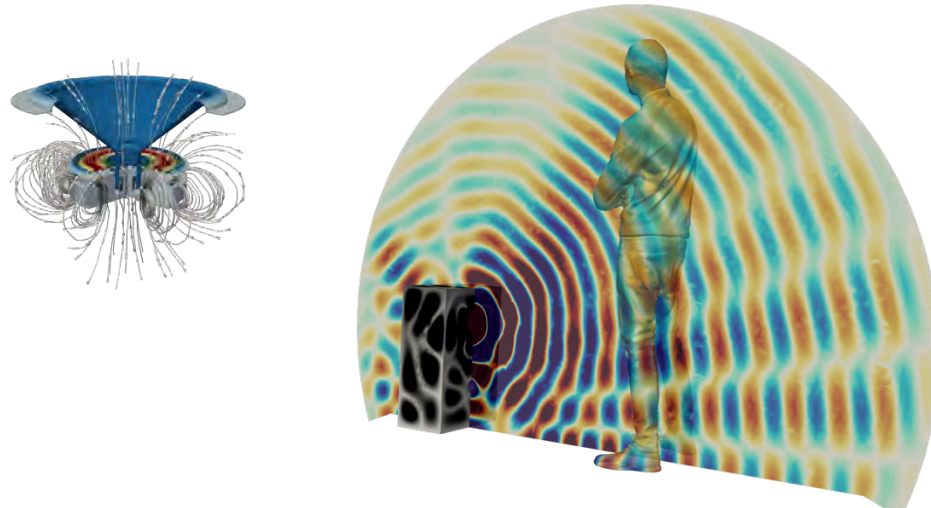


Fig. 6
Loudspeaker driver (left) in 3D Multiphysics simulation with cabinet and resonator (right). Pressure field interpolated after the simulation on a mannequin standing at a distance.

Table 1 shows the run times for the simulations performed in this work. Each of the 2D axisymmetric simulations (altogether 25 simulations running at the same time) was run on a single core for about 3 min 40 sec. The 3D simulation ran for about an hour on 32-core-256-GB machine. Note that the domain decomposition method was not used for this simulation, which may further reduce the run times.

Table 1. Run time statistics.

Simulation	DoFs (million)	Cores	RAM (GB)	Run time
2D Axisymmetric	2.15	1	16	3 min 40 sec
3D with cabinet	12	32 (multithreading)	256	1 hr

4 Conclusion

This work shows the application of the multiharmonic method to the simulation of a loudspeaker driver. The method was successfully applied to a multiphysics problem including electromagnetics, linear elasticity, and acoustics strongly coupled in a finite element framework. The capabilities of the method leveraged by cloud computing are highlighted by quick simulation run times, e.g., less than 4 min for 2.15 million DoFs, to obtain a frequency sweep of sound pressure levels.

5 References

- [1] Quanscient Allsolve: <https://quanscient.com/>, retrieved on 28.04.2024.
- [2] Nakhla M. S. and Vlach J.: "A piecewise harmonic balance technique for determination of the periodic response of nonlinear systems", IEEE Transactions on Circuits and Systems, vol. 23, pp. 85-91, 1976.
- [3] Halbach A.: "Domain decomposition techniques for the nonlinear, steady-state, finite element simulation of MEMS ultrasonic", PhD Thesis, University of Liège, 2017.

Electric drive virtual development and thermal management – project presentation

Michael Hood, Florent Colas, Darren Nunes, Jonathan Brunel (Siemens Digital Industries Software)

1 Summary and Context

The landscape of automotive technology is undergoing a profound transformation because of the increasingly diverse set of requirements emerging from the various market segments and territories, transitioning from the long-established legacy powertrain architecture to electric drivetrains.

Siemens owns several [eRod sport cars](#), made by the Swiss company Kyburz. ERod is a two-seats, 600kg electric vehicle powered with a 45KW motor at a maximum speed of 120kmh. Its expected range is 208km (EU 134/2014).

Siemens is naming those cars Simrod and uses them both to benchmark, demonstrate and validate its simulation and testing solutions. Those physical cars have a digital twin, a digital representation that can serve for simulation, validation and demonstration purposes. In this Simrod context, Siemens is currently running a comprehensive demonstrator project, related to the development and integration of the Simrod's electric drivetrain.

The project covers the V-Cycle of the electric drive development of a racing variant of the Simrod under specific cost constraints, and the presentation will focus on the thermal management of the E-Drive.

The original design intended for leisure and fun is known to face some thermal management limitations in racing conditions: the impact of racing conditions is assessed from its preliminary architectural sizing down to the final detailed engineering of its components, while keeping an up-to-date picture of the project constraints on the design solutions.

2 Integrated Workflow

Developing and integrating an electric drive in a short time, with excellent performance in a wide range of operating conditions, while meeting all requirements imposed by customer and by internal brand image, requires various stakeholders to collaborate efficiently. This ecosystem contains engineers with different scientific fields of expertise, working on conflicting attributes, specialized in the development of different high-end components, working in different teams, and sometimes different companies. All of them need to receive clearly defined design requirements and to make design choices informed by sourcing and manufacturing constraints and the latest data from the design project.

A full-vehicle system model is used to cascade vehicle requirements down to requirements for the electric drive and for each of its components (motor, inverter, transmission). A design exploration approach is used to identify the best e-drive design and thermal management solutions.

Virtual models of the e-motor components are concurrently and iteratively developed and validated. They gain accuracy as the design is converging toward a fully defined 3D model and mature solution. The high-fidelity component characterisations are shared accross the different models and can then be re-introduced in the full-vehicle simulation to verify requirement compliance at all stages of the project.

3 A sport version of the Simrod : Requirements & Design

The project starts with requirements for the vehicle. The drivetrain must power the Simrod through a demanding race track driving cycle derived from real life telemetric data, while keeping an acceptable temperature for the motor and the inverter, a low noise level and the expected range. It must accelerate from 0 to 40kph in 2.5s and from 0 to 60kph in 4.0sec. It must be able to start with a 30% slope.

Those requirements are used as targets of a design space exploration using HEEDS, the design space exploration and optimization software from Siemens. HEEDS drives a complete vehicle system model in Simcenter Amesim, the system simulation platform. The motor design parameters and life expectancy are balanced with the E-Drive architecture sizing, performance, and cost. This analysis allows to identify an architecture of the electric drivetrain and send requirements to the electric motor, transmission, and inverter development teams.

The electric motor is designed with Simcenter E-Machine Design. This is a template-based, vertical product which allows to find the best motor configuration to reach the targets imposed by requirements. Variables are the materials and geometry of the motor components, the motor configuration and type.

The obtained functional design is re-integrated into the initial Amesim model by importing the Simcenter E-Machine Design as a lumped parameter thermal network (LPTN) model for thermal analysis (see Figure 1), such that it can be validated over the entire drive cycle as part of the entire vehicle. The E-Machine Design model is also used as a source of electromagnetic loads used later in the development process, and to generate a detailed CAD-based model of the electric motor.

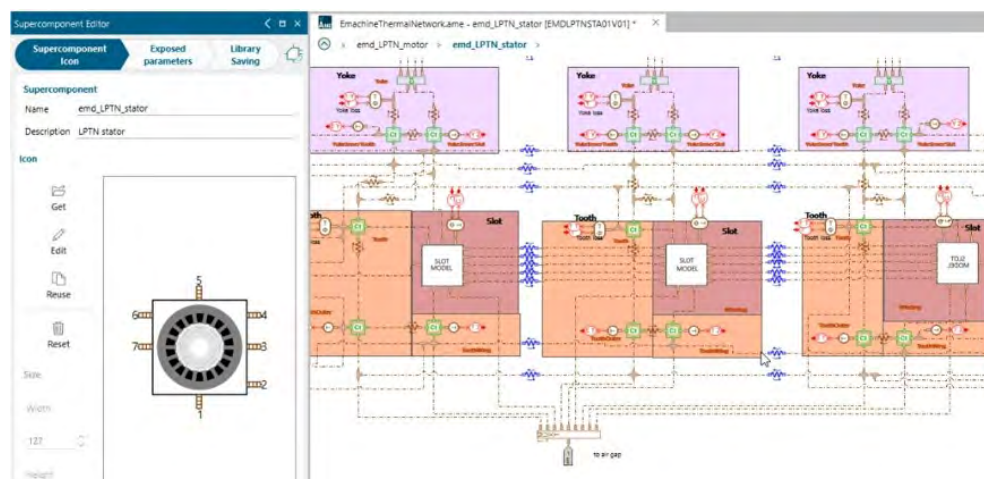


Fig. 1 : Import in Simcenter Amesim of the LPTN model of Simcenter E-Machine Design for the updated Simrod motor design.

The motor, the transmission, the inverter, the housing, are assembled into a full vehicle 3D model, using the integration of the NX platform. This model is used and shared by the mechanical, NVH and thermal teams. If one team edits a component, it is updated for other teams thanks to the Teamcenter integration.

As part of this integrated workflow the temperature of the electric drivetrain over the entire drive cycle is assessed and shows the limitation of the existing passive air-cooled technology and the necessity to use an oil shaft cooling, new rotor and optimized design of the stator teeth and slots. All those results are shared with the program management and other stakeholders, thanks to the PLM backbone.

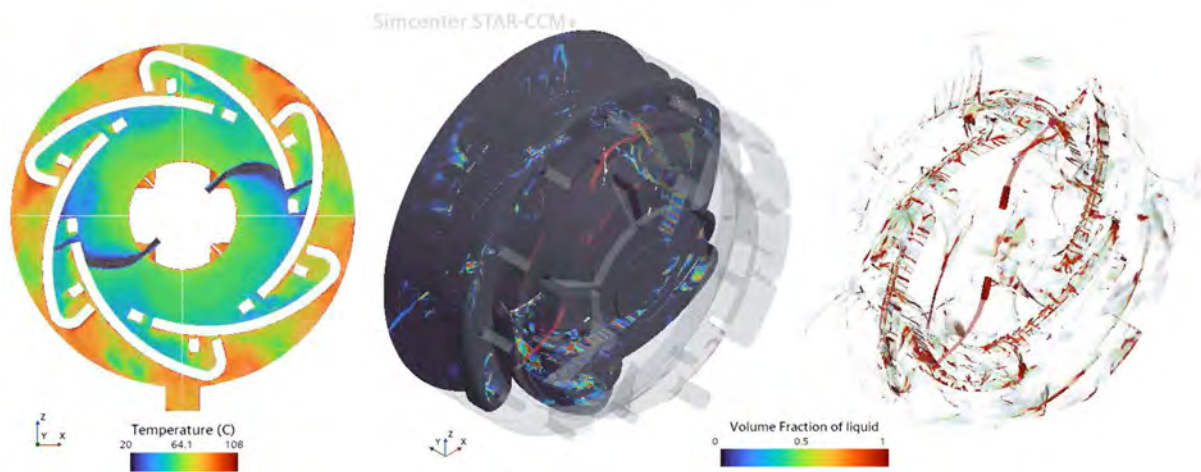


Fig. 2 : Simcenter STAR-CCM+ oil cooling simulation of the Simrod motor design updated with Simcenter E-Machine Design

As the oil shaft cooling is required to satisfy the requirements, the project wants to assess the benefit of adding shaft oil injector to further improve the cooling of the stator end-windings at no significant added cost. Based on the latest CAD model generated from the new E-Machine Design model a detailed simulation of the shaft oil injectors and the resulting oil spray cooling is setup in Simcenter STAR-CCM+ (see Figure 2) and computed over a range of operating points. The results of these high-fidelity simulations allow to predict the improved cooling performance accross the operating range. The Simcenter Amesim LPTN model is easily updated with this design change and its associated performance identification. As was done at every step of the project and design changes, the validity of this final design can be automatically assessed against the original project requirements and propagated to the other stakeholders.

The purpose of the NAFEMS presentation will be to introduce this project.

Building simulation models credibility: What gain can we expect from test-simulation data fusion in solid mechanics?

Pierre Baudoin, Florent Mathieu
EikoSim, France

Nicolas Swiergiel
ArianeGroup, France

Ensuring the credibility of building simulation models is imperative for justifying cost reductions in testing and expediting the development of innovative structures. However, enhancing model credibility with limited test data necessitates the establishment of robust model validation metrics and toolboxes. This presentation will delve into the challenges associated with implementing data fusion techniques, exploring how they can significantly bolster model reliability.

Moreover, we will delve into the integration of Digital Image Correlation (DIC) technology, a pivotal tool aiding in the acquisition of additional test data for enhancing model credibility. DIC technology facilitates the extraction of detailed strain and deformation information by analyzing images, providing valuable insights that contribute to more comprehensive model validation.

The discussion will highlight the intricacies of data fusion and DIC technology, addressing the hurdles and showcasing the rewards they bring to the table. By exemplifying these concepts, we will present a case study involving a test-simulation dialogue of a large-scale structure built by ArianeGroup for the Ariane 6 launcher. The application of data fusion and DIC technology in this real-world scenario will underscore their effectiveness in optimizing model validation processes, ultimately enabling the development of reliable simulation models for complex structures.

1. Introduction and objectives

Building simulation models play a pivotal role in justifying cost reductions and expediting the development of innovative structures. However, ensuring the credibility of these models, especially with limited test data, poses significant challenges. Robust model validation metrics and toolboxes are essential for addressing these challenges effectively.

This presentation focuses on the implementation of data fusion techniques to enhance the reliability of building simulation models. Additionally, it explores the integration of Digital Image Correlation (DIC) technology for acquiring supplementary test data. The objective is to highlight the application of these techniques through a real-world case study involving a large-scale “Dual Launch Structure” (see Fig 1) constructed by ArianeGroup for the Ariane 6 launcher. Through this exploration, we aim to showcase how data fusion and DIC technology can optimize model validation processes, ultimately facilitating the development of reliable simulation models for complex structures.



Figure 1: Ariane 6's Dual Launch Structure (left) and location within the launcher (right)

2. Challenges in Application of Data Fusion Techniques to the Dual Launch Structure

The Dual Launch Structure is a critical component in the Ariane 6 launcher project. With a height of about 9 meters, its primary purpose is to facilitate the simultaneous launch of two similar payloads. A test was conducted at ArianeGroup facilities to validate its behavior at maximum loading and identify possible discrepancies between the FEA and real-life test results.

Data fusion techniques encompass methodologies for integrating disparate data sources to enhance the reliability and accuracy of building simulation models. In the context of the Dual Launch Structure, data fusion involves amalgamating data from various sources, such as DIC measurements, but also about 200 strain gauges, fiber optics, force and displacement sensors. The underlying principle is to leverage the complementary nature of these datasets to gain a more comprehensive understanding of the structure's behavior.

In the context of the Dual Launch Structure, data fusion involves amalgamating data from various sources, such as DIC measurements, but also about 200 strain gauges, fiber optics, force and displacement sensors. Secondly, the scale and complexity of the structure required robust methods for processing, analyzing, and interpreting a large volume of test data with respect to their FEA counterpart. Finally, resource constraints, such as limited time, budget, and computational power, impose challenges in efficiently utilizing available resources for model validation: traditional spreadsheet-based FEA validation can be extremely long to set up in the case of large test datasets, and most of the test data is often discarded.

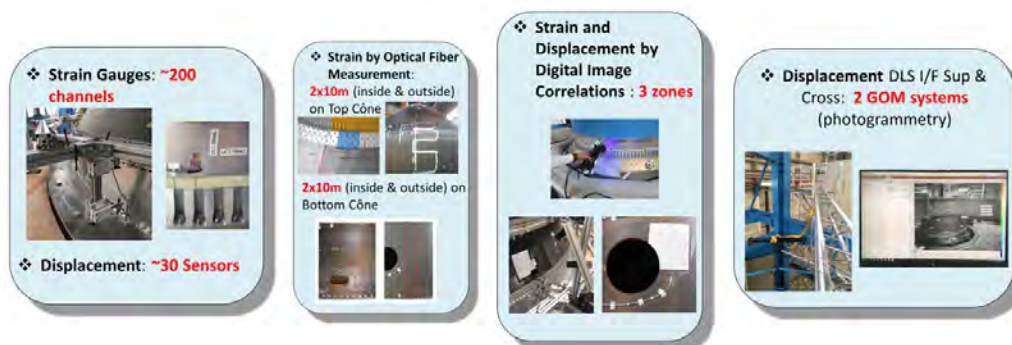


Figure 2: Instrumentation list for the Dual Launch Structure test.

3. Processing

Addressing these challenges required the development of tailored solutions and adaptations. Robust preprocessing techniques were employed to standardize both FEA and test data formats, resolve inconsistencies, and eliminate outliers, ensuring compatibility and coherence among disparate datasets. Within the MUTATION collaborative project, a “Smart testing framework” was developed to seamlessly incorporate diverse data sources into simulation models, enabling comprehensive validation against real-world observations (see Fig 3). The main challenge in assembling these datasets onto the simulation model resided in the fact that these test datasets were not originally well aligned with a 3D model, or synchronized with original simulation predictions.

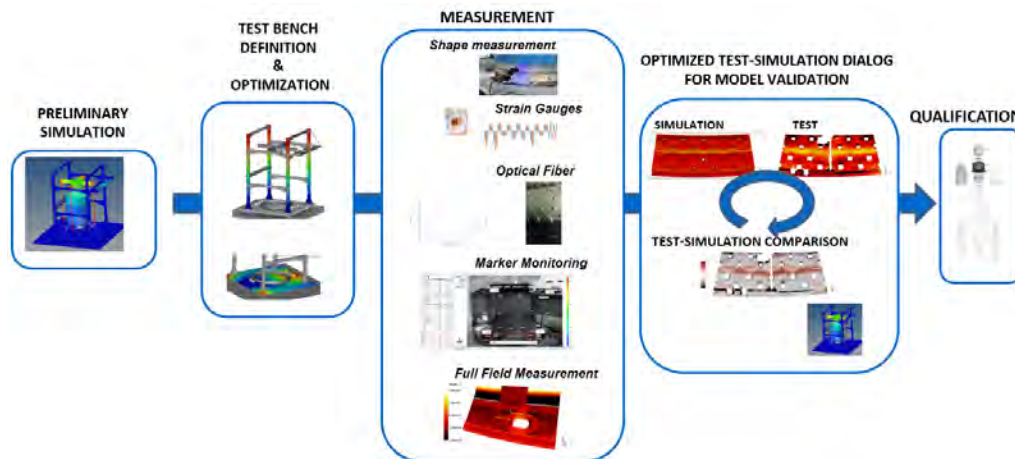


Figure 3: Smart testing framework for the Dual Launch System

4. Results and Conclusion

Through collaborative efforts and a “Smart testing” framework, challenges in validating complex structures were effectively addressed, resulting in an overall validation of the FEA model for future test-less developments.

Having a data fusion framework facilitated the integration of disparate datasets, offering a comprehensive understanding of the structure's behaviour. DIC technology, as well as optical fibers and more traditional sensors, provided detailed insights into structural deformation, validating simulation predictions and identifying areas for optimization.

Key lessons include the importance of robust data preprocessing and convenient tools to aggregate datasets coming from different sources to a 3D model. These insights will guide future endeavours in building models for the DLS, but also ensuring the development of reliable validation methodologies for complex structures in general.

EVIDENT: Investigating Model Validation Approaches

Erik Dartfeldt, Torsten Sjögren (RISE Research Institutes of Sweden)

Toni Bogdanoff, Jakob Olofsson (Jönköping University)

1 Summary

Inspired by the work of Oberkamp and Roy [1], the LIGHTer funded project EVIDENT [2] explores model validation methods to benchmark the current predictive capability of structural cast aluminium components through case studies where results from FE simulations are compared to the corresponding experimental results.

An underlying motivation for the project is the long-term objective of a reduced number of physical prototypes in the product development process to allow for cost reductions and shorter lead times. This, however, requires that the predictive capability of the modelling tools is known and that the tools (and the pertinent guidelines) fulfil the corresponding requirements. One way to evaluate this compliance is through Predictive Capability Assessments which is a key component of EVIDENT.

2 Case study: tensile testing with and without notches

To introduce the concepts and the terminology from the field of model validation an initial case study was carried out using a flat tensile test specimen. The specimens were manufactured through High Pressure Die Casting (HPDC) using the alloy EN AC-46000. No heat treatment was used, and testing was carried out with the casting skin intact. The test specimen geometry is shown in Figure 1.

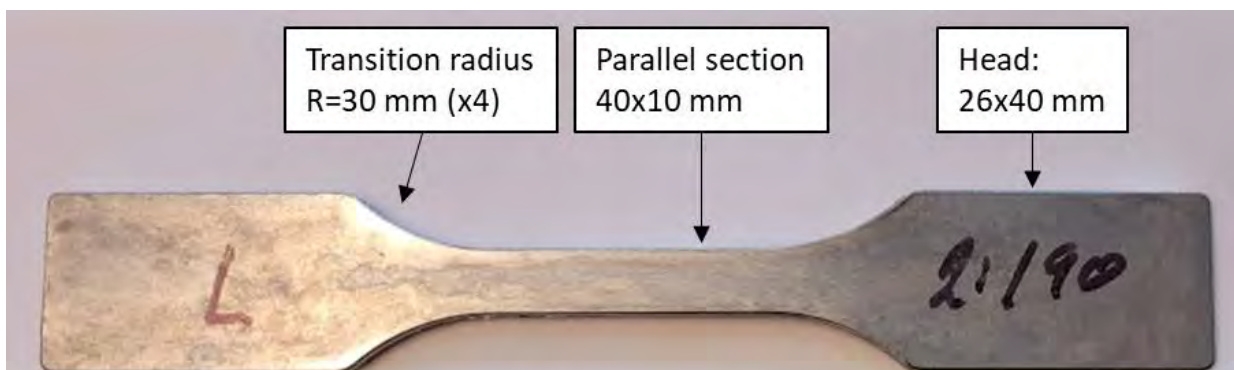


Figure 1. Nominal test specimen geometry (G1).

In order to include the predictive capability of geometrical notch effects in the study, an alternative geometry was also considered in the study, see Figure 2. With this geometry, three regions with locally

higher strains were obtained. The ability to predict the location of the final rupture was one part of the simulation task.

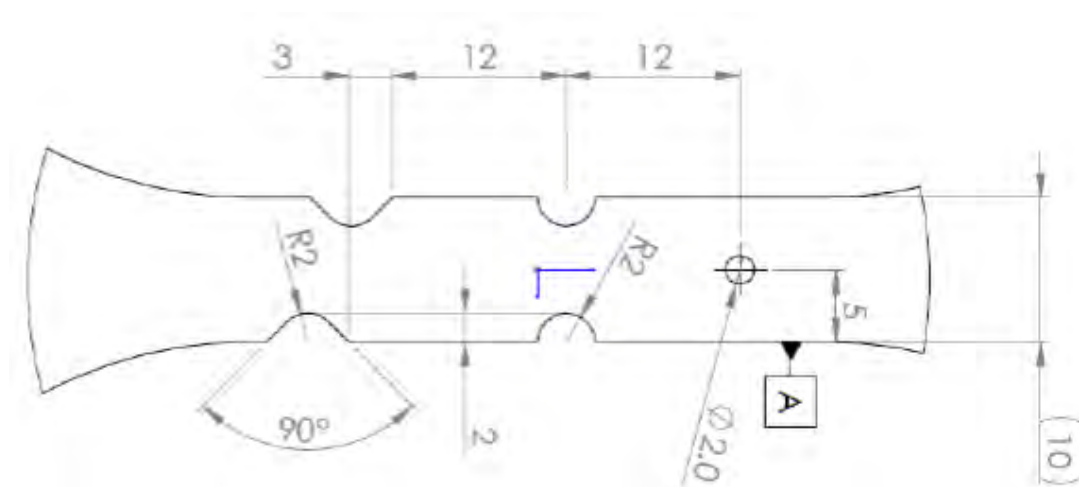


Figure 2. Modified test specimen geometry (G2).

Experimentally, testing was carried out at two test sites (RISE in Borås and Jönköping University). The test specimens were loaded axially by applying a fixed displacement rate at the upper head of the specimen while clamping the lower end. To be able to understand local damage mechanisms (e.g. the impact of local defects), the testing was monitored using Digital Image Correlation (DIC) [3] .

Independent FE based predictions were provided from four groups using different tools and approaches. This gives valuable possibilities to understand the impact of different modelling choices on the agreement between the simulated data and the experimental results. All predictions were made without any knowledge of the experimental results (i.e. blind predictions).

3 Conclusions

By the introduction of full-field measurements, i.e. DIC, more complex load cases can be handled experimentally and enables a quantitative comparison between experimental observations with the corresponding simulation-based predictions. This reasoning is in line with the concept of “Material Testing 2.0” as proposed by Pierron and Grédiac [4]. In the present case study, the ability to predict the strain localization around the notches in the modified geometry is an example of such a possibility. In Figure 3, the observed spatial variation of the major principal strain prior to the final rupture is illustrated.

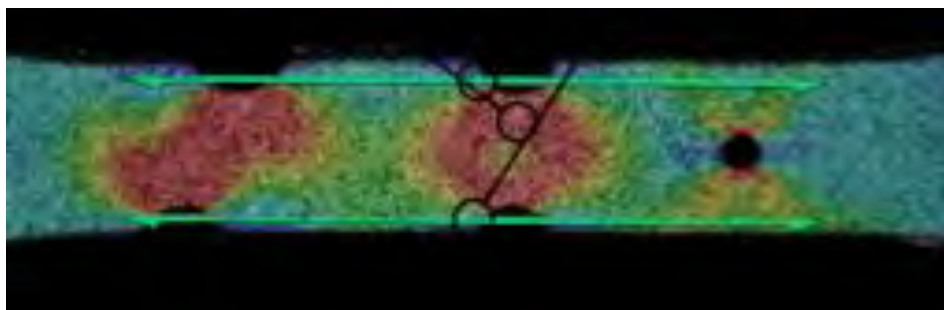


Figure 3. Major principal strain of a G2-specimen prior to the final rupture.

Currently, a second case study is ongoing in the EVIDENT project. A more complex load case using a non-standard test specimen geometry will be evaluated following a similar type of model validation framework as used in the present example. In addition, results from casting simulations (in a similar

approach as found in e.g. [5]) will be used to allow for local properties and manufacturing conditions to be incorporated into the FE-based predictions.

4 References

- [1] W. L. Oberkampf and C. J. Roy, *Verification and Validation in Scientific Computing*, Cambridge University Press, 2010.
- [2] E. Dartfeldt. [Online]. Available: <https://www.ri.se/sv/vad-vi-gor/projekt/utokad-virtuell-produktutveckling>.
- [3] H. Schreier, J.-J. Orteu and M. A. Sutton, *Image Correlation for Shape, Motion and Deformation Measurements*, Springer Verlag, 2009.
- [4] F. Pierron and M. Grédiac, "Towards Material Testing 2.0. A review of test design for identification of constitutive parameters from full-field measurements," *Strain*, 2020.
- [5] J. Olofsson, "Local microstructure-based material performance and damage in design and finite element simulations of cast components," *Journal of Computational Design and Engineering*, vol. 5, no. 4, pp. 419-426, 2018.

Structural Numerical and Experimental Investigation of Urea Mixer Component Thickness to Reduce Cost, Weight, and Thermal Mass

Hemanth Kumar Kuna (DINEX A/S)

1 Summary

The SCR system works by spraying urea-water solution (a liquid) into the hot exhaust gas, which vaporizes and mixes with the gas before it enters the catalyst where the reduction of Nitrogen oxides (NO_x) takes place [1]. At cold engine start, the urea does not vaporize and does not react with the exhaust gasses, so to avoid it being deposited on surfaces inside the exhaust after treatment system (ATS), the injection is cut off until a certain operating temperature is reached. Therefore, it is crucial that the exhaust after treatment system heats up as fast as possible, so the urea is injected and vaporized and the chemical reaction in the catalyst can take place.

The overall purpose of the work is to reduce the thermal mass of the exhaust after treatment system so the time to reach operating temperature is reduced. The reduction of mass is achieved by reducing the plate thickness of some of the exhaust after treatment system parts. The work presents the experimental and numerical estimated structural dynamic behavior when reducing the plate thickness of the parts of the exhaust after treatment system. The experimental results are also used to validate or update numerical Finite Element models so that the reliability of future predictions of structural dynamic behavior is increased.

Commonly in aftertreatment exhaust systems the material thickness used for internal components are 1.5 mm thickness. Considering this as base the investigation been carried. The considered test structure is named Full Assembly and consists of three sub-parts named Doughnut, Mixer and Outer. The Full Assembly and Outer Test structures are produced with plate thickness of 1.5 mm and the Doughnut and Mixer Test structures are produced in three sets with plate thicknesses of 1.5 mm, 1.0 mm and 0.75 mm which gives at total of eight test structures. Impact hammer method is applied for experimental modal analysis (EMA) and modal parameters are estimated by using the Abbravibe toolbox in MatLab [2]. Pretest and correlation analysis are done by using FEMtools [3] software along with a sub-sequent model updating.

1.1 Simulation Model

The simulations were conducted using the ANSYS commercial FEA code and FEMtools. Modal analysis, which studies eigen modes to identify eigen frequencies within the excitation frequency range, also serves as the starting point for dynamic analysis. The geometry model was imported into the software, materials were assigned at room temperature, and mesh type played a major role in the simulations. In the present work, different thicknesses were considered. The study involved shell and solid elements, with the solid elements using the SOLID186 element type. By employing the SOLID186 element type, which is a 20-node element with quadratic displacement behavior, it was determined that even a slightly larger element size would not significantly affect the results. This standard allows for the use of only one solid element through the thickness when a 20-node isoparametric element is employed. The SOLID186 element, defined by 20 nodes with translations in x, y, and z directions, proves capable even with some irregular meshes due to model issues.

1.2 Test Model

1.2.1 Multiple Reference Impact Testing - MRIT

Impact testing has been used for measuring frequency responses on mechanical systems since the seventies. The basic principle is, that a structure is excited, by using a impact hammer with integrated force sensor, in one DOF, and the response is measured with i.e. accelerometer in another DOF.

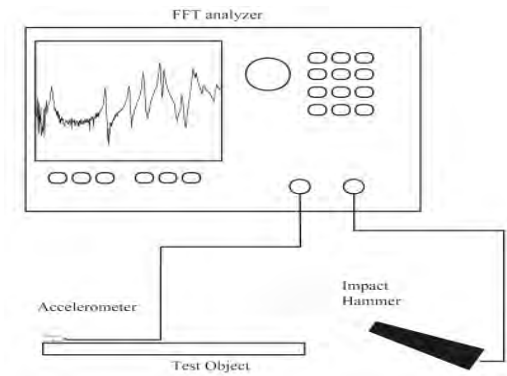


Fig. 1
Impact test setup [4].

The impact hammer and the accelerometer are coupled to a data acquisition system. A Fast Fourier Transform (FFT) analyzer is then used to convert the time data to Frequency Response Functions (FRFs). For modal analysis, impact testing can either be made with a fixed excitation point and multiple output that are measured, or the input is roved between the measuring points with fixed reference accelerometers. The second option is more convenient in most cases, because it is easier to move the impact hammer around the structure than moving the accelerometers to different locations. Furthermore the measurement will be more consistent, i.e. there will be no changes in the mass loading of the system. This is the basics of the MRIT [5, 6] that was developed in the early nineties. MRIT is a single input multiple output method (SIMO). The advantages of using a single input method, is that there is no need for multiple input FRF estimator. However the data set from MRIT can be processed with multiple reference (MIMO) modal parameter extraction methods, because of reciprocity. The FRF matrix for MRIT is a set of many inputs and few outputs and by transposing the matrix it becomes a set of few inputs and many outputs just like MIMO data set.

$$H = \begin{matrix} & \begin{matrix} in_1 & in_2 & \cdots & in_n \end{matrix}^T \\ \begin{matrix} out_1 \\ out_2 \\ \vdots \\ out_m \end{matrix} & \begin{bmatrix} H_{11} & H_{12} & \cdots & H_{1n} \\ H_{21} & H_{22} & \cdots & H_{2n} \\ \vdots & \vdots & \ddots & \vdots \\ H_{m1} & H_{m2} & \cdots & H_{mn} \end{bmatrix} \end{matrix}_{(m \times n)} = \begin{matrix} & \begin{matrix} in_1 & in_2 & \cdots & in_m \end{matrix} \\ \begin{matrix} out_1 \\ out_2 \\ \vdots \\ out_n \end{matrix} & \begin{bmatrix} H_{11} & H_{21} & \cdots & H_{n1} \\ H_{12} & H_{22} & \cdots & H_{n2} \\ \vdots & \vdots & \ddots & \vdots \\ H_{n1} & H_{n2} & \cdots & H_{nm} \end{bmatrix} \end{matrix}_{(n \times m)}$$

Fig. 2

MRIT FRF is the (mxn) matrix and the MIMO FRF ist he (nxm) matrix

A method for improved FRF quality from impact excitation is described in [7]. It is a method of recording all time data prior post processing, instead of confirming or rejecting every single impact. By recording 5 to 10 impacts at DOF, it becomes easier to chose impact with similar magnitude to make an averaging in the FFT processing. This method ensures a better coherence function.

1.2.2 Modal Assurance Criterion - MAC

The Modal Assurance Criterion (MAC), formulated by R. J. Allemang [8, 9], is a widely used technique for quantifying the first level of correlation between two sets of mode shape data and is given by

$$MAC(a,x) = \frac{|\{\psi_x\}^T \{\psi_a\}|^2}{(\{\psi_x\}^T \{\psi_x\})(\{\psi_a\}^T \{\psi_a\})}$$

Fig. 3

Modal Assurance Criterion (MAC), where ψ_x is the mode shape vector of mode x and ψ_a is the mode shape vector of mode a.

The output from this formulation is a matrix whose dimensions are defined by the number of modes which are compared.

1.2.3 Impact location

A Test model is applied in the pretest analysis phase and acts as digital twin of the Test structure that defines the sensor locations and directions. A Test model is applied to ease the process of marking and numbering measurement locations on the Test structure but also to link EMA and FEA data to enable an ease the correlation analysis of numerical and experimental data. The Test model is defined by points and DOF's, that are created when choosing sensor locations and directions from nodes on a FE model. A node point pair table and a DOF pair table is automatically generated to link the FE- and Test model. Different analysis tools can be applied in the pretest analysis phase to determine the optimal sensor locations, thereby reducing the number of sensors and time needed for a satisfying EMA analysis. But unfortunately, for most of the cases in this work, the reduced number of sensors have proven to be insufficient, so a coarse mesh of an increased number of sensor locations have been chosen manually. When the sensor selection process is completed, trace lines are added between the points to give a better visual representation of the Test model, Fig. 4. The point set, which defines the sensor locations, is marked by pen on the prototype structure and point numbers are added to define the impact locations.

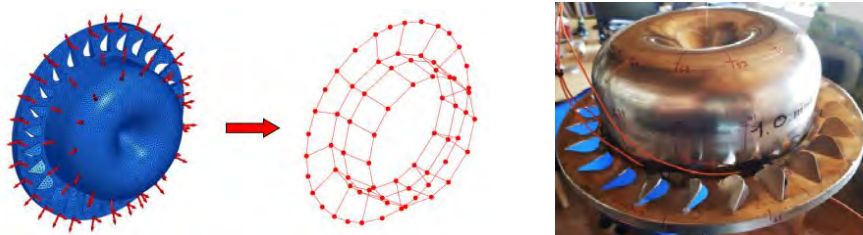


Fig. 4
(Left) Shows a meshed FE model with sensor locations and directions from which a Test model is defined. (Right) Shows a Test model consisting of points with trace lines that have been added manually to give a better visual representation of the model and an example of the 1.0 mm Doughnut structure with marks indicating point numbers and impact locations.

1.2.4 Accelerometer locations and data acquisition

The accelerometer locations are determined from a set of candidate locations which is chosen as the Test model point set. For roving impact hammer method with stationary accelerometers, the initial and potential useful locations can be selected by using pretest analysis metrics. This process can be done automatically and the final selection is determined by a Mode Participation Analysis (MPA) which gives information of how much each of the selected DOF participates in each mode. Fig. 5 shows the experimental setup.



Fig. 5
Experimental setup

2 Test Structures

The test structures are produced of stainless-steel plate material and are assembled from sub-parts by welding. Some of the Test structures are formed or rolled in the manufacturing process to achieve the desired design, which results in deviation from the initial plate thickness. The welding process adds material and the grinding process of the surfaces removes material where both production methods affects the mass and stiffness of the Test structures. Also, the heat effect from the welding process causes internal stress that may bend or deflect the surfaces from their initial shape. This can cause a symmetric structure to become slightly asymmetric. The frequencies and mode shapes of symmetric structures often come in pairs and for slightly asymmetric structures, the double frequencies tend to separate, which also will be case for most of the Test structures in this work. The 1.0 mm and 0.7 mm

test structures (Doughnut and Mixer) are especially influenced by the welding process which have caused great deflections for some surfaces so experimental results been evaluated carefully.



Fig. 6
Produced test structures for EMA

3 Analysis of Doughnut and Mixer

The correlation of EMA results in this section is done to evaluate the effect on the natural frequencies when changing the plate thickness. Though the mode shapes are likely to change significantly, it has still been possible to correlate them so natural frequency differences can be evaluated.

It can be seen that all frequencies decrease when plate thickness decreases, and that mode shape correlation is possible for most modes, even for the 1.5 mm vs. 0.7 mm case. The decreasing frequencies affects the order for which the mode shapes occur. Fig. 7 and Fig. 8 shows the CrossMAC matrices related to Doughnut and Mixer.

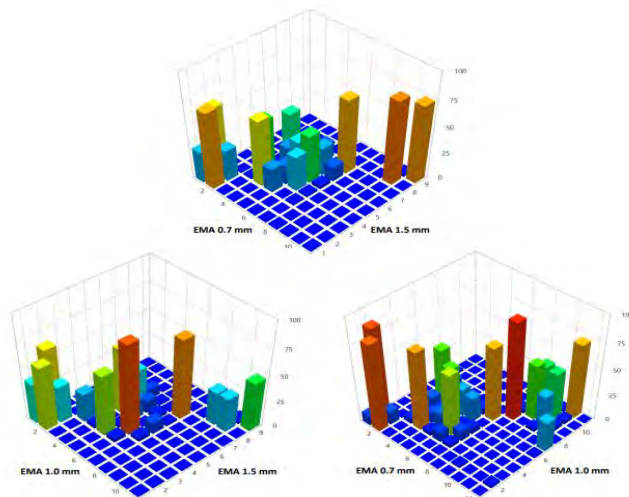


Fig. 7
CrossMAC matrices related to Doughnut

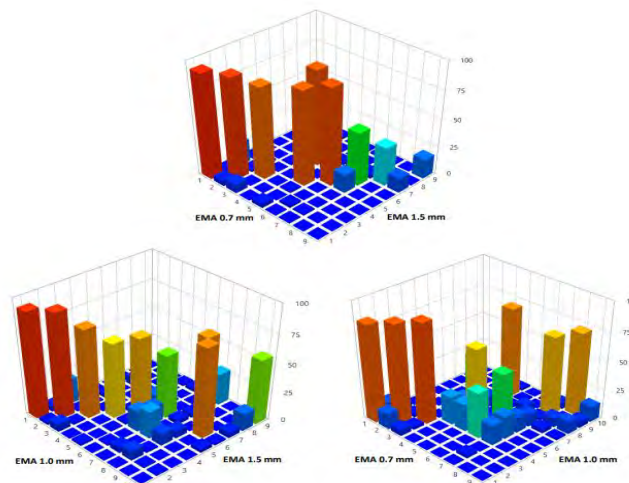


Fig. 8
CrossMAC matrices related to Mixer

4 Analysis of Outer and Full Assembly

The FEA vs EMA correlation results for the Outer shows that the FEA frequencies are 2 to 5 % higher than EMA frequencies except for the 6th mode shape pair where the FEA frequency is 3.6 % lower than EMA. The MAC values range from 61 to 87 %. The FEA vs EMA correlation results for the Full Assembly based on the paired modes shows that all the FEA frequencies range from 2 to 12 % and are higher than the EMA frequencies. The MAC values range from 4 to 65 % and the corresponding CrossMAC matrix for Outer and Full Assembly is presented in Fig. 9 and Fig. 10.

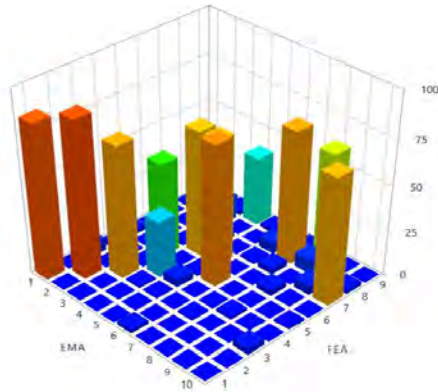


Fig. 9
CrossMAC matrices related to Outer

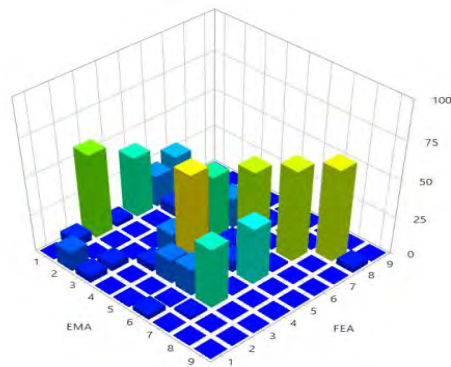


Fig. 10
CrossMAC matrices related to Full Assembly

5 Production Challenges

Reducing the plate thickness makes production challenges in terms of manufacturing process to achieve the desired design. These test structures can be formed or rolled in the manufacturing. CT scan been performed on doughnut for 1.5 mm thickness comparison between produced model with design model as shown in Fig. 11 and thickness check of the produced model been performed. Similar CT scan been also performed for 1.0mm and 0.7mm thickness. 0.7mm thickness have more challenges in terms of deviation, shape and deflection compared to 1.5mm and 1.0mm.

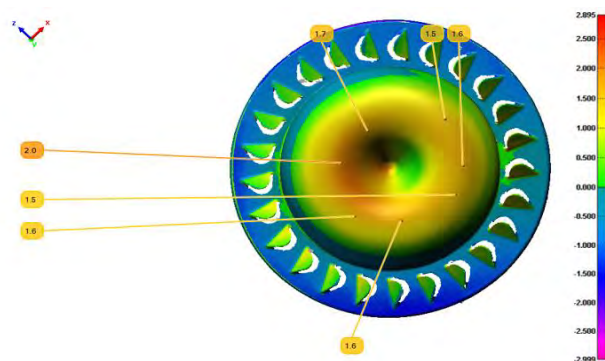


Fig. 11
Comparison of design model with production model 1.5 mm

6 Conclusions

Numerical models of subcomponents were compared to experimental modal analysis through Impact hammer method and correlation analysis are done by using FEM tools so that the reliability of predictions for structural dynamic behavior is known. In Doughnut and Mixer, the natural frequencies decrease when plate thickness is reduced, but the related mode shapes do not change significantly. The decrease in frequencies are far greater for the 1.5 mm to 1.0 mm plate thickness reduction, than for the 1.0 mm to 0.7 mm plate thickness reduction. The modes shapes related to the symmetrical parts of the Outer structure can appear in any orientation around the axis of symmetry, but the mode shapes related to the non-symmetrical parts have a fixed orientation that does not allow mode shapes to be rotated in order to find the best match. This combination of a structure with symmetrical and non-symmetrical parts, have proven to increase the complexity of identifying and pairing the correct modes. Because of mass consistency of the FE model and test structure, it is expected that only a minor global stiffness update is necessary to match FEA and EMA frequencies which then can be considered validated. For the Full Assembly, all modes are paired successfully by applying a combination of MAC values and visual evaluation of the mode shapes. All frequencies are estimated higher for the FE model than the test structure. The natural frequencies of the Doughnut, Mixer and Outer sub-pats becomes much higher when they are assembled into the Full assembly. To improve results, the mass could be corrected for the subparts and DOF resolution could be increased by adding more points and also by adding more DOF per point, by using triaxial accelerometers. The combination of roving accelerometers inside the Full Assembly and roving hammer technique outside on the Full Assembly has worked to satisfying level.

Qualitative evaluation of production challenges through CT scan been presented in the work for 1.5 mm, 1.0 mm and 0.7 mm thickness. 0.7 mm thickness have more challenges in terms of deviation, shape and deflection compared to 1.5 mm and 1.0 mm. Generally 0.7 mm prototype on seeing looks ok, but can clearly feel the deviation due to the manufacturing process and need different assembly method.

Present work was focused on the subcomponents dynamic behaviour and it can be extended through these subcomponents placed into full After Treatment System and applying the road load data for conducting the shaker test to perform the durability on subcomponents.

7 References

- [1] Dieselnet.com, resources on engines, fuels and emissions; Engine & emission technology online since 1997 (https://www.dieselnet.com/tech/diesel_exh_mat.php)
- [2] Abravibe toolbox in MatLab, developed by Prof. Anders Brandt. <http://www.abravibe.com/toolbox.html>
- [3] ANSYS Workbench 18.2 and FEMtools software <https://www.femtools.com/>
- [4] Anders Brandt. Noise and Vibration Analysis Signal Analysis and Experimental Procedures. John Wiley & sons Ltd., 2011.
- [5] D.J. Ewins. Modal Testing: Theory, Practice and Application Second Edition. Research Studies Press LTD, 2000.
- [6] William A. Fladung. THE DEVELOPMENT AND IMPLEMENTATION OF MULTIPLE REFERENCE IMPACT TESTING. Technical report, Masters Thesis University of Cincinnati, 1994.
- [7] A. Brandt and R. Brincker. Impact Excitation Processing for Improved Frequency Resonse Quality, 2010.
- [8] R.J. Allemang and D.L. Brown. CORRELATION COEFFICIENT FOR MODAL VECTOR ANALYSIS. In Proceedings of the International Modal Analysis Conference Exhibit, pages 110–116, Orlando, FL, USA, 1982. Union Coll.
- [9] Randall J. Allemang. The modal assurance criterion (MAC): Twenty years of use and abuse. In Proceedings of SPIE - The International Society for Optical Engineering, volume 4753 I, pages 397–405, Los Angeles, CA, United states, 2002. SPIE.

Modern Digital Twin solutions – Overview and Applications

Pär-Ola Jansell

Altair Engineering AB

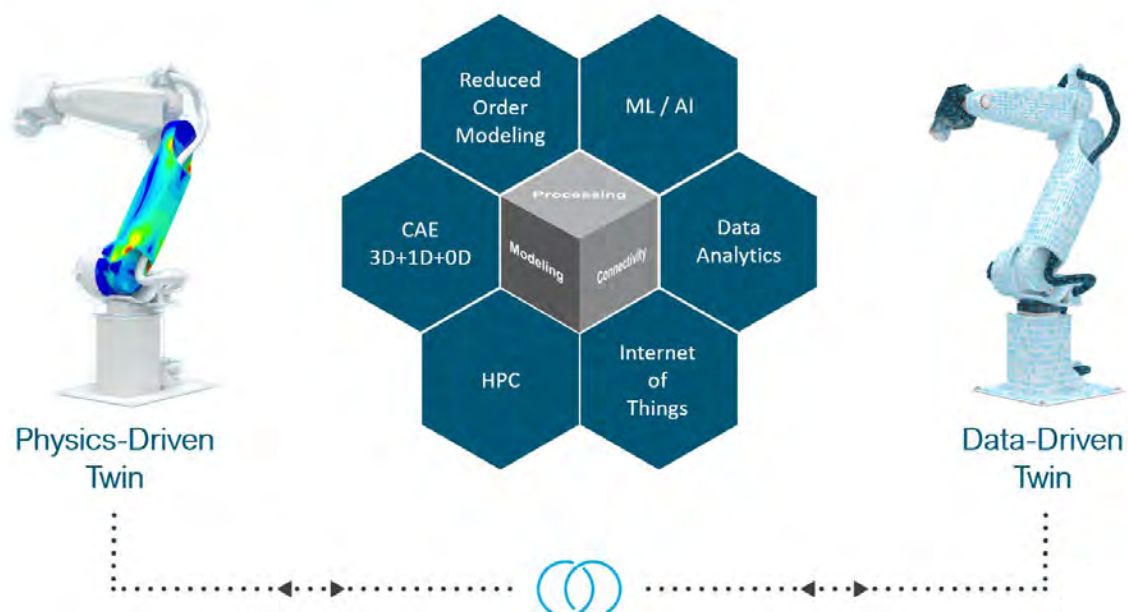
Modern Digital twin solutions empower organizations to transform their products, systems, and processes. By combining simulation, high-performance computing (HPC), artificial intelligence (AI), data analytics and Internet of Things (IoT) capabilities, teams can design, build, test, optimize, evaluate what-if scenarios, perform studies like predictive maintenance, remaining useful life, etc.— with or without the need of physical prototypes.

Modern Digital twin solutions remove the boundaries between and enable the combination of physics and data (real time, historic or synthetic) driven models. This presentation will cover the components of the modern multi-functional/physical/disciplinary Digital twin solution, including reduced order models, fleet data, simulation models etc.

Some different real-life applications will be discussed and outlined:

1. Minimizing vehicle maintenance and warranty costs due to operational loads – using a durability digital twin to predict damage in real-time from on-board sensors.
2. Using digital twins for range calculation of electric vehicles.
3. Using a digital twin to detect and manage deviations in a sheet metal forming process.

Combining connected capabilities and smart product development solutions enable comprehensive cross-functional system evaluation, which eliminates information silos and communication bottlenecks during product development. With modern Digital twin solutions, organizations become more efficient and can deploy Digital twin technology when and where they need it — through any or all lifecycle stages — from pre-production conceptual design through in-service performance.



Recent Advances in Nonlinear Industrial Non-parametric Optimization

Anton Jurinic (Dassault Systèmes), Claus B. W. Pedersen (Dassault Systèmes)

1 Motivation Nonlinear Industrial optimization

The goal to more accurately predict real world loading scenarios mean nonlinear effects are more often necessary to include in FE-analysis.

Sources of nonlinearity can be any or all of the following:

- Geometric nonlinearity (large deformations)
- Boundary nonlinearity (e.g. contact)
- Material nonlinearity (history dependent material behaviour e.g. elastic-plastic deformation)

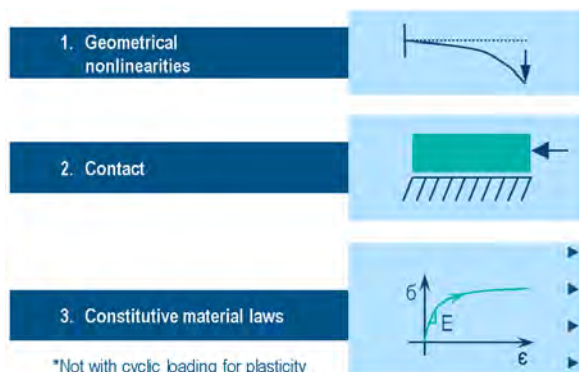


Figure 1 – Sources of nonlinearity.

Performing non-parametric structural optimization on nonlinear FE-models can add challenges in the form of non-convergence of the underlying FE-simulation. Typically, nonlinear effects are removed from the structural optimizations to increase probability of converging optimizations. However, this comes at the risk of the optimized designs not being able to sustain real world loadings. Potentially this will lead to more manual re-design loops in order to find robust structures.

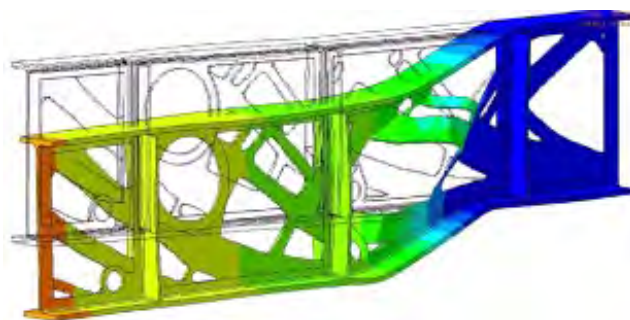


Figure 2 – Example of cantilever beam in global buckling during topology optimization.

This presentation will show selected applications where non-parametric optimization using Tosca Structure is performed on nonlinear FE-models in Abaqus/Standard resulting in more robust designs. Examples cover Topology, Shape, Sizing and Bead optimization. All with some or all of the nonlinear effects mentioned previously.

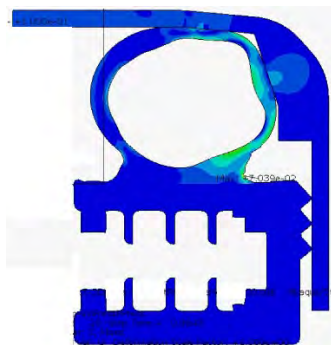


Figure 3 – Example of shape optimization containing hyperelastic rubber material and large sliding friction contact.

2 Numerical and physical stabilization approaches

In order to facilitate successful non-parametric optimizations where nonlinear effects are considered a number of stabilization approaches are used:

- Added artificial forces for suppression of physical post-buckling
- Quasi-static modelling
- Stabilizing void elements [ref. 1]

Depending on the optimization configuration and also the underlying FE-model configuration one or more of the stabilization approaches may be used. It is found that the here mentioned approaches help to stabilize the FE-analysis during optimization. The consequence is that optimization can successfully complete without convergence issues in the FE-solver.

3 Conclusions – Nonlinear industrial optimization

Effects from nonlinearities can be considered in non-parametric optimization given the right tools and settings. Nonlinearities can arise from large displacements, material nonlinearity and/or contact/friction. Also effects from imperfections are crucial for certain types of problems and can be included in the optimizations. Stabilization methods for the underlying FE-analysis allows for successful optimization with less risk of non-convergence.

Correct adjoint sensitivities are calculated by Abaqus/Standard and used by the optimizer engine in Tosca Structure. This means no simplifications are necessary which allows for:

- Analyzing real world models
- Including nonlinear effects
- Including imperfections

Considering nonlinear effects during optimization can help producing more robust designs. This also reduces risk of failure in realistic validation analysis.

4 References

- [1] Scherz, L.; Kriegesmann, B.; Pedersen, C.B.W.: A condition number-based numerical stabilization method for geometrically non-linear topology optimization. Submitted, 2024.

EXHIBITORS

- Altair Engineering
- atNorth
- BETA CAE Nordic
- Dassault Systèmes
- EikoSim
- Hexagon Manufacturing Intelligence
- Magna Powertrain Engineering Center Steyr
- NAFEMS
- Noesis Solutions
- Particleworks Europe
- Quanscient
- Rescale
- Siemens
- sustainedBIZZ



Safe the date!

Abstract submission deadline 22 Nov. 2024

www.nafems.org/congress



NWC25
NAFEMS WORLD CONGRESS
19-22 MAY 2025 | SALZBURG | AUSTRIA
A WORLD OF ENGINEERING SIMULATION

More regional conferences

www.nafems.org/nrc24



NAFEMS Deutschland, Österreich, Schweiz GmbH
Griesstr. 20, 85567 Grafing b. M.
Tel.: +49 176 217 984 01
Fax: +49 3 22 11 08 99 13 41
E-mail: info@nafems.de
www.nafems.org

